Optically Stimulated Luminescence dating of archaeological and environmental sequences in North Africa and Arabia

Natalie Jane Russell

Thesis submitted for the degree of Doctor of Philosophy,
Royal Holloway, University of London

May 2014

Institution of study:
Centre for Quaternary Research
Department of Geography
Royal Holloway
University of London

Declaration of Authorship

I Natalie Jane Russell hereby declare that this thesis and the work presented in it is entirely my own. Where I have consulted the work of others, this is always clearly stated.

Signed:

Date:

Abstract

A major goal in the study of human evolution is to understand the history of migration and expansion of modern humans out of sub-Saharan Africa during the last 150, 000 years. The overarching aim of this thesis is to develop a robust chronology for human occupation and environmental change in Libya (North Africa) and southern Arabia using optically stimulated luminescence (OSL) dating.

This study comprises three main components. The first component explores methodological aspects of OSL dating. In this component, the differences between equivalent doses produced using single-grain, pseudo single-grain and small aliquot are explored using material from Libya. Subsequently, the effects of using different curve fitting functions and data rejection criteria are explored using data from both the North African and Arabian sites.

The second component centres on constructing a robust chronology for the timing of human occupation and environmental change in the landscape surrounding the Haua Fteah cave in northern Libya. This chronology is then used to investigate the relationship between human activity and environmental change in North Africa. In particular, consideration is given to the timing and availability of fresh water in the region, and to how the area may have acted as a refuge during periods of climatic deterioration.

The final component focuses on enhancing the current age model of human occupation and environmental change at the Jebel Faya rock shelter in Arabia. In this component, the importance of Arabia as a potential dispersal route out of sub-Saharan Africa is considered, and the relationship between human activity and climate change in the region is discussed.

Acknowledgements

Firstly, I wish to thank my supervisor Dr Simon Armitage. His encouragement, guidance and support have been invaluable over the last four years and I cannot thank him enough. I feel very fortunate to have worked with such a knowledgeable and patient supervisor, and I can only hope that he realises how grateful I am to him. I would also like to thank Professor Clive Gamble for helping me see the wood through the trees. Having his experience on my team has always made everything seem more achievable. Dr Simon Blockley has also provided an encouraging presence in my supervisory team over the years, and I thank him for his enthusiasm and support.

Thank you to all of the Royal Holloway Geography laboratory, teaching, administration and support staff. In particular I would like to thank Iñaki Valcarcel. Iñaki has supported me in the lab for over 5 years, throughout my undergraduate, masters and PhD. He has always gone out of his way to help, he has been incredibly patient and supportive, and he has been an absolute pleasure to work with. I will miss our time in the labs. I would also like to thank Alice Christie and Peter French for all of their support over the last four years.

Thank you to all of the student and staff members of the CQR for making my time as a PhD student in the department so enjoyable. In particular, thank you to Dr Claire Gallant, Dr Mark Hardiman, Robyn Christie, Lucy Flower and Dr Ian Candy. I also wish to thank my friends and peers in the luminescence community, particularly Dr Georgina King and Dr Julie Durcan. I would also like to thank all of the members of the Libyan (TRANSNAP) and Arabian field teams. Special thanks go to Dr Lucy Farr, Dr Robyn Inglis, Dr Knut Bretzke, and Professor Adrian Parker for all of their help.

Dr Innes Keighren and Dr Tom Stevens, I couldn't have done it without you! Thank you for all of your support, advice and friendship over the last few years. Thank you for all of the coffee rants and never failing to make me laugh. It really has meant a lot.

Thank you to all of my friends and family for your support and encouragement, particularly Jean and David Locke, Stan and Dee Walker, and Jean and Dave Hurley.

Finally, I want to thank my parents John and Wendy Russell. I dedicate this thesis to you. You have always supported and encouraged me in everything that I have done, and I would not have got this far without you. Thank you for your love and support, and for always being there when I need you.

Contents

List of contents

List of Figures

List of tables

Chapter 1 - Introduction

1.1 Introduction

In this introductory chapter the rationale behind this thesis is discussed, specifically focussing on why and how this research will contribute to our understanding of modern human dispersals out of sub-Saharan Africa. A brief introduction into the current understanding of the relationship between Quaternary climatic change and archaeological developments in North Africa and Arabia is presented, although this is discussed in more detail in Chapter 2. The study sites in northern Libya and Arabia are introduced, providing information regarding why these areas were chosen, and how the outcomes of this thesis will contribute to the multidisciplinary projects being undertaken there. Research aims and objectives are then outlined, before the chapter concludes with an explanation of the thesis structure.

1.2 Thesis rationale

Investigating and understanding the history of migration and expansion of modern humans out of sub-Saharan Africa is essential in the study of human evolution. Current fossil, archaeological and genetic data suggests that modern humans originated in sub-Saharan Africa between 150 – 200 ka (Beyin, 2011; Fleagle et al., 2008; McDougall et al., 2005; Tyron, 2006; Willoughby, 2007; Reed & Tishkoff, 2006; White et al., 2003). Whilst the scientific community generally agrees on an African source, debates concerning the timing and geographical routes of modern human dispersal out of Africa remain unresolved, and are amongst the most widely debated topics in Quaternary Science (Abbate & Sagri, 2011; Beyin, 2011).

Improving our understanding of the spatial and temporal distributions of human habitats is key to understanding what may have driven Pleistocene human dispersals and settlement dynamics (Bretzke et al., 2013). Consequently, a primary focus of current research aims to investigate the timing of modern human dispersals out of Africa, the number and success of dispersal events, and the potential drivers of such events (Abbate & Sagri, 2011).

Following Mellars (2006), two alternative mechanisms for the migration of anatomically modern humans (AMH) out of Africa are widely acknowledged. The first suggests that a sudden change in the cognitive capacity of modern human populations (supported by the

emergence of distinctively modern patterns of culture and technology) enabled a massive demographic expansion across and out of Africa, and their subsequent replacement of preceding archaic groups. Alternatively, as environmental change is a causal mechanism for the dispersal and isolation of animal populations (Blome et al., 2012), modern human expansions and contractions are often related to climatic oscillations during the Pleistocene (Petraglia et al., 2011; Foley & Lahr, 1998). Sharp oscillations between arid and humid conditions led to changes in annual precipitation of up to 50% in sub-Saharan Africa (Partridge et al., 1997). These variations in climatic conditions would have had significant effects on modern human populations, specifically those groups occupying the most arid regions of Africa (Mellars, 2006). Consequently, increased consideration is being given to the role of Pleistocene climatic change on modern human dispersals over different spatial and temporal frameworks (Blome et al., 2012).

Whilst climatic change may not have been the sole causal factor of early modern human migrations out of sub-Saharan Africa, it is important to understand the environments in which modern human populations were existing. Due to the generally arid nature of the African continent (specifically the Saharan desert region), changes in water availability would have significantly influenced the timing and routes of early human migrations. In order to migrate out of sub-Saharan Africa, modern humans would have had to cross either the Sahara desert or the Arabian Peninsula. Since both of these areas are uninhabitable under current climate conditions, it would have been necessary for more humid conditions to be present to facilitate migration and expansion of human groups into them. This would have required climatic change.

1.2.1 The "Saharo-Arabian" desert belt

Extending from the Atlantic coast of North Africa, through the Middle East and into Asia, the Saharo-Arabian desert belt separates the African and Eurasian landmasses, presently acting as a geographical barrier to human dispersals out of sub-Saharan Africa (Figure 1.1) (Groucutt & Blinkhorn, 2013). However, periods of increased humidity during the Pleistocene potentially created "windows of opportunity" during which human populations were able to inhabit and traverse these present day deserts. Since modern humans evolved in sub-Saharan Africa, it was necessary for ancient populations to cross the present-day deserts of either, or both of, the Sahara and Arabia (Drake et al., 2013).

Understanding the dispersal of hominins into and through the "Saharo-Arabian belt" is therefore essential to understand how modern human groups dispersed from Africa into the rest of the world (Groucutt & Blinkhorn, 2013; Issar, 2010). Current investigations into this area of research include: 1) establishing when desert barriers were "open" (humid) and when they were "closed" (arid); 2) determining the causes of humid-arid fluctuations; and 3) determining the extent of ancient occupation of the Saharo-Arabian desert belt, and questioning how effective these deserts were at preventing hominin occupation and dispersal (Drake et al., 2013).

Figure 1.1. Map outlining the location of the Saharo-Arabian desert belt (adapted from Groucutt & Blinkhorn (2013).

Four potential routes from sub-Saharan African to the Mediterranean are commonly referred to, including: 1) a northern route along the Nile River Valley (Vermeersch, 2001); 2) a "Green Sahara" route in which Saharan megalakes and riverine belts provided a "humid corridor" across the Sahara (Drake et al., 2011); 3) a "coastal route" along the western Red Sea coastline (Abbate & Sagri, 2011); and 4) an eastern route across the Bab al-Mandab Straits into the Arabian Peninsula (Stringer, 2000, Abbate & Sagri, 2011; Drake et al., 2013; Mellars et al., 2006). Whichever route AMH took, they would have required daily access to drinking water (Sagri & Abbate, 2011; Oppenheimer, 2009).

During glacial and interglacial periods, hydrological variations in North Africa and Arabia have been linked to Middle and Upper Palaeolithic occupations and dispersals (Armitage et al., 2011, Drake et al., 2011, Petraglia et al., 2011). Evidence for hominin penetration into

desert areas under more favourable, humid conditions can be found in the vast deserts of the Sahara and the Arabian Peninsula (Drake et al., 2011; Groucutt & Petraglia, 2012; Petraglia et al., 2012). This "greening" of desert environments is thought to have encouraged the expansion of hominin populations into previously inaccessible areas, whilst increased aridity would have led to population contractions and possible extinctions (Petraglia et al., 2012).

1.2.2 The importance of North African and Arabian research

Testing ideas regarding the relationships between climatic change and human dispersals requires well resolved, and accurately dated, records of environmental change and human occupation. Poor preservation of archaeological sites in desert environments often results in limited information being available to aid our understanding of hominin dispersals in these regions, and thus the potential influence of climatic change on hominin demography (Petraglia et al., 2012). Human fossil records and archaeological sites are scarce and often poorly dated, with large areas along possible migration routes often ill-defined and poorly documented (Abbate & Sagri, 2011). Consequently, in order to track dispersals and compare the distribution of hominins in northern Africa and the Arabian Peninsula, it is essential to increase environmental and archaeological investigations, applying reliable dating techniques wherever possible (Abbate & Sagri, 2011).

Due to their strategic placement at the main gateways between Africa and Eurasia, North Africa and Arabia play a central role in the current debates surrounding hominin dispersal (Beyin, 2011). The lack of precisely dated archaeological records in these regions has resulted in a distinct gap in knowledge concerning dispersal routes out of sub-Saharan Africa (Petraglia et al., 2011). Furthermore, the fragmentary record of climate in these regions prevents investigation of the synchroneity of climatic change between the two areas during the Pleistocene (Drake et al., 2013). Increasing the number, and improving the chronological resolution, of both environmental and archaeological studies, is therefore essential. This will facilitate the comparison of macro scale, coarse temporal frameworks (such as the Marine Isotope Stage boundaries), with micro scale studies (investigating the relationship between small populations and local environmental change over relatively short timescales) (Blome et al., 2012).

In this thesis I set out to answer the following questions:

1. When were modern humans present in the landscape surrounding the Haua Fteah cave, Libya, and the Jebel Faya rock shelter, Arabia?
2. How has regional climate change affected the timing of human activity in these regions?
3. How closely do North African and Arabian Quaternary environmental changes reflect northern hemisphere glacial and interglacial cycles?
4. Do the data presented in this thesis support a "pre" or "post Toba" dispersal model out of sub-Saharan Africa?
5. Did modern humans migrate out of sub-Saharan Africa along a northern or southern route?

1.2.3 How this thesis will contribute to the debate

This thesis uses applications of optically stimulated luminescence (OSL) dating to investigate the timing of human occupation and environmental change in northern Libya and Arabia, during the late Middle to the Late Pleistocene (c. 200 ka to present). Providing a chronology for Palaeolithic sites in these areas (currently under climatic and archaeological (re)investigation), will enhance our understanding of the timing of local human occupation and environmental histories in these regions. Furthermore, this will aid investigations into the human histories in the areas, and their response to both local and regional climatic shifts.

Through multidisciplinary research (Section 1.3 and 1.4) and the application of strong chronological constraints, it will be possible to fill in some of the current gaps in our understanding surrounding the causes, routes and timing of human dispersals out of sub-Saharan Africa. In the context of this thesis, regional and local climates will be investigated through the study of various sedimentary sequences (primarily lacustrine, coastal and palaeosols), as well as via comparison with other regional records (including marine isotope curves, speleothems etc). The timing of modern human occupation in North Africa and Arabia will be investigated through the study of Palaeolithic sites in these regions. Because skeletal material is relatively rare, some types of Middle Palaeolithic lithics have been used in the literature to act as evidence for the presence of AMH (Armitage et al., 2011; C. Hunt, *pers. comm.* 2010).

1.3 The Haua Fteah cave, Libya

This thesis is tied to the European Research Council (ERC) funded "Cultural transformations and environmental transitions in North African prehistory" (TRANSNAP) project, the overarching aim of which is to investigate the relationship between the environment and human settlement over the past 200 ka in the Cyrenaican region of northeast Libya. The primary objective of the TRANSNAP project is the re-excavation of the famous Haua Fteah cave in Cyrenaica (Figure 1.2), initially excavated by Cambridge archaeologist Charles McBurney in the 1950s (Barker et al., 2007; McBurney, 1967). The Haua Fteah is a limestone karstic cave, positioned on the lowest of a series of terraces of the Gebel Akhdar (Green Mountain) massif. The Gebel Akhdar is an upland massif between the Mediterranean Sea and the Sahara (Barker et al., 2007). The Haua Fteah Cave represents one of the longest and most complete records of human occupation in North Africa, yielding a sequence of human occupation stretching from the Graeco-Roman to Middle Palaeolithic (Barker et al., 2007, 2010).

The secondary objective of the project is to investigate the relationship between humans and environmental change. This objective is being addressed using geomorphological and archaeological investigations in the landscape surrounding the Haua Fteah. During the initial excavation of the cave in the 1950s, the McBurney team investigated a number of sites along the coast, in an attempt to investigate the climatic and environmental context of the surrounding landscape (McBurney, 1967; McBurney & Hey, 1955). In the TRANSNAP project, this research is being continued in an attempt to determine the nature of landscapes in the Jebel Akhdar during periods of human occupation, with the aim of determining how human populations responded to these changes (Barker et al., 2007).

Overall the TRANSAP project aims to address three major research questions: 1) when and how did modern humans reach North Africa?; 2) when and how did farming begin in North Africa?; and 3) to what extent was climatic change implicated in these processes?

Figure 1.2. Photographs showing a) the Haua Fteah cave, b) the excavation within the cave, and c) a view of the Mediterranean Sea from inside the cave.

1.3.1 Regional significance

The Gebel Akhdar experiences a Mediterranean climate, with higher precipitation than the neighbouring Sahara. The Haua Fteah is positioned between the desert belt and the Mediterranean coastline (McBurney & Hey, 1955). Recent research suggests that such areas act as refuges during periods of climatic deterioration, and were essential for the survival of modern human populations during these periods (Basell, 2008). In particular, lake margins, coasts and highland areas are thought to have provided refuges due to their habitat stability during (prolonged) periods of aridity (Basell, 2008). Coastal areas, for example, represented ecotones containing a rich diversity of habitats that would have provided modern humans with a range of resources, potentially including improved access to water (Bailey et al., 2008). During periods of rapid climatic fluctuation or increased aridity, it is possible that the "protected" coastal strip may have provided modern humans with a habitable "refuge" during times of climatic and resource stress (Basell, 2008). For example, Shea (2008) reports that the coastal zone in the Levant provided a belt of Mediterranean vegetation that allowed modern humans to survive during periods of desert expansion. It has been proposed that coastal zones may have provided a corridor for human dispersals out of Africa (Stringer, 2000; Bailey, 2008).

The TRANSNAP study area is ideal for studying the interplay of human migration, occupation and adaptation in response to regional environmental change since it occupies an apex position between Europe, the Levant and Africa. Ascertaining the number and timing of occupations within the Haua Fteah cave and wider environment may shed light on the ability of the region to act as a refuge during climatic fluctuations. By comparing the timing of occupation with important climatic and geomorphological changes in the landscape, it is possible to investigate the relationship between humans and climate change in North Africa. Special considerations are given to timing and availability of fresh water in the vicinity of the cave, which would have acted as a valuable resource for human populations residing in the area, especially during periods of climatic deterioration.

1.3.2 Thesis contribution

Whilst the work presented within this thesis forms an important component of the TRANSNAP project, it has distinct stand alone aims and objectives which focus specifically on the timing of human occupation in the region, and the timing of local environmental change (specifically the timing and availability of fresh water resources). Being a part of the project presents an opportunity to examine the multi-proxy records in and around Haua Fteah Cave, whilst providing dates which can be used to derive robust age models of human and environmental change in the area. Comparison of these records with findings from Arabia and other regions of North Africa and the Levant, will enhance our understanding of the spatial and temporal distributions of modern human populations. These data will contribute to debates regarding the timing and dispersal routes of modern humans out of sub-Saharan Africa.

OSL samples were also taken from several localities around the landscape, including the Al Marj palaeolake basin, Latrun, the Chersa Beach coastal strip, Wadi Derna and its tributary Hajj Creiem (Figure 1.3). Modern human activity during the deposition of these deposits was represented by the presence of in-situ lithics that are currently attributed to AMH populations (Section 2.5). OSL dating has been completed at these sites with the aim of constructing a framework for understanding the timing of human presence in the landscape, and major climatic and environmental changes in the region. In addition, the Al Marj, Wadi Derna and Hajj Creiem sites all provide evidence for the presence of fresh water

in the Gebel Akdhar. Consequently, ages from these sites provide information regarding the availability of water resources during periods of human occupation.

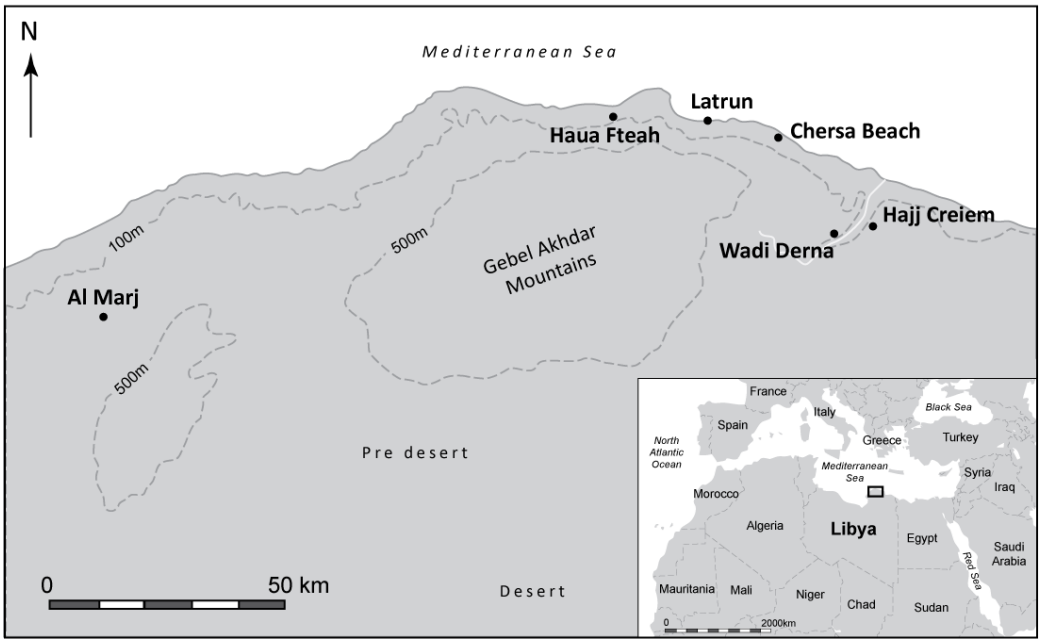

Figure 1.3. Map showing the location of the Haua Fteah cave and other sites from the surrounding landscape. The inset illustrates the positioning of the region within a wider setting.

During initial excavations by Charles McBurney, radiocarbon (^{14}C) dating was used to date the upper part of the Haua Fteah cave sequence. Sediment depth was then used to extrapolate ages for the lower levels, alongside early oxygen isotope measurements that were correlated with deep sea records (Emiliani & McBurney, 1967). As part of the re-excavation of the cave, a suite of chronological techniques are being applied to the cave sequence including tephrochronology, Electron Spin Resonance (ESR) dating, Uranium-Series (U-Series), and renewed ^{14}C dating. OSL dating produced as part of this thesis will contribute to the suite of ages produced for the cave sequence, facilitating the production of an age model for human occupation in the cave.

1.4 Jebel Faya, United Arab Emirates

In addition to the TRANSNAP project in Libya, this thesis also ties to a joint project between the Institute of Early Prehistory of the University of Tübingen (Germany) and the Directorate of Antiquities of the Department of Culture and Information, Government of Sharjah (UAE).

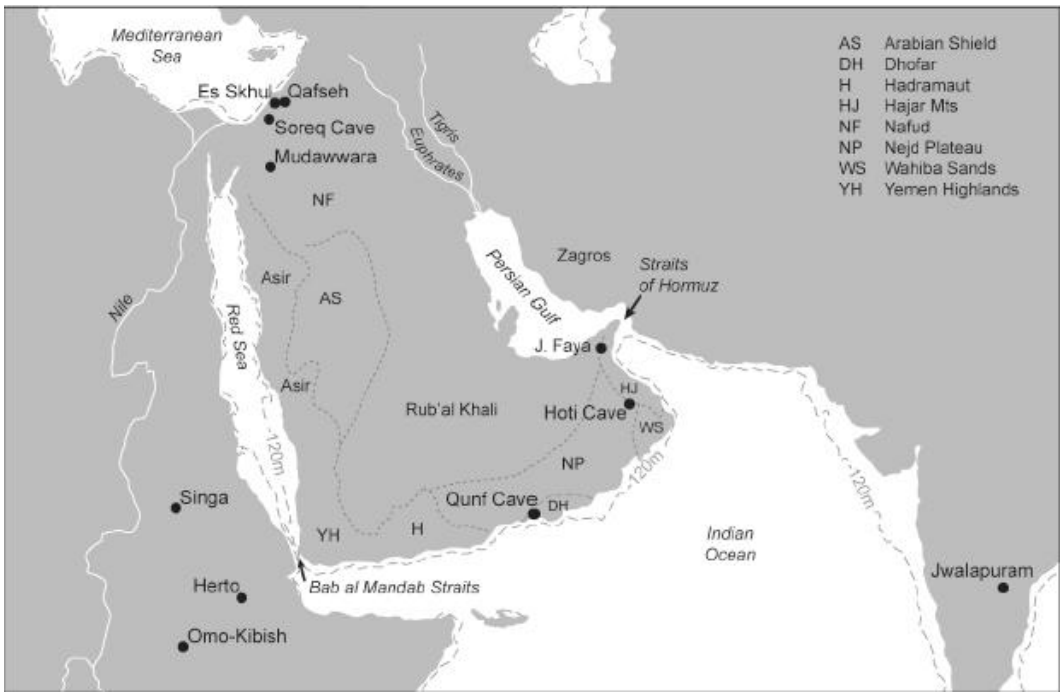

Figure 1.4. Map showing the location of FAY-NE1 (J. Faya), United Arab Emirates, and a number of important geographical barriers. The dashed line represents the -120 m shoreline, which indicates the maximum exposure of land during marine low stands (source: Armitage et al., 2011).

FAY-NE1 is a large rock shelter site situated on the eastern side of Jebel Faya in the central region of the Emirate of Sharjah (UAE). Jebel Faya is the most southerly of four mountains that constitute an anticline structure, located at the western edge of a plain that separates the site from the Hajar Mountains to the east (Figure 1.4). FAY-NE1 is approximately equidistant (60 km) from the Persian Gulf in the west, and the Gulf of Oman in the east. The northern tip of the Oman peninsula is located c 130 km to the north of the site (Bretzke et al., 2013).

1.4.1 Regional importance of the site

The large dune fields of the Rub' al-Khali sand sea extend from the coast of the Persian Gulf to the west, and are separated from the wide plain that reaches the western foot of the Hajar Mountains by the anticline structure containing Jebel Faya (Figure 1.4). This wide plain to the east of the FAY-NE1 site is commonly referred to as the Inland Basin or Dhaid-Madam Plain (Uerpmann, 2008). In comparison with the surrounding areas, the plain is characterised by relatively well developed vegetation. This results from the relatively wet conditions caused by the drainage of precipitation from the Hajar mountains into the Inland Basin via surface runoff and underground flow (Bretzke et al., 2013). Under favourable conditions, flow in the wadis draining precipitation from the Hajar Mountains can reach Jebel Faya and beyond. In the past, the confluence of these wadis near FAY-NE1 resulted in the presence of standing surface water, identified by lake deposits in the local area (Bretzke et al., 2013). Furthermore, runoff from the Jebel Faya periodically results in collection of water in potholes in the wadi c. 200 m north of the site. The availability of fresh water, presence of vegetation, raw material availability for lithic production from the anticline, and sheltered nature of the site would have made it an attractive settlement area for mobile hunter-gatherer groups dispersing into Arabia during the Pleistocene.

Archaeological layers identified inside the rock shelter, and below a barrier of fallen rocks, include artefacts from the Iron and Bronze ages, through the Neolithic, and into the Palaeolithic (Armitage et al., 2011). An archaeological sterile layer separates the Palaeolithic assemblages from overlying archaeological units. The current chronology for the site, produced via quartz single-grain optically stimulated luminescence dating, suggests that the sedimentary and archaeological sequence spans at least 125 ka (Armitage et al., 2011; Bretzke et al., 2013). DNA studies previously suggested that diversion of the human genetic gene pool occurred between 60 – 85 ka (Forster, 2004; Macaulay et al., 2005), indicating that the dispersal of modern humans out of Africa most likely occurred c. 75 – 80 ka (Rosenberg et al., 2011). However, the lithic industries recovered from the site have been used to infer the presence of modern humans at Jebel Faya c. 125 ka suggesting that the dispersal of modern humans out of Africa may have occurred much earlier, during the transition between MIS 6 and 5 (Armitage et al., 2011). Armitage et al. (2011) explain this early arrival of modern humans at this site as being the result of the interplay between global sea-level and regional climate change. As such, the chronology of the FAY-NE1 site is of critical importance for our understanding of the climatic controls upon human migration.

1.4.2 How this thesis will contribute

Through the application of Optically Stimulated Luminescence (OSL) dating, this thesis aims to increase the current resolution of the age model for FAY-NE1. This is necessary because Armitage et al. (2011) only dated key horizons within the site, without providing a chronology for the entire archaeological sequence. Enhancing the chronology will facilitate investigation into the settlement history of the site since the Palaeolithic, contributing to our understanding of the timing of human occupation in Arabia and its relationship to periods of climatic fluctuation. Comparison of results from climatic and archaeological research over a wider geographical area will facilitate exploration of the current debates concerning the potential routes and timings of our ancestors' migration out of sub-Saharan Africa. Furthermore, providing an enhanced chronology for the site enables the testing of the hypothesis that the advantageous geographical setting of Jebel Faya led to a stable populating of the region (Bretzke et al., 2013).

1.5 Research Aims

The overarching aim of this PhD is to develop a robust chronology for human occupation and abrupt climatic and environmental change in Libya (North Africa) and southern Arabia during the Mid to Late Pleistocene, using applications of OSL dating.

The thesis can be split into three key components. The first component aims to develop the most appropriate method for age determination of fine grain sedimentary quartz using OSL dating. Standard methods are applied and tested using four samples from the Libyan field sites. The applicability and affect of the $2D_0$ rejection criterion, and the function used to fit the datasets on age determination are also tested and discussed using the Libyan and Arabian material. Results from the various experiments are compared and discussed in Chapters 8 and 9.

The second component focuses on constructing a robust chronology for the timing of human activity, and important climatic and geomorphological changes in the landscape surrounding the Haua Fteah cave in Libya. This will allow for an investigation into the relationship between humans and climate change in North Africa, specifically testing theories concerning how abrupt climatic and environmental change may have influenced human development and population migration into the area. Special consideration is given

to the timing and availability of fresh water in the region, and the ability of the area to act as a refuge during periods of climatic deterioration.

The third component centres on producing an enhanced age model of human occupation and environmental change at the FAY-NE1 site in Jebel Faya, UAE. Improving the understanding of human occupation history at the site will aid our understanding of the importance of Arabia as a potential dispersal route out of sub-Saharan Africa. Furthermore, providing a chronology of occupation will facilitate investigations into the relationship between climatic change, human activity, and human expansions into the region.

1.6 Thesis Structure

This introduction briefly outlined: 1) the scientific context and rationale behind the thesis; 2) the two study locations and associated multidisciplinary research projects; and 3) the main aims and objectives of the overall project. Chapter 2 provides a review of Quaternary climate, environment and human adaptation in North Africa and Arabia. Chapters 3, 4, 5, 6 and 7 introduce optically stimulated luminescence dating, detailing: 1) the collection and preparation of material; 2) how the luminescence signal is measured; 3) how the environmental dose rate is calculated; and 4) how OSL ages are determined and calculated. Chapter 8 presents experimental work published by Russell and Armitage (2012), which tests the applicability of standard methods when dating fine grain sand from Libyan sites. Chapter 9 assesses the affect of applying the $2D_0$ rejection criteria, and the choice of function used to fit the OSL signal, to the datasets produced for all samples in this thesis. Chapters 10 and 11 introduce the individual study sites from Libya and Arabia respectively, presenting the OSL ages produced at each site, and discussing the significance of the findings in this thesis in the context of current wider environmental and archaeological understanding. Specific focus is given to the impact of these findings on theories concerning the timing and route of modern human migration out of sub-Saharan Africa. The main conclusions of the thesis are presented in Chapter 12.

Chapter 2 - Climate, Environment and Adaptation

2.1 Introduction

This chapter outlines our current understanding of Mid to Late Pleistocene (and Holocene) climatic change in North Africa and Arabia, specifically focusing on the drivers and patterns of change. These patterns are subsequently used to provide the environmental context for theories linking climatic fluctuations to the expansion, contraction and migration of modern humans out of sub-Saharan Africa.

2.2 North African Quaternary Climate Change: Current Understanding

The Pleistocene (c. 2.6 – 0.01 Ma) and Holocene (c. 0.01 Ma – Present) represent the two epochs in the Quaternary, the most recent major period of the geological record. Changes in the Earth's orbital and rotational parameters (eccentricity, obliquity and precession) drive seasonal and latitudinal variations in the distribution of incoming solar radiation over different timescales (100 ka, 41 ka and 21 ka respectively), and are traditionally believed to have caused multiple shifts in global climate between glacial and interglacial conditions during the Pleistocene (Hays et al., 1976; Berger & Loutre, 2007). Throughout the Quaternary, there have been a succession of these glacial-interglacial cycles, however, more rapid, high-amplitude shifts in climate are also frequently recoded in high resolution palaeoclimatic records (Labeyrie et al., 2007; Maslin et al., 2001). These Sub-Milankovitch climatic oscillations, identified in the Greenland ice cores and North Atlantic marine cores (Bond et al., 1992; Bond et al., 1993; Dansgaard et al., 1993), occurred over timescales that were too abrupt and rapid to be explained by orbital forcing (Berger & Labeyrie, 1987; Maslin et al., 2001). Maslin et al. (2001), therefore suggest that the large scale glacial-interglacial cycles were not solely caused by orbital forcing, but driven instead by strong climate system feedback mechanisms. Primary mechanisms are thought to include increased albedo during glacial periods and heat transfer changes via oceanic circulation, whilst secondary feedback mechanisms involved changes in greenhouse gas levels and ice sheet stability (Maslin et al., 2001).

Throughout the Quaternary period, the alternating glacial and interglacial periods are each assigned an Oxygen Isotope Stage (OIS) or Marine Isotope Stage (MIS) number (Figure 2.1). MIS and OIS numbers thus provide a coarse temporal framework for large scale climatic

changes, with even numbers representing glacial periods, and odd numbers denoting interglacials (Lowe and Walker, 1997). Lisiecki and Raymo (2005) present a 5.3 Ma stacked record (LR04; Figure 2.1) of average benthic $\delta^{18}O$ from 57 globally distributed records, which is assigned an age model derived from orbital tuning and average sedimentation rates. Stages are assigned, based on changes in the isotopic composition of marine core records from the Atlantic, Pacific and Indian Oceans, providing a trace of palaeoclimate over time. This stack therefore provides a common record and timescale for global climatic change, which regional records can be compared to.

Within the large scale climate cycles, a number of shorter-term, rapid climatic variations can be observed, known as stadial (cool) and interstadial (warm) episodes. Whilst the timescales of these rapid climatic shifts (which include Heinrich Events and Dansgaard-Oeschger cycles) are too short to be explained by orbital forcing, they have been shown to cause variations in regional climates and environments during glacial and interglacial periods (Bar-Matthews et al., 1997; Blome et al., 2012; Bond et al., 1993; Dansgaard et al., 1993; Maslin et al., 2001). Sub-Milankovitch events are particularly important for African and Arabian regions as rapid changes in ocean and atmospheric circulation induced by Heinrich events have been linked to abrupt changes in climate in tropical and subtropical areas (Carto et al., 2009). Consequently, these abrupt changes would lead to local and regional changes in aridity (Blome et al., 2012).

The Thermohaline Circulation (THC) or Meridional Overturning Circulation (MOC) is an oceanic current responsible for the cross-equatorial transport of heat from low latitudes to northern polar regions (Carto et al., 2009). This circulation pattern, which is driven by salinity and temperature gradients, carries warm and relatively salty surface water from the Gulf of Mexico up to Greenland, Iceland and Norway, releasing heat into the atmosphere and warming the adjacent continents (Carto et al., 2009). Heinrich events, which occur when icebergs surge into the North Atlantic during periods of ice sheet instability, result in the abrupt collapse of the THC, as the associated meltwater leads to a decrease in sea surface temperature (SST) and salinity (Carto et al., 2009). Heinrich events are identified as carbonate-rich layers of ice rafter debris, which last between 100 and 500 years (Carto et al., 2009). These rapid climatic shifts are characterised by an initial, abrupt cooling event followed by an equally abrupt warming event (most likely caused by the re-establishment of the THC) (Carto et al., 2009).

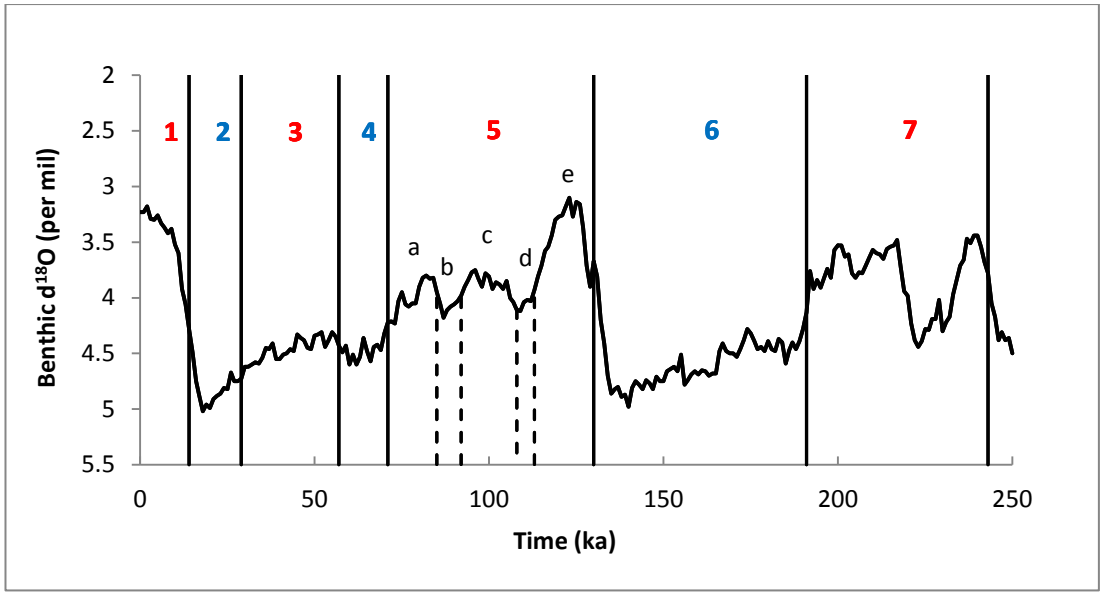

Figure 2.1. Oxygen isotope data from the LR04 stack produced by Lisiecki and Raymo (2005) spanning the last 250 ka. MIS stage boundaries are marked by solid black lines. MIS 5 sub-stage boundaries, reported by Martrat et al. (2004), are represented by dashed lines and labelled accordingly. Interglacial MIS stage numbers are labelled in red, while glacial MIS stage numbers are labelled in blue.

Heinrich events are associated with cooling events throughout the Pleistocene (specifically at 16, 22, 30, 38, 45, 65, 85 and 105 ka) and are thought to have occurred amidst millennial scale Dansgaard-Oeschger cooling climatic oscillations (Figure 2.2) (Carto et al., 2009; Bond et al., 1993; Maslin et al., 2001). A number of studies suggest that fluctuations in the THC over the last 125 ka, caused by Heinrich events, drove much of the observed North Atlantic sea surface temperature (SST) variability, and subsequently terrestrial cooling in Africa. Carto et al. (2009) used climate modelling to suggest that during the occurrence of Heinrich events, Africa experienced profound shifts in climate, with large parts of North, West and East Africa experiencing increased aridity. Cacho et al. (1999) analysed planktonic foraminifera assemblages from an Alboran Sea, western Mediterranean sedimentary sequence, identifying a link between colder SSTs and land surface temperatures with the occurrence of the four most recent Heinrich Events (Carto et al., 2009). Broecker and Hemming (2001) similarly reported a link between Heinrich events and increased aridity in Africa using sediment cores from the equatorial Atlantic. Furthermore, Schefuβ et al. (2003) interpreted variations in the abundance of southern African C4 plant abundance in marine sediment cores as being in phase with tropical SSTs. They suggest that tropical sea

surface temperatures controlled tropical evaporation and atmospheric moisture content, which in turn controlled African precipitation and therefore continental aridity. During glacial periods the tropical SST decreased by up to 5 °C. They suggest that this decrease led to continental aridity resulting from a reduction in tropical evaporation, and therefore reduced African precipitation. North African aridity (brought about by Heinrich events) would have reduced water and food resources, affecting the habitability of these regions for hominins.

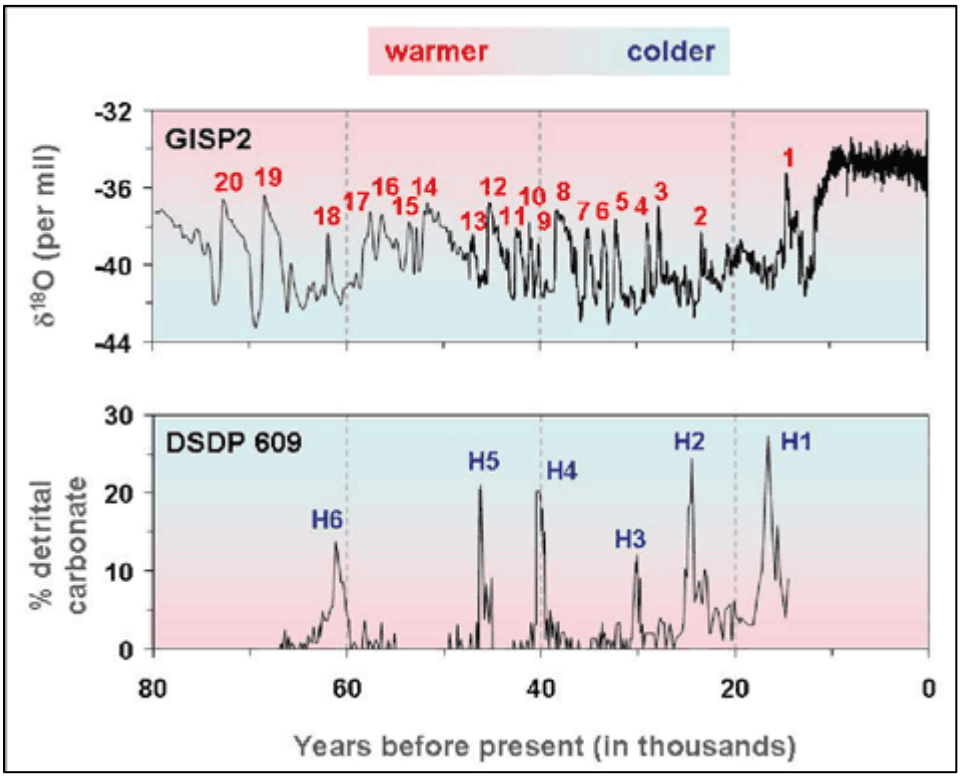

Figure 2.2. NOAA Palaeoclimatology figure showing an $\delta^{18}O$ record from the GISP2 ice core in Greenland over the last glacial period (top), and a record of ice-rafted debris material from a North Atlantic marine core (bottom). Heinrich events are represented by blue letters and numbers on the bottom graph, 20 Dansgaard-Oeschger events are represented by red numbers on the top graph. Red shaded areas represent warmer conditions, whilst blue shaded areas represent colder climate conditions. Source: National Climate Centre Data (2008).

2.3 Regional variations in North Africa and the Arabian Peninsula

To facilitate an accurate reconstruction of Pleistocene climatic change in North Africa and Arabia, modern climates are used to provide a framework for the interpretation of Pleistocene climatic and environmental records (Blome et al., 2012). At present there are

two competing hypotheses concerning the causes of Pleistocene climatic change in tropical deserts, specifically the Saharo-Arabian desert belt. The first hypothesis suggests that high latitude glacial cycles (c. 100 ka) drive change in the deserts, resulting in increased aridity during glacial periods in African and Arabian regions as moisture becomes stored in continental ice sheets (Blome et al., 2012; Cooke et al., 1993; Drake et al., 2008, 2013). Bar-Yosef and Meadow (1995) support this hypothesis, suggesting that during periods of extreme aridity (i.e. the last glacial maximum) large and small lake basins receded, potentially drying up completely. Bar-Matthews et al. (2003) further support this idea. They suggest that oxygen isotope records from Soreq and Perquin cave in Israel reflect higher precipitation levels in the Levant and Northern Arabia during interglacial events. The second hypothesis instead suggests that it is the strength of the monsoon system (driven by precessional cycles (c. 26 ka)) that controls climate change in these desert regions (Drake et al., 2013). Using statistical methods, Trauth et al. (2009) analysed published records of terrigenous dust flux from the eastern Mediterranean Sea, subtropical West Africa, and the Arabian Sea, and lake level records from East Africa, to identify trends in the hydrological cycle in tropical Africa. They suggest that African climate variability and moisture levels are predominantly driven by low-latitude solar heating and its effect on monsoon systems, rather than high-latitude ice volume variations. Issar (2010), further supports the second hypothesis, arguing that field evidence contradicts the conceptual model of the first hypothesis, specifically referring to Bartov et al. (2002) who dated maximum lake levels of Lake Lisan (the precursor to the Dead Sea) to the (last glacial maximum) LGM. Drake et al. (2013) suggest that increasing debates concerning the limitations of this first hypothesis, combined with an increased understanding of climate, lends support to the second hypothesis. DeMenocal et al. (2000) however, argue that the rapid onset and termination of the African Humid Period in their terrigenous sediment record could not have been driven by a simple response to gradual insolation forcing, and that feedback mechanisms are likely to have been important contributory factors. They suggest that the sub tropical monsoon system is in fact a natural consequence of the high latitude deep ocean thermohaline circulation, and therefore support the first hypothesis. Considering both hypotheses, it is possible to suggest that desert climates could in fact be driven by a combination of monsoonal rainfall in the south (driven by hypothesis 2) and rainfall from North Atlantic and Mediterranean Westerlies in the north (driven by hypothesis 2), a notion supported by Drake et al. (2013).

Precipitation patterns across the Saharo-Arabian desert belt are currently driven by mid-latitude Westerlies in the north, and the location of the Intertropical Convergence Zone (ITCZ) in the south (Drake et al., 2013). North Atlantic and Mediterranean Westerlies are high altitude winds that determine the location of "frontal boundaries". These boundaries occur where the warm, moist air from the tropics collides with the cool, dry air from the poles, resulting in rising moist air, cloud formation, and increased precipitation (Blome et al., 2012). Global temperature variations have been shown to influence the position of the Westerlies. During warm periods, the Westerlies strengthen, moving towards the pole and diverting rainfall away from Africa. Conversely, during cold periods they weaken, moving towards the equator, bringing precipitation back to Northern Africa (Blome et al., 2012; Toggweiler and Russell, 2008). As the North African coastline lies beyond the influence of the ITCZ and monsoon systems in the south, precipitation along the Cyrenaican coastline is most likely driven by these mid-latitude Westerlies.

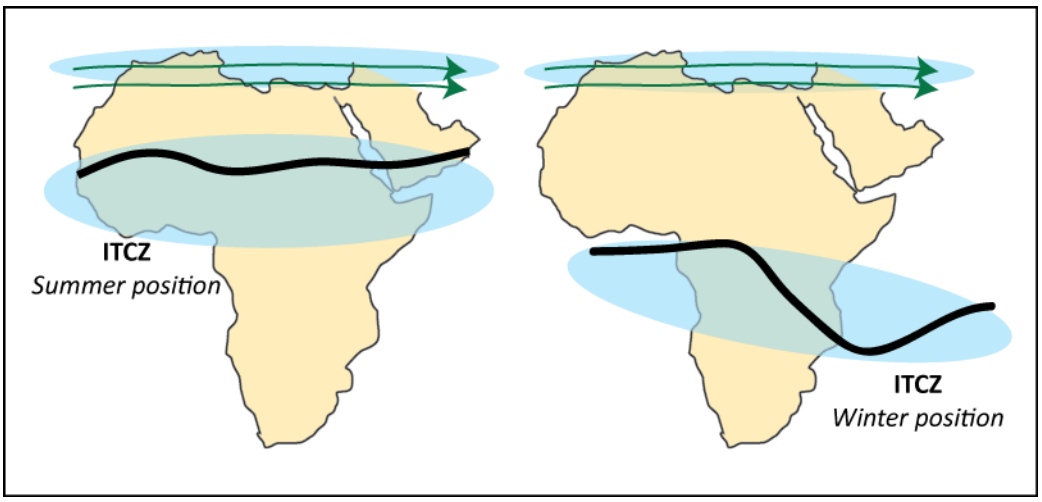

Figure 2.3. Diagram showing the changing position of the ITCZ during summer and winter conditions. Green arrows represent the average location of the Westerlies (based on Blome et al., 2012). Blue shaded areas represent zones of increased rainfall associated with monsoon systems tracking the position of the ITCZ, and the location of the Westerlies.

Precipitation along the southern edge of the Saharo-Arabian desert belt (i.e. central and eastern Africa, and southern Arabia) is controlled by the African and Arabian monsoons respectively. Monsoon systems are caused by differential heating between land and neighbouring oceans, leading to seasonal reversals of wind and increased precipitation over the land (Blome et al., 2012). Due to the high specific heat capacity of water,

terrestrial surfaces heat more rapidly than the adjacent ocean surfaces. Consequently, areas of low pressure develop over the land as the warm terrestrial air masses rise, drawing in moist air from the ocean, resulting in convection over central Africa and southern Arabia (Rose and Petraglia, 2009).

Insolation heats the Earth's surface which in turn warms the overlying air, causing convection and forming areas of low surface pressure. The zone of maximum insolation received by the Earth's surface can be approximated by the location of the ITCZ. The position of the ITCZ is therefore a primary driver of the African and Arabian monsoons (Blome et al., 2012).

Following Carto et al. (2009), variations in the position of the ITCZ and associated monsoonal systems have an important impact on climates and environments in low latitudes, specifically central African and southern Arabia. Whilst variations in the position of the ITCZ over the oceans remains small, seasonal variations associated with increased heating over North Africa during the northern hemisphere summer cause the ITCZ to move north. As the ITCZ moves north, precipitation (resulting from warm, moist southeasterlies) increases over the Sahara, the Horn of Africa, and the Arabian Peninsula (Figure 2.3) (Carto et al., 2009). Conversely, during the northern hemisphere winter, the ITCZ moves south as the land in North Africa cools. The development of colder, denser air over the continent during the northern hemisphere winter, results in an outward flow of dry air that inhibits precipitation. The northward movement of the ITCZ and associated monsoonal systems results in increased precipitation in the central African region, causing increased humidity across the Saharo-Arabian desert belt (Drake et al., 2013; Issar, 2010). Monsoon strength is controlled by insolation strength. In the low-latitudes, insolation strength is primarily controlled by the 23 ka precessional cycle, leading to cyclic strengthening (high insolation) and weakening (low insolation) of monsoon systems.

Drake et al. (2013) suggest that should the strengthening of the monsoon occur in conjunction with a weakening of the Westerlies, there may have been times in the past when precipitation increased both north and south of the desert belt, causing it to contract, therefore reducing its effectiveness as a barrier to human dispersals.

Carto et al. (2009) also suggest that variations in SST can influence the position of the ITCZ. As the North Atlantic SST decreases, a temperature and pressure gradient develops between the northern and southern hemispheres, which causes the ITCZ to move south

towards the equator. Consequently, they propose that if the North Atlantic SST remained cold for an extended time period, monsoon strength would be reduced, resulting in arid conditions in sub-tropical Africa. Blome et al. (2012) report that North and South Atlantic records of SSTs surrounding the African continent indicate that the warmest SSTs occurred during MIS 5e (c. 130-120 ka), with overall patterns that are generally consistent with the global MIS record. However, Indian Ocean records of SST diverge from this pattern, which is likely due to changes in deep water upwelling patterns and variations in local to regional monsoonal winds. Consequently, Blome et al. (2012) suggest that the Indian Ocean records are least similar to the Atlantic records as the adjacent regions (North-East Africa and Arabia) were more likely to have been heavily influenced by the East African and Asian monsoons. Evidence presented by records of SST therefore suggest that the variations observed within African and Arabian palaeoclimate records can be explained by regional, rather than global changes (Blome et al., 2012).

2.4 Climate change in Africa and Arabia over the last c. 200 ka.

Although North Africa and Arabia did not experience glaciations, dramatic changes in regional climate and global sea levels had significant impacts on local environments (Garcea, 2008). Traditionally it is assumed that throughout the Pleistocene, North African and Arabian desert regions were characterised by periods of humidity during interglacials, and aridity during glacials (Drake et al., 2008). Pleistocene lake level evidence from the Fazzan Basin in Libya supports the notion of increased humidity during interglacial periods, with increased lake levels attributed to interglacial periods over the last 420 ka (Armitage et al., 2007). The presence of many smaller lakes, rather than a single giant lake in the Fazzan Basin during the Late Pleistocene and Holocene, however, suggests that water availability may have been more limited during interglacial periods over the last c. 120 ka (Drake et al., 2011). Several authors have developed synopses of Mid to Late Pleistocene African and Arabian climatic change, the results of which are discussed in the following section.

2.4.1 Blome et al. (2012)

Blome et al. (2012) provide a synopsis of African Palaeoclimate from 150 to 30 ka using published proxy evidence from a number of offshore marine cores, African lake cores, and

terrestrial sedimentary archives. In the context of this thesis, the information presented here primarily concerns the information that they provide for North Africa, East Africa and Arabia (Figure 2.4).

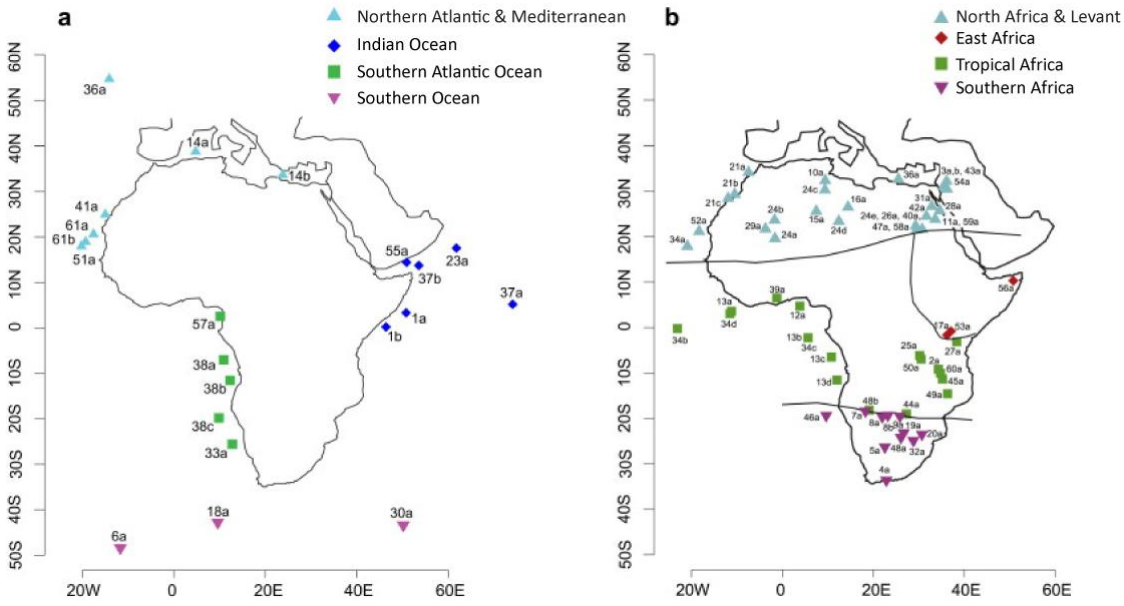

Figure 2.4. Diagram illustrating the regional zones of Blome et al. (2012). The figures show the distribution of a) marine climate sites, and b) terrestrial climate sites. Source: Blome et al. (2012).

Blome et al. (2012) synthesised Eastern Mediterranean $\delta^{18}O$ speleothem, carbonate, marine pollen and dust records to interpret palaeo-rainfall and humidity in North Africa (Figure 2.5). Speleothem records from Arabia and the Levant suggest the presence of a humid period between 135 – 120 ka (MIS 5e), followed by a more arid period extending from 120-90 ka (MIS 5d). A return to more humid conditions between 90-80 ka (MIS 5a-5c) was then identified before the records suggest a return to arid conditions in MIS 4. Similarly, spring-fed, groundwater and speleothem carbonate records from across North Africa indicate the occurrence of wet conditions between 135-115 ka (end of MIS 6 – MIS 5e) and 100-75 ka (MIS 5a-5c), although here, humid conditions appeared to have remained for longer than those observed in the Levant. Furthermore, pollen records from marine cores off the coast of Morocco indicate that Mediterranean vegetation expanded into the Sahara during global interglacial conditions, retreating during global glacial periods (Hooghiemstra et al., 1992). Blome et al., (2012) hypothesise that the expansion and contraction of Westerlies is likely to have affected precipitation in North Africa, specifically during the period between 100-70 ka (MIS 5). North African records appear variable

between 70-35 ka (early MIS 5a – MIS 3), which Blome et al. (2012) suggest is partly caused by the link between precessional forcing, insolation strength and thereby North African precipitation (Westerlies also play a part in North African regional climate). Overall, however, North Africa experienced arid climate conditions during this time (70-35 ka), with the Sahara expanding between 65-50 ka (MIS 4).

Blome et al. (2012) also investigated East African lake level reconstructions and vegetation histories, suggesting that humid conditions prevailed between c. 145-120 ka (late MIS 6 – MIS 5e), c. 110-95 ka (MIS 5c-5d), c. 80-65 ka (MIS 5a- early MIS 4), and c. 55-50 ka (MIS 3) (Figure 2.6). This interpretation suggests that during the 105-75 ka humid period observed in North Africa, areas in East Africa were affected by arid conditions from c.95-80 ka (MIS 5b). Blome et al. (2012) suggest that these variations observed between North and East Africa reflect changes in the East African monsoonal system, and Westerlies, associated with insolation. Climate change, in this case, was found to be asynchronous across Africa, with the complex interaction between a number of different factors contributing to regional changes throughout the Pleistocene (Blome et al., 2012).

North and East Africa both experienced humid conditions c. 80 ka (MIS 5a), turning to arid conditions at the start of MIS 4 (c. 75 ka), potentially restricting the timing of human dispersal out of sub-Saharan Africa (Blome et al., 2012). Consequently, if the desert belt acted as a barrier to human movements during these periods, it is assumed that modern human populations migrated to the North African coast prior to 75 ka (start of MIS 4) when arid conditions characterised much of the African continent (Blome et al., 2012). Humid periods across North Africa and the Levant c. 135-115 ka (MIS 5e) and c. 105-75 ka (MIS 5a-5c), would have provided multiple opportunities for such northward dispersals of human populations out of Africa. Furthermore, humid conditions in East Africa between c. 145-120 ka, c. 110-95 ka, and c. 80-65 ka would have facilitated multiple opportunities for an early modern human exodus from East Africa to Arabia over the Bab al-Mandab Straits (Blome et al., 2012).

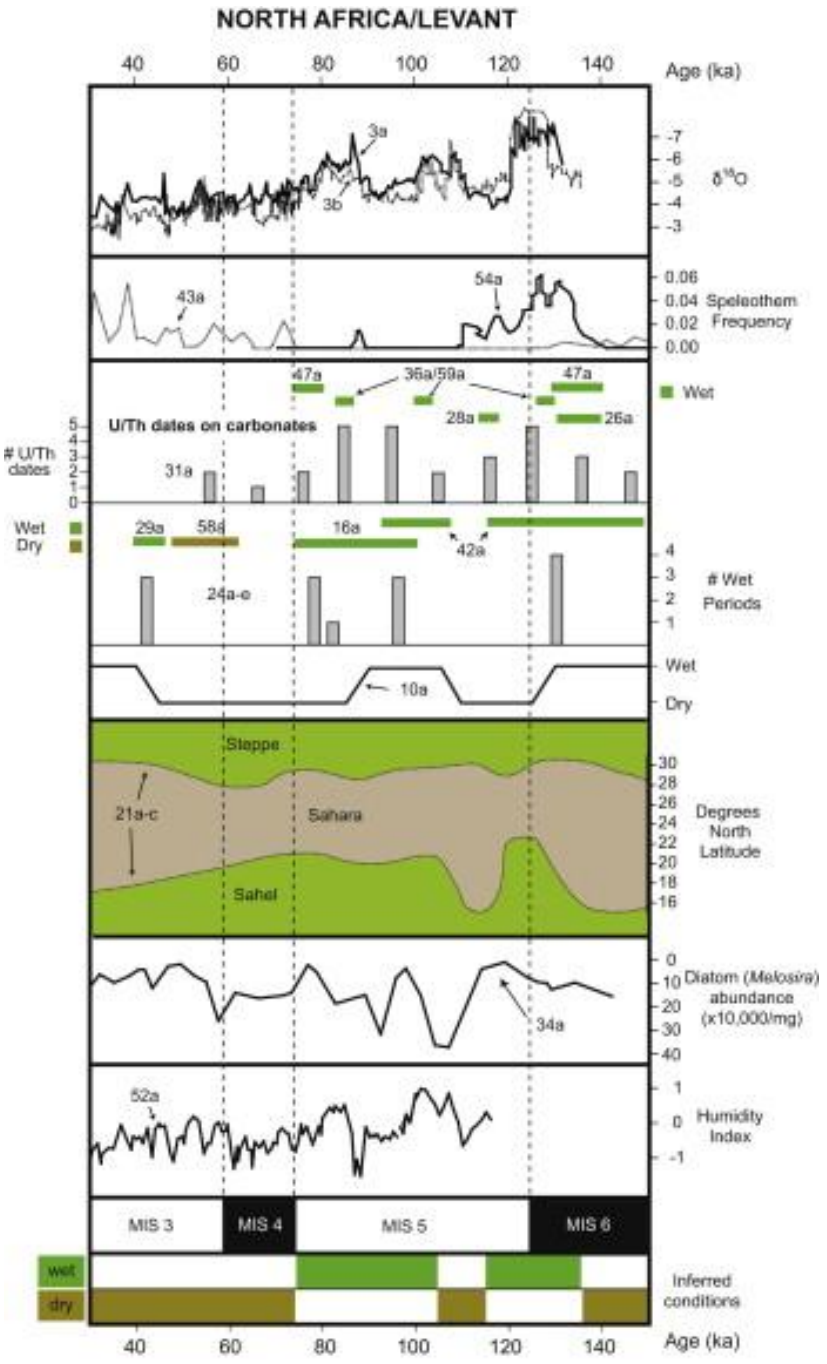

Figure 2.5. Summary diagram from Blome et al. (2012) displaying information from the North African (and Levant) datasets.

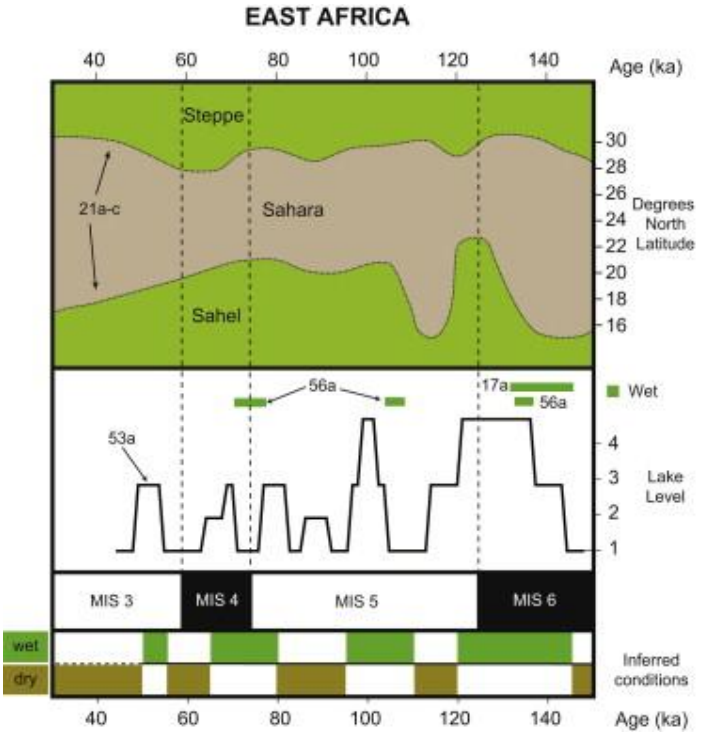

Figure 2.6. Summary diagram from Blome et al. (2012) displaying information from the East African terrestrial datasets.

2.4.2 Drake et al. (2013)

Drake et al. (2013) used probability density function (PDF) analysis to investigate data from lacustrine, tufa, calcrete, travertine and fluvial deposits, in order to identify periods of humid climate in the Saharan and Arabian deserts (Figure 2.7).

While MIS 6 is traditionally thought of as a period of aridity, there is some evidence of humidity in the Saharan and Arabian deserts. Caution must be applied, however, as dating over this timeframe is frequently limited by large associated errors. An increase in the probability peak for humidity occurs in the Sahara at the terminus of MIS 6 c. 138 ka, preceded by a significant decline in humidity. Humid sites are only located in northern and central Saharan regions during MIS 6, suggesting the absence of humid corridors across the Sahara during this time period. The decline in humidity appears reduced in the Arabian Peninsula, with the presence of scattered evidence for humidity throughout MIS 6 centred around 138, 154 and 180 ka. Clear troughs in humidity occur between each of these peaks, indicating increased aridity in the Arabian Peninsula during these periods.

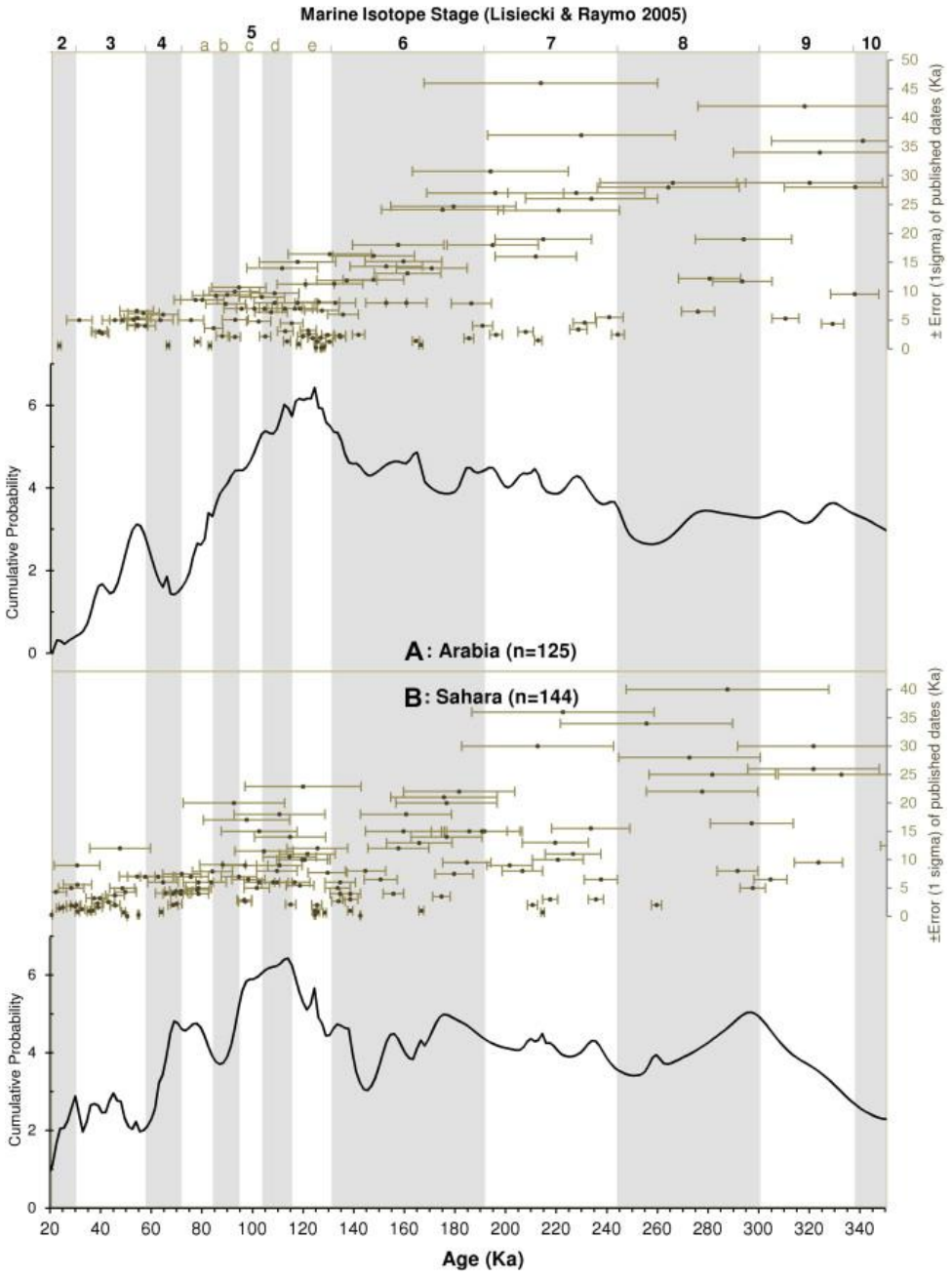

Figure 2.7. Regional PDF curves produced by Drake et al. (2013) displaying cumulative probability fluctuations for the Saharan (B) and Arabian (A) humidity over the last 20 – 350 ka BP. Mean ages used in the construction of the PDF are shown above each plot with an associated one sigma error. Ages are separated vertically according to error size for display. Source: Drake et al. (2013).

Parker (2009) also presents a summary of climatic change over the last 350 ka using palaeoenvironmental records, providing evidence for one or more phases of increased precipitation in Arabia during MIS 3. He too provides evidence for a series of pluvial stages during MIS 6, which was originally believed to be a period of prolonged aridity. It is therefore possible that MIS 6 represented a period of climatic variability in Arabia, with

short fluctuations in climate that are too rapid to be accurately reflected by the probability density functions developed by Drake et al. (2013), with the large errors commonly greater than the rapidity of change.

In Arabia, evidence from the northern and southern regions suggests that MIS 5 was a predominantly humid interglacial, potentially including short arid intervals. Increased dust levels in Arabian Sea marine cores, combined with changes in palaeolake and dune records, suggest that MIS sub-stages 5d and 5b were characterised by lower humidity levels (although not severe aridity). This reduced humidity is also reflected in the global climate stacked marine record of Lisiecki and Raymo (2005) (Figure 2.1), where cool, dry stadials are identified as lower oxygen isotope levels during these periods. Increased speleothem growth in Arabia (Yemen, southern and northern Oman) was most pronounced between 130 – 120 ka (MIS 5e), with oxygen isotope values heavily depleted during this period. Additional speleothem evidence also suggests increased humidity in Yemen during MIS stages 5a and 5c. 48 dates from Arabia suggest that MIS 5e was the most pronounced humidity peak during MIS 5. Lacustrine evidence from lakes in the Rub' al Khali region indicates increased humidity c. 80, c. 100, 104 ka, c. 125 ka and 132 ka, further supporting increased humidity levels during MIS 5a, c and e. During MIS 5, the Sahara appears to be characterised by two prominent humidity peaks centred on 76-78 ka (MIS 5a) and 114-104 ka (MIS 5d/e), separated by a less humid period centred around 87 ka (MIS 5b). Whilst the evidence for the increase in humidity during MIS 5a comes from sites concentrated in the eastern Sahara regions, the MIS 5e evidence is more widespread, suggesting increased humidity at this time affected the entire Sahara region. Both humidity peaks in the Sahara region correspond with the timing of insolation maxima (principally precessional peaks) over the Sahara, and thus are likely related to enhancement of the African monsoon. Whilst this correlation may explain an increase in humidity during these periods, Drake et al. (2013) suggest that there appears to be no further correlation between Saharan climate and insolation during the rest of MIS 5. In contrast with the widespread evidence across the Sahara, a lack of evidence for humidity in central Arabian regions may indicate that dispersal could have been easier north across the Sahara than through Arabia during MIS 5. Armitage et al. (2011), however, report evidence for "wetter" phases in southern Arabia between 135-120 ka (MIS 6-5e) and 82-78 ka (MIS 5a) based on cave speleothem records from Oman (Burns et al., 2001; Fleitmann & Matter, 2009), phases of lacustrine development in Jordan (Petit-Marie, 2010), and cave speleothem records in Israel (Bar-Matthews et al., 2003). The synthesised evidence from Armitage et al. (2011) is presented

in Figure 2.8. It is possible, therefore, that as evidence for central Arabian sites remain undiscovered due to the lack of focused research in this region, Arabia remains a potential route for AMH at this time. Once again, the evidence suggests that variations in the timing of humid periods during MIS 5 in Arabia and the Sahara, is most likely a result of regional changes in weather/monsoon systems.

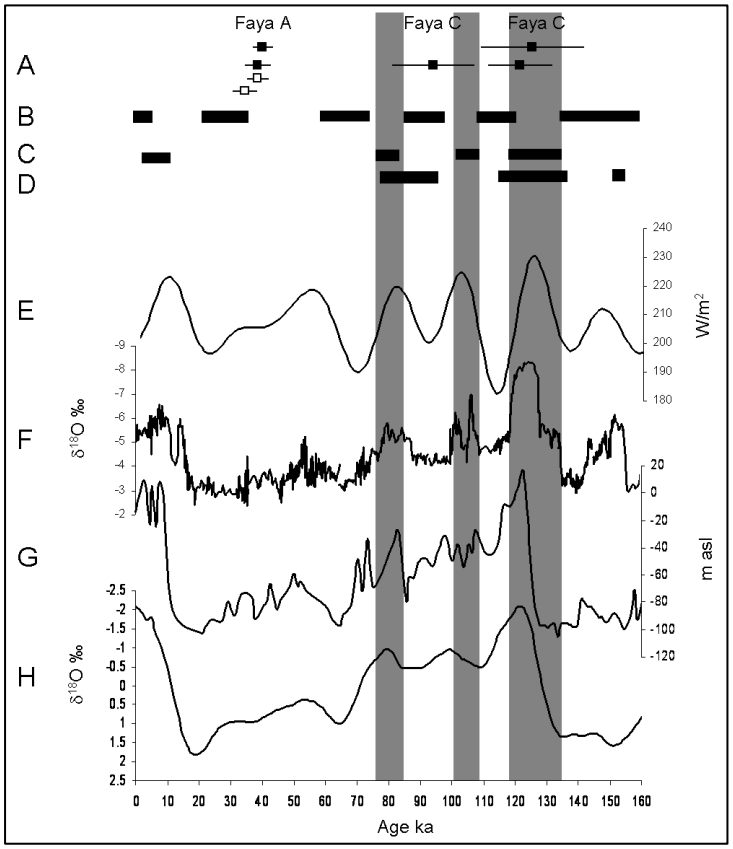

Figure 2.8. Compilation diagram from Armitage et al. (2011) showing the Jebel Faya chronology with regional and global proxy records. Gray bars represent periods of humidity in the region. (A) shows OSL ages from occupation (solid squares) and sterile (open squares) layers at Jebel Faya (error bars indicate 1 SE). (B) shows phases of aeolian dune accumulation in the Wahiba Sands, Oman. (C) illustrates the timing of wet phases in Oman from cave speleothem records in Hoti and Qunf. (D) represents phases of lacustrine development recorded in Mudawwara, Jordan. (E) shows the Indian Ocean Monsoon Index. (F) Is an oxygen isotope (*d*18O) record from Soreq Cave, Israel (‰ indicates per mil). (G) shows Red Sea eustatic changes. (H) is the SPECMAP stacked oxygen isotope record.

MIS 4 appears to be a period of climatic transition in both the Sahara and Arabia, with limited evidence of humidity in either region. There is, however, direct evidence for aridity

in both regions, with the activation of dune systems in the Liwa (63 ka and 60-50 ka) and Wahiba Sands (throughout MIS 4 until c. 64 ka) (Drake et al., 2013).

During MIS 3, Drake et al. (2013) suggest a trend of increased humidity in both regions, with humidity peaks occurring at 40 ka and 54 ka in Arabia, and 37 ka (Morocco) and 44 ka (eastern and central regions) in the Sahara. Mediterranean humidity appears to be closely related to the timing of humidity in the Sahara. There is widespread evidence for humidity 44 ka, although evidence for humidity is generally identified along the desert margins. Arabia experienced several pluvial episodes during early and mid MIS 3. A small peak in humidity c. 40 ka, indicated by the presence of lacustrine and fluvial sediments, is thought to be related to the 44 ka humidity peak in the Sahara. However, MIS 3 in Arabia was dominated by a much earlier (c. 54 ka) humidity peak, with evidence from a wide range of proxies across large regions of the peninsula. At this time there was increased flow in the Nile, as well as increased humidity in surrounding regions (recorded by increased speleothem growth in the Levant). Supporting evidence from Lake Naivasha in east Africa (Trauth et al., 2003) suggests that the increase in Arabian humidity at this time may have been related to the Indian Ocean South-Western Monsoon. Variations in the timing of increased humidity in the Sahara and Arabian desert belts during MIS 3 suggests that the Indian and Atlantic Ocean monsoons were responding to climatic change in slightly different ways. Little evidence of humidity was identified in northern Arabia, suggesting that the Indian Ocean monsoon was only able to penetrate as far as north and central Arabia during the 54 ka humidity event. Thus, northern Arabia would have remained arid, even during relatively humid events in the rest of the region. Evidence suggesting that northern Arabia remained arid, while the southern peninsula experienced humid conditions would have potentially impacted upon migration routes taken by modern humans (Drake et al., 2013), with dispersal routes through the north seemingly unlikely.

They found little evidence for humidity in Arabia during MIS 2; however, in the eastern Sahara region there appeared to be a sharp rise in humidity at the start of MIS 2, peaking near the boundary with MIS 3.

The PDF analysis presented by Drake et al. (2013) is limited by temporal and spatial bias, which may result in artificial peaks and troughs, or gaps in the spatial distribution of humid sites. The preservation potential of humid sites, lack of research in some areas, and large errors associated with some of the older dates, will further bias the datasets, potentially reducing the ability of the PDF to identify rapid climatic events.

In summary, the work of Drake et al (2013) suggests that the Saharan and Arabian deserts experienced periods of humidity during the beginning of MIS 2, and during MIS 3, 4 and 6, although within each region the timing of humidity varied. On two occasions, increased humidity roughly corresponded with insolation maxima (c. 30 ka in the Sahara, and c. 55 ka in Arabia); however, this correlation was not observed at any other point. Both regions experienced humidity throughout MIS 5, with periods of increased humidity appearing to correspond with the timing of insolation maxima in each area. Variations in the timing of humidity in Arabia and the Sahara during MIS 3, 4 and 6, suggest that the Indian Ocean and Atlantic Ocean West African Monsoons responded differently to insolation forcing.

2.4.3 Climate summary

Blome et al. (2012), Drake et al. (2013), and Parker (2009) have demonstrated broad similarities in their climatic investigations from African and Arabian climate over the last c. 250 ka. Evidence from speleothems, lacustrine sediments, sand dune deposits, marine cores, as well as other records, indicate that the Saharo-Arabian desert belt experienced significant climatic oscillations between wet and dry periods. Interglacial periods in North and East Africa, and southern Arabia, are generally characterised by increased levels of precipitation across the region, while glacial periods appear to have experienced increased dune mobility, making large areas of Arabia uninhabitable (Petraglia et al., 2012). MIS 5e represents the most dominant period of humidity for all areas in each of the studies, with MIS 5a and MIS 3 also consistently providing evidence of increased humidity. Evidence for aridity is widespread across Arabian and African records during MIS 4 and MIS 2. Whilst records suggest that MIS 5b and 5d were less humid than other interglacial periods, there is no evidence that these times were particularly arid in Arabia or Africa. Variability in climate records between the two regions can be observed in every MIS stage investigated. Furthermore, variations in the timing of humidity across the Saharo-Arabian belt appear to reflect different response times of the African and Indian Ocean monsoon systems. It is unlikely, therefore, that African and Arabian climates are solely driven by high latitude processes. Changes in regional climate are instead, most likely driven by regional variations in the position of the ITCZ and associated monsoon systems in central and southern Africa, and Westerlies along the coast of North Africa.

This thesis will use evidence of important archaeological, climatic and geomorphological changes in the landscape surrounding the Haua Fteah cave (Libya) to test the two competing hypotheses concerning the causes of Pleistocene climatic change in tropical deserts. Firstly, primary evidence from Libya and the reported synopses of Arabian climate will be used to test the extent to which regional changes in North Africa and southern Arabia are coincident with northern Hemisphere glacial and interglacial cycles. Secondly, evidence of environmental changes (specifically fresh water availability) from northern Libya will be used to assess the importance of the strength of the westerlies as a control for humidity in the region.

2.5 Anatomically Modern Humans

The Out of Africa 2 model suggests that all modern humans descend from a single population of *Homo Sapiens* that evolved in Africa c. 200 ka, before migrating and expanding out of Africa c. 100 ka later (Carto et al., 2009). Modern human fossils found in Skhul and Qafzeh, which date to between 119 and 85 ka, represent the oldest modern human fossil remains identified outside of Africa (Carto et al., 2009). Walter et al. (2000) also provide some of the oldest evidence for AMH outside of sub-Saharan Africa, reporting the discovery of Middle Stone Age artefacts along the Red Sea coast in an emerged reef terrace that has been dated to c. 125 ka using U-Th dating. They suggest that the presence of old and new tool technologies (including bifacial hand axes, obsidian flakes and blade tools), and the adaptation to the coastline signals the onset of modern human behaviour in the region, supporting an early expansion of modern humans out of Africa. Recent work by Armitage et al. (2011) also supports an early expansion of modern humans out of Africa. They suggest that the archaeological sequence attributed to modern humans at Jebel Faya spans at least 125 ka. Assemblage C lithics at this site bearing technological affinities to modern human African Assemblages are thought to represent modern human populations expanding out of Africa during the transition from MIS 6 to early MIS 5. However, based on the majority of existing fossil, genetic, and archaeological records, many authors propose that modern humans did not successfully expand out of Africa until c. 60-80 ka (Eriksson et al., 2012).

Traditionally, genetic data suggests the dispersal of modern humans out of Africa occurred during MIS 4, c. 60-70 ka (Petraglia et al., 2012). Mellars (2006, and references therein)

further support this proposal, providing mtDNA genetic evidence, which suggests that an episode of rapid population growth in ancestral African populations centred around 60-80 ka. Recently, Mellars et al. (2013) argue against an early dispersal of modern humans out of Africa and into South Asia prior to the Toba super-eruption 74 ka. They suggest that the most recent genetic evidence from Africa and Asia supports a coastally oriented modern human dispersal out of Africa 60 – 50 ka, with no genetic evidence for a "pre Toba" dispersal of modern humans from Africa. They argue that a complete lack of a pre-L3 mtDNA haplogroup (i.e. one predating the source for all known, extant maternal lineages in Eurasia) represents either 1) the complete extinction of all modern human groups that migrated out of Africa < 74 ka, or 2) modern humans did not disperse out of Africa until after (post) the Toba eruption.

The expansion, contraction and migration of modern human populations within and out of Africa are commonly thought to be linked to climatic oscillations in the Late Pleistocene (Foley & Lahr, 1998; Petraglia et al., 2011). Specifically, the expansion of populations, and migrations into new areas, is believed to occur during periods of environmental amelioration, as increased resource availability facilitates movement across previously uninhabitable areas (Petraglia et al., 2011). The migration of both archaic and modern humans out of Africa was most likely the result of both push (i.e. environmental change) and pull (the opening up of new niches) factors (Bar-Yosef & Cohen, 2001). During periods of aridity, a lack of freshwater resources would have rendered the Saharo-Arabian desert belt uninhabitable, acting as a barrier against modern human expansions, occupations and migrations out of sub-Saharan Africa. The incompleteness of the fossil and climatic record makes it difficult to fully quantify the effectiveness of this relationship.

As the discovery of human fossils is rare, stone tools represent the most common archaeological finds. Consequently, the presence of lithics at a site is used to indicate the presence of hominins in different environments around the world. Using the method of production, shape and size of the lithics, archaeologists assign stone artefacts to prehistoric cultures, each associated with different hominin groups (Bar-Yosef & Cohen, 2001). There is no easy way to identify the manufacturers of lithics, which are limited by a number of reduction strategies, and the quality and availability of raw materials (Straus & Bar-Yosef, 2001). In the case of this thesis, as well as many other studies, however, the presence of lithics from Middle Stone Age industries with affinities relating to modern human Middle Palaeolithic industries in Europe is taken to indicate the presence of modern humans.

Lithics identified in the stone tool assemblage found in association with the Skhul and Qafzeh skeleton remains, for example, are reported as typically Middle Palaeolithic or MSA in form (Mellars, 2006).

2.6 Migration out of Africa

Until recently, there were two opposing models for the origins of modern humans (*Homo sapiens*). The multiregional model suggests that modern humans simultaneously evolved from archaic hominin populations distributed worldwide (Wolpoff et al., 2000). Continuous interbreeding and genetic exchanges between the evolving human populations in different regions resulted in similar evolutionary pathways, facilitating the development of modern humans in several places at once. Local and regional variations observed in modern humans today, were believed to be a result of adaptation to local environmental conditions. The increasing availability of genetic evidence, however, means that this model is now largely rejected (Close & Minichillo, 2007).

Following the investigation of fossil, genetic and archaeological data, our current understanding of modern human populations is that they evolved in sub-Saharan Africa between 200-150 ka (Beyin, 2011). The Out-of-Africa model suggests that modern humans evolved solely in Africa before migrating, and replacing all other archaic hominin populations without interbreeding or genetic exchanges. Debates concerning whether these populations expanded out of Africa in a single event or over multiple dispersals remain unresolved (Beyin, 2011).

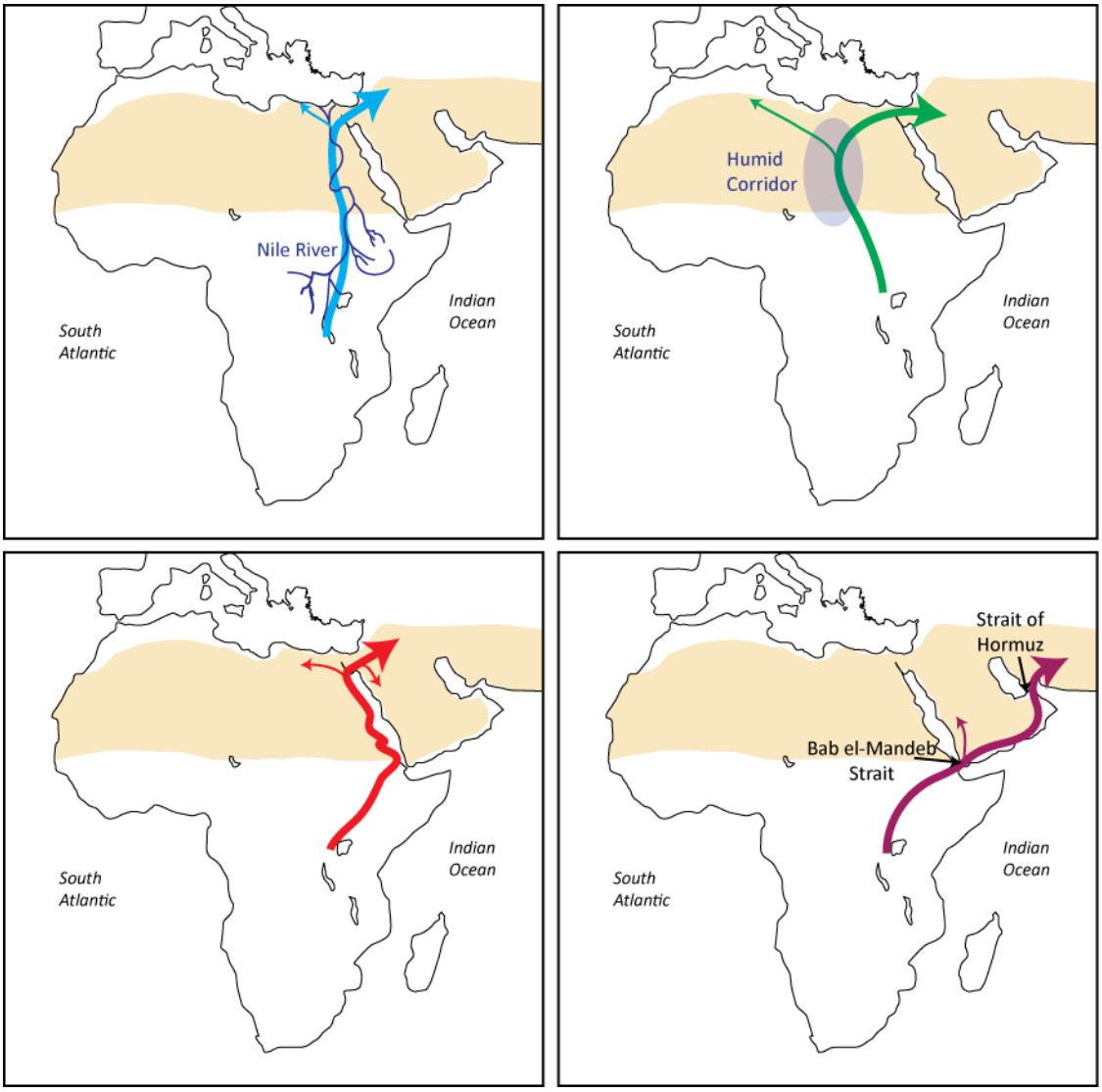

Figure 2.9. Maps showing the potential routes taken by modern human during their expansion and migration out of sub-Saharan Africa. The blue arrow (top left) represents the northern "Nile-Sinai Corridor", whereby modern humans followed the course of the Nile River Valley out of sub-Saharan African and into the Levant (Section 2.6.1). The green arrow (top right) illustrates the "Green Sahara" migration route, which modern humans may have used when mega lakes and riverine belts transected across the central Saharan desert (Section 2.6.2). The orange arrow (bottom left) shows the "coastal route", taking modern humans north along the western Red Sea coastline out of sub-Saharan Africa (Section 2.6.3). The purple arrow (bottom right) displays the "southern route" out of Africa across the Bab al-Mandab Straits, across southern Arabia, and into southwest Asia via the Straits of Hormuz (Section 2.6.4)

There are currently two widely accepted dispersal routes potentially taken by modern humans expanding out of sub-Saharan Africa. The "northern route" suggests that modern

humans travelled north across the Sahara desert, out of North Africa, and into the Levant (Beyin, 2011). Human migrations north from sub-Saharan Africa and across the Saharan desert belt, is thought to have occurred in one of three ways. Current hypotheses suggest that the Sahara was crossed either along the "Nile-Sinai corridor", via the western Red Sea "coastal route", or across a "Green Sahara" desert along a transect of mega lakes or riverine belts during periods of climatic amelioration (Figure 2.9) (Abbate & Sagri, 2011; Beyin 2011). Parker (2009) and Beyin (2011) suggest that this northern route is supported by the presence of the Skhul and Qafzeh fossils in the Levant during MIS 5, however attempts to link the Nile Valley archaeology with the Levantine record have not always indicated a strong cultural connection (Marks et al., 1992a, 1992b). Furthermore, whilst the presence of a dry land bridge across Sinai makes this route accessible, it is likely that this route would have been most favourable during periods of "wetter" climatic conditions such as MIS 5 (Beyin, 2006; Osborne et al., 2008; Field & Lahr, 2005). Movement of the ITCZ south towards the equator during North Atlantic cooling in MIS 4 would have caused increased aridity in the Sahara and the Levant, potentially closing this route out of Africa, and acting as a barrier to human migration (Beyin, 2011).

Alternatively, the "southern route" suggests that modern humans, who had successfully adapted to coastal regions, dispersed into southern Arabia via the Straits of Bab al-Mandab during low sea level stands associated with glacial periods (Figure 2.9). These human populations then expanded across Arabia, before entering southwest Asia via the Straits of Hormuz. This route remains unclear due to the lack of well dated archaeological and fossil evidence in the Arabian Peninsula. Genetic evidence presented by Eriksson et al. (2012), however, supports the idea of an initial, ephemeral expansion of modern humans out of Africa via the southern route, facilitating the presence of modern humans in Southwest Asia between 130-90 ka. They suggest that at this time, low sea levels and more favourable climatic conditions enabled modern humans to cross the Bab al-Mandab Straits into the Arabian Peninsula, and the Straits of Hormuz into Southwest Asia.

The emergence of modern humans out of sub-Saharan Africa remains widely debated. Suggested drivers for Upper Pleistocene dispersals out of Africa include climate change, population expansion, and the emergence of complex behaviours such as language (Beyin, 2011). While modern humans are traditionally believed to have taken the northern inland route out of Africa through the Levant, and into the Middle East and on into Eurasia, the alternate "southern route" (centred around the potential role of the Arabian Peninsula) is

gaining support. New theories suggesting that modern humans may have migrated along a southern route, using the coastline of the Red Sea or a land bridge into the Arabia and southwest Asia during periods of low sea level, continue to gain support with an increased level of research in this previously understudied region (Armitage et al., 2011; Beyin, 2011; Carto et al., 2009; Petraglia et al., 2012).

2.6.1 A northern route along "the Nile-Sinai Corridor"

Traditionally, the agreed dispersal route of modern humans out of Africa through the Sahara desert was thought to be via the Nile River valley corridor (Drake et al., 2011). It is argued that the availability of fresh water and food resources along the river were fundamental for the survival of modern human populations migrating across the otherwise uninhabitable desert barrier (Garcea, 2008). The identification of fossils in the Near East from Qafzeh and Skhul between 119-81 ka supports the notion of a northern route along the Nile corridor and onwards into the Levant (Armitage et al., 2011). A later dispersal (c. 40-65 ka) along the same route is commonly thought to have led to the colonisation of Eurasia (Armitage et al., 2011). A lack of fossil and archaeological evidence with sound chronologies along the Nile corridor, combined with new evidence and theories concerning alternative routes, has led to uncertainties surrounding this route in recent years (Drake et al., 2011).

2.6.2 The "Green Sahara" route

The Sahara desert has frequently been considered an effective obstacle to human dispersals, acting as a barrier between the more humid regions to the north and south (Drake et al., 2011). A major limiting factor for the occupation of desert environments is the availability of fresh water (Groucutt & Blinkhorn, 2013). During the Holocene, however, the Sahara desert was home to some of the largest fresh water lakes on Earth (Drake & Bristow, 2006). Using Landsat TM imagery and digital elevation models (DEMs), Drake et al. (2011) mapped the Palaeohydrology of the Sahara, identifying a series of large freshwater lakes, whose catchments aligned, potentially providing a corridor of humidity across the desert. The "Green Sahara" theory suggests that during periods of increased humidity (specifically during MIS 5), the currently hyperarid Sahara desert may have been inhabitable, with the presence of these large freshwater lakes facilitating the expansion,

occupation and migration of hominids and animals north out of sub-Saharan Africa. Through reanalysis of the Saharan zoogeography, Drake et al. (2011) identified 25 North African animal species with population centres distributed north, south and within the Sahara region. The presence of these populations across the Sahara supports the notion that dispersal across the desert was possible during humid phases. Furthermore, stone tools have been identified in all megalake basins across the Sahara, suggesting modern humans and their ancestors not only migrated along the humid corridor of the megalakes, but also occupied them during past humid periods (Drake et al., 2011). Middle Stone Age (MSA) lithics identified in the Lake Megafazzan basin (which has a catchment that does not extend outside the hyperarid core of the Saharan desert) provide strong evidence for hominin migration into, and the occupation of, the central Sahara during humid periods (Drake et al., 2008). Research conducted by Blome et al. (2012) supports the Green Sahara theory, suggesting that during humid climatic periods, the contraction of the Saharo-Arabian desert belt would have enhanced modern human occupation in these areas. Furthermore, they report a link between increasing humidity and hominin site densities both along the Nile river valley, as well as a number of interior North African sites, which experienced significant population increases and decreases coinciding with humid and arid periods respectively (Blome et al., 2012).

2.6.3 Migrations along the western Red Sea "Coastal Route"

Migration along the western coast of the Red Sea has also been suggested as a potential route for modern human migration from sub-Saharan Africa to the Mediterranean coast of Northeast Africa.

Coastal landscapes are considered to be one of the most important areas for modern human expansions and migrations, (Rose & Petraglia, 2009). Finlayson et al. (2006) suggest that Neanderthal populations were able to survive along the Gibraltar coastline for several thousand years longer than anywhere else in Europe. Coastlines represent areas of enriched habitats with greater diversity and productivity of terrestrial resources, which could be exploited by modern human populations (Bailey et al., 2008). There is increasing evidence that coastal regions provided important areas of refugia and potential corridors for expansion and migration of modern humans (Stringer, 2000; Basell, 2008; Beyin, 2011). The spatial distribution of Acheulean sites in Arabia suggests that Early Pleistocene hominin

populations most likely migrated into Arabia along the coastlines, before expanding inland along river valleys during wet periods (Rose & Petraglia, 2009). The availability of molluscs, migratory birds and sea mammals along the coastline would have provided rich sources of energy that would have been present throughout the Pleistocene, irrespective of sea level and global climate changes (Bailey et al., 2008). The discovery of a number of coastal sites in South Africa dated between c. 75 – 125 ka supports the idea that Pleistocene hominins adapted to the coastal environments during periods of lower sea level, increased aridity and reduced access to fresh water (Carto et al., 2009; Marean et al., 2007; Trinkaus, 2005). During periods of low sea levels, freshwater springs are likely to have been exposed along the new coastal gradients, presenting attractive new areas for modern human occupation (Beyin, 2011, Walter et al., 2000). Once humans had developed strategies to exploit coastal environments, migration along these margins may have become a favourable route out of Africa (Beyin, 2011).

2.6.4 The "Southern Route" via Arabia

The Red Sea currently has an average width of 354 km, a maximum depth of 2850 m, and extends 2000 km along a north-south axis. With a width of 29 km and a depth of 137 m, the southern part of the Red Sea basin is connected to the Indian Ocean by the Bab al-Mandab Straits, an area that is potentially shallow enough to have been crossed during low sea level stands. Under present day conditions, travelling up the Nile River through the Sahara deserts, along the Mediterranean coastline to the north of the Red Sea, and along the Red Sea coast, represents the only terrestrial route out of sub-Saharan Africa, into Arabia. During periods of aridity, these routes through the Sahara desert are likely to have become uninhabitable. The extension of the coastal landscape associated with low sea level stands during these periods, however, may have facilitated expansion of modern humans out of Sub-Saharan Africa and into Arabia, via the shallow Bab al-Mandab Straits (Rose & Petraglia, 2009).

Over the last 1 Ma, Rose and Petraglia (2009) suggest that modern humans from Africa and Eurasia episodically expanded into the Arabian Peninsula during periods of climatic amelioration. Mellars et al. (2006) suggest that modern humans dispersed across the Bab al-Mandab Straits, along the Arabian coastline, and onwards into Asia via the Straits of Hormuz, prior to 50 ka. The Out of Africa 3 model suggests that modern humans from East

Africa migrated along this southern route in Arabia c. 60 ka, potentially using the Indian Ocean or Red Sea shorelines during one or multiple wet phases (Delanges et al., 2013). In the present day, three quarters of the Arabian Peninsula is covered by desert (Delanges et al., 2013). Consequently, the poor preservation, and hence paucity, of archaeological and hominin fossil evidence, has resulted in a gap in our understanding of the role that this region played in the dispersal of modern humans during the Late Pleistocene (Petraglia et al., 2011). Throughout the Quaternary, the different ecological niches within Arabia have been subjected to the extreme glacial and interglacial climatic cycles. With increased precipitations levels and surface water availability, an increase in environmental diversity would be expected across the Arabian Peninsula (Rose & Petraglia, 2009). During the Mid to Late Pleistocene, it is therefore likely that human development within the region was influenced by fluctuations associated with environmental change (Rose & Petraglia, 2009). No Pleistocene modern human fossils have yet been found in the Arabian Peninsula (Delanges et al., 2013).

Bretzke et al. (2013) consider four major obstacles that modern humans would have faced should they have taken the "southern route" through Arabia, suggesting that the opening up of routes across the Arabian Peninsula was a complex phenomenon closely related to fluctuations in the regional climate (Figure 1.3). In order to facilitate the crossing of the Bab al-Mandab Straits (into Arabia), and the Straits of Hormuz (out of Arabia), low sea levels associated with glacial conditions would have been required. Conversely, in order to cross the internal, arid regions of the Njed Plateau and Wahiba Sand Sea, increased precipitation levels associated with strengthened monsoons, typical of interglacial conditions, would have been necessary. Consequently, contrasting climatic conditions were required to facilitate human migration and dispersal out of Africa, across the Arabian Peninsula and on into Asia, and potentially the Levant (Armitage et al., 2011). During the transition from MIS 6 to MIS 5e, the low sea levels resulted in a reduction in the width of the Bab al-Mandab Straits, whilst Arabia experienced increased levels of precipitation (Armitage et al., 2011 and references within). This phasing of increased moisture availability and lower sea levels would have facilitated expansions of modern humans along this southern route. Research undertaken by Bretzke et al. (2013) and Armitage et al. (2011), suggests that human occupation in southern Arabia was reliant on periods of increased precipitation in the region, with populations withdrawing from the area during drier phases. It is feasible that populations retreating from the area during climatic deteriorations sought refuge in the Asir and Dhofar Mountains, and in the basin of the

Persian Gulf, in southern Arabia. Both areas are thought to represent potential refugia sites which provided resources including fresh water and stable environments even in the drier climatic periods (Bretzke et al., 2013; Rose & Petraglia, 2009).

Evidence for increased humidity during MIS 6 increases the feasibility of hunter gatherer dispersals into Arabia as early as c. 200 ka (Rose & Petraglia, 2009). Rose and Petraglia (2009) suggest that there is a possibility that early groups of modern humans expanded into the peninsula during these pluvial periods in MIS 6, hypothesising that identification of Arabian technologies between 200 and 100 ka may indicate the presence of early modern human populations. Increased precipitation in the mountainous and upland plateau areas of south-western Arabia, which trap moisture from the Indian Ocean monsoon, creates favourable highland areas for human occupation. Furthermore, runoff into the surrounding coastal plains makes these areas very attractive to modern human populations (Rose & Petraglia, 2009). Highland areas and lake margins would also have offered areas of comparative habitat stability, supporting human populations through the availability of fresh water and other associated resources, such as increased vegetation (Basell, 2008).

The most recent evidence from Arabia suggests that modern humans initially expanded out of Africa and into Arabia during the transition between MIS 6 and 5 (Armitage et al., 2011). Once the region was occupied, an increase in the regional diversity of the archaeology suggests that populations would have contracted into discontinuous areas of environmental refugia during periods of climatic and environmental degradation in MIS 3 (Delanges et al., 2013). Newly emerging evidence also suggests that distinctive technological industries developed across different geographical areas in Arabia as a result of varying adaptations and source populations (Petraglia et al., 2012).

As discussed in Section 2.5, genetic data suggests the dispersal of modern humans out of Africa occurred during MIS 4, c. 60-70 ka (Petraglia et al., 2012), after the Toba eruption 74 ka (Mellars et al., 2013). Cabrera et al. (2009), however, used mtDNA evidence from Arabia to investigate the likely number and timing of modern human dispersal events. They suggest that the modern phylogeographic patterning supports a modern human expansion out of Africa during the favourable climates of MIS 5, around 100 ka. Semi-arid savannahs and arid steppes, and the deserts of Arabia may have become populated during humid phases, driven by the northwards migration of the ITCZ during precessional maxima (Delanges et al., 2013). The deterioration of the climate and environment during arid phases, on the other hand, may have resulted in the contraction of modern human

populations into areas of environmental refugia (Delanges et al., 2013). Due to the lack of evidence for continuous human occupation in the Arabian Peninsula between the end of MIS 5 and the beginning of MIS 3, it is hypothesised that during the harshest climatic periods the entire region became depopulated (Delanges et al., 2013).

Armitage et al. (2011) report the presence of modern humans at Jebel Faya in the UAE c. 125 ka, supporting the theory of an early, southern dispersal from East Africa into southern Arabia via the Bab al-Mandab Straits. Located at a pivotal location en route between northeast Africa and South Asia, Jebel Faya represents a potential key to increasing our understanding of timing and routes of early modern human dispersals (Beyin, 2011). With modern human lithic evidence dated to c. 125 ka at the site, it is suggested that modern humans migrated into Arabia during MIS 6 via the southern route (Beyin, 2011). An increase in the ratio of C3 to C4 plants in the local area during the accumulation of Assemblage C (c. 127-123 ka) at Jebel Faya suggests that during this period of occupation, the local region was experiencing cooler, wetter conditions (Bretzke et al., 2013). Further evidence for a "wetter" period during the site occupation related to Assemblage C is supported by the presence of local fluvial sands, gravels, calcarenites, and lacustrine sediments dated to MIS 5e (130-115 ka) and MIS 5a (90-76 ka). Armitage et al. (2011) suggest that the technological patterns from the basal lithic assemblage at Jebel Faya (dated to c. 125 ka) show greater similarities to East and northeast Africa Middle Stone Age (MSA) sites, than lithics identified at other sites in Arabia. This basal assemblage (Assemblage C) is, therefore, attributed to early modern human populations expanding out of Africa during MIS 5, supporting the idea of rapid migration along a southern route across the Bab al-Mandab Straits, along the Arabian Sea rim, up to the Straits of Hormuz, and on to the Central and South Asia (Delanges et al., 2013). Similar technological patterns identified in the Dhofar region of Oman and Yemen, further support this expansion model (Delanges et al., 2013). Whilst Jebel Faya provides exciting evidence of technological connections between Arabian and Northeast African MSA industries, the absence of corroborative evidence from other Arabian sites complicates ideas surrounding human migrations across Arabia (Beyin, 2011).

Delanges et al. (2013) investigated two tributaries of Wadi Surdud (the only site in western Arabia that directly faces the African continent), producing 19 OSL ages for sediments containing artefacts. Whilst the upper unit contains dense Middle Palaeolithic archaeological concentrations (dated to MIS 3, between 63 and 42 ka), the lower unit

(dated to MIS 5, c. 85 ka) provided only a few non-diagnostic scattered artefacts. The area surrounding Wadi Surdud is believed to have represented a favourable area of refugia for human occupation, exhibiting a stable water supply and access to animal resources over long time periods. Similar to the situation identified at Jebel Faya, where the deposition of Palaeolithic artefacts with no known affinities to other lithic industries in the surrounding areas were reported, a succession of human occupation is assumed due to the development of a local MSA industry. Both Wadi Surdud and Jebel Faya represent ecozones characterised by higher annual precipitation levels than their surrounding desert and semi-desert areas. It is likely, therefore, that these two areas represent refugia, where Middle Palaeolithic groups could retreat to under harsh environmental conditions, before once again expanding during periods of climatic amelioration. Human dispersal trajectories from these sites are therefore likely to have been influenced by natural pathways and barriers, specifically relating to humid periods and therefore the availability of fresh water (Delanges et al., 2013). For example, dispersals along the flat coastal plain would only have been possible during humid periods when fresh water resources would have been more readily available (Delanges et al., 2013).

Petraglia (2011) suggests an alternative multidirectional model of modern human expansions and migrations across inland Arabia via a number of rivers and lakes, facilitated by the humid conditions present in MIS 5 (Delanges et al., 2013). A potential inland pathway would have been from west to east along the major Wadi channels that spring in the Western highlands to the east. Beyond the highlands to the east lies an internal plateau containing the south-western portion of the Rub' al-Khali desert, an area likely to be unattractive to human populations due to its arid nature (Delanges et al., 2013). Recent evidence suggests the modern humans successfully expanded far into the interior of the Arabian Peninsula during periods of ameliorated climate, adapting to the marginal environments. Petraglia et al. (2012) present the results from three stratified Middle Palaeolithic sites associated with the Jubbah palaeolake basin in the Nefud Desert, Saudi Arabia, the northern interior region of the Arabian Peninsula. Petraglia et al. (2012) identified 28 lithic artefacts at Jebel Qattar, at the southern end of the Jubbah lake basin, which they dated to 211 ± 16 ka. The presence of two Levallois flakes has enabled a tentative association of this assemblage with a modern human source. If this attribution is correct, it would suggest that modern humans were in fact present in Arabia at a time thought to correspond with the origin of the species in Africa. Located in the upper part of a palaeosol unit related to MIS 7, the majority of these artefacts do, however, also

correlate with the upper age range of fossils thought to be of Neanderthal origin, potentially representing the presence of archaic humans in Arabia. 115 lithic artefacts were identified within a palaeosol attributed to MIS 5a (75 ± 5 ka), which was overlain by massive sands (indicative of climatic desiccation at the start of the last glacial period (MIS 4), and thought to be associated with the Toba eruption (74 ka)). The presence of humans during MIS 5a overlaps with mitochondrial DNA ages for the dispersal of modern humans out of Africa between 75-62 ka. A palaeosol is also identified at the site relating to MIS 5c (95 ± 7 ka).

The presence of Middle Palaeolithic technology along the shorelines of Jebel Qattar, adjacent to the Jubbah palaeolake basin has enabled Petraglia et al. (2011) to suggest an initial expansion of modern human populations into the Arabian interior during the latter stage of MIS 5 (sub-stage 5a). They suggest that modern human expansions would have been concentrated along the attractive habitats associated with riverine valleys and lakeshores. In addition to the route across the Bab al-Mandab Straits, therefore, they suggest that it may have been possible for modern humans to expand into Arabia from the Levant along major riverine channels (Petraglia et al., 2012). Thus modern humans occupying the Jubbah palaeolake region could have migrated from the north or south along a dense network of river channels, under humid conditions.

2.7 Summary

The current understanding of regional climatic change in North Africa and Arabia, and the timing and distribution of modern humans in these areas, is fragmentary. An improved regional understanding of Palaeoclimate and human occupation is therefore necessary to determine how and when modern humans dispersed out of sub-Saharan Africa. Increasing archaeological and palaeoclimatic research across African and Arabian regions will therefore improve our understanding of modern human evolution and demographics. Until that point, it is not possible to accurately determine which route or routes were utilised by early modern human populations.

Recent debates surrounding the timing of modern human dispersals out of sub-Saharan Africa centre on differences between the genetic and archaeological evidence, which is complicated further by a lack of human fossils in North Africa and Arabia. Dates produced in association with evidence for modern human presence in northern Libya and southern

Arabia as part of this thesis will be used to discuss the likely timing of modern human dispersals out of Africa. Specific consideration will be given to the "pre" vs. "post Toba" debate, concerning whether or not modern humans were able to migrate out of sub-Saharan Africa earlier than traditionally thought.

In order for modern humans to expand out of sub-Saharan Africa, it was necessary for modern humans to cross the Saharo-Arabian desert belt. Several potential migration routes have been discussed including the "Nile-Sinai Corridor", the "Green Sahara" route, the "Coastal Route" along the western Red Sea coast, and the "Southern Route" across the Bab al-Mandab Straits and through Arabia. In order to establish which route(s) were taken by modern humans, an increased understanding of the palaeoclimate of Africa and Arabia during the Pleistocene is required. Using the dates produced at Jebel Faya and in the landscape surrounding the Haua Fteah cave, this thesis will discuss which routes represent the most likely taken by modern humans migrating out of Africa, specifically focussing on whether a northern or a southern route was favourable.

The widespread distribution of humid sites during MIS 5 supports the notion that modern humans may have dispersed out of sub-Saharan Africa into North Africa and Southern Arabia earlier than previously thought. On one hand, the presence of an arid barrier in Northern Arabia during this period, suggests that modern humans dispersing into the Levant came from North Africa, utilising a northern, rather than a southern route. Whilst there is some evidence for humidity in the southern Sahara during MIS 6, no humid corridors required to facilitate the early dispersal of modern humans across the Sahara or Arabia have been found (Drake et al., 2013).

Chapter 3 – Optically Stimulated Luminescence dating

3.1 Introduction

Optically stimulated luminescence (OSL) dating is a radiometric dating technique that can be used to directly date the time elapsed since sediment was last exposed to sunlight (typically the time of sediment deposition), based on the cumulative effect of nuclear radiation on the crystal structure of a mineral (Aitken, 1998).

Utilising some of the most common detrital minerals, including quartz and feldspar (which are very common in terrestrial surface settings), OSL dating is well suited to a wide range of geological, archaeological and anthropogenic contexts (Duller, 2008a). Consequently, OSL dating can be used in association with other absolute dating methods, or independently where the absence of datable material (e.g. organic carbon) prevents the application of other techniques such as radiocarbon (^{14}C) dating (Rhodes, 2011). OSL dating utilises the signal from quartz minerals, while infrared stimulated luminescence (IRSL) is used for dating feldspar (Duller, 2008a). OSL dating of quartz has been deemed preferable in this study due to qualities including a prevalence in most environments, a rapidly bleaching signal, high resistance against weathering and a lack of anomalous fading, which are discussed later in Section 3.4.

With a dating range of between c. 100 and 200,000 years and an optimum accuracy of ca. 5%, the OSL dating range surpasses that of the frequently used radiocarbon (^{14}C) dating, which exhibits a range of c. 50 ka (Higham et al., 2011; Reimer et al., 2009; Rhodes, 2011). OSL dating also has the advantage of directly dating the zeroing / bleaching of the luminescence signal and is therefore directly related to the depositional event of interest. OSL therefore allows us to determine the amount of time that has passed since a sediment was last exposed to sunlight (Duller, 2008a; Tsukamoto et al., 2009).

Consequently, as the extended age range covers the timescale of interest across the diverse range of potential study environments involved in this project, OSL dating has the potential to be applicable in this case.

3.2 Basic Principles (Physical Process)

Quartz and feldspar record the amount of ionising radiation that they have been exposed to as a latent signal within their crystal lattice (Duller, 2008a; Preusser et al., 2009). The decay of ^{235}U, ^{238}U, ^{232}Th (and their daughter products), ^{40}K and ^{87}Rb from within a sediment grain and its surroundings, causes the emission of alpha (α), beta (β) and gamma (γ) radiation (Lian, 2007). This leads to the absorption of dose by mineral grains. Cosmic radiation generated in outer space also provides a further, smaller, contribution (typically less than 10%) (Rhodes, 2011). Incoming energy from this ionising radiation causes electrons to become detached (ionized) from their parent nuclei in the crystal lattice (Aitken, 1998). As summarised by Preusser et al. (2009), all natural crystals, despite their purity, are known to contain a number of defects within their lattice. In quartz, electron traps and recombination centres (Section 3.5) are examples of defects in the mineral lattice. Any detached electrons that diffuse into the vicinity of an electron trap may become trapped at this location, thus representing the "memory" of the accumulated exposure to radiation (Aitken, 1998). It is this accumulation of electrons within the electron traps that allows minerals such as quartz to act as natural dosimeters, recording the cumulative radiation exposure over time (Aitken, 1998).

3.3 Calculation of a quartz OSL age

The two principle components necessary for the calculation of a luminescence age are the equivalent dose (D_e) and the environmental dose rate (D_r). The D_e refers to the amount of laboratory radiation that is required to generate a luminescence intensity identical to that caused by the radiation dose received in nature (the palaeodose). Thus, in OSL the D_e represents the laboratory equivalent (hence the "equivalent" dose) of the palaeodose (Aitken, 1998). The D_r represents the rate at which incoming radiation energy (Section 3.2) is absorbed (Aitken, 1998).

OSL dating is based on the assumption that a sample's luminescence signal is entirely "bleached" (i.e. the electron population of the OSL source trap is reduced to zero) prior to deposition, during pre-depositional transport processes. Should any residual charge remain trapped in the mineral grain at deposition, the age of deposition will be overestimated. This is especially important in younger samples, where even relatively small amounts of residual signal would significantly affect the measured D_e (Thomas et al.,

2005). Using the single-aliquot regenerative-dose (SAR) technique (Murray & Wintle, 2000; Section 5.2), it is possible to calculate the amount of radiation to which a sample was exposed during burial (D_e). By dividing this value by the rate at which exposure to ionising radiation occurred during burial (D_r), it is possible to determine the amount of time that has elapsed since the sample was last exposed to sunlight.

Following Aitken (1998) calculation of the OSL age is thus achieved using Equation 1:

$$Age = \frac{D_e}{D_r}$$

The equivalent dose is measured in the SI unit Gray (Gy), whereby 1 Gy is equivalent to 1 $J.kg^{-1}$. Standard publishing procedures result in OSL ages being quoted as one central value with 1 σ errors associated (representing 68% uncertainty) (Rhodes, 2011).

3.4 Quartz v Feldspar

Quartz and feldspar both have the ability to act as luminescence dosimeters, and are both abundant in most sedimentary deposits. Whilst feldspar has several advantages as a dosimeter over quartz (including a higher intrinsic luminescence intensity, lower thermal transfer effects and higher dose-response saturation levels) it is also a more complicated dosimeter (see Lian, 2007 Figure 7 for a recent summary). This is partly because the term "feldspar" covers a wide range of minerals with an equally wide range of luminescence characteristics (Duller, 2008a). However, the most significant problem associated with dating feldspars is anomalous fading (Wintle, 1973). This is a process whereby the observed luminescence signal decreases over time, despite the physical trap parameters suggesting that it should be stable (Duller, 2008a, Huntley & Lian, 2006).

Quartz is the most common mineral grain in sedimentary deposits at the Earth's surface (Preusser et al., 2009), which means that it was expected to be present in all samples from the research sites presented in this thesis. Further advantages of using quartz include a high resistance to weathering and a lack of anomalous fading (Lian, 2007). Duller (2008a) further supports the use of quartz over feldspar by reporting that the OSL signal of quartz is more rapidly bleached than that of feldspar, and therefore more likely to have been fully reset prior to burial.

Despite ongoing research focussing on improving the luminescence dating of feldspars (discussed further in Buylaert et al., 2012, and Duller, 2004), a more rapidly bleaching signal, a higher resistance to weathering and an apparent lack of anomalous fading makes quartz the mineral of choice for this study.

3.5 Mechanism of OSL stimulation

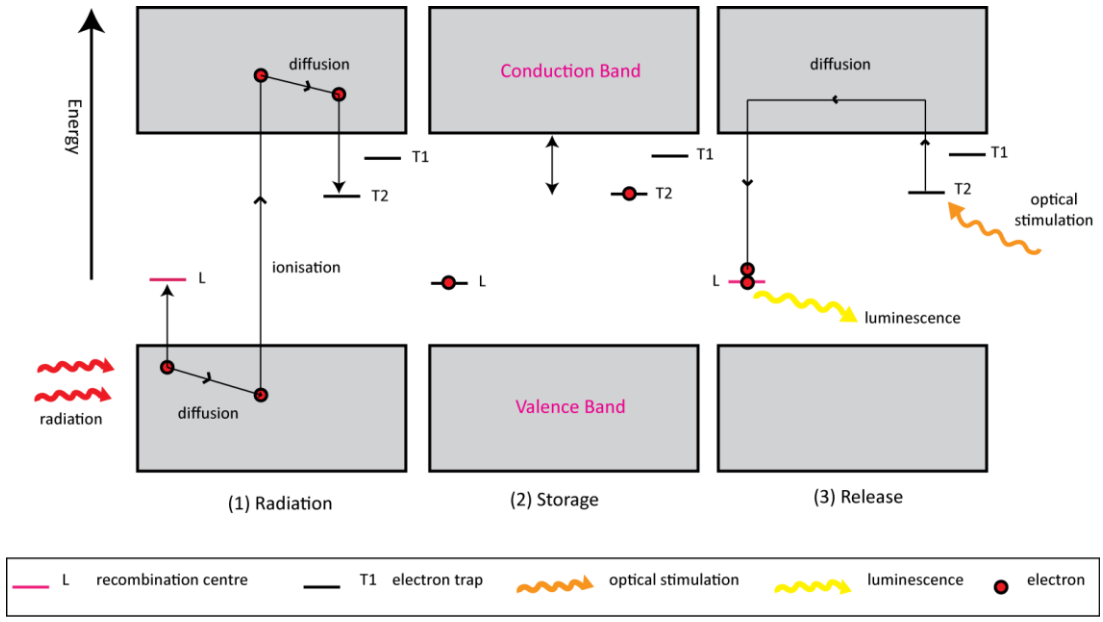

Figure 3.1. A "Band Gap" energy level diagram illustrating the response of electrons to ionising radiation (after Aitken, 1998). (1) Energy from ionising radiation causes electrons to migrate via the conduction band from their parent nuclei to electron traps, where they are stored. (2) During burial, storage of the electrons occurs, providing the sample is not exposed to light and that the traps are geologically stable at ambient burial temperature. (3) Eviction of the electrons from the traps occurs when the sample is exposed to photons of sufficient energy to promote them to the conduction band, allowing them to diffuse freely through the crystal lattice. Evicted electrons then migrate back through the crystal lattice until they unite with a recombination centre, causing the emission of a visible photon, known as luminescence.

Following the simplified “band gap” energy level diagram explanation of Aitken (1985), when sufficient energy (light in the case of OSL) has been supplied to de-trap an electron, it can either become re-trapped in an electron trap or it can recombine with a hole at a recombination centre. Upon recombination of an electron at a recombination centre, energy is released in the form of a photon or heat (Figure 3.1). OSL dating is principally concerned with recombination centres which emit a photon upon recombination (also termed luminescence centres). The number of photons emitted from a sample during stimulation is therefore, proportional to the number of trapped electrons, which is itself proportional to the total ionising radiation dose to which the mineral has been exposed since burial.

The depth of a given trap below the conduction band is related to its thermal (and therefore geological) stability, and thus determines that trap’s ability to retain electrons over time. In shallow traps, lattice vibrations at ambient burial temperature are sufficient to cause the loss of a significant proportion of trapped electrons, thereby rendering the trap unsuitable for use in dating. In deeper traps, it is only with the provision of sufficient energy (e.g. the absorption of a photon) that the detrapping of an electron can occur (Aitken, 1998). Preusser et al. (2009) report that whilst the exact position of peaks in a TL growth curve vary with experimental conditions, at a heating rate of 20 °C / s (used in early TL dating), the most commonly observed traps can be located at c. 110 °C, 230 °C, 270 °C, 325 °C and 375 °C. Spooner et al. (1988) suggest that in quartz the 325 °C TL peak represents the only trap that is easily bleachable by visible wavelengths of light, and thus it is assumed that this is the main source trap for OSL. Lower temperature peaks are normally only found in artificially irradiated samples due to their relative instability over time. Examples include the 110 °C and 230 °C TL peaks, which were found to exhibit trapping lifetimes of a few hours and a few centuries at 20 °C respectively (Spooner & Questiaux, 2000).

Similar to electron traps, as recombination centres are located at various depths their characteristic light / heat wavelength will vary accordingly. Any centres exhibiting lower energy emissions (i.e. at a wavelength undetected by the photomultiplier tube) are thus regarded as non-luminescence centres.

3.6 The Fast component

Many authors have investigated the shape of the OSL decay curve, with the aim of identifying the number of components that contribute to the final signal. It has long been agreed that the signal can broadly be broken down into fast, medium and slow components, each with different bleaching and growth characteristics (Bailey et al.. 1997). The fast and medium components represent the most readily bleachable signals (i.e. source traps which are most readily bleached under optical stimulation) and dominate the initial part of the signal, whilst the slow components exhibit much slower bleaching characteristics (i.e. a slower eviction rate of charge from the associated trap) (Bailey et al., 1997). Essentially, upon exposure to light, an electron stored in the traps responsible for the fast component will be evicted first, followed by those from the medium and then slow components. Each component exhibits different bleaching properties, which may in turn lead to variations in the determination of D_e due to differing bleaching conditions. Detailed research into the components has been completed by Adamiec (2005), Bailey et al. (1997), Bailey (2000), Li and Li (2006a), and Smith and Rhodes (1994).

As the most readily bleachable, the fast component is the most commonly selected for dating as it is considered less likely to be affected by partial bleaching than the less sensitive slower components. A potential limitation of using the fast component, is its relatively early dose-response saturation. Several studies (e.g. Ballarini et al., 2007; Murray et al., 2008; Wintle, 2008) have indicated that calculated equivalent doses become less accurate as the dose response curve reaches saturation.

Measurement of the OSL signal can be completed using either continuous-wave (CW) or linearly modulated (LM) stimulation, whereby the light source is held at a constant power or ramped from zero to a maximum value respectively. LM-OSL has the advantage of being able to separate and record the various components which contribute to the OSL decay curve (Bulur, 1996). Whilst CW stimulation can also be used to identify the various components, LM-OSL presents the data in a format considered more amenable to mathematical analysis (Bulur, 1996).

Past studies using LM-OSL, including those by Choi et al. (2006), and Jain et al. (2003), have led to the identification of at least 6 different components within the main OSL signal, including the ultrafast, fast, medium and three slow (s1, s2 and s3) components. Individual peaks in the LM-OSL curve can be identified when luminescence output is displayed as a

function of illumination time and mathematically analysed to identify the various individual components, as shown in Figure 3.2 (Wintle & Murray, 2006).

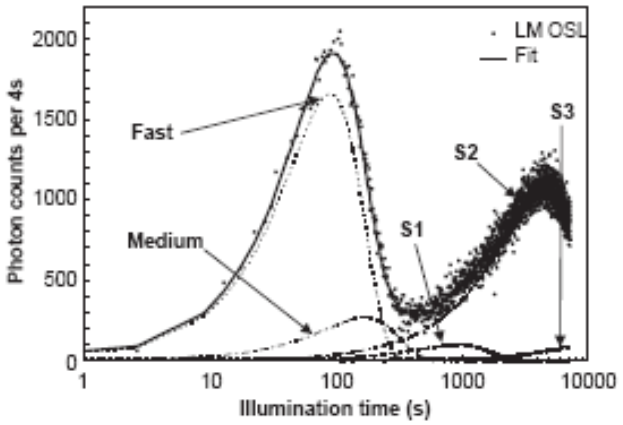

Figure 3.2. An example LM OSL curve from a typical quartz sample. The LM OSL curve has been deconvoluted to separate the different component contributions. The plot displays five individual components from the full OSL signal, including the fast, medium and three slow components. Source: Singarayer et al. (2005).

Jain et al. (2003) report that while dating quartz samples dominated by the fast component is relatively free of complications, this may not be true for samples in which other components constitute an appreciable proportion of the OSL signal measured. They suggest that further investigation into the behaviour of the different OSL components is necessary to ensure accurate equivalent dose evaluations for samples lacking a dominant fast component (Choi et al., 2006).

3.7 Small aliquot vs. single-grain measurements

OSL dating can be completed using either individual single grains or small aliquots (i.e. a small subsample composed of multiple grains, c. 1 – 5 mg of quartz (Duller, 2008a; Galbraith et al., 1999)). Depending on the grain size of quartz used, between 20 and 1,000,000 grains can be contained within a single aliquot, leading to the averaging of D_e signals from each of the individual grains within a sample (Duller, 2008b). A key assumption when dating aliquots, is that all grains in the aliquot have the same equivalent dose, a situation typically associated with sediments which were fully bleached prior to

deposition. However, this assumption is likely to be violated to some degree in the majority of natural environments. Development of single-grain OSL dating has facilitated the ability to investigate the extent to which all of the grains within a sample can produce the same apparent luminescence age. Furthermore, the ability to observe signals from individual grains has led to improvements in our understanding of the inherent grain to grain variability within samples (Roberts et al., 1997). Displaying single-grain results on a radial plot, as first demonstrated by Galbraith et al. (1999), allows the scale of variation in D_e values and potential presence of more than one sediment population within a sample to be more readily identified (Figure 3.3). Single grains can vary greatly in both luminescence intensity and the precision with which the D_e can be estimated. Radial plots represent a graphical solution for comparing and displaying these patterns in a single grain dataset (Galbraith et al., 1999).

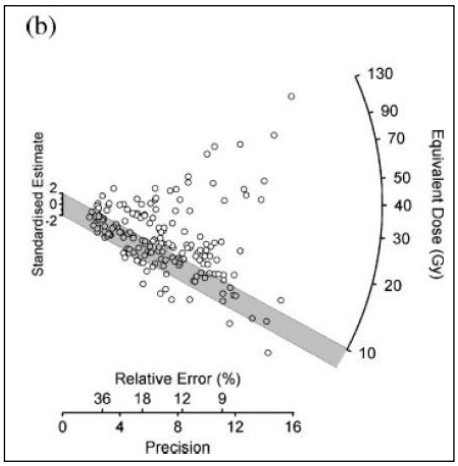

Figure 3.3. An example of a radial plot for a sediment which was partially bleached prior to burial. Source: Duller (2004). Open circles represent the D_e values from the measured single-grain signals. The y axis displays the length of a two sigma error bar, which is applicable to any point on the plot. The x axis provides two scales, a scale of precision / relative standard error of the individual palaeodose estimates. The circular scale represents the D_e value in Gy. The grey bar is centred along the mean D_e value for the dataset, which is usually calculated by applying the central age model (Section 5.2.2). All of the points that lie within the bar are consistent within 2 standard errors of the mean dose. The majority of data points in this radial plot cannot be included in the 2 sigma band, suggesting that the sample consists of a set of grains with very different D_e values, suggesting that the sample may have been partially bleached.

Duller et al. (2000) measured over 3000 individual quartz grains from 7 different sites and demonstrated that, for these samples, 95% of the total luminescence signal was derived from only 5% of the grains measured. Their data indicates that only a small proportion of quartz grains contribute a significant OSL signal. Furthermore, where grains were inherently dim, counting statistics were thought to be the dominant source of uncertainty. Conversely, where grains were bright, uncertainty appeared to be predominantly related to instrumental error. Duller et al. (2000) also discovered large variations in the luminescence characteristics of individual grains, notably in their dose saturation characteristics and luminescence sensitivities, which will subsequently affect the overall contributions to the sample D_e. The upper age limit for the OSL dating of quartz is controlled by the saturation of the traps within the crystal lattice of the mineral, and saturation occurs where no further trapping of electrons can occur regardless of exposure to radiation since the OSL trap(s) are full (Rhodes, 2011). Yoshida et al. (2000) present the results from a study of individual quartz grains from Australian sedimentary deposits, which highlights the variability in luminescence and saturation characteristics of the individual grains. In this thesis, c. 15-20% and 28-58% of the total Libyan and Arabian grains measured respectively were termed "Class 1" grains, which exhibit intrinsically 'bright' signals and high saturation dose limits. Yoshida et al. (2000) suggest that these favourable characteristics may enable this type of grain to provide reliable optical ages for deposits up to 1 Ma. These class 1 grains are of particular interest in the present study since samples from Libyan sites are relatively bright.

While Olley et al. (1998) reported that measurements carried out on small aliquots are able to accurately reflect variations in the D_e distribution, Russell and Armitage (2012) demonstrated that the presence of individual grains with poor luminescence properties in small aliquots can lead to discrepancies between D_e distributions generated by single-grain and multi grain OSL measurements. By utilising single-grain analysis, it is possible to exclude such unreliable grains from D_e determination with the use of a robust grain rejection criteria, as reported in Jacobs et al. (2008a) and Armitage et al. (2011), thereby potentially enhancing the reliability of the sample D_e.

Development of the single-grain method continues to increase our understanding of grain to grain variability, whilst allowing for complications such as partial bleaching to be better identified. Advancements in technological design enable 100 grains per aliquot to be individually analysed with a laser, significantly increasing the rate at which these types of

investigations can be completed (Figure 3.4) (Duller et al., 1999; Duller, 2004). Single-grain technology was used throughout this project.

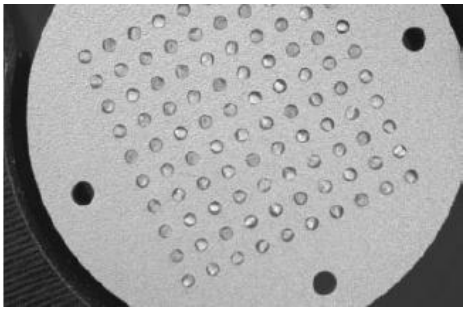

Figure 3.4. Image of the single-grain holder used during single-grain analysis. Discs contain 10x10 or 8x8 holes within which a single-grain is placed. Source Duller (2004).

3.8 Summary

- Following Aitken (1998), OSL dating uses the cumulative effect of nuclear radiation on the crystal structure of a mineral to determine the time that has elapsed since a sediment was last exposed to sunlight.
- The emission of α, β, γ and cosmic radiation leads to the absorption of dose by mineral grains. Defects in the crystal lattice of the minerals act as electron traps which store detached electrons that diffuse into their vicinity. Accumulation of these electrons represents the memory of the mineral (i.e. the cumulative radiation exposure over time).
- The equivalent dose (D_e) represents the amount of laboratory radiation required to generate a luminescence intensity identical to that caused by the palaeodose (i.e. the radiation dose received in nature). Thus, it is essential that the luminescence signal of a sample is reduced to zero prior to burial in order to avoid overestimation of the burial age.
- The environmental dose rate (D_r) represents the rate at which incoming radiation energy is absorbed by the mineral. By dividing the D_e by the D_r, it is therefore possible to calculate the time that has elapsed since the mineral was last exposed to sunlight.

- Quartz was chosen as the luminescence dosimeter in this thesis due to an absence of anomalous fading, a high resistance to weathering, a rapidly bleaching signal, and a prevalence of this mineral in most environments.
- Trapped electrons become de-trapped following the application of sufficient light levels. These electrons can then become re-trapped in an electron trap or recombine at a recombination centre. Upon recombination at a recombination centre, energy is dissipated as a photon or heat. Recombination centres that emit photons are also known as luminescence centres, which OSL is primarily concerned with. The number of photons released is proportional to the number of trapped electrons, which are in turn proportional to the total absorbed ionising radiation dose since burial of the mineral.
- The depth of a trap below the conduction band is related to its thermal stability. Deeper traps are able to retain electrons over longer time periods as higher energy levels are required to de-trap the electrons. In quartz, the 325 °C peak is thought to represent the main source trap for OSL. Lower temperature peaks (i.e. 110 °C and 230 °C), with trapping lifetimes of c. a few hours to centuries, are commonly only found in artificially irradiated samples.
- The OSL decay curve can broadly be resolved into fast, medium and slow components (Singarayer et al., 2005). As the most readily bleachable signal that dominates the initial part of the OSL signal, the fast component is the most commonly chosen component for dating.
- Small aliquot dating is used for samples that are thought to have been fully bleached prior to burial. Single-grain dating represents a more recent method that allows the investigation of the extent to which all grains within a sample can produce the same apparent luminescence age. Consequently, single-grain dating allows for the identification of grain to grain variability, partial bleaching and post depositional mixing, and unreliable grain characteristics (Duller, 2008b).

Chapter 4 – Sample collection and preparation

4.1 Introduction

The following chapter outlines the procedures and protocols used to collect and prepare the luminescence samples reported in this study. Specifically, this chapter focuses on the sampling methods used at the field sites, and the subsequent laboratory procedures used to extract pure quartz from these samples.

4.2 Sample Collection

In the field samples were collected either in opaque plastic tubes (40 mm diameter, 20 cm length) hammered into the vertical face of a freshly cleaned section, or as ~10x10x10 cm sediment blocks. Prior to sampling, the tubes were packed at one end using clean laboratory tissue in an attempt to prevent vibrations from mixing the sediment in the tube during sampling. Once the tube was fully inserted into the section, the tube was removed, packed at both ends and then taped to ensure the sediment within remained securely in place. Where compaction or cementation of a sediment prevented the insertion of tubing into the face of a section, block samples were carved from the cleaned, vertical section using a geological hammer and Swiss army knife. Once sampled, all tube and block samples were individually packed in three layers of opaque black plastic bags, labelled, and sealed with tape, ready for transportation to the laboratory in the UK.

Where possible, samples were taken at least 30 cm away from any stratigraphic boundaries to avoid accidental mixing of the different sedimentary layers and to maximise the probability that the sample was retrieved from a context with a homogenous gamma field. The depositional history of the sampling location was also taken into consideration, avoiding sections where the sediments were unlikely to have been fully bleached prior to deposition. In some cases it was impossible to avoid contexts where complex dosimetry or mixed populations might be present. In these contexts, both single-grain (SGLL) dating and careful modelling of the dose rates are required to extract reliable age estimates (Section 4.5 and Chapter 7.

4.3 Sample Preparation

In the laboratory, all stages of sample preparation and measurement were completed under subdued orange (a Philips Master SOX-E 18W low pressure sodium-vapour lamp) or red (using Fluorescent light tubes equipped with 226 (UV), 209 (Neutral density) and 027 (red) Lee Filters) light conditions to avoid bleaching of the luminescence signal. Where possible, the outer 2cm of light exposed material from each surface and end of the block and tube samples respectively, was removed. This material was retained for moisture content and radionuclide determination (as discussed in Section 4.4).

Heavily cemented block samples were prepared via multiple cycles of etching in 10% hydrochloric acid, following the method of Armitage and King (2013). After the removal of a small sample for radioisotope concentration analysis, the three axes of the block were measured before immersion in 10% hydrochloric acid. Once no further effervescence was observed, the block was extracted from the solution and cleaned to remove any liberated, light exposed sediment, and the 3 axes were re-measured. This procedure was repeated until the length of each axis had been reduced by 2cm (ensuring all light exposed material had been removed), samples were treated using the procedures outlined in sections 4.3.1 to 4.3.5.

4.3.1 Carbonate removal

Carbonates were removed from the sample via immersion in a 10% solution of HCl, which was frequently replaced to ensure completion of the chemical reaction. Once no further effervescence was observed, concentrated (11 M) HCl was added to the samples before they were stirred, left to settle and rinsed three times with deionised water.

All samples reported in this thesis that were obtained from the Libyan study sites demonstrated an extremely vigorous reaction to the HCl, suggesting a high carbonate concentration. Conversely, the Jebel Faya samples from Arabia displayed only a moderate reaction to the HCl.

4.3.2 Removal of organic material

Organic matter was removed from the sample by oxidation in hydrogen peroxide solution. Samples were immersed in hydrogen peroxide solution for one week, during which time the samples were regularly stirred, and H_20_2 was refreshed. Samples were rinsed three times with deionised water to remove the H_20_2 in preparation for sieving.

4.3.3 Separating the various size fractions

After the removal of carbonates and organic matter, samples were wet sieved at 250, 210, 180, 150, 125, 90, 60 and 40 µm. < 40 µm material was Stokes' settled 4 times at 11 µm and 4 µm to obtain the 4 - 11 µm size fraction.

Samples extracted from the Jebel Faya site contained a significant proportion of grains in the 180 – 212 µm size fraction, the preferred size for single-grain dating, and therefore the subsequent sample preparation procedures were carried out on this size fraction alone.

Conversely, samples from the Libyan sites contained very little coarse grain (>60 µm) quartz, with the greatest mass present in the < 125 µm fraction. Subsequently only the 60 – 125 µm and 4 – 11 µm (where applicable) fractions were used in the following preparation stages.

4.3.4 Density separation

Grain size fractions >60 µm were density separated prior to hydrofluoric acid (HF) etching. Heavy minerals and feldspars were separated from quartz in two stages using sodium polytungstate solution (SPT) which had been prepared at a density of 2.75 and 2.62 g/cm^3 respectively. A maximum of 3 g of each sample was placed into a centrifuge tube with c. 20 ml of SPT at a density of 2.75 g/cm^3, before being inserted into a centrifuge rotating at 3000 rpm for 15 minutes. Upon extraction from the centrifuge, the bottom third of the SPT was frozen inside the tube using liquid nitrogen, and the unfrozen liquid was decanted into a separate beaker. This latter fraction contains mineral grains with a density below 2.75 g/cm^3, principally quartz and feldspar. SPT was removed from the decanted fraction using deionised water, and the separated sediment was dried in the oven overnight at 50 °C. The oven dried sediment was separated a second time using SPT at a density of 2.62 g/cm^3,

with the sunken fraction consisting principally of quartz, and the floating fraction consisting principally of feldspar.

4.3.5 Etching

The quartz rich fractions obtained by density separation were further purified with respect to feldspar via chemical etching. The 212-180 μm grain size fractions (those from Jebel Faya) were immersed in 27.6 M Hydrofluoric (HF) acid for one hour. Conversely, the finer grain size fractions (those from Libyan samples), including those obtained by Stokes settling, were etched using fluorosilicic acid (H_2SiF_6). HF etching typically removes a 10 μm "rind" from the outside of quartz grains (Hong, 1998) and hence HF etching is inappropriate for the finer grain sizes extracted from Libyan samples. Consequently, the Libyan samples were prepared using long fluorosilicic acid etches, which dissolve feldspars without having a significant effect upon quartz. 20 ml of Fluorosilicic acid (H_2SiF_6) was added to each sample, which were contained in small plastic bottles. These bottles were then placed on an orbital shaker for one week to ensure the continual mixing of the sample with the chemical. After this time the sediments were allowed to settle. Once the allotted time period had passed, the HF or H_2SiF_6 was decanted off, before the samples were rinsed 3 times with deionised water to remove all of the remaining chemicals. Samples were then immersed in 11 M HCl for 24 hours in order to remove any fluoride precipitates which may have formed on the surface of the sediment grains following hydrofluoric or fluorosilicic acid treatment. Subsequently, the samples were rinsed three times with deionised water. Following treatment with HF or H_2SiF_6, the purified quartz samples were re-sieved to their original size fractions. This step allows the removal of any partially dissolved grains remaining in the sample, based upon the assumption that these grains are likely to be feldspars. Samples were dried overnight in the oven at 50 °C and stored in light tight containers prior to measurement.

4.4 Sample for moisture content and dosimetry measurement

Sample moisture contents were measured using approximately 100 g of the light exposed material that had been removed from each sample during the first stage of preparation. In each case, sediment was placed into a pre-weighed empty beaker and then weighed again

before being placed in the oven at 50 °C overnight. Once the sample was completely dry the beaker and dry sediment was once again weighed. The observed change in mass was attributed to water loss and percentage water content was calculated.

4.5 Disc Preparation

As discussed in Section 3.7, in environments where partial bleaching or post depositional mixing is likely to have occurred, it is preferable to utilise single-grain dating (Duller, 2008b). Conversely, for homogenous samples where it is unlikely there will be a mixed age population, small aliquots represent an equally suitable method. Due to the variability of depositional environments sampled for this thesis, both single-grain, small aliquot, and fine grain dating was employed. The latter was utilised where the paucity of coarse grain quartz resulted in only the 4 – 11 µm size fraction being available for dating.

When dating multiple grains from the fine sand size fraction (c. 60 – 125 µm), it was important to consider the number of grains present on a standard 9.8 mm diameter disc. Duller (2008b) suggests that with increasing number of grains on a disc, there will be a reduction in the variation in D_e observed due to averaging caused as the grains are measured simultaneously as part of the aliquot. In an attempt to reduce the sample size, and thus the observed D_e variation, masks were used to control the size of the individual aliquots (Section 4.5.2).

Each of these measurements were completed using a different type of disc, which are loaded with grains using the methods discussed in the following sections.

4.5.1 Single-grain preparation

As the holes on a standard aluminium (Al) single-grain disc are 300 µm deep and 300 µm wide (Figure 6), the optimum size fraction for single-grain analysis is ~200 µm, as this should prevent more than one grain residing in each recess. Prior to use, each single-grain disc was cleaned in an ultrasonic bath containing deionised water and checked under a microscope to ensure that no grains had become stuck in any of the recesses.

When measuring 180 – 212 µm grains, an excess of quartz was poured onto the surface of an aluminium single grain disc. All excess grains were then removed with a fine brush which was swept across the surface of the disc.

Due to the paucity of coarse grain quartz in the Libyan samples, it was not possible to employ the same standard method of disc preparation. As a result, individual smaller grains were hand-picked and manually loaded into the recesses of a single-grain disc under a microscope using thin electrical wire, ensuring only one grain was present in each recess (as reported in Russell and Armitage, 2012). Whilst this was a very time consuming process, this was the most effective way to ensure the measurement of a true single-grain age.

4.5.2 Small aliquot preparation

Small aliquots were prepared by mounting a monolayer of the 60 – 90 µm or 90 – 125 µm quartz grains on to the surface of a 9.7 mm diameter aluminium discs using Silkospray that had been applied to the disc via a mask. A medium sized mask (c. 5 mm in diameter) was used for initial and experimental measurements of the samples, while a small mask size (c. 2 mm in diameter) was used to generate aliquots for age determination. This approach was adopted since initial measurements are intended to determine the bulk properties of a sample (appropriate D_e, optimal preheating conditions etc), whereas for age determination, small aliquots maximise the probability of detecting mixed age populations or partial bleaching.

Very small aliquot, or "Pseudo single grain" (Russell and Armitage, 2012) discs were generated by pouring an excess of the 60 – 90 µm or 90 – 125 µm quartz grains on to the surface of an aluminium single-grain disc. Similar to the single-grain disc method, the excess grains were then swept off the surface of the disc using a fine brush, which resulted in c. 20 – 14 grains becoming trapped in each recess depending on the sample size fraction used.

4.5.3 Fine grain preparation

Some Libyan samples contained no quartz grains larger than silt-sized, and hence these samples were measured using the 4 – 11 μm size fraction. Due to its fine grain nature, the 4 – 11 μm size fraction could not be oven dried and was therefore stored in deionised water.

9.7 mm Al discs were placed into the bottom of a glass vial and filled with 700 μl of deionised water. An additional 700 μl of the sample was then inserted into the glass vial. The samples were then left to settle for c. 3 hours, before the top 700 μl of deionised water was removed using a small amount of laboratory roll. The discs were then placed into the oven and left overnight at 50 °C allowing all of the water to evaporate away, thus leaving a monolayer of the dry 4 – 11 μm material on the surface of the disc.

4.6 Summary

This chapter outlines the sampling and preparation methods utilised for samples in this thesis, including the chemical and manual preparation of the material in the laboratory that was necessary to isolate pure quartz for measurement. Disc preparation methods discussed in this chapter are fundamentally driven by the investigations discussed in Chapter 8, where the variations between single-grain, 'pseudo single-grain' and small aliquot measurements are considered.

Chapter 5 - Measurement of the Luminescence signal

5.1 Introduction

The OSL signal from quartz is most commonly measured using the single aliquot regenerative-dose (SAR) protocol, discussed in Section 5.2 (Murray & Roberts, 1998). In summary, the protocol involves measuring the natural OSL signal followed by a succession of luminescence measurements which result from a series of increasing laboratory irradiations (Murray & Wintle, 2000; Wintle & Murray, 2006). These laboratory irradiations allow the OSL signal growth characteristics of the aliquot to be determined, allowing the D_e to be calculated.

In order to accurately measure OSL, it is necessary to use a stimulating light source with a wavelength clearly different from that emitted as luminescence from the sample. As light with a shorter wavelength causes more rapid eviction of the luminescence signal (Aitken, 1998; Spooner, 1994), blue – green light-emitting diodes (LEDs) (470 nm) or green lasers (514 or 532 nm) are commonly used to stimulate a sample, as their relatively short wavelength is clearly distinguishable from the UV light emitted from luminescence quartz centres (ca. 365nm) (Lian, 2007; Rhodes, 2011). Alternately, IR diodes (800–900 nm) are employed to detect the presence of feldspars (Duller, 2003; Rhodes, 2011). The photons emitted by the sample in response to stimulation by the LEDs or lasers pass through two U340 filters directly into the photomultiplier tube where they are detected (Bøtter-Jensen et al., 2003).

A further consideration for the accurate measurement of OSL concerns the temperature at which the sample is held whilst optical stimulation occurs. Increasing the temperature results in a more rapid eviction of the luminescence signal, however, it also contributes to the process of thermal quenching, whereby the efficiency of luminescence centres is reduced with increasing temperature (Wintle and Murray, 2000). Figure 5.1, illustrates the variation in integrated OSL signal with increasing temperature.

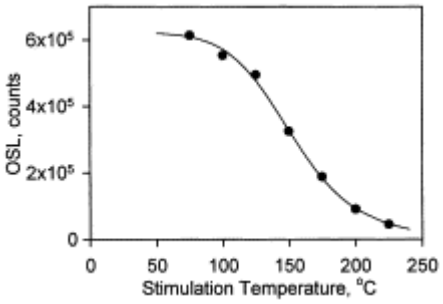

Figure 5.1. Integrated OSL signals as a function of stimulation temperature, demonstrating the effect that increasing temperature has on OSL light sums (Wintle and Murray, 2000).

Murray and Wintle (1998) demonstrated that heating a sample to 125°C provides optimum conditions for rapid stimulation, alongside minimal thermal quenching, hence resulting in a strong signal to noise ratio. Measuring luminescence at this elevated temperature also prevents the re-trapping of electrons in low temperature traps during stimulation. In particular, raised temperature stimulation prevents the re-trapping of electrons in the 110 °C trap, which would subsequently be thermally transferred back to a stable dating trap during a subsequent preheating (Aitken 1998; Lian, 2007; Murray & Wintle, 1998; Stokes et al., 2000).

An OSL decay curve is a representation of luminescence output during laboratory stimulation, displaying OSL intensity as a function of illumination time (Figure 5.2). The shape of the curve follows the depletion of the OSL signal as electrons are evicted from the electron traps in the mineral (Lian, 2007). Bailey et al. (1997) demonstrated that the OSL decay curve is not a simple exponential decay, but instead comprises several components which reflect different electron trap populations and which exhibit various sensitivities to light stimulation. It is the sum of the individual exponential decay curves produced by each component that is therefore represented by the signal decay curve (Lian, 2007). Assuming that the stimulation intensity remains constant, the most light-sensitive traps contribute to the first part of the signal, followed by contributions from progressively less light sensitive traps. While the OSL signal is undoubtedly derived from the number of electrons in a particular trap, it is also affected by the relative proportion of luminescence and non-radiative recombination centres (Aitken, 1998; Lian, 2007; Wintle & Murray, 2006).

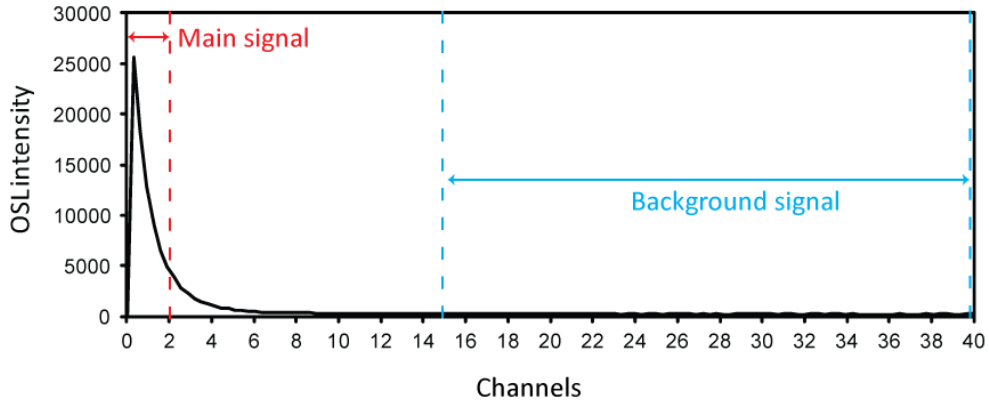

Figure 5.2. An example of a multigrain OSL decay curve, displaying the luminescence output (number of photons detected), on the y axis, as a function of illumination time, on the x axis. The main signal is commonly taken from the first 2 channels (0.32 seconds) of measurement, while the background readings are taken from the final 25 channels (4 seconds).

5.2 The SAR Protocol

Sensitivity is the radiative recombination probability, however, in practice it is commonly defined as "luminescence per unit dose" (Armitage et al., 2000). Therefore, a change in sensitivity affects the amount of OSL emitted per unit of dose absorbed. Such changes are known to occur during laboratory procedures (e.g. preheating and irradiation) and in nature (Armitage et al., 2000). In 2000, Murray and Wintle introduced the single-aliquot regenerative-dose (SAR) technique. Whilst single aliquot protocols were already in use for quartz OSL, the key advantage of the SAR protocol was that sensitivity could be corrected for. SAR also represented a new method whereby a reliable D_e determination could be achieved with improved dating precision via an incorporated assessment of internal consistency (i.e. the recycling ratio, see Section 5.2.1.1.). Based on the protocol first suggested by Murray and Roberts (1998), the response of OSL to a fixed radiation test dose administered following each regenerated luminescence dose point is used to monitor sensitivity changes (Table 5.1). The natural and regenerated doses are normalised to a fixed test dose in order to monitor sensitivity change throughout the SAR cycle.

Irradiation (Natural or Regenerated)
↓
Preheat (PH 1)
↓
Measurement of OSL (L_n or L_x)
↓
Test Dose
↓
Preheat (PH 2)
↓
Measurement of OSL (T_n or T_x)

Table 5.1. Summary of the SAR protocol (after: Murray and Wintle, 2000). L_n refers to the natural luminescence intensity while L_x refers to the regenerated luminescence intensity. Similarly, T_x and T_n refer to the respective test dose intensities. PH 1 and PH 2 are the preheats used prior to measurement of the natural / regenerated and test dose OSL respectively.

Natural (L_n) and regenerated (L_x) luminescence intensities are divided by their respective test dose (T_x or T_n) intensities, producing a sensitivity-corrected luminescence response. By attempting to correct for changes in sensitivity in this way, if working properly, then "the corrected OSL response should be independent of prior dose and thermal/optical treatment, i.e. there should be no change in the sensitivity-corrected dose-response curve on re-measurement" (Murray & Wintle, 2000. pp57)). By then comparing the sensitivity-corrected natural luminescence intensity (L_n/T_n) with the sensitivity-corrected dose response curve, it is possible to interpolate a sensitivity-corrected D_e (Figure 5.3) (Armitage et al., 2000; Murray & Roberts, 1998; Murray & Wintle, 2000; Murray & Wintle, 2003; Wintle & Murray, 2006).

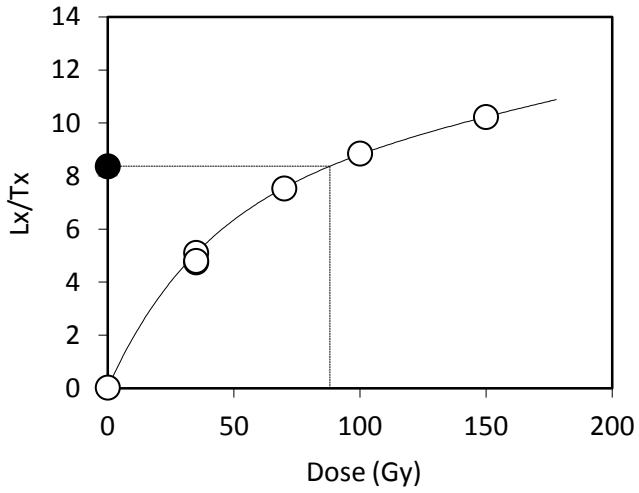

Figure 5.3. An example of a sensitivity-corrected dose response curve. The sensitivity-corrected natural luminescence intensity (L_n/T_n) is compared with the dose response curve, composed of the sensitivity-corrected regenerated luminescence signals (L_x/T_x).

The fundamental assumption underlying the SAR protocol is that the OSL sensitivity measured using a test dose is directly proportional to the OSL sensitivity of the associated regenerated dose (Wintle & Murray, 2006). It is therefore assumed that sensitivity change can be adequately monitored and corrected for using the OSL response to a fixed radiation test dose (Murray & Wintle, 2003). The key assumption of SAR is that the sensitivity changes which occur between L_x and T_x are negligible and/or constant. Consequently, for SAR to work effectively, the OSL signal must be measured following every dose and simulation cycle, allowing the effects of sensitivity change in both the natural and regenerated signals to be corrected for (Murray & Wintle, 2000). Furthermore, it is assumed that any changes in sensitivity during measurement of the natural signal will be similar to those changes experienced during the subsequent regenerated cycles (Wintle & Murray, 2006).

Another fundamental assumption of the SAR protocol is that the samples being measured are dominated by the fast component. It is generally accepted that samples dominated by the fast component produce the most reliable D_e estimates due to potentially poor signal behaviour and partial bleaching of the medium and slow components (Bailey, 2010; Choi et al., 2006b). Samples that are not dominated by the fast component are more likely to be

affected by partial bleaching, due to the dominance of less light-sensitive components, which may be thermally unstable (Section 3.6) (Roberts, 2008).

5.2.1 Modifying the SAR Protocol

While SAR cannot prevent the process of sensitivity change, it can monitor the effects. In fact, the deliberate generation of sensitivity change can commonly be utilised in an attempt to test the technique (Lian, 2007; Wintle and Murray, 2006). Within the technique there are a number of internal checks that have been developed to ensure that the sensitivity correction system is working efficiently, allowing greater confidence to be assigned to the final OSL ages produced (Armitage et al., 2000; Murray & Wintle, 2003; Wintle & Murray, 2006). These checks attempt to ensure that the SAR measurement conditions utilised for determining the equivalent dose used for age determination are appropriate, and that the underlying assumptions of the SAR protocol are valid (Wintle, 2008). They include the recycling ratio test, the recuperation test, and the dose recovery test.

In addition, a series of screening protocols (rejection criteria) are applied to the raw dataset. These rejection criteria facilitate the removal of any data from the measured dose distributions that may provide erroneous or unreliable D_e estimates as a result of their luminescence characteristics. In this thesis, the recycling ratio and recuperation test (mentioned above) were routinely applied to each dataset as part of the rejection criteria.

Due to a combination of intrinsic and extrinsic factors (including bleaching and the structure of the quartz mineral), it is assumed that there will be at least a small degree of inter-grain / inter-aliquot variability within all samples measured as part of this thesis. As a result, variations are likely to be observed between the individual D_e values produced by the different grains and aliquots measured for each sample.

5.2.1.1 Recycling Ratio

Sensitivity change, which is often cumulative, has been identified as being at its greatest between the first and last measurement cycles of a SAR sequence (Armitage et al., 2000). The recycling ratio is designed to test the efficiency with which SAR has corrected for this

change, by comparing the ratio between two sensitivity-corrected OSL responses (Murray & Wintle, 2000). In order to do this, a repeat of the first regenerated dose is carried out following completion of all of the other measurements, and the two signals are then compared. If SAR has successfully corrected for sensitivity change then the ratio of Rx:R1 (i.e. the second measured point : the first measure point) should be consistent within unity (Ballarini et al., 2007; Jacobs et al., 2006; Roberts et al., 1998). Any aliquots displaying a recycling ratio value outside ± 10% of unity were therefore rejected.

5.2.1.2 IR depletion Ratio

Whilst both quartz and feldspar luminescence signals can be reset to zero by a few minutes of exposure to visible light, only feldspars are sensitive to IR stimulation (Hütt et al., 1988). IRSL can therefore only be used to extract the luminescence signal from feldspars, due to the insensitivity of quartz to IR photons. Accordingly, the IR test provides a method for assessing the purity of quartz by enabling the presence of any feldspar contamination to be identified via stimulation of the sample with IR light. Following the application of a regeneration dose (equivalent to that of the first regeneration dose) and preheat, aliquots were exposed to IRSL. Should any signal be emitted during this stimulation, resulting in a loss of OSL, the presence of the contaminating mineral can be confirmed (Ballarini et al., 2007; Duller, 2003; 2008a)). The OSL signal from the IRSL SAR cycle was compared to the OSL signal from a standard SAR cycle using the same regeneration dose. Any aliquots displaying an IR depletion ratio (measured dose / expected dose) value outside ± 2 σ of unity were rejected.

5.2.1.3 Recuperation

By applying a zero dose to the sample, the recuperation test identifies the presence of thermal transfer (Sections 3.5 and 5.2.2.2) by identifying the redistribution of electrons from light-insensitive, thermally stable traps into more light sensitive, shallower traps following irradiation, optical stimulation and preheating (Li & Li, 2006b); Murray & Wintle, 2000; 2006). Assuming no thermal transfer or recuperation has occurred, the measured luminescence signal should be less than 5% of L_n / T_n. Values within ± 5% of unity are generally accepted as it is thought that they are close enough to unity to be unlikely to

cause problems associated with recuperation (Wintle & Murray, 2006). Murray and Wintle (2000) suggest that only a small test dose should be used in SAR, as this will minimise the risk of thermal transfer during measurement of the sample (Bailey, 2004; Murray & Wintle, 2000; Singarayer et al., 2005; Wintle & Murray, 2006). All samples in this thesis displaying a recuperation value outside ± 5% of unity were rejected.

5.2.1.4 Natural interception of the Growth Curve

As growth curves are produced using the increase of an OSL signal with increasing laboratory irradiated doses, it is important that the resulting growth curve is fitted using a function which accurately describes the curve. Whilst in most circumstances the natural signal is capable of intercepting the growth curve, occasionally the sensitivity corrected natural signal is greater than that of the largest laboratory irradiated regeneration dose (Armitage et al., 2000; Yoshida et al., 2000). Consequently, the inability of the natural signal to intersect the dose-response (growth) curve (Figure 5.4) results in the rejection of the relevant data, as no equivalent dose can be calculated.

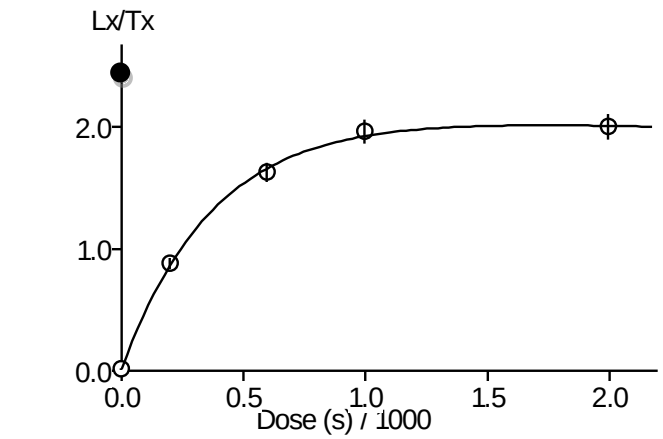

Figure 5.4. An example of where the sensitivity corrected natural OSL (L_n/T_n) does not intersect the growth curve.

To avoid the largest regenerative dose being too small to incorporate the natural signal in the growth curve, raw data was checked prior to the removal of the discs from the Risø

reader. Where the highest regeneration dose did not yield a sensitivity-corrected OSL intensity larger than L_n / T_n, an additional dose was applied at the end of the sequence.

Despite these attempts, some samples were still unable to intercept the growth curve, suggesting another underlying process was responsible for lack of interception. No explanation for the occurrence of this observation has yet been identified, although similar results can be observed in Armitage et al. (2000) and Bailey (2004). Bailey et al. (2005) suggest that in instances where the natural signal level exceeds the maximum signal level obtained through laboratory regeneration, the application of pulsed laboratory irradiations may facilitate the production of a growth curve capable of incorporating the natural signal. Their paper suggests that the laboratory-regenerated dose response of quartz OSL may become suppressed as a result of the difference between laboratory and natural dose rates. Using the pulsed-irradiation procedure in combination with the fast component of the OSL decay, they successfully demonstrate how the problem of an irrecoverable natural signal level can be overcome.

5.2.1.5 The Fast Ratio

As discussed in Section 5.2, an underlying assumption of the SAR protocol is that there is a dominant fast component present within the sample being measured. Durcan and Duller (2011) and Duller (2012), developed the fast ratio test, which is a method for verifying the dominance of the fast component in the initial part of the quartz OSL signal from small aliquots and single grains. The fast ratio is calculated by taking the initial OSL signal minus a background (fast component), which is then divided by an assessment of the contribution from the medium component minus a background (Duller, 2012). Essentially, the fast ratio compares the proportion of fast to medium components within the OSL signal. Samples with a fast ratio value greater than 20 are believed to exhibit a dominant fast component. Therefore, any aliquots in this thesis with a fast ratio less than 20 were rejected.

Stimulation powers and photo ionisation cross-sections of the measurement equipment are incorporated into the calculation. This ensures that the ratio is transferable between different samples and readers, thus making signal comparisons straightforward (Durcan & Duller, 2011). Where comparison of the natural and regenerative dose signals from the same sample produces discrepancies, the fast ratio can also be used to suggest the presence of signals from thermally unstable traps (Durcan & Duller, 2011).

In this thesis, the fast ratio represents a rapid method that was used to screen the OSL signals in an attempt to remove any aliquots that did not display a dominant fast component.

5.2.1.6 Signal visibility

With only a small proportion of the grains likely to provide a luminescence signal it was important to only utilise those grains capable of producing a strong signal. As mentioned previously, bright grains are preferred to inherently dim grains as uncertainty is less likely to be associated with the counting statistics. Therefore, following the rejection criteria outlined in Jacobs et al. (2008a), any weak signals exhibiting a T_n less than three times the instrumental background were rejected.

5.2.1.7 Removal of saturated signals

While the upper age limit of OSL dating is generally thought to be c. 200 ka (Section 3.1), this will vary between samples and is dependent on the saturation level of the mineral. The rate at which saturation is reached will depend on dose saturation properties and environmental dose rate for each quartz grain. Consequently, samples exhibiting high saturation characteristics that have been exposed to low environmental dose rates will provide the longest dateable age range.

Following Singarayer and Bailey (2003), assuming a single trap is responsible for the fast component, the OSL signal can be fitted with the single saturating exponential function:

$$I = I_0 + I_{max}\left(1 - exp^{-D/Do}\right)$$

Equation 2 (above). Where I is the OSL intensity due to dose D, I_0 is the luminescence intensity at 0 dose, I_{max} is the maximum luminescence intensity, and D_0 is the dose level that is characteristic of the dose response curve.

Using this single saturating exponential function, Bailey (2001) suggests that it is possible to accurately determine D_e values that are close to a dose value of $2D_0$. Measurements beyond this limit are thought to generate larger, asymmetric uncertainties, and are thus thought to reflect a saturated signal (Wintle & Murray, 2006). Typical published values of D_0 vary from 55 Gy (Roberts & Duller, 2004) to about 190 Gy (Singarayer & Bailey, 2004).

In this thesis, two criteria were initially used to determine which OSL signals appeared to be in saturation. Firstly, using the classification of Yoshida et al. (2000), any "class 3" grains (those which exhibit a natural signal that is unable to intercept the growth response curve) were removed in the initial screening of the data (Section 5.2.1.4.). The second criteria (used following the application of the rejection criteria discussed in the previous sections) involved using $2D_0$ as an upper limit for D_e. It has been suggested that any grains or aliquots displaying a $D_e > 2D_0$ are saturated, and should therefore removed from further analysis. As discussed in Chapter 9, however, investigations into the $2D_0$ rejection criterion suggested that it was not appropriate for the samples in this thesis.

In some instances, where high laboratory doses are required for the construction of the dose response curve, several authors (including Murray et al. (2008) and Pawley et al. (2008)) report that dose response curves are better fitted with an exponential plus linear function. For samples in this thesis that passed all rejection criteria, but failed the application of $2D_0$, an exponential plus linear function has been applied. It remains unclear why some samples using high laboratory doses require an exponential plus linear function. Investigations into the processes responsible for the additional linear component are still ongoing (Lowick et al., 2010).

5.2.2 Testing the appropriateness of the SAR protocol

In the following sub-sections, the tests utilised to identify the most appropriate range of regenerative doses and preheat conditions for age determinations of each sample are outlined. The application of the dose recovery test, suggested by Wintle and Murray (2006), is also discussed below.

5.2.2.1 Initial D_e Test

In order to accurately determine the equivalent dose of a sample using the SAR protocol, it is necessary to irradiate and measure regenerative dose points that bracket the D_e. At sites where other independent age controls are available, it may be possible to estimate the highest regenerative dose point necessary to encompass the natural signal. However, in the majority of sites, the age of a particular sample is not known, and therefore it is necessary to investigate the doses required prior to commencement of the main OSL measurement sequence.

In this study, initial tests were performed on five aliquots of a sample (generated using a medium sized mask), using an SAR measurement sequence consisting of regenerative doses of 20, 60, 100, 200, 300 and 400 Gy. By measuring a small number of aliquots in this way, it was possible to modify the SAR protocol so that the regenerative doses used in each measurement were applicable to the sample being measured.

5.2.2.2 Preheat Plateau Test

During measurement of OSL it is not possible to select only those traps that are thermally stable over geological time (Lian, 2007). As explained by Wintle and Murray (2006), following optical bleaching of a sample in the laboratory an observable signal is commonly detected when the OSL signal is subsequently measured. This phenomenon, often referred to as thermally transferred charge, is a relic of the preheat administered immediately prior to stimulation. Thermal transfer occurs when charge that has been thermally released from a relatively shallow (i.e. exhibiting a lower thermal stability), optically insensitive trap during preheating, and is subsequently recaptured by a deeper, geologically stable, OSL trap (Wintle & Murray, 2006). Smith et al. (1986) were the first to identify recuperation (i.e. a thermally transferred signal seen at a zero dose point) of charge from the 110 °C TL peak into the OSL trap (Wintle & Murray, 2000). Thus, to avoid this recuperation, grains are usually held at 125 °C during stimulation (Murray & Wintle, 2003) (Section 5.1). It is believed that the traps responsible for the thermal transfer observed at higher preheat temperatures lie in the range of 200-300 °C (Wintle & Murray, 2006). Consequently, in an attempt to remove and redistribute electrons from thermally unstable traps that may have become filled during laboratory irradiation, samples are preheated. By testing the response of aliquots to a range of preheat temperatures prior to measurement in a preheat

plateau test, it is possible to identify the most suitable preheating regime for the main SAR sequence. Capable of emptying any light sensitive shallow traps which may be filled during laboratory irradiations, this preheating reduces any negative impacts of thermal transfer (Wintle & Murray, 2006). Variations in the inherent properties of a single grain, such as its opacity, chemical composition, mineralogical structure, sensitivity and light absorption capabilities, can result in the differing luminescence signals emitted by a sample (Adamiec, 2005; Duller et al., 1999). As a result, preheat plateau tests must be completed for each site to identify the most suitable preheat conditions, and subsequently account for such variation and produce optimal age determinations for every sample (Rhodes, 2011).

5.2.2.3 Dose Recovery Test

As the largest sensitivity change appears to occur following the initial heating of a sample (Armitage et al., 2000), the dose recovery test is designed to identify whether the first sensitivity measurement is appropriate to the preceding natural signal (Wintle & Murray, 2006). Any sensitivity change that occurs during the measurement of the natural signal cannot be detected by the subsequent test dose measurement, and will therefore not be identified by the recycling ratio test. Accordingly, within the laboratory, the unheated sample is fully bleached prior to being irradiated with a known dose. The sample is then measured using a standard SAR measurement sequence. This allows the calculation of a D_e for the aliquot, and the ratio of the OSL resulting from this known dose to the known dose is calculated. Samples that produce a dose recovery ratio (measured dose / known dose) consistent with unity demonstrate the ability to return a known D_e, suggesting that the SAR protocol is working correctly (Wintle & Murray, 2006). It is imperative for the success of the dose recovery test that the laboratory dose delivered gives rise to a trapped charge as close as possible to the palaeodose. Should significant variations be apparent between the two, then the D_e determination cannot be assumed to be an accurate reflection of the palaeodose (Bailey, 2004; Bailey et al., 2005).

5.2.2.4 The combined Dose Recovery Preheat Plateau Test

The dose recovery preheat plateau test represents a method for assessing the performance of the SAR protocol under a range of preheat temperature regimes. 24 aliquots from each

sample were prepared by a controlled optical bleaching of the natural dose (40 s at 20 °C, followed by a 10 ks pause, and then a second 40 s bleach at 20 °C), followed by the application of a known laboratory dose. The laboratory dose used was as close to the natural D_e as possible, and was identified following the initial D_e measurements. Splitting the aliquots into groups of three, the D_e values were measured using the standard SAR method under a range of preheating regimes. Following Armitage et al. (2011), Preheat 1 (PH1) temperatures of 160-280 °C at 20 °C intervals, held for 10 s, all with a 160 °C, 0 s Preheat 2 (PH2), and a 260 °C PH1 with a 220 °C PH2, both held at temperature for 10 s were used. Essentially this test provides an ability to simultaneously test for the complications discussed in the previous two sub-sections by combining the preheat plateau test and dose recovery test into a single measurement. Due to the low availability of quartz from the samples measured in this thesis, utilising this combined method reduced the volume of quartz used in the internal tests.

5.3 Measurement of the equivalent dose

Optical stimulation of all aliquots (including fine grains) and single grains during standard measurements in this thesis were completed at 125°C for 40 seconds and 1 second respectively. Samples were heated at a rate of 5 °C/s and held at 125 °C for 10 s to account for the thermal lag between the heater plate (monitored by the instrument using a thermocouple) and the sample. The 40 s and 1 s measurements were split into 250 and 60 channels respectively, allowing the OSL signal from specific sections of the OSL decay curve to be isolated and analysed. A background signal obtained from the last 4 s (channels 225 - 250) and 0.3 s (channels 40-55) of each small aliquot and single-grain signal was subtracted from the corresponding main luminescence signal produced during the first 0.32 s (channels 1-2) and 0.3 s (channels 6-20) of stimulation. OSL response curves from all samples measured exhibited a rapid initial decay, indicative of a dominant fast component.

A 5 Gy test dose was used for all measurements in this thesis. All OSL measurements reported in this thesis were completed on one of two Risø TL/OSL-DA-15 or a Risø TL/OSL-DA-20 automated luminescence system equipped with a $^{90}Sr/^{90}Y$ beta source. The Risø mounted β sources were calibrated following the methods of Armitage and Bailey (2005) for single aliquots and of Armitage et al. (2011) for single grains. The Risø mounted β source used for single grain measurement gave a mean dose of ~6 Gy/min. Due to the spatial inhomogeneity of beta emitters across the active face of our $^{90}Sr/^{90}Y$ beta source, an

individual calibration value was calculated for each position on the single grain disc. As reported in Armitage et al. (2011), 4,800 grains of calibration quartz were measured, yielding 1,815 dose rate estimates (18±3 per grain position). The results suggested that dose rates for individual grain positions differed from the mean single grain disc calibration by up to 20%. All single grain discs were placed into the Risø instrument at the same angle relative to the $^{90}Sr/^{90}Y$ beta source, and rotated 0.04±0.03° per measurement cycle within the single aliquot regenerative-dose method. Consequently it was possible to calculate the grain position correction factors shown in Table 5.2. These values were used to accurately correct for the effects of inhomogeneity in our $^{90}Sr/^{90}Y$ beta source. Position-corrected equivalent doses were used in all single grain age calculations.

	1	2	3	4	5	6	7	8	9	10
1	1.081	1.068	1.025	1.005	1.024	0.968	0.927	0.886	0.827	0.788
11	1.095	1.099	1.092	1.062	1.043	1.011	0.943	0.900	0.859	0.790
21	1.132	1.160	1.111	1.084	1.023	1.067	0.936	0.926	0.863	0.827
31	1.165	1.130	1.143	1.066	1.086	1.006	0.981	0.926	0.868	0.840
41	1.132	1.168	1.106	1.139	1.068	1.046	0.971	0.931	0.864	0.867
51	1.172	1.181	1.125	1.099	1.085	1.024	0.998	0.963	0.882	0.864
61	1.179	1.135	1.117	1.105	1.056	0.996	1.012	0.952	0.906	0.828
71	1.116	1.108	1.128	1.050	1.042	1.007	1.022	0.921	0.908	0.867
81	1.134	1.104	1.133	1.059	1.074	1.006	0.973	0.927	0.891	0.854
91	1.093	1.083	1.092	1.047	1.029	1.007	0.972	0.942	0.896	0.825

Table 5.2. Grain position correction values (after: Armitage et al., 2011) used to correct for the effects of inhomogeneity in the $^{90}Sr/^{90}Y$ beta source on single grain measurements in this thesis.

Single aliquot measurements were made using a blue LED (470±30nm) stimulation source typically operating at 60 mW/cm^2, while a green laser (532 nm), operating at 10 W/cm^2, was used to stimulate individual grains during single-grain measurements. A bialkali photomultiplier tube (EMI 9235QB) coupled with a 7.5mm Hoya U-340 filter was used to detect the photons. Infrared diodes were used to stimulate the aliquots for 40 seconds at 20°C during IR Depletion tests (Bøtter-Jensen et al., 2003).

5.4 Calculation of a sample D_e

All OSL data generated in this thesis was fitted and analysed using Luminescence Analyst version 3.22b, developed by Prof. Geoff Duller in 2005. Small aliquot (including fine grains)

and single-grain growth curves were fitted using the "exponential plus linear fit" function. Monte Carlo simulation was used to estimate the uncertainty of the individual D_e values based on counting statistics and instrumental error (Duller, 2007).

Small aliquot and single-grain D_e values that passed all of the rejection criteria discussed above were accepted (assumed to be devoid of any luminescence characteristics likely to produce erroneous age estimates), while a record was kept of the number of rejected grains along with the reason for their rejection.

5.5 Summary

- The single-aliquot regenerative-dose (SAR) protocol, introduced by Murray and Wintle (2000), represents a protocol with the ability to check and correct for sensitivity change.
- An SAR protocol involves the measurement of a natural signal followed by a number of luminescence measurements from a series of increasing laboratory irradiations (regenerated doses). The response of OSL to a fixed test dose administered following each natural and regenerated dose is measured to monitor any changes in sensitivity. Dividing the natural and regenerated luminescence intensities by their respective test dose intensities produces a sensitivity-corrected luminescence response.
- A series of screening protocols (also referred to as rejection criteria) applied to all datasets in this thesis have been discussed. These include the recycling ratio, the IR depletion ratio, the recuperation test, an assessment of the natural interception of the growth curve, the fast ratio, an assessment of signal visibility, and the use of D_0 to identify saturation of the signal.
- The appropriateness of the SAR protocol measurement conditions were also assessed via the completion of a number of tests. An initial D_e test assesses the appropriateness of the range of regenerative doses used (i.e. will the growth curve generated incorporate the natural signal). Finally, the ability of the SAR protocol to recover a known dose under a range of preheat conditions was assessed via the completion of a dose recovery preheat plateau.

Chapter 6 - Calculating the environmental dose rate

6.1 Introduction

The rate at which a mineral absorbs energy as a result of exposure to ionising radiation in the natural environment is known as the environmental dose rate (D_r). Since the parent isotopes of the decay series responsible for the environmental dose rate (^{238}U, $4.47x10^9a$; ^{235}U, $7.04x10^8a$; ^{232}Th, $1.41x10^{10}a$; ^{40}K, $1.25x10^9a$ (Aitken 1985)) are long-lived relative to the timescales covered by OSL dating, D_r is effectively constant throughout the burial period (Aitken, 1998; Bailey, 2004; Lian, 2007; Murray & Olley, 2002). Accurate determination of the D_r is essential for the calculation of a luminescence age, since it is the denominator in the age equation (Equation 1, Section 3.3).

6.1.1 Internal contributions to the D_r

Natural radiation affecting a sample can include both external and internal components. Internal components are derived from radioisotopes within the grains themselves. Sutton and Zimmerman (1976) suggested that up to 5% of the total radiation dose could originate from an internal alpha component, following their discovery of trace amounts of U and Th in quartz minerals. However, further research by Mejdahl (1987) investigating the potential dose contributions of the internal alpha dose of quartz, suggested that contributions were in fact likely to be negligible. More recent studies have included a small internal alpha dose rate (e.g. Jacobs et al., 2008a assumed 0.033 ± 0.008 Gy/ka), though Vandenberghe et al. (2008) have suggested that radioisotope concentrations in quartz separates actually derive from imperfect mineral separation. In the present case, the internal dose rate has been assumed to be zero, based upon the reasoning of Vandenberghe et al. (2008). Where the external radiation levels are low, it is considered more important to check the internal contribution (Aitken, 1998).

6.1.2 External contributions to the D_r

External sources of radiation are derived from radioactive isotopes within the surrounding sediment matrix, in addition to a small contribution from cosmic radiation. The external dose rate from the radioactive isotopes is comprised of several radiation types, including

alpha particles, beta particles, and gamma rays; each able to penetrate different sediment thicknesses (Figure 6.1) (Aitken, 1998). Mejdahl (1979) reports that approximately one third of radiation received can be attributed to gamma radiation, while two thirds can be attributed to beta particles emitted by U, Th and K series.

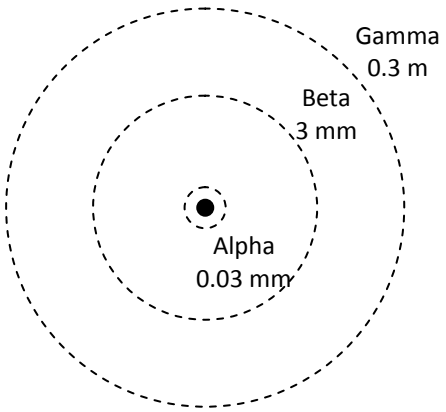

Figure 6.1. Maximum spheres of influence (not to scale) for alpha, beta and gamma radiation surrounding a silt-sized grain of sediment (after Aitken, 1998).

Alpha particles have short ranges, and are only able to penetrate ~0.03 mm. This is due to their heavily ionizing nature, which causes them to lose their energy rapidly (Aitken, 1998). As a result, it is possible to remove the alpha component from the coarse Arabian mineral grains used in this study (180-212 µm) during sample preparation, via the removal of the alpha irradiated outer-rind (~ 10 µm) with HF acid. Consequently, only the less strongly ionising beta and gamma contributions were used in the calculation of D_r. The Libyan samples only yielded finer grained material (4-11 µm, 60-90 µm, and 90-125 µm) and so it was not possible to HF etch these samples. Quartz was extracted using H_2SiF_6 treatment instead, which does not significantly corrode the outer layer of quartz grains. Consequently, the alpha, beta and gamma contributions were taken into consideration when calculating the D_r for the Libyan samples in this study.

Beta particles and gamma rays have much larger penetration ranges than alpha particles (~3 mm and ~30 cm respectively). As the sphere of gamma radiation penetration is thought to be 30 cm, where possible, all samples in this study were taken at least 30 cm away from any lithostratigraphic boundaries in an attempt to avoid inhomogeneity of the D_r.

6.1.3 Cosmic radiation contributions

Cosmic radiation typically contributes less than 10% to the overall D_r and can be split into two main components. The soft component is fully absorbed within the top 50 cm of sediment, while the hard component (which consists of muons – particles similar to electrons) is much less readily absorbed. Consequently, for the calculation of D_r, the hard component is of primary interest (Prescott & Hutton, 1988). With increased depth below the Earth's surface, the intensity of cosmic rays (and thus their contribution to the D_r) diminishes in relation to the density of the material it is passing through. Similarly, latitude and elevation can affect the cosmic ray intensity (Prescott & Hutton, 1988, 1994). Further information concerning calculation of the cosmic dose rate can be located in Section 6.5.

6.2 Standard method for D_r calculation

To calculate the rate at which energy has been absorbed in a mineral, it is necessary to take into consideration the rate at which energy is being deposited by the various forms of radiation (Aitken, 1985). The environmental D_r is therefore calculated by combining the alpha, beta, gamma and cosmic dose rate contributions (Appendix 2). Uranium, Thorium and Potassium concentrations were measured using ICP MS, ICP AES, and in-situ gamma spectrometry. The contribution of U (ppm), Th (ppm) and K (%) concentrations were converted into dry alpha, beta and gamma dose rates using the conversion factors of Adamiec and Aitken (1998). Source calibration errors from Armitage and Bailey (2005) and a standard 10% error on all ICP data were applied to all D_r calculations.

6.3 Limitations and uncertainties associated with calculation of the D_r

Variations in the D_r may arise as a result of the nature of the sediment, i.e. the water and organic material content of a sample, mineral in-homogeneity, secular disequilibrium in the U and Th decay chain, and the depth of the sample below the Earth's surface (discussed further in Section 6.5) (Lian, 2007).

6.3.1 Mineral in-homogeneity

Where radioisotopes vary spatially within a sediment, spatial variations in the levels of ionising radiation intensity may also occur. Specifically, beta particles (which only ionise over c. 3 mm) when non-uniformly distributed within a sediment can produce significant dose rate heterogeneity at a grain to grain scale. As the D_r is assumed to be constant, both spatially and temporally, these variations can have a significant effect on the overall calculation of the dose rate for single grain samples (Nathan et al., 2003). Where small aliquots are measured, the distribution of radioisotopes over the bulk sample has no effect.

6.3.2 Radioactive disequilibrium

Further complications include the potential occurrence of radioactive disequilibrium. This occurs when a parent or daughter in the ^{232}Th or ^{238}U decay chain is moved into or out of a system, leading to a parent/daughter activity ratio different from unity. During the calculation of the OSL ages in this study, it was assumed that the decay series remained in secular equilibrium over the burial period (Olley et al., 1996).

6.3.3 Attenuation via water

The presence of water within the interstices of a sediment matrix leads to a reduction in the environmental dose rate by absorbing radiation that would otherwise have been absorbed by mineral grains. Consequently, water content must be taken into consideration when calculating the D_r to avoid underestimation of the final age (Lian, 2007). Whilst it is possible to measure the current moisture content of a sample (see Section 4.4.), it is the average water content over the entire burial period that must be calculated. For example, a sample which is now dry may have originally been deposited as part of a lacustrine sediment, and therefore may have been saturated with water for some portion of its burial history. Sedimentology at the sampling sites can be used to interpret the transport and depositional processes responsible for the formation of the different sedimentary sequences over time. Consequently, this information can be used to infer how the water content of a sediment may have changed in the past (i.e. water lain deposits overlain by aeolian sediments suggests the reduction of water in the environment). Accordingly, this

information was used to determine whether or not the present day measurements appeared to appropriately represent the water content over the entire burial period.

6.4 Measurement of the environmental dose rate

This section outlines the methods utilised for calculating the alpha, beta and gamma contributions to the D_r. Two methods were used to calculate the radioisotope concentration of the sediments measured in this study. Firstly, inductively coupled plasma mass spectrometry (ICP MS) was used to measure U and Th, while atomic emission spectroscopy (ICP AES) was used to measure K concentrations. In addition, for some samples, in-situ gamma spectrometry was used. Owing to the inhomogeneous nature of some of the sampled sediments, measurements were made using both methods where possible. When both methods were used on a single sample, ICP-MS/AES measurements were used to calculate external alpha and beta dose rates, while in-situ gamma-spectrometry measurements were used to calculate the gamma dose rate. Where only one technique was used on a sample, radioisotope concentrations derived using this technique were used to determine the alpha, beta and gamma dose rates.

6.4.1 ICP MS and ICP AES

ICP MS/AES were used to quantify the alpha beta contribution from U, Th and K in the surrounding sediment matrix. Measurements were performed on dried, homogenised samples taken from the light exposed material removed from the outside of each sample. Sample preparation and measurement was completed by the ICP AES and ICP MS facilities at Royal Holloway, University of London. Using standard methods, ICP MS and ICP AES measurements were used to measure the K and U / Th components respectively. Samples were prepared using a dissolution lithium metaborate fusion procedure. Analytical runs included measurements of calibration standards to monitor the accuracy of the measurements.

6.4.2 In-situ gamma spectrometry

In-situ determinations of gamma ray contributions to the D_r were made using a portable gamma spectrometer, which had been calibrated against the Oxford concrete blocks (Rhodes & Schwenninger, 2007). Direct measurement of the sediment allows any in-situ spatial heterogeneity in gamma contribution around the sample to be measured. Gamma ray contributions from the U, Th and K decay series produced scintillations in the NaI crystal, which were converted into electrical pulses by a photomultiplier tube (Figure 6.2)(Aitken, 1985).

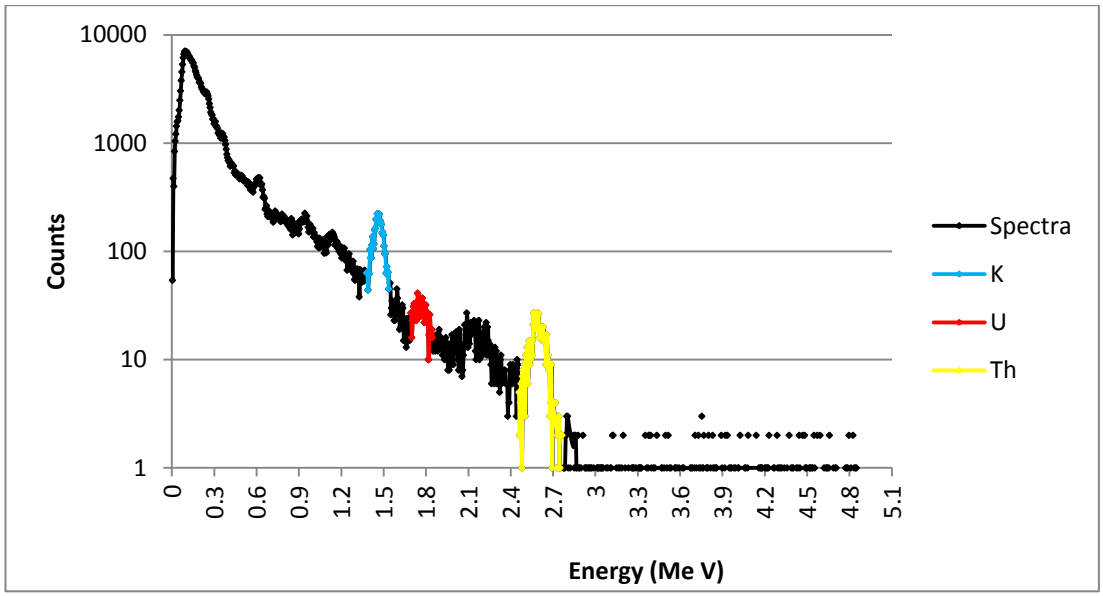

Figure 6.2. A field-gamma energy spectrum for OSL 21, Chersa Beach. Pulses were recorded over a measurement period of 3600 s. The K (1.38-1.53 MeV, blue), U (1.69-1.84 MeV, red), and Th (2.46-2.76 MeV, yellow) elemental contributions are identified as photopeaks observed within the gamma spectrum. By integrating the count associated with each photopeak, and applying the relevant calibration and stripping factors, the elemental contributions can be calculated (Aitken, 1985, Appendix L).

It was not possible to obtain field gamma spectrometer measurements for some of the samples due to the cemented nature of the sediments. Consequently, the gamma contribution for these samples was calculated using radioisotope concentrations from the ICP MS / AES data. Following Armitage et al. (2011) and Bretzke et al. (2013), it is possible that this approach may provide an overestimation of the gamma dose rate for some

samples. For the FAY-NE1 samples measured in their study, the total gamma dose rates determined using ICP-MS/AES radioisotope concentrations were c. 10% higher than those calculated using field gamma-spectrometer. However, due to the homogenous nature of the Libyan sediments lacking gamma spectrometry measurements in this study, the ICP-MS/AES measurements were deemed appropriate for calculation of the gamma contribution in this instance.

6.5 Water Attenuation

For reasons discussed in Section 6.3.3., it is necessary to correct beta and gamma dose rates for the effect of mean burial water content. Dry beta and gamma dose rates have been corrected for water content using Equation 3 and Equation 4 respectively:

(Equation 3)

$$D\beta = \frac{D\beta dry}{1 + (1.25\mathrm{W})}$$

(Equation 4)

$$D\gamma = \frac{D\gamma dry}{1 + (1.14\mathrm{W})}$$

where Dβ refers to the corrected "wet" beta dose rate, Dγ refers to the corrected "wet" gamma dose rate, and W refers to the water content (%) of the sample over the burial period.

In this study, the majority of water contents are based on the present day values. As such, the water contents of the Libyan samples varied between 2% and 23% (see Table 6.1), whilst for the Arabian samples a standard water content value of 5% was utilised (this was thought to encompass the full range of likely burial conditions (Armitage et al., 2011). Due to the uncertainty associated with calculating an "average" water content value for the entire burial period, an error of ± 5% was associated with the water content values generated (Aitken, 1998).

Site	Sample number	Water Content (%)	Site	Sample number	Water Content (%)
Al Marj (EM 4)	OSL 1	2 ± 5	Chersa Beach	OSL 22	3 ± 5
Al Marj (EM 4)	OSL 3	6 ± 5	Chersa Beach	OSL 23	3 ± 5
Lh' Atrun	OSL 7	4 ± 5	Chersa Beach	OSL 24	12 ± 5
Lh' Atrun	OSL 8	10 ± 5	Chersa Beach	OSL 25	13 ± 5
Al Marj (EM 4)	OSL 9	9 ± 5	Haua Fteah	HF10	23 ± 5
Al Marj (EM 4)	OSL 10	12 ± 5	Haua Fteah	HF09	26 ± 5
Al Marj (EM 4)	OSL 11	11 ± 5	Hajj Creiem	Hajj Creiem	2 ± 5
Wadi Derna	OSL 17	5 ± 5	Al Marj core	OSL 28	18 ± 5
Wadi Derna	OSL 18	3 ± 5	Al Marj core	OSL 29	19 ± 5
Hajj Creiem	OSL 19	3 ± 5	Al Marj core	OSL 30	17 ± 5
Hajj Creiem	OSL 20	4 ± 5	Al Marj core	OSL 31	19 ± 5
Hajj Creiem	OSL 21	12 ± 5			

Table 6.1. Present day water content values for the Libyan samples.

6.6 Calculating the cosmic dose contribution

Calculations of the cosmic ray dose rates were completed using the COSMIC programme developed by Dr Robert Clark at Durham University. Cosmic ray contributions depend primarily on the thickness and density of the overlying sediments, and to a lesser extent upon the sample location longitude, latitude and altitude. Data relevant to the calculation of cosmic dose rates are presented in Table 6.2.

Longitude and latitude must be considered as the Earth's magnetic field causes cosmic contributions to be greater with proximity to the poles (specifically at latitudes greater than 60 ° N/S), where shielding is lowest (Duller, 2008a). Altitude must also be taken into consideration, but in practice only causes significant variations at heights greater than 500 m OD.

The thickness and density of the material overlying the sample is the most significant factor to be considered. At mid latitudes Duller (2008) reports that the cosmic dose is c. 0.2 Gy/ka at a depth of 30 cm, however, at a depth of 10 m it falls to *c* 0.07Gy/ka. In situations

where the thickness of the overburden may have changed dramatically over time, additional considerations were given to the cosmic contribution. At Jebel Faya (Arabia) and Haua Fteah (Libya), the presence of a rock shelter / cave provided a more complex cosmic contribution scenario. As a result the cos2 Φ- zenith angular distribution of cosmic rays protocol reported in Smith et al. (1997) was applied (Appendix 2).

A systematic error of ± 10% was applied to each cosmic dose rate calculation.

6.7 Calculating the sample D_r

Water content, depth, and radioisotope values for every sample in this thesis are reported in Table 6.2. The environmental dose rate is comprised of the sum of the alpha (where applicable), beta, gamma and cosmic dose rate contributions. The conversion factors of Adamiec and Aitken (1998) were used to convert the contribution of U (ppm), Th (ppm) and K (%) concentrations (obtained via ICP MS, ICP AES and in-situ gamma spectrometry) into dry alpha, beta and gamma dose rates. Alpha and beta dose rates have been corrected for grain size (Mejdahl, 1979) and water content (Aitken, 1985). Gamma dose rates have been corrected for water content (Aitken, 1985) only. Alpha efficiency factors from Rees-Jones (1995) have also been applied to alpha dose rates. Errors from Murray and Olley (2002) associated with conversion factors, dosimetry calibration, alpha attenuation, beta attenuation and water content calculation have been propagated in quadrature through the environmental D_r calculation. Source calibration errors (Armitage and Bailey, 2005) and a standard 10% error on all ICP data were also applied to the D_r calculations. Total environmental dose rates used in age calculations in this thesis are presented in Table 6.3 A worked example of the D_r calculation is presented in Appendix 2.

Sample ID	Water Content	Gamma			ICP			Cosmic					
		K (%)	U (ppm)	Th (ppm)	K (%)	U (ppm)	Th (ppm)	Lat (°)	Long (°)	Elevation (m)	Depth (cm)	Value (Gy/ka)	Cos2Theta (Gy/ka)
HF09	0.23 ± 0.02	X	x	x	2.16 ± 0.21	2.58 ± 0.26	12.83 ± 1.28	32	22	60	750	0.09	0.02
HF10	0.26 ± 0.03	X	x	x	1.83 ± 2.30	2.34 ± 0.23	10.40 ± 1.04	32	22	60	630	0.10	0.02
OSL 1	0.02 ± 0.001	X	x	x	1.47 ± 0.15	3.03 ± 0.30	13.04 ± 1.30	32	21	290	440	0.11	X
OSL 3	0.60 ± 0.003	1.09 ± 0.04	2.21 ± 0.16	11.24 ± 0.65	1.40 ± 0.14	2.50 ± 0.25	14.18 ± 1.42	32	21	290	190	0.16	X
OSL 7	0.04 0.002	X	x	x	0.07 ± 0.01	1.30 ± 0.13	0.30 ± 0.03	32	22	0	1130	0.06	X
OSL 8	0.10 0.01	X	x	x	0.58 ± 0.06	0.87 ± 0.09	4.30 ± 0.43	32	22	0	800	0.08	X
OSL 9	0.09 ± 0.01	0.86 ± 0.03	2.01 ± 0.15	9.31 ± 0.56	1.42 ± 0.14	2.74 ± 0.27	14.30 ± 1.43	32	21	290	340	0.13	X
OSL 10	0.12 ± 0.01	0.86 ± 0.03	2.11 ± 0.15	9.50 ± 0.56	1.54 ± 0.15	2.83 ± 0.28	14.20 ± 1.43	32	21	290	440	0.11	X
OSL 11	0.11 ± 0.01	1.06 ± 0.04	2.25 ± 0.16	10.81 ± 0.64	1.69 ± 0.17	3.06 ± 0.31	15.80 ± 1.58	32	21	290	395	0.12	X
OSL 17	0.05 ± 0.003	X	x	x	1.97 ± 0.20	2.29 ± 0.23	13.10 ± 1.31	32	22	120	4000	0.01	X
OSL 18	0.03 ± 0.002	X	x	x	1.42 ± 0.14	2.79 ± 0.28	7.60 ± 0.76	32	22	120	338	0.13	X
OSL 19	0.03 ± 0.002	0.87 ± 0.03	2.94 ± 0.22	3.10 ± 0.37	1.13 ± 0.11	2.22 ± 0.22	9.40 ± 0.94	32	22	100	105	0.18	X
OSL 20	0.04 ± 0.002	0.87 ± 0.03	2.94 ± 0.22	3.10 ± 0.37	1.14 ± 0.11	2.24 ± 0.22	8.65 ± 0.87	32	22	100	140	0.18	X
Hajj Creiem	0.02 ± 0.001	0.87 ± 0.03	2.94 ± 0.22	3.10 ± 0.37	1.15 ± 0.11	2.50 ± 0.25	7.90 ± 0.79	32	22	100	130	0.17	X
OSL 21	0.12 ± 0.01	0.42 ± 0.02	0.95 ± 0.08	2.35 ± 0.17	0.66 ± 0.06	2.09 ± 0.20	2.20 ± 0.22	32	22	0	540	0.10	X
OSL 22	0.03 ± 0.002	X	x	x	0.10 ± 0.01	2.31 ± 0.23	6.94×10^{-3} *	32	22	0	170	0.16	X
OSL 23	0.03 ± 0.002	X	x	x	0.10 ± 0.01	2.31 ± 0.23	6.94×10^{-3} *	32	22	0	450	0.11	X
OSL 24	0.12 ± 0.01	0.74 ± 0.03	1.14 ± 0.09	4.55 ± 0.30	1.05 ± 0.10	1.71 ± 0.17	5.20 ± 0.52	32	22	0	550	0.10	X
OSL 25	0.13 ± 0.01	X	x	x	0.18 ± 0.02	1.30 ± 0.13	1.60 ± 0.16	32	22	0	500	0.11	X
OSL 28	0.18 ± 0.02	X	x	x	2.07 ± 0.20	3.03 ± 0.30	12.80 ± 1.28	32	21	290	157.5	0.16	X
OSL 29	0.19 ± 0.02	X	x	x	2.08 ± 0.20	2.54 ± 0.25	13.90 ± 1.39	32	21	290	318.5	0.14	X
OSL 30	0.17 ± 0.02	X	x	x	1.80 ± 0.18	2.27 ± 0.23	13.40 ± 1.34	32	21	290	1021.5	0.06	X
OSL 31	0.19 ± 0.02	X	x	x	1.81 ± 0.18	2.65 ± 0.27	13.00 ± 1.30	32	21	290	298.5	0.14	X

Sample ID	Water Content	Gamma			ICP			Cosmic					
		K (%)	U (ppm)	Th (ppm)	K (%)	U (ppm)	Th (ppm)	Lat (°)	Long (°)	Elevation (m)	Depth (cm)	Value (Gy/ka)	Cos2Theta (Gy/ka)
Faya NR1	0.05 ± 0.00	0.58 ± 0.04	1.06 ± 0.10	0.87 ± 0.08	0.73 ± 0.07	0.90 ± 0.09	1.20 ± 0.12	25	56	180	45	0.205	0.19
Faya NR2	0.05 ± 0.00	0.42 ± 0.04	0.90 ± 0.09	0.42 ± 0.04	0.71 ± 0.07	1.00 ± 0.10	1.20 ± 0.12	25	56	180	85	0.181	0.16
Faya NR3	0.05 ± 0.00	0.18 ± 0.02	0.82 ± 0.10	0.11 ± 0.01	0.74 ± 0.07	1.00 ± 0.10	1.80 ± 0.18	25	56	180	155	0.165	0.15
Faya NR4	0.05 ± 0.00	0.23 ± 0.02	1.01 ± 0.11	0.32 ± 0.03	0.47 ± 0.05	1.00 ± 0.10	0.90 ± 0.09	25	56	180	40	0.209	0.18
Faya NR6	0.05 ± 0.00	0.20 ± 0.02	0.78 ± 0.09	0.12 ± 0.01	0.44 ± 0.04	0.90 ± 0.09	0.90 ± 0.09	25	56	180	95	0.178	0.15
Faya NR7	0.05 ± 0.00	0.31 ± 0.03	0.72 ± 0.08	0.52 ± 0.05	0.56 ± 0.06	0.80 ± 0.08	1.60 ± 0.16	25	56	180	195	0.157	0.09
Faya NR8	0.05 ± 0.00	0.25 ± 0.02	0.81 ± 0.09	0.37 ± 0.04	0.70 ± 0.07	1.70 ± 0.17	1.70 ± 0.17	25	56	180	235	0.15	0.13
Faya NR9	0.05 ± 0.00	0.23 ± 0.02	0.83 ± 0.09	0.28 ± 0.03	0.70 ± 0.07	1.10 ± 0.11	1.70 ± 0.17	25	56	180	290	0.14	0.13

Table 6.2. Depth, radioisotope and water content values used for the calculation of the sample environmental dose rates. The Cos2Theta value represents the cosmic dose rate calculated following the application of the cosmic correction factor (Appendix 2).

*** An error of ± 3.94 x 10^{-4} was applied to the OSL 22 and OSL 23 Th values.**

Sample ID	Alpha dose rate (Gy/ka)	Beta dose rate (Gy/Ka)	Gamma dose rate (Gy/ka)	Cosmic dose rate (Gy/ka)	Total Environmental dose rate (Gy/ka)
HF09	0.07 ± 0.03	1.78 ± 0.15	1.13 ± 0.08	0.02 ± 2 x 10^{-3}	3.00 ± 0.17
HF10	0.06 ± 0.03	1.47 ± 0.13	0.93 ± 0.06	0.02 ± 2 x 10^{-3}	2.48 ± 0.14
OSL 1	0.08 ± 0.04	1.77 ± 0.13	1.29 ± 0.08	0.11 ± 0.01	3.25 ± 0.16
OSL 3	0.07 ± 0.03	1.60 ± 0.12	0.99 ± 0.04	0.16 ± 0.02	2.82 ± 0.13
OSL 7	0.13 ± 0.06	0.24 ± 0.02	0.17 ± 0.02	0.06 ± 0.01	0.59 ± 0.07
OSL 8	0.09 ± 0.04	0.61 ± 0.05	0.40 ± 0.03	0.08 ± 0.01	1.18 ± 0.07
OSL 9	0.07 ± 0.03	1.59 ± 0.12	0.80 ± 0.04	0.13 ± 0.01	2.59 ± 0.13
OSL 10	0.07 ± 0.03	1.63 ± 0.13	0.80 ± 0.04	0.11 ± 0.01	2.61 ± 0.13
OSL 11	0.08 ± 0.03	1.8 ± 0.14	0.91 ± 0.04	0.12 ± 0.01	2.91 ± 0.15
OSL 17	0.06 ± 0.03	1.97 ± 0.16	1.29 ± 0.09	0.01 ± 0.001	3.34 ± 0.19
OSL 18	0.07 ± 0.03	1.56 ± 0.12	0.99 ± 0.06	0.13 ± 0.01	2.76 ± 0.14
OSL 19	0.06 ± 0.03	1.32 ± 0.10	0.81 ± 0.04	0.18 ± 0.02	2.37 ± 0.11
OSL 20	0.06 ± 0.03	1.29 ± 0.10	0.80 ± 0.04	0.18 ± 0.02	2.33 ± 0.11
Hajj Creiem	0.07 ± 0.03	1.35 ± 0.10	0.82 ± 0.04	0.17 ± 0.02	2.40 ± 0.12
OSL 21	0.19 ± 0.09	0.76 ± 0.06	0.28 ± 0.01	0.10 ± 0.01	1.33 ± 0.11
OSL 22	0.23 ± 0.12	0.40 ± 0.04	0.28 ± 0.03	0.16 ± 0.02	1.06 ± 0.13
OSL 23	0.23 ± 0.12	0.40 ± 0.04	0.28 ± 0.03	0.11 ± 0.01	1.01 ± 0.13
OSL 24	0.16 ± 0.08	1.04 ± 0.09	0.46 ± 0.02	0.10 ± 0.01	1.77 ± 0.12
OSL 25	0.12 ± 0.06	0.32 ± 0.02	0.23 ± 0.02	0.11 ± 0.01	0.78 ± 0.07
OSL 28	0.27 ± 0.13	1.95 ± 0.16	1.21 ± 0.08	0.16 ± 0.02	3.59 ± 0.22
OSL 29	0.23 ± 0.11	1.90 ± 0.16	1.20 ± 0.08	0.14 ± 0.01	3.48 ± 0.21
OSL 30	0.22 ± 0.10	1.72 ± 0.14	1.12 ± 0.08	0.06 ± 0.01	3.11 ± 0.19
OSL 31	0.24 ± 0.11	1.73 ± 0.14	1.12 ± 0.07	0.14 ± 0.01	3.24 ± 0.19

Sample ID	Alpha dose rate (Gy/ka)	Beta dose rate (Gy/Ka)	Gamma dose rate (Gy/ka)	Cosmic dose rate (Gy/ka)	Total Environmental dose rate (Gy/ka)
Faya NR1	-	0.57 ± 0.06	0.29 ± 0.02	0.19 ± 2 x 10^{-3}	1.05 ± 0.06
Faya NR2	-	0.56 ± 0.06	0.21 ± 0.02	0.16 ± 2 x 10^{-3}	0.93 ± 0.06
Faya NR3	-	0.60 ± 0.06	0.13 ± 0.01	0.15 ± 2 x 10^{-3}	0.88 ± 0.06
Faya NR4	-	0.41 ± 0.04	0.18 ± 0.01	0.18 ± 2 x 10^{-3}	0.76 ± 0.04
Faya NR6	-	0.38 ± 0.04	0.13 ± 0.01	0.15 ± 2 x 10^{-3}	0.66 ± 0.04
Faya NR7	-	0.46 ± 0.05	0.17 ± 0.01	0.09 ± 2 x 10^{-3}	0.72 ± 0.05
Faya NR8	-	0.63 ± 0.06	0.16 ± 0.01	0.13 ± 2 x 10^{-3}	0.92 ± 0.06
Faya NR9	-	0.58 ± 0.06	0.15 ± 0.01	0.13 ± 2 x 10^{-3}	0.86 ± 0.06

Table 6.3. Calculated dose rate values for all Libyan and Arabian samples dated in this thesis. Summary tables reporting all D_e and D_r values used for age calculation of the Libyan and Arabian Samples are reported in Appendix 3 and Appendix 4 respectively.

6.8 Conclusions

- The environmental dose rate is the rate at which a mineral absorbs energy resulting from exposure to ionising radiation in the natural environment.
- Natural radiation can include internal and external components. In this study, the internal dose rate was assumed to be zero.
- The calculation of the D_r is completed by combining the alpha, beta, gamma, and cosmic dose rate contributions.
- ICP MS/AES and in situ field gamma spectrometry were used to measure concentrations of U, Th and K.
- Cosmic ray dose rates were calculated using the COSMIC programme.
- Dose rates were corrected for grain size and water content. Errors associated with source calibrations, ICP measurement, dosimetry calculation, alpha and beta attenuation, conversion factors, and water content calculation were propagated in quadrature through the D_r calculation.

Chapter 7 - Age determination and calculation

7.1 Introduction

In order to calculate a reliable age estimate for a given sample, procedures must be followed to ensure the accurate and precise calculation of the D_e and D_r.

In this thesis, samples were dated via small aliquot or single-grain dating methods. Due to the averaging effect encountered when measuring more than one grain at a time, any grain to grain variation present within that sample would not be observed when utilising the small aliquot technique. Consequently, small aliquot dating was only applied where samples were thought to contain grains that would all yield the same apparent luminescence age. Accordingly, to obtain a representative D_e value for these datasets, an effective weighted mean was applied via the use of the Central Age Model (Section 7.2.2).

For samples thought to contain complex dose distributions, single-grain dating was applied, and more extensive investigations were undertaken to extract the individual age components and produce the most statistically likely age(s). The following chapter will discuss how the single-grain datasets were assessed, and subsequently why specific age models were then applied.

7.2 Investigating complexity within single-grain datasets

Due to the presence of grain to grain variability, and the potential complexity of the depositional and burial histories, the majority of samples dated using single-grain techniques in this thesis exhibit varying degrees of dose distribution complexity. Using statistical analysis, it was possible to further investigate the dose population, allowing the identification and extraction of several discrete age populations from within a single sample. Implementation of statistical modelling (in this case) should be carried out in conjunction with an understanding of the potential intrinsic and/or extrinsic mechanisms responsible for the spread in the D_e distribution. Almost all samples of quartz will exhibit some overdispersion between individual D_e estimates. Galbraith and Roberts (2012) suggest that once a suitable understanding of the depositional and post depositional history of a sample has been obtained, the most appropriate model for the specific dataset can be applied. By taking into consideration prior knowledge of such complex

environmental histories, it may even be possible in some cases to explain why certain anomalous populations are present in a sample.

The following sections present a selection of statistical models which can be used to enhance our understanding of a sample dose distribution, and subsequently improve the overall age calculation.

7.2.1 Overdispersion

In order to identify whether samples are consistent with a single component D_e distribution, or whether more than one component is present, the overdispersion parameter (σ) is utilised (Jacobs et al., 2008). This represents the relative standard deviation of the D_e distribution after taking into consideration measurement uncertainties (e.g. counting statistics and instrument reproducibility) (Galbraith et al., 1999; Olley et al., 2004; Rodnight et al., 2006). Where the grain population of a sample displays significant σ between individual D_e determinations, single-grain dating is essential as the averaging effect of the single aliquot technique may lead to the generation of an incorrect age estimate (Duller, 2008b; Jacobs et al., 2008a). Despite believing their samples to have been well bleached at the time of deposition, many authors, including Duller et al. (2000), Jacobs et al. (2006) and Olley et al. (2004), have reported overdispersion values of 9-22% (Jacobs et al., 2008b). Whilst Guérin et al. (2013) express concern that the 20% limit is potentially subjective, following Olley et al. (2004), it is widely accepted that a sample displaying < 20% overdispersion, is most likely consistent with a single component D_e distribution (Galbraith et al., 2005; Olley et al., 2004). Consequently, samples yielding overdispersion values > 20 % in this study were assumed to contain more than one D_e component.

Causes of dispersion in D_e estimates can be thought of as both intrinsic and extrinsic. Intrinsic factors comprise uncertainties relating to the laboratory measurement of dose (i.e. counting statistics and instrument reproducibility)(Thomsen et al., 2005), while extrinsic factors include bioturbation, bleaching heterogeneity, beta dose rate heterogeneity, and natural variability (including the non uniform emptying of optically sensitive traps and thermal transfer) (Mayya et al., 2006; Wintle & Murray, 2006). Sample depositional and post depositional history (Section 3.3), local variations in dosimetry (Section 6.3), and inherent grain to grain variability (Section 3.7) may also have a significant effect on the overdispersion of a sample; thus an understanding of these mechanisms within the

environment being dated is required (Nathan et al. 2003; Galbraith & Roberts, 2012; Yoshida et al., 2000). A final consideration and observation reported by several authors is that the sample aliquot size can also significantly affect the generated overdispersion values and the potential success of the models applied. Galbraith et al. (2005), for example, identified that as the number of grains in an aliquot is reduced, the degree of overdispersion is increased.

Where overdispersion within a sample is significant, and will affect the overall age estimation, the application of various statistical models, including the central age model (CAM) (Galbraith et al., 1999), minimum age model (MAM) and finite mixture model (FMM), can aid the extraction of the statistically most likely age of the sample (Lian, 2007; Galbraith et al., 1999).

7.2.2 Central Age Model

The Central Age Model is a method for producing a weighted mean for a dataset. A CAM assumes that the luminescence signals of all constituent grains from a sample are representative of a single component. While the grains within the sample may potentially yield a range of doses, all signals are assumed to be centred on some average value of the D_e, with any dispersion of measured D_e values being described by the overdispersion parameter (Galbraith and Roberts, 2012). While able to take overdispersion into account when determining the weighted mean and associated standard error, the use of a CAM is therefore most appropriate for samples whereby the constituent grains were fully bleached prior to burial, and where no post depositional mixing has occurred (Galbraith et al., 1999, Galbraith & Roberts, 2012). Olley et al. (2004), recommend the use of the CAM for well bleached samples. Where instances of partial or heterogeneous bleaching occur they suggest the utilisation of a different model which has the ability to take partial/homogenous bleaching into account. Rodnight et al. (2006) support this idea, demonstrating that the use of a CAM on their partially bleached fluvial sediments was inappropriate. Optical ages produced by the CAM in their study overestimated the burial age due to the presence of several grain populations, resulting from residual signals that remained following incomplete bleaching of the samples during turbulent river flow.

7.2.3 Minimum Age Model

The Minimum Age Model essentially represents a method for identifying the youngest component within a dataset. In circumstances like those observed by Rodnight et al. (2006), whereby only some grains were fully bleached prior to deposition, the MAM of Galbraith et al. (1999) may be more appropriate (Galbraith & Roberts, 2012). The MAM is used to accurately estimate the burial dose (D_b) for the population of fully bleached grains within a sample that has been affected by partial bleaching or post depositional mixing (Galbraith & Roberts, 2012). Olley et al. (2004) demonstrated how the MAM successfully produced the most accurate estimate of D_e for partially bleached Holocene sediments from a variety of depositional environments. They concluded that obtaining reliable ages for Holocene environments was dependent upon successfully identifying the youngest D_e population. Conversely, Rodnight et al. (2006) suggested that utilisation of the MAM in their fluvial sediments was not preferred, with results underestimating the burial ages following the strong influence of one or two low D_e values. Their analysis demonstrated that neither the CAM nor the MAM were able to successfully derive reproducible burial ages from the sampled palaeochannel deposits, where a mixed population of D_e values was present (Rodnight et al., 2006). For samples where 'younger grains' may have become incorporated into a sediment during a post depositional mixing event, it would also be inappropriate to use the MAM.

7.2.4 Finite Mixture Model

Finite Mixture Models are used to determine the number of discrete D_e components, the relative proportion of grains within each component, and the associated weighted mean of each component within the overall population of a single grain sample D_e distribution (Jacobs et al., 2008a). If a sample is believed to contain a number of discrete D_e components, Galbraith and Roberts (2012) suggest the use of the FMM as a viable alternative to the CAM and MAM. The FMM is commonly used with samples where post depositional sediment mixing is thought to have occurred (e.g. archaeological sites where the mixing of units is common). Accordingly, the FMM is designed to identify discrete individual components, and their associated weighted averages, in an attempt to generate a central D_e value for each component of the D_e distribution (Jacobs et al., 2008a). Galbraith (2005) utilises the maximum log likelihood (llik) and Bayesian Information

Criterion (BIC) statistical measures to identify the number of components that best fits the dataset. Based on the highest supported llik and lowest supported BIC estimate values, the optimum number of components and overdispersion values are thus identified (Jacobs et al., 2008a). Following the application of the FMM to samples in this thesis, the number of components, their relative proportions, and value of overdispersion obtained using the optimum Bayesian Information Coefficient (BIC), are reported.

7.3 Age Model Selection

Due to the depositional histories of the samples measured in this thesis, the utilisation of the MAM was deemed inappropriate for the reasons discussed in Section 7.2.3. In each case, all accepted D_e values from a sample were inserted into a CAM model in order to obtain a weighted mean equivalent dose and also a measurement of overdispersion. Where overdispersion was < 20%, the CAM D_e was used to calculate the age of the sample, on the assumption that only one equivalent dose population was present in this sample. Lacustrine, raised beach, and aeolianite samples (which are assumed to be fully bleached and devoid of post-depositional bleaching), are examples of where the CAM proved to be the most appropriate model in this study. In circumstances where overdispersion was > 20%, the FMM was utilised. Cave sediments, palaeosols and alluvial material represent the sample types where the FMM was necessary here. Where the FMM was applied, all identified components are reported. In each case, using prior knowledge of the sedimentary environment, depositional history, and likely dosimetry variations, the most likely / appropriate component has been utilised in the production of the luminescence age. Whilst components containing > 50% of a sample population are thought to provide a true representation of the sample population, an explanation of why each chosen component was deemed appropriate is presented for each sample.

7.4 Summary

- Where complex dose distributions were apparent within a sample, statistical analysis was used to investigate the dose population, and extract the most appropriate age population(s) for each sample.
- Overdispersion represents the quantitative measure of dispersion within a dataset that is beyond that accounted for by measurement uncertainties.

- Where overdispersion < 20%, the sample was thought to comprise of a single dose component. Thus, the Central Age Model was utilised to generate a weighted mean value for the dataset.
- Samples yielding an overdispersion value of > 20% were believed to contain a complex dose distribution comprising more than one component. The Finite Mixture Model was applied to these samples to determine the number of discrete components within the sample population, the relative proportion of grains within each component, and a weighted mean value for each component. These weighted mean values were then used to generate ages for each individual component.

Chapter 8 - A comparison of single-grain and small aliquot dating of fine sand.

Due to the paucity of coarse grain quartz in the Libyan samples, it was not possible to produce true single-grain discs (i.e. one grain per recess) using standard methods (Section 4.5.1). Consequently, experimental work was undertaken to identify whether or not very small aliquots containing c. 20 to 50 grains yielded similar results to true single-grain dating. In this chapter true single-grain and very small aliquot data are compared for four samples from the Cyrenaican region of Libya. The results from hand loading individual grains into a single-grain disc are compared to very small aliquots generated by brushing 60-125 µm grains across the surface of a single-grain disc. True small aliquots were also produced for each sample for additional comparisons. Should the results prove to be comparable, the time consuming process of manually loading a single-grain disc with individual quartz grains could be avoided.

8.1 Introduction

Single-grain dating has significantly enhanced our understanding of Quaternary environmental and archaeological sediments over the last decade. In particular, single-grain work has increased our understanding of grain to grain variability, and specifically the extent to which all of the grains within a sample can produce the same apparent luminescence age (Section 3.7, Roberts et al. 1997). Whilst small aliquot dating was utilised for the majority of the Libyan sites studied in this thesis, several sedimentary layers exhibited evidence for post depositional mixing or partial bleaching of the sediments. Consequently, where OSL samples were taken from these layers, single-grain dating was deemed the most appropriate method for obtaining accurate age estimations.

Conventionally, standard single-grain methods utilise the ~ 200 µm size fraction, as this results in a single-grain residing in each 300 by 300 µm recess (Section 4.5.1). Due to the paucity of coarse grain quartz in the Libyan samples, utilisation of the standard method with grains < 200 µm would result in multiple occupancy of each recess of a single-grain disc, thus precluding true single-grain measurements. Accordingly, to produce true single-grain measurements it is necessary to manually load individual grains into each recess. However, this is very time consuming.

Several authors have advocated the use of small, multi grain aliquots of quartz as a viable alternative to manual loading of a single-grain disc when the optimum size fraction is not available for single-grain dating (e.g. Rodnight, 2008). It has been proposed that this method may yield results that are comparable to true single-grain measurements, since it is widely observed that a very small proportion of sedimentary quartz grains are luminescent (Duller et al., 2000). This approach has the advantage of avoiding laborious manual loading of single-grain discs. As part of this thesis, the results obtained from true single-grain (SG), small aliquot (SA) and "pseudo single-grain" (PSG) (i.e. small, multi grain aliquots) measurements from four samples were compared to test the applicability of the PSG technique to the Libyan samples (for disc preparation information, see Section 4.5).

8.2 Sites and samples

HF10 and HF09 were taken from the Haua Fteah cave (Section 10.3) at depths of 6.3 and 7.5 m respectively. Micromorphological investigations surrounding HF10 indicated post depositional mixing and partial bleaching were likely to have occurred, with slope wash material and inwash events dominating the transport and depositional processes (Inglis, 2012, unpublished thesis). Whilst micromorphological analysis was not completed in the lower section of the cave, where HF09 was collected, it was thought that similar depositional processes were likely to have occurred (R. Inglis, *pers. comm*. 2012). Additionally, during sampling, animal burrow holes were identified across the section face, suggesting bioturbation was an active process in the cave sediments.

OSL 3 and OSL 1 were collected from section EM 4 in the Al Marj basin (Section 10.6.1). OSL 1 was taken from a silty clay at the base of the section (4.5 m below the surface), while OSL 3 was collected from a capping palaeosol layer at a depth of 1.4 m. Due to the inclusion of roots and rootlet channels throughout the palaeosol, bioturbation was considered to be a potential cause of post depositional mixing of the sediment. Accordingly, single-grain dating was deemed necessary for this sample. Conversely, the uniform nature of the silty clay deposit at the base of the section provided minimal sedimentary evidence for post depositional mixing or partial bleaching. It was expected that small aliquot and single-grain measurements would yield comparable results for this sample.

Samples from the Haua Fteah cave were collected in opaque plastic tubes, whilst Al Marj samples were collected as blocks. Standard methods reported in Chapter 2 were used to extract the 60-90 µm and 90-125 µm fractions of pure quartz from the Haua Fteah and Al Marj samples respectively. These size fractions represented the coarsest size fraction available for each site.

8.3 Disc preparation and measurement

True single-grain (SG) discs were prepared by hand picking individual quartz grains and manually loading them into each recess of a standard (300 µm hole diameter) single-grain disc. Hand picking was performed using thin electrical wire, with the disc being illuminated using a sodium lamp and viewed under a microscope. Pseudo single-grain (PSG) discs were prepared using standard single-grain methods (i.e. brushing an excess of grains across the surface of a single-grain disc), resulting in c. 20 and 14 grains within each recess for the Haua Fteah (60 – 90 µm) and Al Marj (90 – 125 µm) samples respectively. Finally, small aliquots (SA) for both samples were mounted on an aluminium disc using silkospray silicone oil applied via a 2 mm diameter mask (Section 4.5.2).

All OSL measurements in this experiment were carried out using a Risø TL/OSL-DA-15 automated dating system (Bøtter-Jensen et al., 2003), fitted with a single-grain OSL attachment (Section 5.3). Optical stimulation of single and pseudo single-grains was carried out using a 10 mW Nd:YVO_4 solid state diode-pumped green laser (532 nm) focussed to yield a nominal power density of 50 W/cm^2, while small aliquots were stimulated using a blue (470 nm) light emitting diode with a power density of 33 mW/cm^2 (Bøtter-Jensen et al., 2003). Infra-red stimulations were carried out using an IR (870 nm) laser diode array yielding a power density of 132 mW/cm^2. A ^{90}Sr/^{90}Y beta source (calibrated relative to the National Physical Laboratory ^{60}Co g-source (Armitage & Bailey, 2005)) providing c. 6 Gy/min was used for irradiation. Dose rates for individual single-grain positions on the single-grain disc were calibrated according to the procedure outlined in Armitage et al. (2011) due to the spatial inhomogeneity of beta emitters across the active face of the ^{90}Sr/^{90}Y beta source.

Equivalent doses were calculated using the SAR protocol of Murray and Wintle (2000). OSL was measured at an elevated temperature of 125 °C. Small aliquots were stimulated using blue diodes for 40 s, with the OSL measured during the first 0.32 s of illumination minus a

background signal from the last 4 s. Single and pseudo single-grains were stimulated with the green laser for 1 s, with the OSL recorded during the first 0.3 s of stimulation minus a background signal from the last 0.3 s.

8.4 Equivalent dose determination

Small aliquot dose recovery preheat plateau tests (Section 5.2.2.4) were completed to determine the optimal preheating conditions for each of the four samples. 24 small aliquots from each sample (prepared using a 5 mm diameter mask) were measured using PH1 temperatures ranging from 160-280 °C at 20 °C intervals, held for 10 s, all with a 160 °C PH2 held for 10 s. An additional measurement was made with a PH1 of 260 °C and a PH2 of 220 °C, both held for 10 s. As shown in Figure 8.1, all samples were relatively insensitive to preheating conditions, and a PH1 of 260 °C and PH2 of 220 °C were chosen accordingly.

Additional dose recovery testing was completed for OSL 3 using 6 hand-picked SG and 6 PSG discs to test the efficacy of the preheating regime. Each disc was given a 12.5 Gy dose and measured using a 260 °C PH1 and a 220 °C PH2. As illustrated in Figure 8.2, both methods yielded D_e values consistent with the administered dose.

Growth curves were fitted using an exponential plus linear function, and Monte Carlo simulation was used to estimate the uncertainty for individual D_e values, using 1000 "Monte Carlo Repeats" in Analyst version 3.24 (Duller, 2007). Following publication, additional testing of the datasets included fitting growth curves with an exponential function and utilisation of the $2D_0$ rejection criteria; the results of which are discussed in Chapter 9.

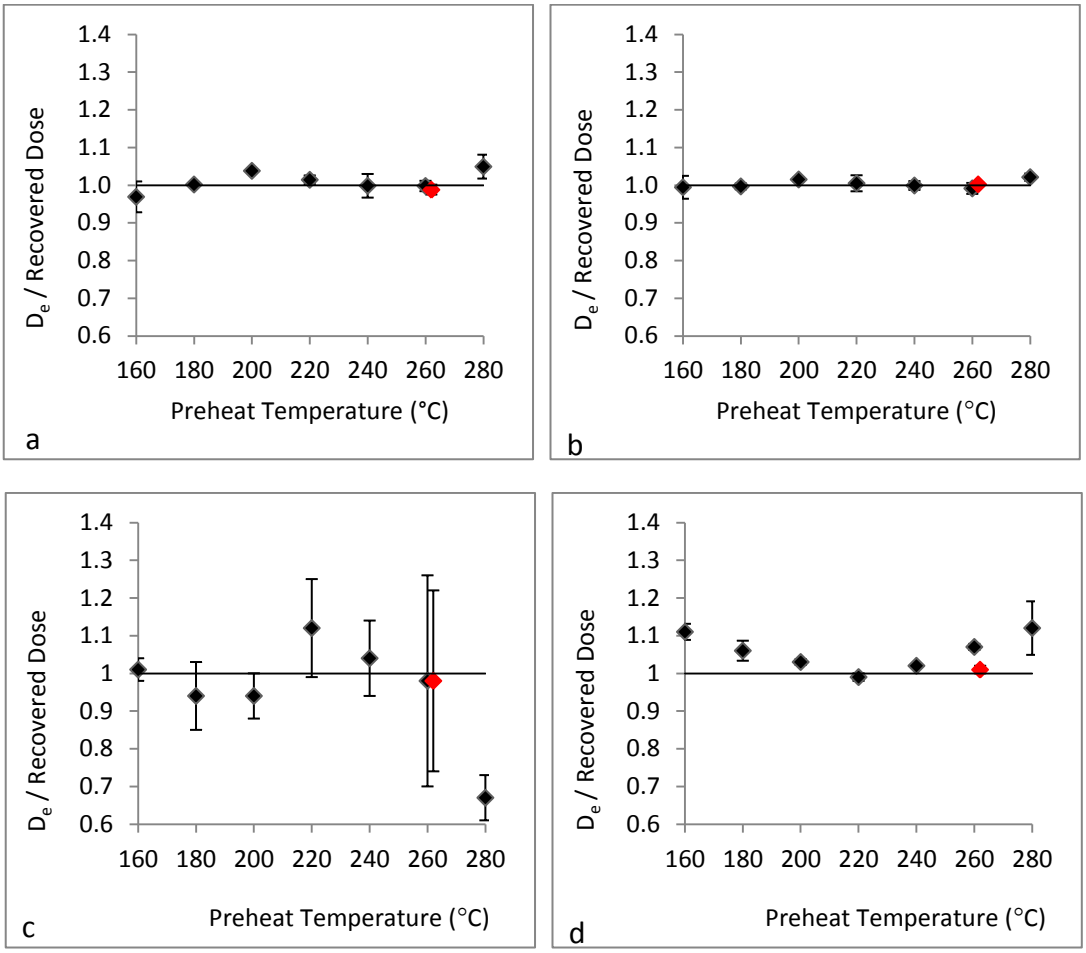

Figure 8.1. Dose recovery preheat plateaus for a) HF09 (10.3 Gy), b) HF10 (10.3 Gy), c) OSL1 (316 Gy) and d) OSL3 (12.5 Gy). All four samples were able to successfully recover the given dose. Data for the preheating regime chosen for subsequent D_e measurements (PH1, 260 °C for 10 s and PH2, 220 °C for 10 s) is offset by 2 °C on the *x*-axis and red for clarity. All other data were generated using a PH2 of 160 °C for 0 s. Mean dose recovery ratios for the samples are: a) HF09 0.99 ± 0.01, b) HF10 1.00 ± 0.01, c) 0.98 ± 0.24, and d) 1.01 ± 0.01.

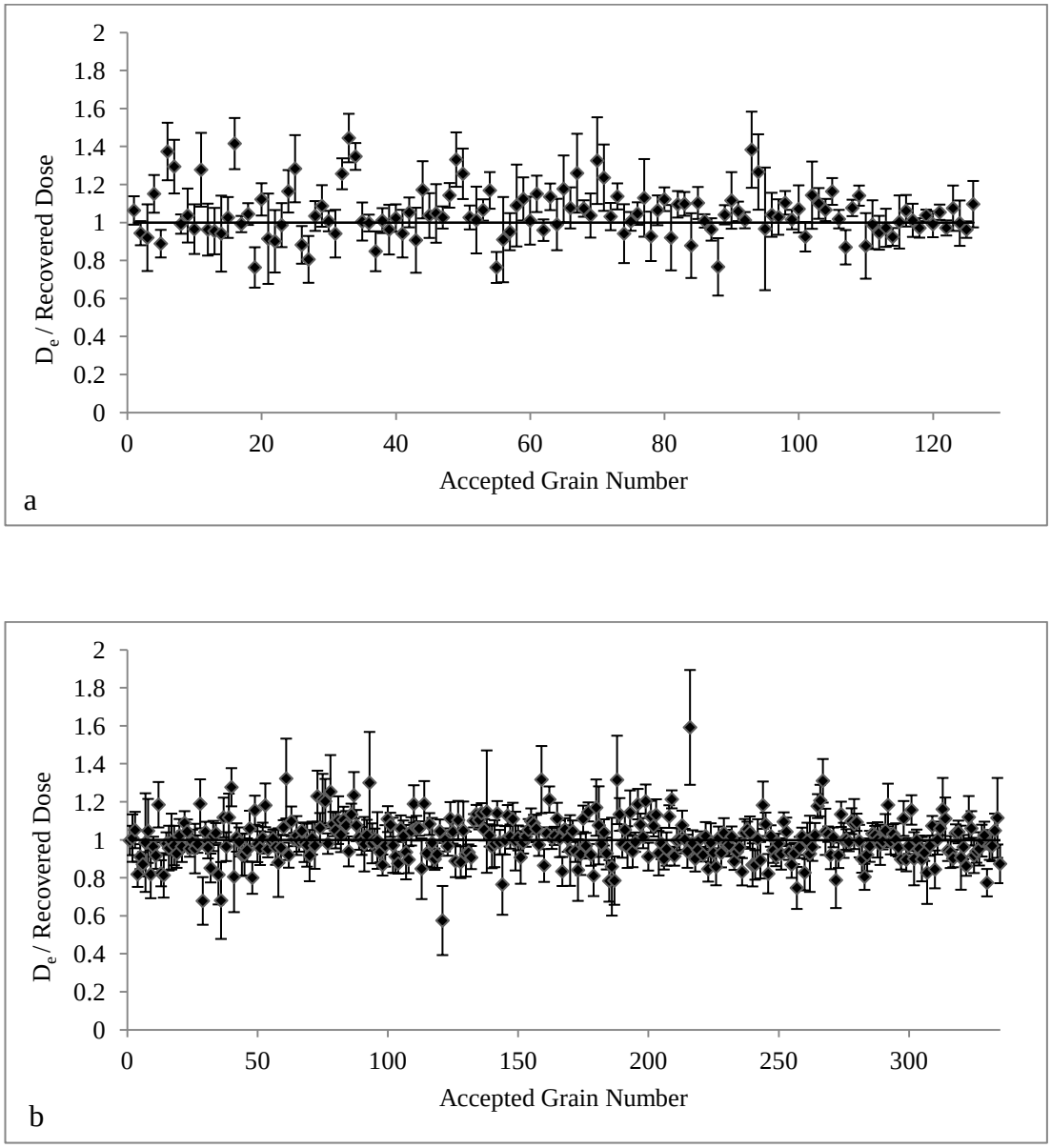

Figure 8.2. a) single-grain and b) pseudo single-grain dose recovery experiment results for OSL 3. All discs were given a 12.5 Gy dose. Standard deviation values of 1.6 and 1.4 Gy, and overdispersion (σ_d) values of 4% and 5% were produced by the single-grain and pseudo single-grain datasets respectively. CAM D_e values produced by both datasets were within errors of the 12.5 Gy dose given (13.1 ± 1.6 Gy (4% σ_d) and 12.5 ± 1.4 Gy (5% σ_d) for the single-grain and pseudo single-grain datasets respectively).

As discussed in Section 5.2.1, it was important to ensure that the SAR measurement conditions utilised for determining the D_e were appropriate. Additionally, it was vital to exclude any grains/aliquots displaying luminescence properties that were not conducive to accurate D_e determination. Consequently, the grain/aliquot rejection criteria of Jacobs et al. (2008a) as modified by Armitage et al. (2011) was adopted for this experiment. In summary, grains were rejected where one or more of the following conditions were met: 1) the natural signal was less than three times the size of the background signal; 2) the recycling ratio of Murray and Wintle (2000) differed from unity by greater than 10%; 3) the IR depletion ratio was greater than 2σ below unity for single or pseudo single-grains (Duller, 2003), or differed from unity by more than 10% for small aliquots; 4) the L_x/T_x for the 0 Gy regenerated dose was greater than 5% of L_n/T_n (Murray & Wintle, 2000); 5) the natural signal (i.e. L_n/T_n) did not intercept the growth curve (Armitage et al., 2000; Yoshida et al., 2000); or 5) the shape of the dose response curve precluded the generation of a meaningful D_e.

Table 8.1 summarises the total number of grains measured, the total number of grains rejected following application of the rejection criteria (outlined above), and the total number of grains accepted for inclusion in the calculation of the burial dose. Due to poor recycling ratio values, a total of 7 and 4 small aliquots were rejected out of the 24 small aliquots measured for OSL 1 and OSL 3 respectively.

Fast ratio values were generated for small aliquot measurements from each of the four samples using the method of Durcan and Duller (2011) (Section 5.2.1.5). Values ranged from 22.4 to 131, suggesting the dominance of a fast component within the initial part of the OSL signal.

8.5 Initial comparison of the D_e

Initial comparison of the true single grain (SG), pseudo single grain (PSG), and small aliquot (SA) datasets was completed through the application of the Central Age Model (CAM) of Galbraith et al. (1999) (Section 7.2.2). As illustrated by Table 8.2, the CAM D_e values produced for the PSG datasets are, in every case, higher than those produced for the SG measurements. Furthermore, for each sample (excluding OSL 3) the SA CAM D_e is consistently higher than that produced by the PSG dataset. It can therefore be observed that SG and PSG / SA measurements do not produce comparable D_e values in this case.

Sample	HF09 SG HP	HF09 PSG	HF10 SG HP	HF10 PSG	EM-OSL1 SG HP	EM-OSL1 PSG	EM-OSL3 SG HP	EM-OSL3 PSG
Total grains measured	1600	600	2000	600	1100	600	1100	600
Grains rejected for the following reasons								
Tn <3* σBG	755	0	1070	0	560	5	568	21
Poor recycling ratio	574	183	611	117	282	178	312	274
Depletion by IR	20	1	13	2	5	9	12	8
0 Gy dose >5% of Ln	7	0	3	1	2	0	79	125
No Ln/Tn intersection	66	138	48	42	96	113	4	0
Poor DR curve	93	146	131	87	64	136	8	9
Sum of rejected grains	1515	468	1876	249	1009	441	983	437
Acceptable individual grains	85	132	124	351	91	159	117	163
Grains rejected (%)	94.6	78	93.8	41.5	91.7	73.5	89.3	72.8

Table 8.1. A summary of the number of grains measured, rejected, and accepted following the application of the rejection criteria outlined in Section 8.4 to the Haua Fteah and Al Marj samples under investigation.

Sample	HF09		HF10		EM-OSL1		EM-OSL3	
	D_e (Gy)	σ (%)	D_e (Gy)	σ (%)	D_e (Gy)	σ (%)	D_e (Gy)	σ (%)
SG	168.4 ± 12.1	55 ± 5	103 ± 6	51 ± 4	154.2 ± 9	42 ± 4	10.7 ± 0.6	45 ± 3
PSG	251.4 ± 10.6	30 ± 2	160.4 ± 5.6	27 ± 1	237.5 ± 9.8	33 ± 2	12.6 ± 0.6	54 ± 3
SA	352.1 ± 13.5	1 ± 1	233.7 ± 20.3	25 ± 7	269.6 ± 19.7	21 ± 6	12.6 ± 0.6	15 ± 3
Synthetic	218.6 ± 17	36 ± 6	109.3 ± 8.6	45 ± 5	207.4 ± 14.5	26 ± 5	12.1 ± 1.3	57 ± 8

Table 8.2. A summary of CAM D_e and σ values for single-grain (SG), pseudo single-grain (PSG), small aliquot (SA), and synthetic aliquot (synthetic) datasets from Haua Fteah and Al Marj samples. D_e uncertainties are based on the propagation, in quadrature, of the standard error derived from the CAM and a 3% beta source calibration error (Armitage & Bailey, 2005).

	63-90µm Hand Picked Single-Grain		**63-90µm Pseudo Single-Grain**		**90-125µm Hand Picked Single-Grain**		**90-125µm Pseudo Single-Grain**		**90-125µm Small Aliquot**	
	Value	±	Value	±	Value	±	Value	±	Value	±
Measured dose rate (Gy/s)	0.100	0.014	0.101	0.005	0.101	0.005	0.102	0.007	0.105	0.006
n (measured/accepted)	12 / 10		12 / 11		12 / 11		6 / 6		24 / 20	
180-212 µm (Gy/s)	0.099	0.005	0.099	0.005	0.099	0.005	0.099	0.005	0.099	0.005
Ratio (correction factor)	**1.008**	0.149	**1.020**	0.073	**1.020**	0.069	**1.034**	0.091	**1.064**	0.083

Table 8.3. Results from the calibration experiments completed using the 60–90 µm and 90–125 µm size fractions, prepared as explained in Section 8.3. The small aliquot rejection criteria outlined in Section 8.4 was adopted for all samples in this instance. Dose rates for PSG and SG measurements were calculated using D_e values derived from summed single-grain signals from each disc. These dose rates are presented in the row entitled "Measured dose rate". The number of single-grain and small aliquot discs measured are presented in the row entitled "n (measured/accepted)". The single-grain dose date for 180–212 µm grains in presented in the row entitled "180–212 µm (Gy/s)".

8.6 Investigating the cause of variation between the datasets

Three hypotheses were tested in an attempt to explain the discrepancy between the SG, PSG and SA datasets. Hypothesis 1 suggests that disparity may have been caused by variation of the effective beta dose rate, resulting from the different irradiation geometries of each disc. Hypothesis 2 postulates that exposure to higher intensity sodium light conditions over extended time periods during hand picking, may have bleached some of the SG signal. Finally, Hypothesis 3 suggests that the inclusion of grains with poor luminescence properties in PSG and SA measurements has adversely affected the CAM D_e values.

8.6.1 Hypothesis 1. The discrepancy between D_e values obtained from SG, PSG and SA measurements is due to the different irradiation geometries employed for each sample.

In order to test Hypothesis 1, measurements were made to investigate whether or not the variation in the irradiation geometries between the three discs had an impact on the effective beta dose rate delivered to each sample. In this instance, shielding of the beta dose rate by overlying grains in a PSG disc recess was a primary concern.

There are several potential causes for variations in the effective beta dose rate delivered to each sample. Firstly, due to the different thicknesses of the discs used for small aliquot and pseudo/single-grains, there would potentially be differences in the associated backscattering effects. Furthermore, as the pseudo single-grain and true single-grains are recessed in the single-grain discs, additional variations in backscatter may occur. Finally, as mentioned above, the stacking of grains in a pseudo single-grain recess may potentially shield the underlying grains from the beta dose, causing variations between the SG and PSG measurements.

In order to test Hypothesis 1, the Risø instrument was calibrated using 60-90 and 90-125 µm annealed quartz (450 °C, 1 hr) from a Nigerian sand sample that had been given a 4.5 ± 0.15 Gy gamma dose using the National Physical Laboratory Hotspot 800 ^{60}Co gamma source. Calibrations were performed using SG, PSG, and SA discs, prepared using the methods outline in Section 8.3.

The results from the calibration experiment (displayed in Table 8.3) demonstrate that the laboratory beta dose rates for all sample geometries and grain sizes were within errors of each other. SG and PSG calibration measurements were all consistent with each other and the 180-212 μm single-grain calibration completed by Armitage et al. (2011) on the same instrument. The SA calibration was also consistent with the calibration performed using the method of Armitage and Bailey (2005). Hypothesis 1 was therefore rejected.

8.6.2 Hypothesis 2. The discrepancy between D_e values obtained from SG, PSG and SA measurements is due to an increase in laboratory light exposure times during the manual loading of the grains

Hand-picking and manually loading single-grains of quartz into individual recesses on a single-grain disc is a time consuming process, resulting in the exposure of quartz to light from a sodium lamp for extended periods of time (c. 30 min). Consequently it was important to ensure that these exposure periods were not responsible for reducing the SG CAM D_e values via bleaching of the OSL signal.

Accordingly, Hypothesis 2 was tested by exposing small aliquots of quartz under a bright sodium lamp over a range of time periods. In groups of three, small aliquots were exposed to the sodium light for periods of 0, 1, 2, 4 and 6 hours. As illustrated by Figure 8.3, average D_e values obtained after 1 and 2 hours of exposure to the sodium lamp were consistent (within errors) with aliquots that had not been exposed. A gradual decline in average D_e was observed after 2 hours of exposure, suggesting that direct exposure under the sodium lamp may impact the samples beyond this point. Using the equation of the line (Figure 8.3) a constant signal bleaching rate of < 2% per hour was calculated for the samples.

Since manual loading of each disc was completed in c. 30 minutes (unused quartz grains were stored in light-tight conditions between hand-picking of each disc) it was possible to reject the hypothesis that exposure to direct sodium light conditions may have reduced the overall D_e of true single-grain measurements. During all other preparation, samples were exposed to ambient subdued orange light conditions for short time periods. Furthermore, due to the shielding of individual grains by the wall of each single-grain disc recess, bleaching rates measured in the experiment were likely to exceed those experienced

during the manual loading of a single-grain disc, as direct exposure to the sodium lamp was minimal. Hypothesis 2 was therefore rejected.

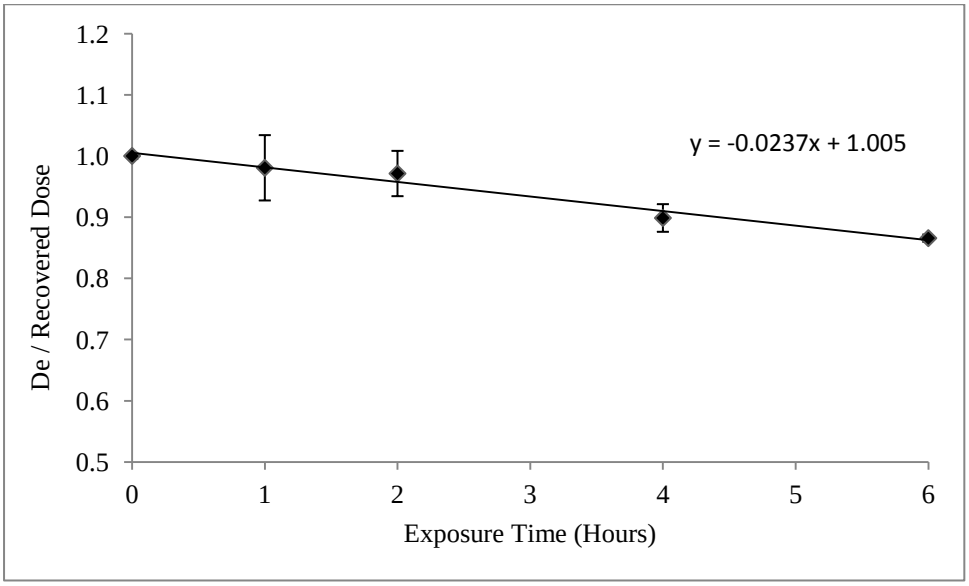

Figure 8.3. Results from the bleaching experiment. All reported data were normalised to those for the unbleached aliquots (i.e. 0 hours of exposure).

8.6.3 Hypothesis 3. The discrepancy between D_e values obtained from SG, PSG and SA measurements is due to the inclusion of grains with poor luminescence properties in small aliquots

Following the rejection of Hypothesis 1 and 2, Hypothesis 3 was tested to investigate whether the inclusion of grains with poor luminescence properties (i.e. those that would have been rejected from the single-grain datasets on the basis of the rejection criteria outlines in Section 8.4) in pseudo single-grain and small aliquots adversely affected the equivalent doses measured for these measurement geometries.

Each individual grain in a SG dataset was subjected to the stringent rejection criteria presented in Section 8.4. and Section 5.2.1. Grains presenting poor luminescence properties were rejected from these datasets. Where a "rogue grain" (i.e. a grain with poor luminescence properties) is present within a small aliquot (including PSG discs), it is unlikely that the averaged signal of several grains will be poor enough to warrant the removal of the aliquot from the dataset. Thus, "rogue grains" rejected from the single-grain datasets

were unlikely to have been removed from the small aliquot datasets, which may cause the variation in D_e observed between the datasets.

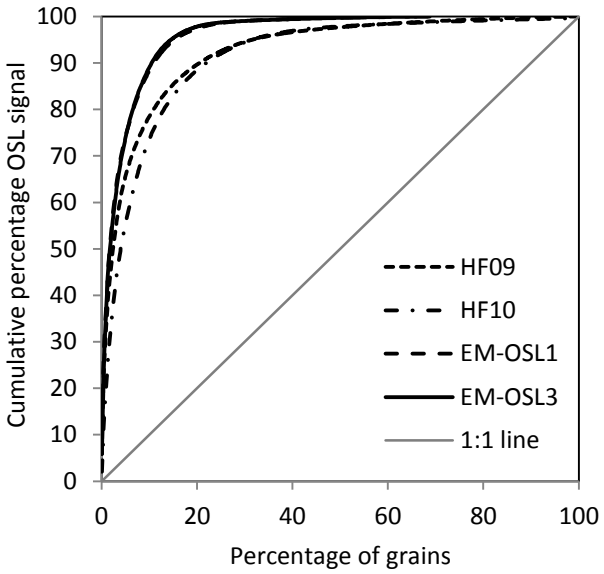

Figure 8.4. Cumulative light sum plots for the Haua Fteah and Al Marj samples measured in this study. Grains are ranked by brightness, with the brightest grain being plotted first.

To test Hypothesis 3, synthetic aliquots were generated using a number of randomly selected single-grain measurements (including those that would fail the single-grain rejection criteria) that were collated and analysed as if those grains constituted a small aliquot. Synthetic aliquots therefore represent artificial "small aliquots" or composites, produced by randomly combining a number of signals (14 or 20) from existing single-grain measurements. Grains used in the synthetic aliquots were drawn from the entire population of measured single-grains for each sample respectively. The rejection criteria were subsequently applied to the synthetic aliquots as a whole, rather than to the individual grains residing within them.

As shown in Figure 8.4, a relatively high proportion (15-20%) of the grains in each of the four samples measured in this experiment contribute 90% of the total light sum. In comparison with data reported by Duller (2000), which suggests that only c. 5% of grains yield a luminescence signal, the Libyan material in this contains a significantly higher proportion of luminescent grains. Haua Fteah and Al Marj PSG samples consisted of 20 and

14 grains respectively. Accordingly, it was assumed that there would be 5 and 3 "bright" grains in the Haua Fteah and Al Marj PSG measurements, and consequently synthetic aliquots were generated using this number grains.

The synthetic aliquot (Synthetic) CAM D_e values (shown in Table 8.2) were compared to the corresponding SG, PSG and SA D_e measurements. In every case, the Synthetic CAM D_e values were higher than the corresponding SG measurements. This evidence supports the supposition that the differences between the single-grain and multiple grain measurements to OSL signals can be attributed to the inclusion of "rogue grains" in small aliquots, which are rejected during single-grain analysis.

Supporting evidence can also be observed in Table 8.1, where the high rejection rate of grains during SG analysis suggests the removal of a substantial number of individual grains exhibiting poor luminescence properties (between 89 – 95% of all grains being rejected. Similar results are demonstrated by Jacobs et al. (2008a) who rejected between 80 – 90% of all grains measured. Consequently we can accept Hypothesis 3.

8.7 Complex D_e distributions and the application of the Finite Mixture Model (FMM)

Whilst the CAM D_e values facilitate the identification of discrepancies between the different datasets, σ_d values of > 20% suggest the presence of more than one D_e component (Section 7.2.1 and 5.1.2) in the SG and PSG datasets. The CAM was therefore not deemed appropriate for age calculation of the SG and PSG datasets. Accordingly, the FMM was adopted for samples displaying an σ_d > 20% (Section 7.2.4).

The FMM D_e distributions presented in Figure 8.5, Figure 8.6 and Table 8.4 suggest that HF10, HF09 and OSL 1 contain complex D_e distributions. Using the SG data, only OSL 3 appears to contain a single dominant component.

Sample	Technique	Components	Component 1 (Gy)	%	Component 2 (Gy)	%	Component 3 (Gy)	%	Component 4 (Gy)	%	Component 5 (Gy)	%
HF09	SG	3	63.39 ± 5.88	16	142.01 ± 8.97	38	274.57 ± 18.45	46	-	-	-	-
	PSG	2	149.2 ± 15.92	15	275.9 ± 12.06	85	-	-	-	-	-	-
HF10	SG	3	40.9 ± 5.15	12	89.1 ± 6.39	53	177 ± 13.21	35	-	-	-	-
	PSG	3	94.85 ± 7.73	8	155.09 ± 5.46	77	244.31 ± 16.87	15	-	-	-	-
EM-OSL 1	SG	2	106.13 ± 8.73	45	209.23 ± 15.26	55	-	-	-	-	-	-
	PSG	3	99.3 ± 13.43	4	190.1 ± 13.29	39	294.6 ± 16.47	57	-	-	-	-
EM-OSL 3	SG	3	9.4 ± 0.35	91	31.64 ± 2.66	8	100.25 ± 22.56	1	-	-	-	-
	PSG	5	10.03 ± 0.36	77	19.06 ± 1.07	14	36.7 ± 2.82	5	82.1 ± 6.95	3	226.6 ± 49.37	1

Table 8.4. FMM results for each single-grain (SG) and pseudo single-grain (PSG) D_e distribution.

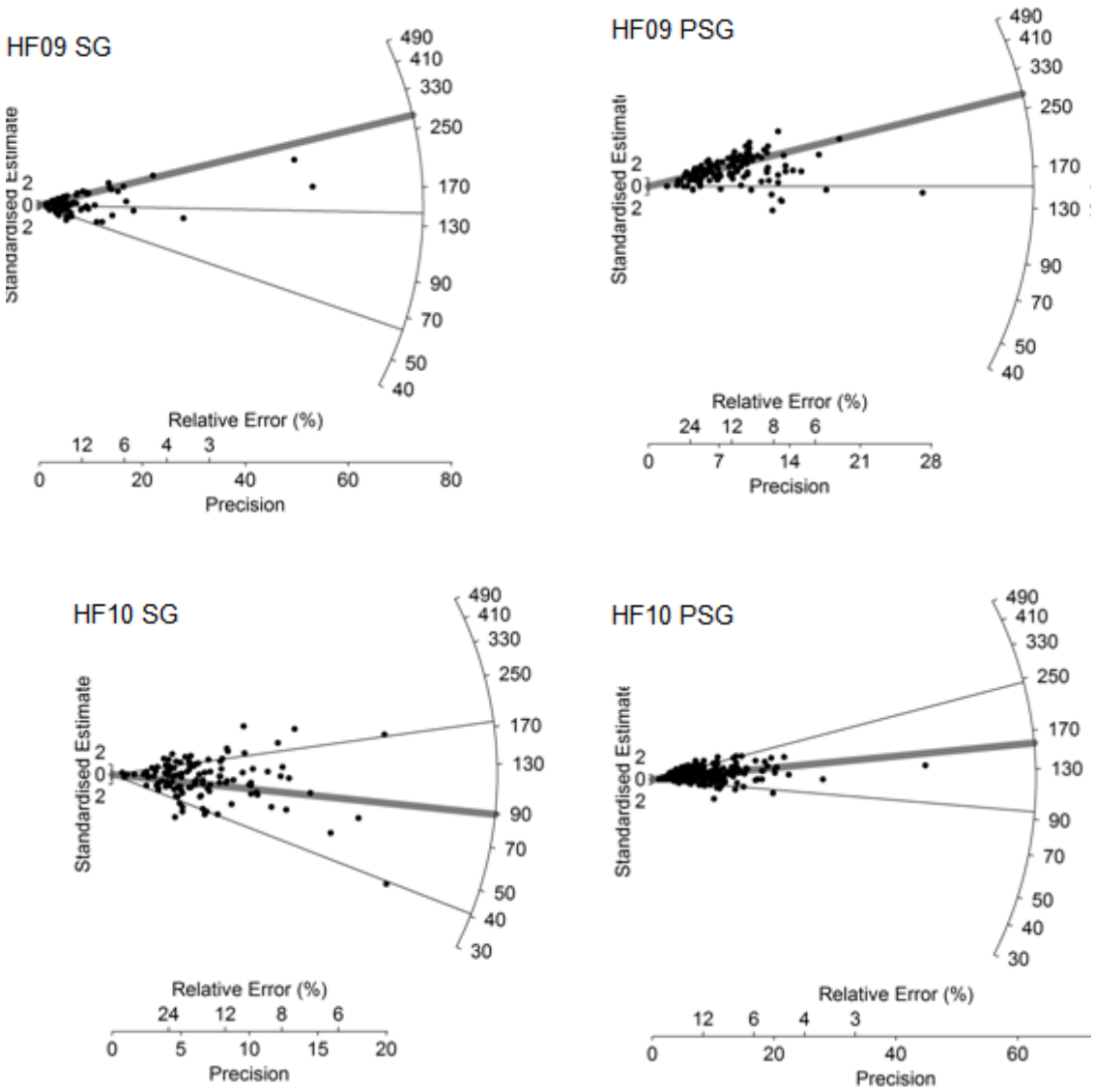

Figure 8.5. Radial plots showing the pseudo single-grain (PSG) and single-grain (SG) D_e distributions obtained from samples HF09 and HF10. The grey bars represent the dominant (>40%) components identified using the FMM. Black lines identify minor components, containing less than 40% of the grains measured.

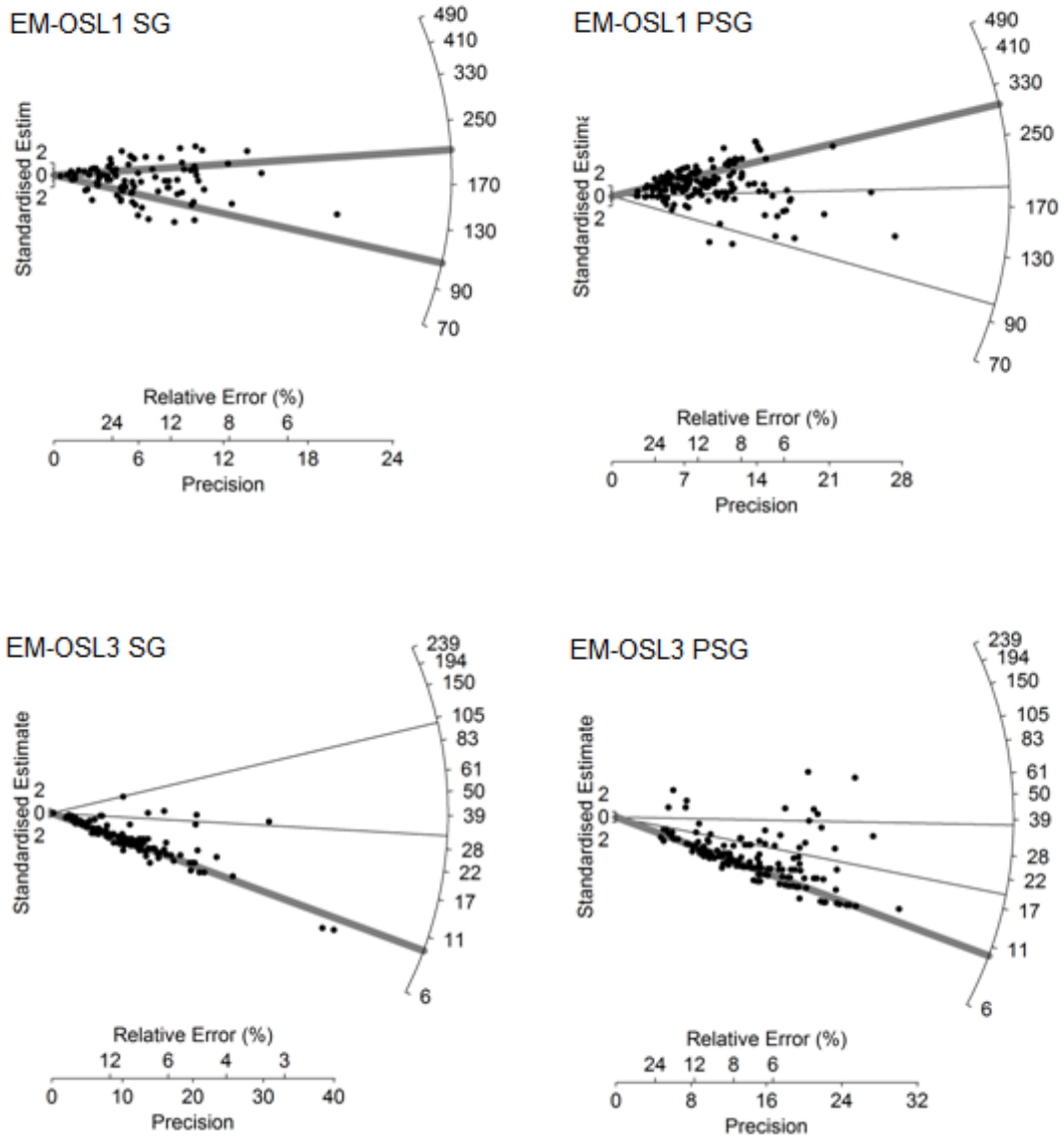

Figure 8.6. Radial plots showing the single-grain (SG) and pseudo single-grain (PSG) D_e distributions obtained from samples EM-OSL1 and EM-OSL3. The grey bars represent the dominant (>40%) components identified using the FMM. Black lines identify minor components, containing less than 40% of the grains measured. Components that comprise of <5% of the grains measured are not shown.

Using the Haua Fteah PSG datasets, the FMM suggests the presence of a dominant component, whilst the SG datasets indicate a more complex distribution of the D_e, with three different components being identified. Figures 6.5 and 6.6 show radial plots of the SG and PSG D_e distributions for both Haua Fteah and Al Marj samples. These plots illustrate the variation between the D_e measurements in each dataset, supporting the argument for complexity within the D_e distributions.

Interestingly, the younger components identified by the FMM in the SG datasets appear absent from the PSG results. Considering the findings discussed in Section 8.6.3, it is likely that the inclusion of "rogue grains" in the PSG dataset is adversely affecting the FMM results. Additionally, it is likely that the discrepancies between the datasets may represent an averaging effect observed when dating multi grain aliquots (Section 3.7), thus preventing the FMM from identifying the younger OSL signals in the PSG datasets. Arnold and Roberts (2009) caution against the use of the FMM on multi grain aliquots, having identified the presence of 'phantom' dose components, which result from similar averaging effects to those observed in this study.

8.8 Supporting Research

Whilst the combination of high inherent sensitivity of our samples and complex dose distributions may contribute to the findings of this research, comparable patterns have been identified by Arnold et al. (2012). Arnold et al. (2012) investigated the effect of measuring single-grain discs containing more than one quartz grain per recess, with the aim of identifying the extent of averaging effects on D_e measurements, and the suitability of PSG dating. They found that SG and PSG measurements were not comparable, attributing these variations to the inclusion of grains with aberrant luminescence behaviours in multi grain aliquots. Furthermore, their PSG and SG FMM D_e distributions also produced significantly different characteristics, with "phantom" dose components arising from averaging effects produced during the PSG measurements.

8.9 Conclusions

In conclusion, the evidence presented in this chapter suggests that the inclusion of "rogue grains" in multi grain measurements adversely affects the measurement of D_e. Whilst only

four samples were measured in this study, the findings published by Arnold et al. (2012) support the findings presented here. PSG datasets yield different apparent equivalent dose distributions to SG datasets, indicating that it is inappropriate to apply a PSG measurement strategy to our samples. Furthermore, caution should be exercised when interpreting PSG results obtained from other sites, especially where a relatively large proportion of grains are luminescent. For these reasons, I have applied a single-grain measurement strategy for samples where mixed grain populations may be present.

Chapter 9 - Application of the $2D_0$ rejection criterion

9.1 Introduction

As discussed in Section 5.2.1.7, the upper age limit of OSL dating is controlled by the radiation dose at which the sensitivity-corrected luminescence intensity ceases to grow with increasing dose. When this point is reached, the dosimeter is said to be in "saturation", and it is not possible to generate a chronologically meaningful equivalent dose. The dose at which saturation occurs varies both between and within samples, a phenomenon which is particularly marked when analysing single quartz grains (e.g. Yoshida et al., 2000). Whilst some samples appear to grow up to an upper limit, other signals exhibit continued growth at high laboratory doses (Yoshida et al., 2000; Duller, 2012). Singarayer and Bailey (2003) used LM-OSL measurements to construct component resolved dose response curves for a Moroccan quartz (TQN: Grey dune deposit, Thomas Quarries, Morocco), demonstrating that a single saturating exponential function (Equation 2, Section 5.2.1.7) could be used to fit each component, based on the assumption that each component is derived from a single trap (Wintle & Murray, 2006).

Wintle and Murray (2006), and Bailey (2000) suggest that when a dose response curve is produced for the fast component (fitted using a single saturating exponential function (Equation 2, Section 5.2.1.7)), it is possible to determine accurate D_e values up to a dose value of around $2*D_0$ ($2D_0$ hereafter, c. 15% below the saturation value observed in the laboratory dose-response curve (Wintle & Murray, 2006)). Where the natural signal is close to saturation, Athanassas (2011) suggests that growth curves are characterised by variable shapes and small slope angles at the point of natural signal intersection. OSL signals which intersect the growth curve at doses greater than $2D_0$ are therefore sufficiently close to saturation to generating large, asymmetric, uncertainties in the D_e (Murray et al., 2002; Murray & Funder, 2003; Wintle & Murray, 2006). In addition, it is not clear that for signals derived from the initial channels of OSL measurement (as opposed to component resolved signals) the shape of the growth curve above $2D_0$ is dominated by the fast component. Consequently, Wintle and Murray (2006) suggest that any aliquots/grains which yield a $D_e > 2D_0$ can be considered to be saturated and therefore excluded from further analysis.

A single saturating exponential function should accurately describe the OSL growth curve where the signal derives from a single trap, and might therefore be preferred where the

dominance of a single trap is assumed. However, where high laboratory doses are required for the construction of a dose response curve which "brackets" the natural luminescence intensity, some authors have suggested that a saturating exponential plus linear function (Equation 4) is more appropriate since, whatever the source, a linear component is visibly present in these growth curves. Duller (2012) suggests that the addition of a linear component is unsurprising in some samples due to the wide range of D_0 values from single grains contributing the luminescence signal.

$$I = I_0 + I_{max}\left(1 - e^{-D/D_0}\right) + k.D$$

Equation 5 (above) describes the exponential plus linear function, following Jacobs et al. (2003). Where *I* is the luminescence intensity following a dose *D*, I_0 is the luminescence intensity at 0 dose, I_{max} is the maximum luminescence intensity, and D_0 and *k* are constants that define the shape of the dose response curve.

Pawley et al. (2010), suggest that the addition of a linear term enables much higher equivalent doses to be measured. Pawley et al. (2010) also argue that the application of the $2D_0$ criterion usually limits dose measurements to c. 200 Gy, often much less. They argue that for a typical sandy sediment experiencing an environmental dose rate of ~ 1 Gy/ka, this would artificially limit the maximum measurable age to 150-200 ka.

The dose response characteristics of the upper part of the growth curve are not well understood. A strong variability in luminescence response in the upper part of the growth curve (i.e. beyond c. 100 Gy) was reported by Athanassas (2011). Consequently, they suggest that when large doses are measured, there is a relationship between the growth curve shape, mode of D_e distribution, and potentially scatter in dose response characteristics. Kim et al. (2010), however, report that the utilisation of an additional linear component is equivocal, with some studies demonstrating an ability to produce reliable results (e.g. Murray et al., 2008), whilst others (including their own) resulting in age underestimations. For example, using the sum of two saturating exponentials, systematic age underestimations of c. 10% were identified when Eemian shallow marine and fluvial sediments were dated by Murray and Funder (2003). The presence of a clearly defined high-dose tail in the datasets was, in this case, considered likely to have been influenced by

the shape of the growth curve. Kim et al. (2010) and Choi et al. (2006b) dated fine grain samples from the archaeological site of Jeongokri on the Korean Peninsula using a saturating exponential plus linear function. Both investigations reported that the samples were close to saturation and the additional linear component (which grew to high doses) was required to generate OSL ages. However, relying on this linear component was again shown to yield age underestimations in this case. In contrast, numerical modelling and empirical measurements, completed by Bailey (2004) and Bailey et al. (2005) respectively, suggests that dose rate effects (the reduced probability of an OSL trap capturing electrons from the conduction band at laboratory dose rates relative to the trapping probability at natural dose rates) may lead to equivalent dose overestimations where the sample has received a large natural dose. Murray et al. (2008) on the other hand, successfully used a saturating exponential plus linear function to produce accurate age determinations for Seyda River deposits from northern Russia. Using the high dose linear region of the growth curve, the OSL results were in excellent agreement with independent age controls for these Eemian deposits. Despite continuing investigation into the application of an additional linear function to the growth curve, the processes responsible for the linear component remain uncertain (Lowick et al., 2010). Consequently, the choice of function used to fit datasets requiring high laboratory doses, as well as the appropriateness of utilising the $2D_0$ rejection criterion, are still under debate.

In this chapter, the effect of applying the $2D_0$ rejection criterion to datasets from the Arabian and Libyan samples studied in this thesis is investigated. Mean D_e values were calculated for each sample (after application of the standard single-aliquot/single-grain rejection criteria outlined in Section 5.2) before and after the application of the $2D_0$ rejection criterion, and then compared. As high laboratory doses were required for the construction of the growth curve for several of the Libyan and Arabian samples, the equivalent doses were calculated using a saturating exponential plus linear function (which appeared to best fit the datasets). However, D_0 was obtained from the same datasets fitted with a saturating exponential function using Analyst v3.22b (developed by Professor Geoff Duller in 2005), following the suggestion of Durcan (2012). Subsequently, comparisons of mean D_e values obtained from the single-grain Arabian datasets generated using a single saturating exponential function versus an exponential plus linear function were also completed, to investigate how the choice of fit affects the overall D_e of each sample. Consequently, these comparisons provide an opportunity to investigate the effect of

applying an additional linear function during interpolation of the luminescence signal, as well as the potential impact of the $2D_0$ rejection criterion on a range of different samples.

9.2 Investigating the effect of the $2D_0$ rejection criterion on mean D_e

Following the application of standard rejection criteria (Section 5.2), mean D_e values for the Libyan and Arabian samples ranged from 12.4 – 526.5 Gy and 8.1 – 113 Gy respectively. As high doses were measured for several of the Libyan and Arabian samples, following Wintle and Murray (2006), the $2D_0$ rejection criterion was applied to all samples in an attempt to remove any saturated signals. By comparing mean D_e values before and after the application of the $2D_0$ rejection criterion, the following sections (9.2.1 and 9.2.2) assess the effect of applying $2D_0$ to the Libyan and Arabian datasets. The single-grain Libyan and Arabian datasets were then analysed using a Finite Mixture Model, both before and after the application of the $2D_0$ rejection criterion, to further assess the effect of applying $2D_0$ by comparing the number, size and D_e for the components generated (Section 9.2.3).

Typical decay curves and growth curves for single-grain Arabian and Libyan measurements are shown in Figures 9.1 and 9.2. Luminescence signals from all of the Libyan and Arabian material are characterised by a rapid signal decay and fast ratio values of > 20 (Durcan and Duller, 2011), suggesting the presence of a dominant fast component within the initial part of the OSL signal.

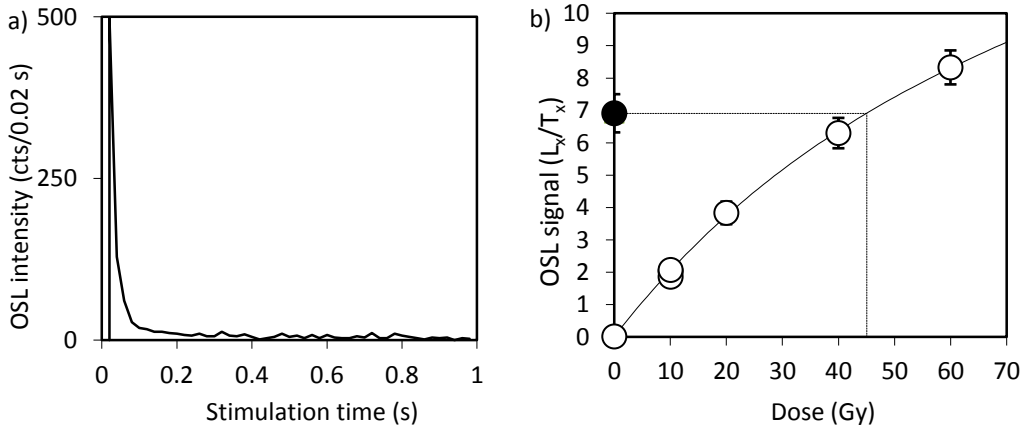

Figure 9.1. A typical a) single-grain decay curve and b) growth curve for Faya NR 1 (Arabia).

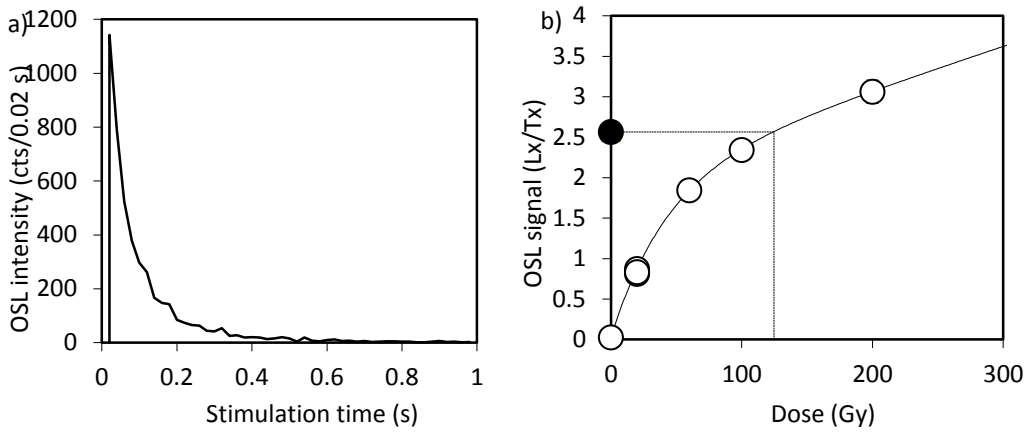

Figure 9.2. A typical a) single-grain decay curve and b) growth curve for OSL 1 (Libya).

9.2.1 Libyan Samples

Single-grain, small aliquot and fine grain mean D_e values calculated before and after the application of the $2D_0$ rejection criterion are displayed in Tables 9.1, 9.2 and 9.3 respectively. Graphical representations of the change in mean D_e following the application of the $2D_0$ rejection criterion are presented in Figures 9.3, 9.4, 9.5, and 9.6.

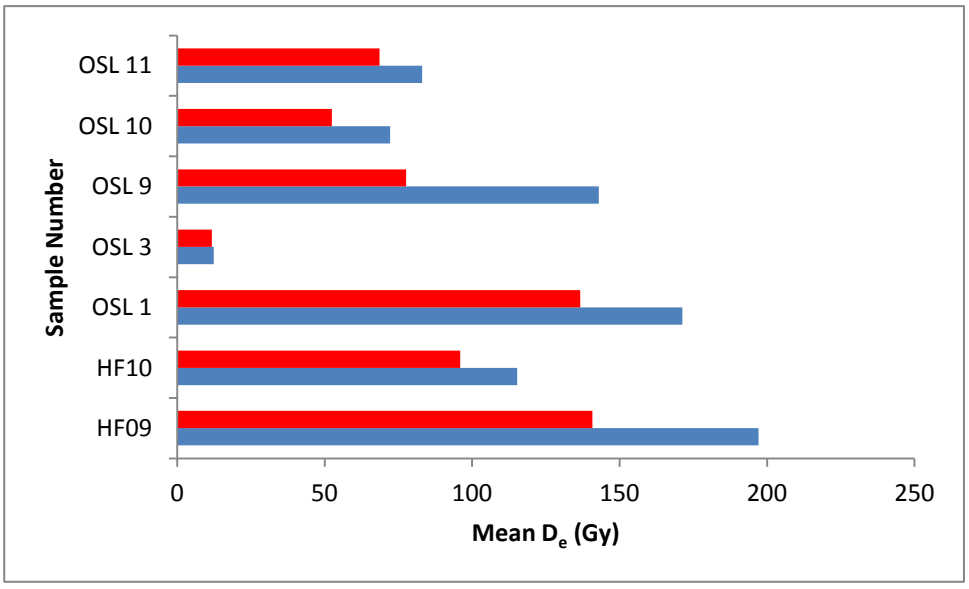

Figure 9.3. Bar chart showing the absolute change in mean D_e observed following the application of the $2D_0$ rejection criterion to each single grain dataset. Blue bars represent the mean D_e before the $2D_0$ rejection criterion was applied. Red bars represent the mean D_e after the $2D_0$ rejection criterion was applied.

Sample ID	pre-$2D_0$			post-$2D_0$			Change in D_e (Gy)	Change in D_e (%)
	Mean D_e	±	*n*	Mean D_e	±	*n*		
HF09	197.1	98.8	84	140.8	78.8	28	-56.3	-29
HF10	115.3	61.7	123	95.9	42.7	85	-19.4	-17
OSL 1	171.3	78.2	92	136.7	49.2	30	-34.6	-20
OSL 3	12.4	10.8	115	11.7	6.9	114	-0.7	-6
OSL 9	142.9	87.9	74	77.6	31.4	34	-65.3	-46
OSL 10	72.2	50.7	117	52.4	25	86	-19.8	-27
OSL 11	83.0	34.7	47	68.6	20.1	33	-14.4	-17

Table 9.1. Mean D_e values produced before (pre-$2D_0$) and after (post-$2D_0$) the application of the $2D_0$ rejection criterion to each single-grain sample. Negative values indicate where the application of $2D_0$ has resulted in the reduction in the absolute and percentage mean D_e values. *n* is the number of signals accepted for each dataset.

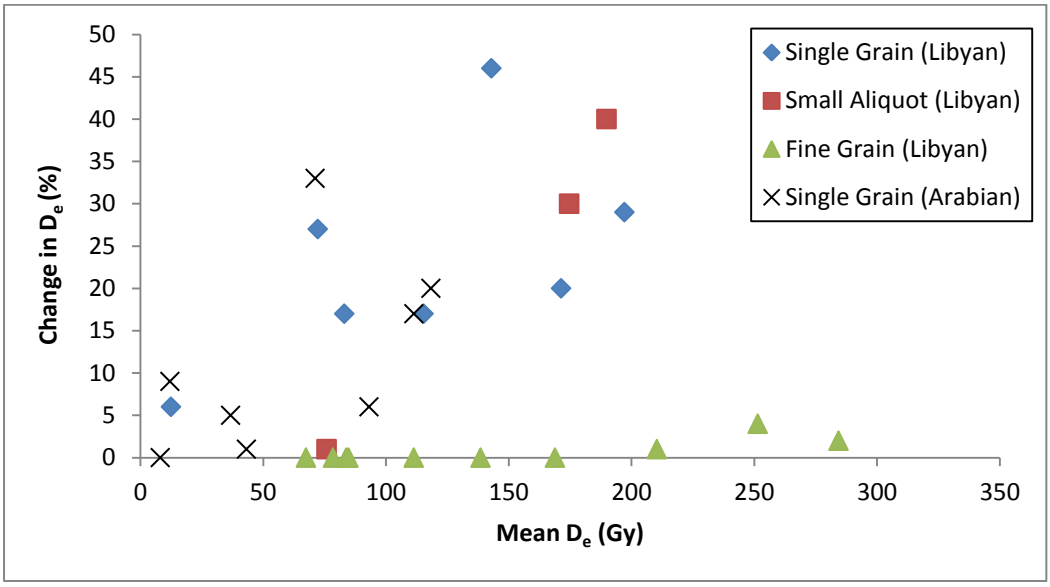

Figure 9.4. Graph illustrating the percentage change in mean D_e following the application of the $2D_0$ rejection criterion to all Libyan and Arabian datasets (produced using an exponential plus linear function).

In every case where single-grain (SG) measurement has been employed, the application of the $2D_0$ rejection criterion to the Libyan datasets results in a reduction in the mean D_e value (Table 9.1; Figure 9.3). Reductions in mean D_e range from 6% (OSL 3, which exhibits the lowest mean D_e) to 46% (OSL 9, exhibiting one of the highest mean D_e values), with an

average reduction of c. 23% associated with the Libyan SG samples. In this instance, samples exhibiting higher mean D_e values appear to have experienced a greater reduction than those experiencing lower mean dose values (Figure 9.4).

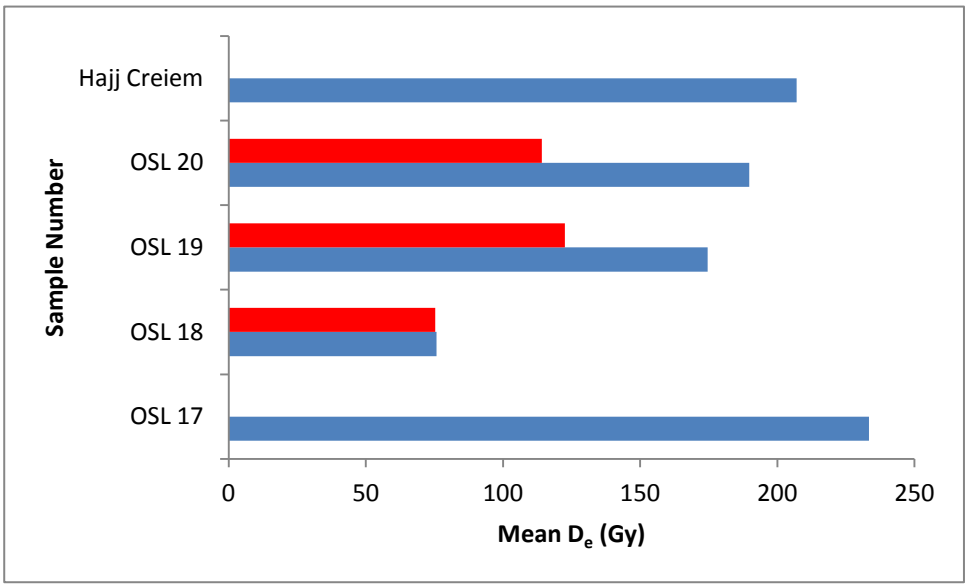

Figure 9.5. Bar chart showing the absolute change in mean D_e observed following the application of the $2D_0$ rejection criterion to each small aliquot dataset. Blue bars represent the mean D_e before the $2D_0$ rejection criterion was applied. Red bars represent the mean D_e after the $2D_0$ rejection criterion was applied. Where no red bar is present, all aliquots were rejected by application of the $2D_0$ rejection criterion.

Sample ID	pre-$2D_0$			post-$2D_0$			Change in D_e (Gy)	Change in D_e (%)
	Mean D_e	±	*n*	Mean D_e	±	*n*		
OSL 19	174.6	55.9	20	122.5	6.4	10	-52.1	-30
OSL 20	189.8	87.3	31	114.1	36.7	9	-75.7	-40
Hajj Creiem	207.0	62.3	15	0	0	0	-	-
OSL 17	233.4	45.6	7	0	0	2	-	-
OSL 18	75.8	8.5	24	75.3	8.7	24	-0.5	-1

Table 9.2. Mean D_e values produced before (pre-$2D_0$) and after (post-$2D_0$) the application of the $2D_0$ rejection criterion to each small aliquot sample. Negative values indicate where the application of $2D_0$ has resulted in the reduction in the absolute and percentage mean D_e values. *n* is the number of signals accepted for each dataset.

Small aliquot (SA) measurements present a more varied response to the application of the $2D_0$ rejection criterion (Table 9.2; Figure 9.5). Three of the samples (OSL 18, 19 and 20) experience a reduction in D_e (ranging from 0.7% to 75.7%) following the application of the $2D_0$ rejection criterion (Figure 9.4). The application of $2D_0$ to the Hajj Creiem (taken adjacent to OSL 19 and OSL 20) and OSL 17 sample datasets results in the rejection of all aliquots measured, which, according to Wintle and Murray (2006) would suggest that all aliquot signals in this sample were saturated. Coincidentally, the reduction in mean D_e for OSL 18 (which exhibits the lowest dose) is significantly lower than the other small aliquot samples, which supports observations in the SG data, suggesting that lower doses are less affected by the application of the $2D_0$ rejection criterion. Furthermore, OSL 17 and Hajj Creiem, which exhibit the highest mean D_e values, represent the samples that experience the greatest change following the application of the $2D_0$ rejection criterion.

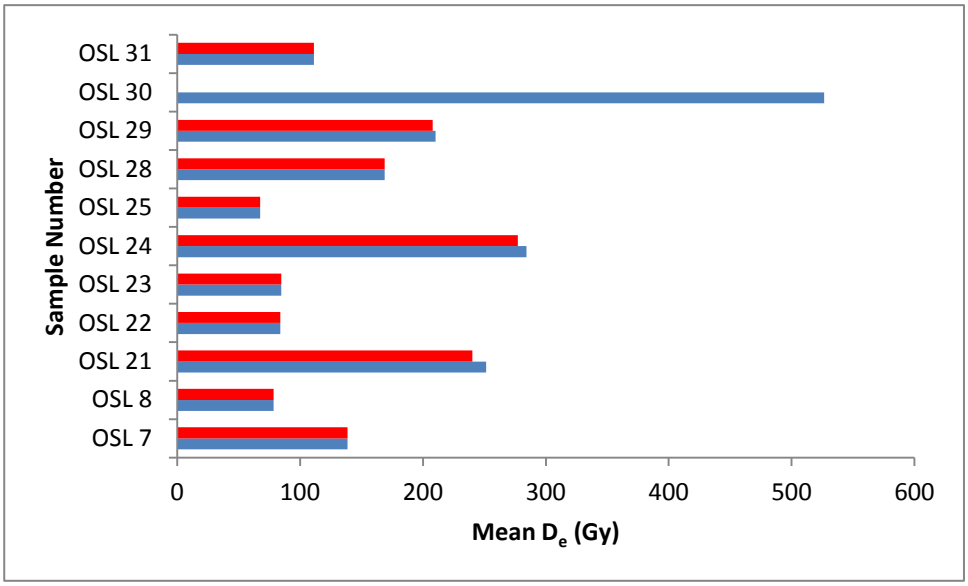

Figure 9.6. Bar chart showing the absolute change in mean D_e observed following the application of the $2D_0$ rejection criterion to each fine grain dataset. Blue bars represent the mean D_e before the $2D_0$ rejection criterion was applied. Red bars represent the mean D_e after the $2D_0$ rejection criterion was applied. Where no red bar is present, all aliquots were rejected by application of the $2D_0$ rejection criterion.

Sample ID	pre-$2D_0$			post-$2D_0$			Change in D_e (Gy)	Change in D_e (%)
	Mean D_e	±	*n*	Mean D_e	±	*n*		
OSL 7	138.5	22.9	22	138.5	22.9	22	0	0
OSL 8	78.4	3.8	23	78.4	3.8	23	0	0
OSL 21	251.4	47.3	20	240.3	41.7	16	-11.1	-4
OSL 22	83.8	6.2	21	83.8	6.2	21	0	0
OSL 23	84.7	9.0	9	84.7	9.0	9	0	0
OSL 24	284.3	34.3	23	277.2	32.7	19	-7.1	-2
OSL 25	67.4	7.2	6	67.4	7.2	6	0	0
OSL 28	168.8	12.1	23	168.8	12.1	23	0	0
OSL 29	210.3	30.5	14	207.8	30.2	11	-2.5	-1
OSL 30	526.5	53.2	10	0	0	0	-	-
OSL 31	111.3	4.7	18	111.3	4.7	18	0	0

Table 9.3. Mean D_e values produced before (pre-$2D_0$) and after (post-$2D_0$) the application of the $2D_0$ rejection criterion to each fine grain sample. Negative values indicate where the application of $2D_0$ has resulted in the reduction in the absolute and percentage mean D_e values. *n* is the number of signals accepted for each dataset.

Datasets from 7 of the 11 fine grain (4-11 μm) samples were unaffected (i.e. no aliquot expressed a $D_e > 2D_0$) by the application of the $2D_0$ rejection criterion (Table 9.3; Figure 9.6). OSL 21 and 24 from Chersa Beach, and 29 from the Al Marj core, however, all experienced a reduction in mean D_e by 11.1%, 7.1%, and 2.5% respectively. All aliquots of one fine grain sample (OSL 30) failed the $2D_0$ rejection criterion. Once again, samples with higher mean D_e values appear to be the most affected following the application of the $2D_0$ rejection criterion (Figure 9.4).

In every case where the application of $2D_0$ has resulted in the reduction of mean D_e, there is also a reduction in the associated D_e error. Whilst this evidence for a reduction in D_e uncertainty could be used to support Wintle and Murray (2006) (suggesting that erroneous equivalent dose values produced from saturated grain(s) have been successfully removed), it is also possible that the $2D_0$ rejection criterion is in fact truncating the higher-dose end of the dose population for each sample. As illustrated in Figures 9.7, 9.8 and 9.9, following the application of the $2D_0$ rejection criterion, it is predominantly the individual grains and aliquots which exhibit the highest equivalent doses that are being rejected. Duller (2012) suggests that as higher equivalent dose values are measured, the proportion of saturated grains will increase. Duller (2012) and Singarayer and Bailey (2003), however, also report

that there is significant variability in the saturation characteristics of individual grains. This would suggest that $2D_0$ should reject signals from grains exhibiting both high and low equivalent dose values. As Figures 9.7, 9.8 and 9.9 demonstrate, however, significantly more signals are being rejected from the top end of the equivalent dose distribution. This, in addition to the lack of low dosed grains being rejected from the datasets, suggests that the $2D_0$ rejection criterion is disproportionately removing the higher dose, top end of each sample population.

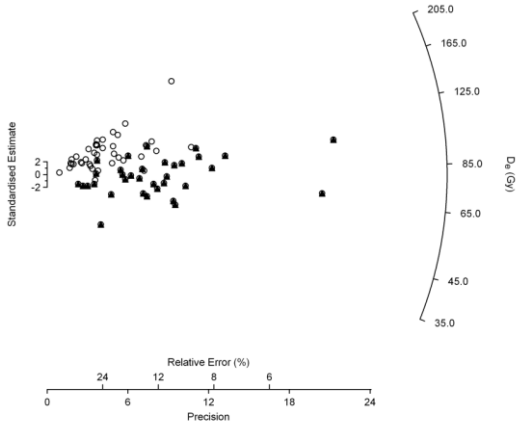

Figure 9.7. Radial plot showing the single-grain D_e distributions obtained from the Libyan sample OSL 9. Open circles represent D_e values accepted prior to the application of the $2D_0$ rejection criterion, but rejected after the application of this criterion. Closed circles represent D_e values that are accepted following the application of the $2D_0$ rejection criterion.

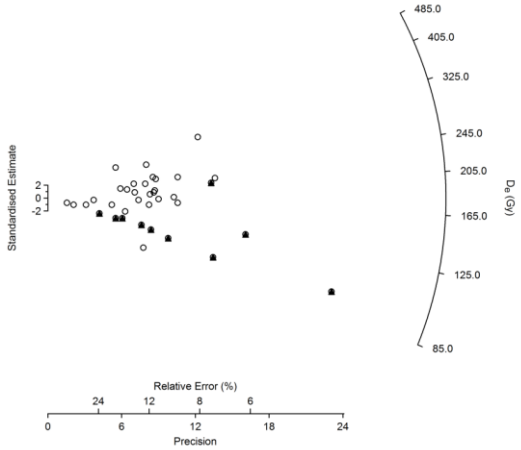

Figure 9.8. Radial plot showing the small aliquot D_e distributions obtained from the Libyan sample OSL 20. Open circles represent D_e values accepted prior to the application of the $2D_0$ rejection criterion, but rejected after the application of this criterion. Closed circles represent D_e values that are accepted following the application of the $2D_0$ rejection criterion.

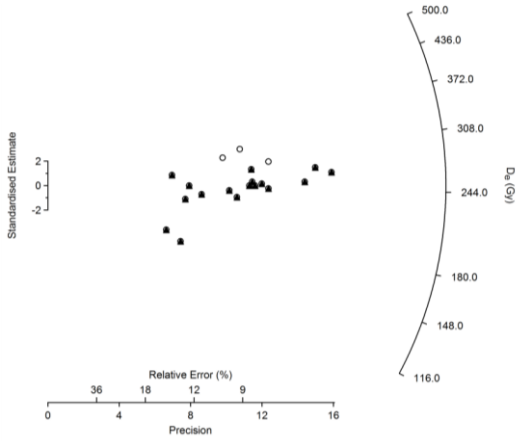

Figure 9.9. Radial plot showing the fine grain D_e distributions obtained from the Libyan sample OSL 21. Open circles represent D_e values accepted prior to the application of the $2D_0$ rejection criterion, but rejected after the application of this criterion. Closed circles represent D_e values that are accepted following the application of the $2D_0$ rejection criterion.

9.2.2 Arabian Samples

All of the Arabian samples in this thesis were measured using single-grain dating techniques. Datasets used to generate previous ages for lithic assemblages at Jebel Faya (published by Armitage et al., 2011), were not subjected to the additional $2D_0$ rejection criterion as the samples were not thought to be in saturation as shown in Figure 9.10 (taken from Armitage et al. (2011) supplementary information). Furthermore, as the figure shows, the use of an exponential plus linear function appeared to provide an appropriate fit for the data.

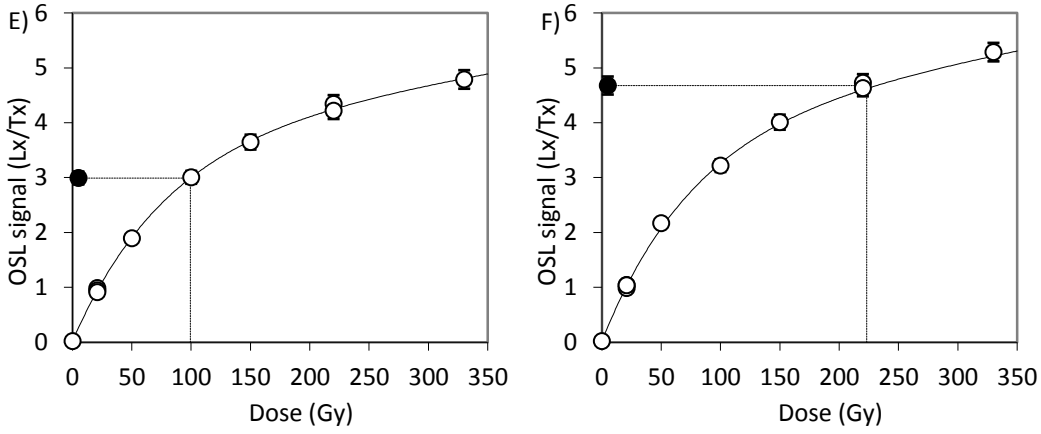

Figure 9.10. Typical growth curves produced by Armitage et al. (2011) for samples from Jebel Faya, Arabia. E) represents a grain yielding a dose value close to the mode. F) provides an example of a grain yielding a high dose value.

The application of the $2D_0$ rejection criterion reduced the measured D_e for 8 out of the 9 Arabian samples dated in this thesis (Table 9.4; Figure 9.11). Faya NR6 is the only sample for which no change in mean D_e occurred when the $2D_0$ rejection criterion was applied. Following Wintle and Murray (2006), this would suggest that Faya NR6 is the only sample which does not contain saturated grains. Faya NR 3, 8 and 9 (which are three of the Arabian samples with the highest D_e values) exhibit the largest change in mean D_e, experiencing a reduction in mean D_e of 20%, 17% and 33% respectively. Consequently, a similar trend to that observed in the Libyan datasets can also be seen here (i.e. samples with higher doses experience greater reductions in mean D_e following the application of the $2D_0$ rejection criterion) (Figure 9.4).

A reduction in equivalent dose uncertainties following the application of the $2D_0$ rejection criterion could again provide supporting evidence for Wintle and Murray (2006), who suggest the saturated grains removed by $2D_0$ exhibit large, asymmetric uncertainties. However, the predominant removal of higher dose signals from the top end of the D_e distribution may also result in a reduction in the dispersion of the data, and therefore the associated D_e uncertainty. Evidence for this truncation of the upper end of the dataset can be observed in Figure 9.12. The radial plot clearly demonstrates that a significantly larger proportion of higher dosed signals are being rejected, with no evidence for the removal of lower dose grains.

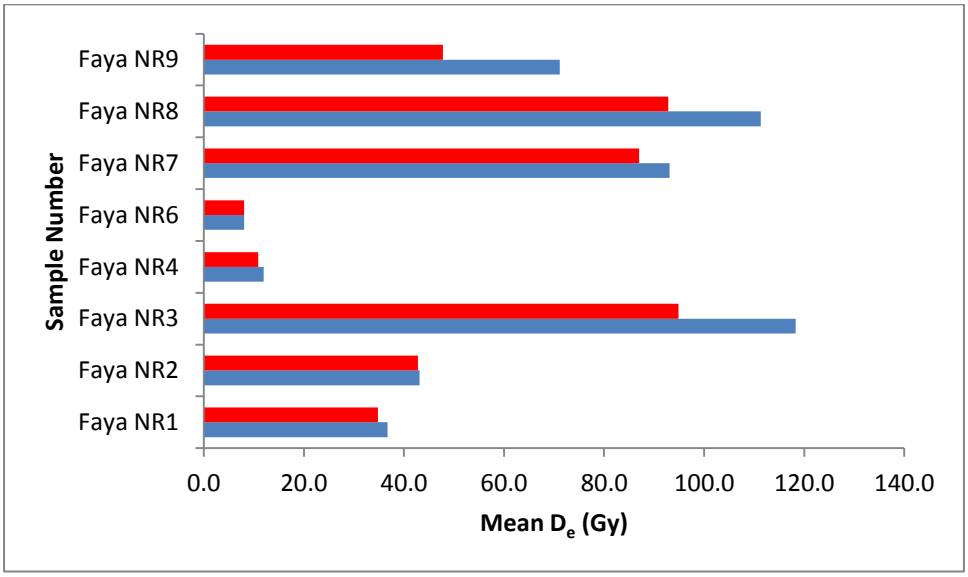

Figure 9.11. Bar chart showing the absolute change in mean D_e observed following the application of the $2D_0$ rejection criterion to each single-grain dataset. Blue bars represent the mean D_e before the $2D_0$ rejection criterion was applied. Red bars represent the mean D_e after the $2D_0$ rejection criterion was applied.

Sample ID	pre-$2D_0$			post-$2D_0$			Change in D_e (Gy)	Change in D_e (%)
	Mean D_e	±	*N*	Mean D_e	±	*n*		
Faya NR1	36.7	21.0	54	34.8	20.8	49	-1.9	-5
Faya NR2	43.1	19.1	78	42.8	18.8	75	-0.4	-1
Faya NR3	118.3	50.6	27	94.9	37.1	19	-23.4	-20
Faya NR4	12.0	15.0	38	10.9	13.5	37	-1.1	-9
Faya NR6	8.0	7.9	17	8.0	7.9	17	0.0	0
Faya NR7	93.1	38.6	29	87.0	35.8	24	-6.0	-6
Faya NR8	111.3	58.0	57	92.8	49.5	37	-18.5	-17
Faya NR9	71.1	53.4	37	47.8	34.3	24	-23.4	-33

Table 9.4. Mean D_e values produced before (pre-$2D_0$) and after (post-$2D_0$) the application of the $2D_0$ rejection criterion to each fine grain sample. Negative values indicate where the application of $2D_0$ has resulted in the reduction in the absolute and percentage mean D_e values. *n* is the number of signals accepted for each dataset.

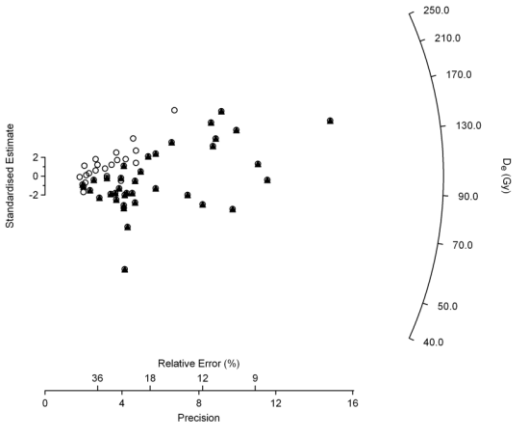

Figure 9.12. Radial plot showing the single-grain D_e distributions obtained from the Arabian sample Faya NR8. Open circles represent D_e values accepted prior to the application of the $2D_0$ rejection criterion, but rejected after the application of this criterion. Closed circles represent D_e values that are accepted following the application of the $2D_0$ rejection criterion.

9.2.3 Assessing the effect of the $2D_0$ rejection criterion on Finite Mixture Model components

Observations made from both the Arabian and Libyan datasets in Section 9.2.1 and 9.2.2 suggest that samples with higher doses experience greater reductions in mean D_e following the application of the $2D_0$ rejection criterion (Figure 9.4). Raw data and radial plot evidence appears to suggest that the higher dose signals are predominantly removed from the high-dose end of the D_e distribution, resulting in a reduction in the dispersion of the dataset. To test the notion that the removal of these higher dose signals is truncating the upper end of the dataset, the components produced by the Finite Mixture Model both before and after the application of the $2D_0$ rejection criterion are compared. Following the suggestions made by Arnold and Roberts (2009) and Russell and Armitage (2012), only the single-grain Libyan and Arabian datasets have been analysed using the Finite Mixture Model (Section 7.2.4).

The single-grain data in Tables 9.5 and 9.6 show that 6 out of the 7, and 5 out of the 7, Libyan and Arabian datasets respectively exhibit complex dose distributions. Only OSL 3, Faya NR2 and Faya NR3 yield a single dominant dose component, with the remaining samples yielding at least two significant components. Data for Faya NR6 is not presented in the tables and figures in this section as the application of $2D_0$ made no difference to the single-grain dataset.

In every case for the Libyan datasets, the highest dose component experiences a reduction in D_e following the application of the $2D_0$ rejection criterion (Table 9.5). In three cases, the highest dose component is completely removed (OSL 3, OSL 9 and OSL 10). D_e values from the smaller dose components experience either a small or no reduction in D_e.

Following the application of the $2D_0$ rejection criterion to the Arabian datasets, there is a more complex response (Table 9.6). The highest dose components from Faya NR3, Faya NR7 and Faya NR8 all experience a reduction in D_e. Component 3 from Faya NR 1 and Faya NR2, and component 4 from Faya NR4, remain unchanged (as does Faya NR6, which is not presented here). In comparison, the highest dose component from Faya NR9 experiences a small increase in D_e following the application of the $2D_0$ rejection criterion.

Sample	Component 1			Component 2			Component 3			Component 4		
	D_e (Gy)	±	%	D_e (Gy)	±	%	D_e (Gy)	±	%	D_e (Gy)	±	%
HF10	40.9	5.0	12	89.1	5.8	53	177.0	12.1	35	-	-	-
HF10 ($2D_0$)	40.0	5.6	13	78.3	8.5	50	133.0	12.4	37	-	-	-
HF09	63.4	5.6	16	142.0	7.9	38	274.6	13.5	46	-	-	-
HF09 ($2D_0$)	57.0	8.0	28	135.7	14.4	50	252.0	32.6	22	-	-	-
OSL 1	106.1	8.1	45	209.2	13.9	55	-	-	-	-	-	-
OSL 1 ($2D_0$)	103.2	23.4	46	164.3	26.1	54	-	-	-	-	-	-
OSL 3	9.4	0.2	91	31.7	2.5	8	100.3	22.4	1	-	-	-
OSL 3 ($2D_0$)	9.4	0.2	92	31.7	2.5	8	-	-	0			
OSL 9	10.9	3.3	1	62.6	4.5	28	114.3	6.6	48	280.7	24.8	23
OSL 9 ($2D_0$)	10.9	3.0	3	60.8	3.4	51	100.3	5.5	46	-	-	0
OSL 10	21.6	1.0	25	70.5	2.1	69	221.9	29.5	6	-	-	-
OSL 10 ($2D_0$)	21.6	0.9	33	66.2	2.0	67	-	-	0	-	-	-
OSL 11	51.4	2.9	34	88.0	4.1	66	-	-	-	-	-	-
OSL 11 ($2D_0$)	49.9	2.8	41	77.2	4.0	59	-	-	-	-	-	-

Table 9.5. Finite Mixture Model results for each of the Libyan single-grain D_e distributions. ($2D_0$) represents data that have been subjected to the $2D_0$ rejection criterion.

Sample	Component 1			Component 2			Component 3			Component 4		
	D_e (Gy)	±	%	D_e (Gy)	±	%	D_e (Gy)	±	%	D_e (Gy)	±	%
FAYA NR1	6.7	0.5	23	22.3	3.6	11	47.7	2.6	66	-	-	-
FAYA NR1 ($2D_0$)	6.7	0.5	26	22.3	3.6	12	47.1	2.7	62	-	-	-
FAYA NR2	8.3	0.9	8	41.7	1.5	92	-	-	-	-	-	-
FAYA NR2 ($2D_0$)	8.3	0.9	8	41.3	1.5	92	-	-	-	-	-	-
FAYA NR3	16.8	6.5	4	119.1	7.4	96	-	-	-	-	-	-
FAYA NR3 ($2D_0$)	16.8	6.5	5	106.6	7.6	95	-	-	-	-	-	-
FAYA NR4	1.8	0.2	25	5.6	0.5	42	16.0	2.1	22	39.8	11.4	11
FAYA NR4 ($2D_0$)	1.8	0.5	26	5.6	0.5	43	16.0	2.1	22	39.9	12.6	9
FAYA NR7	7.3	1.8	3	56.9	14.7	25	108.0	10.9	72	-	-	-
FAYA NR7 ($2D_0$)	7.3	1.6	4	53.9	10.5	28	103.7	8.7	68	-	-	-
FAYA NR8	9.1	2.9	2	67.8	5.4	49	155.7	10.8	49	-	-	-
FAYA NR8 ($2D_0$)	9.1	2.8	3	65.8	8.4	62	150.4	11.9	35	-	-	-
FAYA NR9	6.8	1.2	8	20.7	2.0	13	50.3	3.7	48	117.2	11.9	31
FAYA NR9 ($2D_0$)	6.7	1.2	12	20.8	2.1	21	48.2	3.5	57	120.9	20.2	10

Table 9.6. Finite Mixture Model results for each of the Arabian single-grain D_e distributions. ($2D_0$) represents data that have been subjected to the $2D_0$ rejection criterion.

Data presented in Table 9.7 appear to show a positive correlation between the size of the component D_e, and the subsequent percentage reduction in D_e following the application of the $2D_0$ rejection criterion. 6 out of the 7 single-grain Libyan samples experienced a higher percentage reduction of D_e as the corresponding component dose increased. HF10, for example, experiences a 2%, 12% and 25% reduction in D_e in its smallest, medium and highest dose components respectively. HF09 is the only exception, exhibiting a 10% reduction in D_e for the lowest dose component following the application of the $2D_0$ rejection criterion. Evidence from the Libya datasets, therefore suggests that, in general, the highest dose components experience the greatest reduction in D_e.

Sample	% Change in Component 1 D_e	% Change in Component 2 D_e	% Change in Component 3 D_e	% Change in Component 4 D_e
HF10	-2	-12	-25	-
HF09	-10	-4	-8	-
OSL 1	-3	-21	-	-
OSL 3	0	0	X	-
OSL 9	0	-3	-12	X
OSL 10	0	-6	X	-
OSL 11	-3	-12	-	-

Table 9.7. Percentage change in the D_e values produced for each component by the FMM following the application of the $2D_0$ rejection criterion to each single-grain Libyan sample. Negative values indicate where the application of $2D_0$ has resulted in the reduction in the D_e value of the component. X indicates where a component has been removed following the application of the $2D_0$ rejection criterion.

Evidence from the Arabian datasets is, however, less conclusive. Here, Faya NR1, Faya NR 2 and Faya NR3 are the only samples that experienced a coherent reduction in the D_e as the component dose increased (Table 9.8). None of the components from Faya NR 4 experienced a reduction in D_e. Component 2 and 3 from Faya NR8 exhibited a consistent 3% reduction in D_e following the application of the $2D_0$ rejection criterion. Finally, the highest dose components from Faya NR7 and Faya NR9 did not experience the greatest percentage reduction in D_e. Instead, it was the second largest components from these samples that experienced a higher percentage reduction in D_e.

Sample	% Change in Component 1 D_e	% Change in Component 2 D_e	% Change in Component 3 D_e	% Change in Component 4 D_e
FAYA NR1	0	0	-1	
FAYA NR2	0	-1		
FAYA NR3	0	-10		
FAYA NR4	0	0	0	0
FAYA NR7	0	-5	-4	
FAYA NR8	0	-3	-3	
FAYA NR9	-1	0	-4	-3

Table 9.8. Percentage change in the D_e values produced for each component by the FMM following the application of the $2D_0$ rejection criterion to each single-grain Libyan sample. Negative values indicate where the application of $2D_0$ has resulted in the reduction in the D_e value of the component.

Table 9.9 reports the percentage change in the proportion of grains present in each Finite Mixture Model component for the Libyan samples. With the exception of HF10, following the application of the $2D_0$ rejection criterion, the greatest reduction in the proportion of grains in the components can be identified in the highest dose components. Furthermore, the Libyan datasets show an increase in the proportion of grains in the lower dose components as more signals are removed from the higher dose components. Consequently, it appears that it is the largest dose components that lose the majority of grains following the application of the $2D_0$ rejection criterion.

Overall, the evidence presented in this section suggests that it is the higher dose components that are predominantly affected by the application of the $2D_0$ rejection criterion. Further evidence is provided in Table 9.10, which reports percentage change in the proportion of grains present in each Finite Mixture Model component for the Arabian samples. With the exception of Faya NR2 (which does not exhibit any change), the highest dose component for each single-grain Arabian dataset experiences the greatest reduction in size (i.e. the proportion of grains). Additionally, Faya NR8 and Faya NR9, which yield some of the highest dose values in the Arabian dataset (Table 9.6), experience the greatest

overall change in terms of the proportion of grains contained in each component. Furthermore, as identified in the Libya datasets above, most samples experience an increase in the proportion of grains in the lower dose components (e.g. Components 1, 2 and 3 from Faya NR9 experience an increase in size of 4%, 8% and 9% respectively). This effect is caused by the removal of grains from the highest D_e populations due to the application of the $2D_0$ rejection criterion, resulting in an increase in the proportion of grains in the lower dose components.

Sample	Change in Component 1 size (%)	Change in Component 2 size (%)	Change in Component 3 size (%)	Change in Component 4 size (%)
HF10	1	-3	2	
HF09	12	12	-24	
OSL 1	1	-1		
OSL 3	1	0	-1	
OSL 9	2	23	-2	-23
OSL 10	8	-2	-6	
OSL 11	7	-7		

Table 9.9. Percentage change in the proportion of grains in each FMM component following the application of the $2D_0$ rejection criterion to each single-grain Libyan sample. Negative values indicate where the application of $2D_0$ has resulted in the reduction in the size (i.e. % of all grains) of the component.

Sample	Change in Component 1 size (%)	Change in Component 2 size (%)	Change in Component 3 size (%)	Change in Component 4 size (%)
FAYA NR1	3	1	-4	
FAYA NR2	0	0		
FAYA NR3	1	-1		
FAYA NR4	1	1	0	-2
FAYA NR7	1	3	-4	
FAYA NR8	1	13	-14	
FAYA NR9	4	8	9	-21

Table 9.10. Percentage change in the proportion of grains in each FMM component following the application of the $2D_0$ rejection criterion to each single-grain Arabian sample. Negative values indicate where the application of $2D_0$ has resulted in the reduction in the size (i.e. % of all grains) of the component.

In summary, evidence from the finite mixture model data indicates that the application of the $2D_0$ rejection criterion to the single-grain Arabian and Libyan datasets results predominantly in the rejection of grains contained within the highest ("oldest") dose components. This supports the argument that the $2D_0$ rejection criterion is artificially truncating the upper end of the D_e distribution. An increase in the proportion of grains in the lower dose components following the application of $2D_0$, further suggests that utilisation of the rejection criterion would reduce the luminescence age produced, as components containing higher percentages of luminescence signals are generally chosen for age determination.

9.2.4 Changing the function used to fit the Arabian datasets before $2D_0$ is applied

As discussed in Section 9.1, the dose response characteristics from the upper part of the growth curve are not well understood. As a result, the choice of function used to fit datasets (particularly those requiring high laboratory doses) remains a subject under debate.

To explore the effect of using a saturating exponential rather than a saturating exponential plus linear fit to growth curves, both fits were applied to the Arabian single-grain datasets. The equivalent doses produced using a saturating exponential plus linear fit are those used in Section 9.2.2 (Appendix 5), whereas those for the saturating exponential fit have not yet been discussed.

Having calculated mean D_e values using single saturating exponential and exponential plus linear functions for all of the Arabian samples, both datasets were additionally analysed using the $2D_0$ rejection criterion. It should be noted that, following Durcan (2012), the D_0 value used for this analysis is that calculated when fitting the growth curve with a single saturating exponential function, irrespective of the fit used to generate the equivalent dose.

Initial comparisons were made between the mean D_e values produced for each dataset using an exponential plus linear and a single saturating exponential function, without the application of the $2D_0$ rejection criterion. Following the removal of the additional linear function, mean D_e values from each of the Arabian datasets (with the exception of Faya NR6, which experienced no change) have been reduced (Table 9.11). Faya NR3, Faya NR8

and Faya NR9 experience the largest reduction in mean D_e following the removal of the additional linear function, falling by 11.6%, 17.3% and 20.4% respectively.

Sample ID	Exponential + Linear			Exponential			Change in D_e (Gy)	Change in D_e (%)
	Mean D_e (Gy)	±	*n*	Mean D_e (Gy)	±	*n*		
Faya NR1	36.7	21.0	54	35.1	19.9	53	-1.6	-4.4
Faya NR2	43.1	19.1	78	42.2	17.7	77	-0.9	-2.1
Faya NR3	118.3	50.6	27	104.6	43.6	22	-13.7	-11.6
Faya NR4	12.0	15.0	25	11.7	18.5	24	-0.3	-2.6
Faya NR6	8.0	7.9	17	8.0	7.9	17	0.0	0
Faya NR7	93.1	38.6	29	87.2	34.5	26	-5.9	-6.3
Faya NR8	111.3	58.0	57	92.0	46.8	48	-19.3	-17.3
Faya NR9	71.1	53.4	37	56.6	37.5	32	-14.5	-20.4

Table 9.11. Mean D_e values produced using an exponential plus linear (Exponential + Linear) and a single saturating exponential (Exponential) function, prior to the application of the $2D_0$ rejection criterion to each single-grain Arabian samples. Negative values indicate where the removal of the linear function has resulted in the reduction in the absolute and percentage mean D_e values. *n* is the number of signals accepted for each dataset.

Datasets yielding lower mean D_e values experienced smaller reductions in mean D_e following the removal of the additional linear component and vice versa, a response similar to the effect of applying the $2D_0$ rejection criterion to datasets in Sections 9.2.1 and 9.2.2. As D_0 values are produced using a saturating exponential function, it is possible therefore, that the application of the $2D_0$ rejection criterion and the removal of the linear function are having a similar effect on the datasets (i.e. disproportionately more higher dose grains are being rejected).

In an attempt to understand why the use of a single saturating exponential function resulted in lower mean D_e values for the majority of Arabian samples, the reasons for grain rejections from 4 datasets were studied. The rejection criteria data presented in Table 9.12 suggests that following the removal of the additional linear function, there was a significant increase in the number of grains rejected due to a lack of L_n/T_n intersection (i.e. the natural signal failed to intersect the growth curve). Whilst some of these signals had previously been rejected from the exponential plus linear datasets due to a poor dose response curve,

several of the signals had previously been accepted. Figure 9.13 and 9.14 show examples of grains that were accepted using an exponential plus linear function, but then rejected due to a lack of L_n/T_n intersection following the application of a single saturating exponential function. It appears that the removal of the linear function results in these higher dosed grains appearing to be in saturation as their natural signal now exceeds the maximum point in the single saturating exponential growth curve. Inspection of the growth curves presented in Figures 9.10 and 9.11 suggests that, whatever the origin of the high-dose linear growth curve component, the inclusion of this component produces a growth curve which fits the measured data better than a single saturating exponential fit.

Sample	Faya NR3 (E+L)	Faya NR3 (Exp)	Faya NR4 (E+L)	Faya NR4 (Exp)	Faya NR8 (E+L)	Faya NR8 (Exp)	Faya NR9 (E+L)	Faya NR9 (Exp)
Total grains measured	2200	2200	1200	1200	3800	3800	2300	2300
Grains rejected for the following reasons								
T_n <3* σBG	1550	1550	850	850	2557	2557	1542	1542
Poor recycling ratio	469	469	296	296	1043	1043	656	656
Depletion by IR	7	7	5	5	5	5	0	0
0 Gy dose >5% of L_n	9	9	16	16	7	7	8	8
No L_n/T_n intersection	126	131	6	7	54	80	16	29
Poor DR curve	12	12	2	2	77	60	41	33
Sum of rejected grains	2173	2178	1175	1176	3743	3752	2263	2268
Acceptable individual grains	27	22	25	24	57	48	37	32

Table 9.12. The number of grains measured, rejected following application of the rejection criteria outlined in Section 5.2, and accepted for inclusion in the calculation of the burial dose. Data is provided for samples Faya NR3, Faya NR4, Faya NR8 and Faya NR9 datasets that were produced using a single saturating exponential (E) and an exponential plus linear function (E+L).

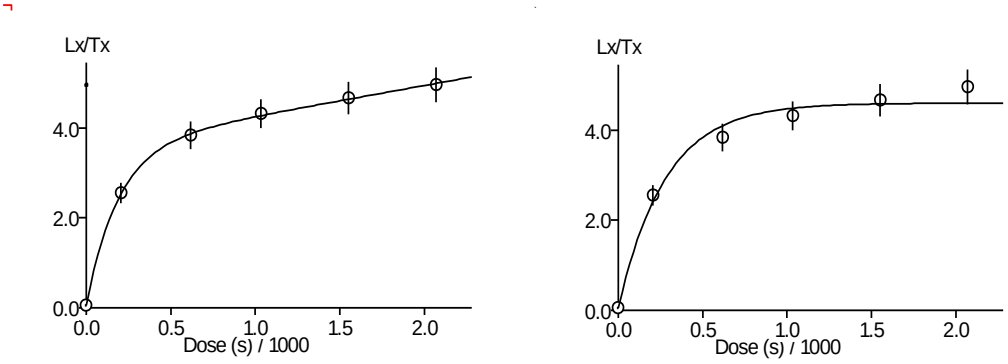

Figure 9.13. Exponential plus linear (left) and single saturating exponential (right) growth curve functions for Faya NR3, disc 7, grain 27. The red line indicated where the natural intersects the growth curve.

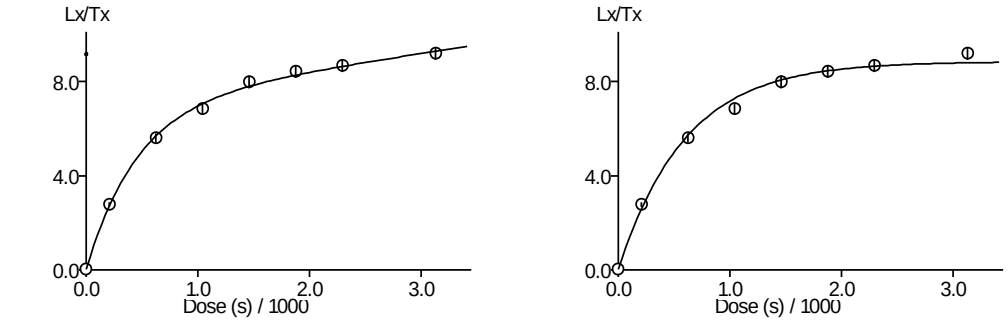

Figure 9.14. Exponential plus linear (left) and single saturating exponential (right) growth curve functions for Faya NR8, disc 23, grain 16. The red line indicated where the natural intersects the growth curve.

When fitting growth curves with a saturating exponential plus linear function, the application of the $2D_0$ rejection criterion results in a reduction of the mean D_e value in most cases (Section 9.2.2). Furthermore, it is predominantly the higher dose signals that are being rejected from the Arabian datasets (Figure 9.12). In several instances (e.g. Figure 9.13 and 9.14), grains rejected by the $2D_0$ criterion produced dose response curves that continued to grow at higher doses, and therefore did not appear to be in saturation when an additional linear function was used.

Whilst the number of grains in saturation will increase with increasing dose, the highly variable dose response characteristics of individual grains (Yoshida et al., 2000) means that

some grains in any given sample are likely to saturate at doses which, for a single aliquot dataset, would be considered low (e.g. a few Gray). As such, for relatively low D_e samples, the $2D_0$ rejection criterion would theoretically be expected to reject grains throughout the dose distributions, thereby exerting minimal influence on the mean D_e. However, since the samples exhibiting lower dose values appear to experience smaller reductions in mean D_e, it is probable that the $2D_0$ rejection criterion is disproportionately rejecting signals obtained from the upper (linear) part of the growth curve. The appropriateness of applying the $2D_0$ rejection criterion to a dataset which is better fitted with an exponential plus linear function is therefore questionable. This would support the theory of Pawley et al. (2010), who suggest that the $2D_0$ rejection criterion is limiting the dose (age) range to which the OSL dating technique is applicable. Duller (2012) explains that there are two reasons why the application of the $2D_0$ rejection criterion may provide an upper age limit for OSL dating. Firstly, the upper age is dependent on the range of D_0 values obtained for the individual quartz grains within a sample. For example, a sample containing individual grains that exhibit lower D_0 values will be limited to lower ages than a sample containing individual grains that exhibit a range of D_0 values that reach higher levels. Secondly, it is possible that the upper age limit will be determined by the amount of time available for analysis. Increasing the analysis time would in turn increase the time available in which to identify grains with a sufficiently high D_0, subsequently increasing the upper age limit for dating.

An alternative possibility is that the addition of a linear function may have enabled saturated grains to be included, erroneously, in the equivalent dose calculation. Whilst it is important to recognise the uncertainty associated with using the upper part of the growth curve, a linear component is clearly visibly in some samples. In these circumstances, not using an exponential plus linear function purely because its origin is not fully understood is debatable in itself. To test for the inclusion of "saturated" grains, the $2D_0$ rejection criterion was applied to both the saturating exponential, and the saturating exponential plus linear datasets produced using the Arabian samples. Mean D_e values produced before and after $2D_0$ was applied were then compared to investigate the effect of the additional rejection criterion (Table 9.13). The results obtained from the datasets produced using a single saturating exponential fit were then compared to the results obtained from the datasets produced using the exponential plus linear function (Table 9.14).

Sample	Function	pre-$2D_0$		*n*	post-$2D_0$		*N*
		D_e (Gy)	D_e (Gy) ±		D_e (Gy)	D_e (Gy) ±	
Faya NR1	E+L	36.7	21.0	55	34.8	20.8	50
	Exp	35.1	19.9	53	34.4	20.2	50
Faya NR2	E+L	43.1	19.1	79	42.8	18.8	76
	Exp	42.2	17.7	77	41.8	18.1	71
Faya NR3	E+L	118.3	50.6	27	94.9	37.1	19
	Exp	104.6	43.6	22	92.8	36.7	18
Faya NR4	E+L	12.0	15.0	38	10.9	13.5	37
	Exp	11.7	18.5	37	9.1	9.7	36
Faya NR6	E+L	8.0	7.9	17	8.0	7.9	17
	Exp	8.0	7.9	17	8.0	7.9	17
Faya NR7	E+L	93.1	38.6	29	87.0	35.8	24
	Exp	87.2	34.5	26	86.3	35.6	24
Faya NR8	E+L	111.3	58.0	57	92.8	49.5	37
	Exp	92.0	46.8	48	91.2	49.7	40
Faya NR9	E+L	71.1	53.4	37	47.8	34.3	24
	Exp	56.6	37.5	32	48.6	36.8	25

Table 9.13. Mean D_e values produced before (pre-$2D_0$) and after (post-$2D_0$) the application of the $2D_0$ rejection criterion to the Arabian datasets generated using a single saturating exponential (Exp) and an exponential plus linear (E+L) function. *n* represents the number of signals accepted for each dataset.

Sample	Pre $2D_0$ (E+L : Exp) Change in D_e (%)	Post $2D_0$ (E+L : Exp) Change in D_e (%)	E+L (Pre : Post $2D_{0)}$ Change in D_e (%)	Exp (Pre : Post $2D_0$) Change in D_e (%)
Faya NR1	-4.4	-5.0	-5.2	-1.9
Faya NR2	-2.1	-7.2	-0.8	-1.1
Faya NR3	-11.6	-13.8	-19.8	-11.3
Faya NR4	-2.6	23.3	-9.4	-22.2
Faya NR6	-0.2	0.7	0	0
Faya NR7	-6.3	-10.6	-6.5	-2.6
Faya NR8	-17.3	-19.2	-16.6	-1.8
Faya NR9	-20.4	-29.7	-32.8	-14.1

Table 9.14. Percentage change in the mean D_e values following the removal of the additional linear component from the Arabian datasets, both before the application of the $2D_0$ rejection criterion (pre $2D_0$) and after (post $2D_0$). The difference in percentage change following the application of the $2D_0$ rejection criterion is then presented for datasets fitted with an exponential plus linear (E+L) and single saturating exponential (Exp) function.

Overall, the mean D_e values from the exponential plus linear datasets were reduced by a greater amount following the application of the $2D_0$ rejection criterion than were the mean D_e values for the exponential fit (with mean reductions of 11.4 ± 4.2% and 6.9 ± 3.1% for each function respectively). Thus, suggesting that many of the grains rejected by the $2D_0$ rejection criterion would have already been removed by the single saturating exponential function. Faya NR 2 and 4, however, provide exceptions, with the exponential fit datasets experiencing greater reductions in mean D_e than the exponential plus linear datasets. This is significant for Faya NR4, which experiences a 12.8% reduction in mean D_e, when a single saturating exponential function is used without the additional linear fit.

Regardless of the function used to fit the Faya NR 6 dataset, there is no change in the mean D_e value following the application of $2D_0$. Conversely, a significant difference can be observed in the results from Faya NR8 and Faya NR9 following the application of the $2D_0$ rejection criterion. Using an exponential plus linear function, the mean D_e for these samples is reduced by 16.6% and 32.8% respectively. However, when the dataset is produced using an exponential function, following the application of $2D_0$, there is a far lower reduction in mean D_e (1.8% and 14.1% respectively). The difference between the two functions therefore results in an additional 14.8% and 18.7% reduction in the mean D_e for Faya NR8 and 9 respectively, if the additional linear function is used. Faya NR4 is the only sample that exhibits a significantly larger reduction in the mean D_e value following the application of the $2D_0$ rejection criterion when a single saturating exponential function is used instead of an exponential plus linear fit. This reduction of 22.2% potentially suggests the presence of grains that saturated at lower dose values.

Whilst the $2D_0$ rejection criterion causes a reduction in the mean D_e for the majority of Arabian samples (regardless of the function used), it once again appears that the samples with higher mean D_e values experience greater variations following the application of $2D_0$.

Unlike the exponential plus linear datasets (which all experience a reduction in D_e uncertainty as "saturated" signals are removed by the application of the $2D_0$ rejection criterion), in some instances (e.g. Faya NR1, 2 and 8), the exponential datasets exhibit an increased D_e uncertainty as signals are rejected. This evidence contradicts the assertion made by Wintle and Murray (2006) that the $2D_0$ criterion rejects only saturated signals, as any large asymmetric uncertainties in the D_e should have been removed.

9.2.5 Summary

65% of all Libyan and Arabian datasets produced with an exponential plus linear fit experienced a reduction in D_e following the application of the $2D_0$ rejection criterion. Only 9 of the samples (comprising mainly of fine grain, low D_e measurements) remained unaffected (Figure 9.4). All of the measurements from two samples (OSL 30 and Hajj Creiem) were rejected when the $2D_0$ rejection criterion was applied, preventing the production of a standard OSL age. Following Durcan (2012), in these circumstances a minimum age for both samples could be produced using the mean $2D_0$ value as a minimum D_e for the sample. In order to reflect the unknown levels of uncertainty associated with this estimate of minimum D_e, Durcan (2012) suggests that no error term should be provided.

The application of the $2D_0$ rejection criterion has had a significant effect on the Arabian datasets, particularly for samples FAYA NR3, NR8 and NR9, which have higher equivalent doses. At such an important site, which potentially provides evidence for the earliest modern humans to leave Africa, limiting the age of samples would result in dramatic changes to our understanding of early human migrations. It is therefore, important to ensure that the application of $2D_0$ is not limiting the OSL age, as suggested by Pawley et al. (2010).

As $2D_0$ can only be calculated when using an exponential function (Durcan 2012), it may not be appropriate to apply this criterion to a dataset that has been generated using an additional linear component. When an exponential fit is utilised without the addition of a linear function, the degree by which the sample mean D_e is reduced is lessened. Furthermore, an increase in the number of grains rejected due to a lack of L_n/T_n intersection following the removal of the linear function (and thus the upper part of the growth curve), suggests that as with the application of $2D_0$, the removal of the linear function may be artificially truncating the upper part of the D_e distribution. However, if as suggested by Singarayer and Bailey (2003), a single saturating exponential function should fit the fast component, the addition of a linear component may result in the inclusion of erroneous signals that would otherwise not have been included.

The assertion made by Wintle and Murray (2006) that the removal of saturated signals exhibiting large, asymmetric uncertainties following the application of the $2D_0$ rejection criterion will result in a reduction in associated D_e uncertainties, is based on experiments

completed using single component datasets. Consequently, any large uncertainties associated with mean D_e would most likely reflect signals in saturation. Where mixed populations are under investigation, however, uncertainties in mean equivalent doses are more likely to reflect dispersion in the natural D_e distribution. A reduction in the associated uncertainty under these circumstances is therefore more likely to reflect a truncation of the upper end of the D_e distribution.

As mentioned in the previous sections, there is currently debate concerning whether or not a single saturating exponential function provides the most appropriate fit when higher doses are being extrapolated. Kim et al. (2010) suggest that the application of an additional linear term, and the use of the upper part of the growth curve has produced mixed results, with some studies producing reliable age estimates, and others experiencing age underestimations. As a mixture of laboratory doses (i.e. high and low) were required to construct a dose response curve for the SG Arabian samples in this thesis, it was possible to use either a single saturating exponential or an exponential plus linear fit. Armitage et al. (2011) produced dates for the same Arabian site using an exponential plus linear function, stating that this function gave the best fit for the data (Figure 9.10). As Table 9.11 shows, prior to the application of the $2D_0$ rejection criterion, a single saturating exponential fit consistently produces mean D_e values that are lower than those produced by an exponential plus linear function. Once again samples with higher mean D_e dose values appear to experience the most dramatic variation. Evidence from changes in the single-grain rejection criteria results (Table 9.12) combined with changes in the growth curve fits (shown in Figure 9.13 and 9.14) suggest that the removal of the additional linear function from the Arabian datasets caused previously accepted signals to now be rejected. Using a single saturating exponential function therefore caused grains with a natural dose that exceeded $2D_0$ to appear saturated (i.e. no L_n/T_n interception) even though the exponential plus linear growth curve demonstrated convincing and continued growth above D_e.

Murray et al. (2008), who were able to produce accurate OSL ages in excellent agreement with independent age controls utilised an exponential plus linear function to fit the signals in their datasets. Furthermore, many of the natural doses included in their age calculations exhibited natural doses which intercepted the upper part of the growth curve at levels high above the $2D_0$ limit. Considering the success of this research, use of an additional rejection criterion (i.e. $2D_0$), or a function (i.e. a single saturating exponential) that may artificially limit or truncate the D_e distribution of a dataset is difficult to justify. Furthermore, where a

visual inspection of the dataset suggests that it is best fitted with the additional linear function, evidence from this chapter suggests that the use of an exponential function or the $2D_0$ rejection criterion is inappropriate.

9.3 Conclusions

In conclusion, it is apparent that the application of the $2D_0$ rejection criterion and the removal of the additional linear function from the growth curve have a significant effect on the majority of samples presented in this thesis, particularly single-grain measurements with higher equivalent doses (Figures 9.4, 9.5, 9.6, 9.7 and 9.11). Evidence presented in this chapter suggests that in most cases, the application of the $2D_0$ rejection criterion is limiting the upper age of each sample by truncating the D_e distribution at higher doses. Similarly, use of a single saturating exponential fit limits the maximum level of the growth curve, causing some grains/aliquots to fail the "no L_n/T_n intersection" rejection criterion. Whilst some authors suggest that using the upper part of the growth curve for dating may result in underestimations / overestimations of the age (e.g. Murray & Funder, 2003; Bailey 2004), research completed by Murray et al. (2008) suggests that accurate results are obtainable when using an exponential plus linear function. Additionally, they have demonstrated that the $2D_0$ rejection criterion, in this case, was not necessary to produce accurate age estimates for old samples.

Armitage et al. (2011) demonstrated that an exponential plus linear function best fitted their data from Jebel Faya (this is also the case for the Libyan and Arabian datasets presented in this thesis). Furthermore, all of the datasets in the research completed by Armitage et al. (2011), Murray et al. (2008), and this thesis had already passed stringent standard rejection criteria (Section 5.2, which includes the removal of signals where the shape of the dose response curve precludes the generation of a meaningful D_e). Taking everything discussed in this chapter into consideration, therefore, all of the Libyan and Arabian datasets in this thesis have been fitted with an exponential plus linear function, and the $2D_0$ rejection criterion has not been applied.

Chapter 10 - Libya

10.1 Introduction

The aim of the TRANSNAP project (formerly the Cyrenaica Prehistory Project) is to understand long-term environmental change, human history, and the relationships between the two in Cyrenaica, Libya, a critical boundary zone between the Saharan desert and the Mediterranean basin (Figure 10.1) (Barker et al., 2007, 2008, 2009, 2010). By integrating excavations in the Haua Fteah cave with geomorphological, palaeoecological, and archaeological studies in the wider landscape, it is anticipated that this project will contribute to our understanding of changes in the surrounding landscape over time, and the potential implications that these changes had on prehistoric human settlement in the region. In addition, data produced during this project will provide an enhanced understanding of the climatic history of North Africa during periods of high-latitude northern hemisphere glaciation, a time when the Sahara is thought to have been abandoned by hominins. In this context, North Africa may provide a climate/landscape refuge for human/hominin populations north of the Sahara during periods where the Sahara itself is uninhabitable.

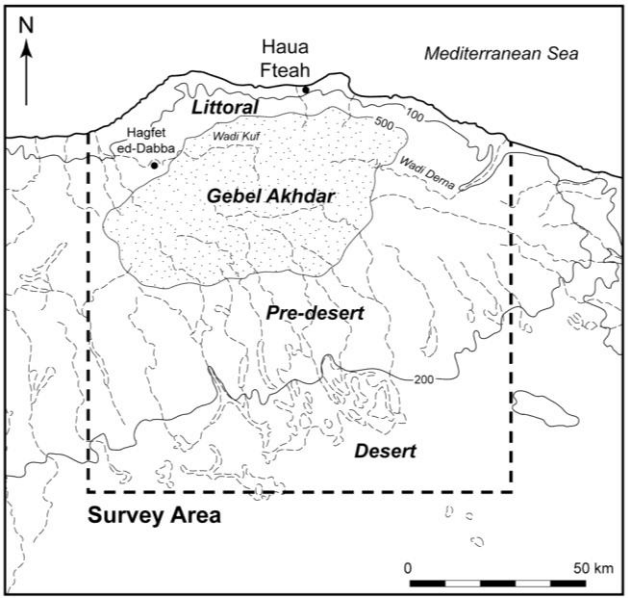

Figure 10.1. The location of the Haua Fteah cave in northeast Libya. The dashed line represents the original survey area of the Cyrenaica Prehistory Project, which was later expanded to include al Marj, further to the west, during the TRANSNAP project (Source: Barker et al., 2007).

Optically Stimulated Luminescence (OSL) dating samples were taken from six locations around the Cyrenaican landscape (Figure 10.2), including the Haua Fteah cave. Establishing a chronology at these sites will enhance our understanding of the timing of human presence and environmental change within the Cyrenaican landscape, facilitating investigations into the relationship between the two during the Quaternary period. By comparing these local chronologies with regional and global archaeological and climatic records, it will also be possible to assess the role of the region as a potential area of refuge during periods of climatic deterioration in adjacent regions, notably the Sahara.

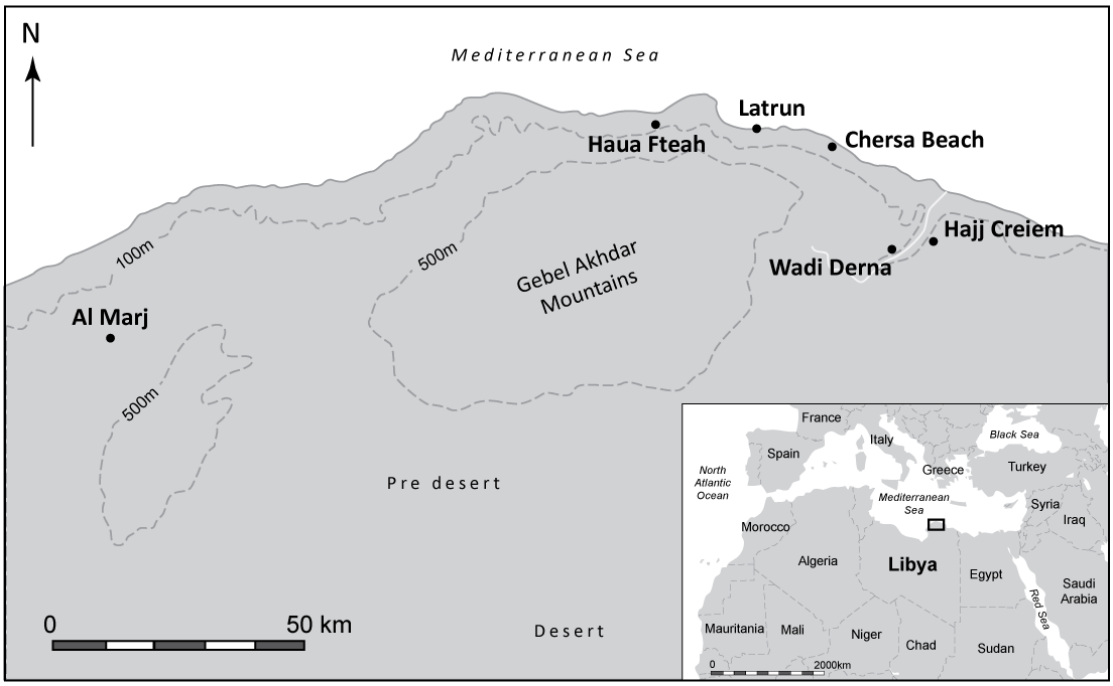

Figure 10.2. Map showing the OSL sampling locations in the landscape surrounding the Haua Fteah cave. Three sites were located at Chersa Beach and two sites were located at al-Marj. The inset illustrates the positioning of the region within a wider setting.

Following the main aims of this thesis (Section 1.5), this chapter presents a chronology for environmental change and human activity in the landscape surrounding the Haua Fteah cave in northern Libya. This chronology is then compared to published climatic and archaeological records. Background information for the study areas, the climatic and anthropogenic significance of each site, and the sampling strategies employed at each locality, are summarised in this chapter.

10.2 Luminescence properties

All OSL samples were collected and prepared using the methodology outlined in Chapter 4. Little or no quartz in the preferred size range (212-180 µm) was present in the Libyan samples, and hence dating work was carried out on the coarsest grain size fractions available in each sample (90 – 125 µm, 60 – 90 µm, and on occasions 4 – 11 µm). Whilst small aliquot and fine grain dating was appropriate for some of the samples measured (i.e. samples thought to contain grains which all belong to a single age population), in several localities single-grain dating was considered necessary (i.e. for samples thought to contain complex dose distributions). In these locations single-grain dating was required to identify the presence of mixed grain populations (potentially caused by partial bleaching of the sample prior to deposition and/or post-depositional mixing of sediment units). This approach should allow the mathematical separation of individual age components, and therefore the production of the most statistically likely age(s). Where quartz grains with diameters greater than > 60 µm were present in a sample, it was possible to hand pick individual grains of quartz, facilitating the production of a single-grain age. However, at certain sites such as Chersa Beach, the paucity of quartz grains with diameters larger than 40 µm prevented such measurements. Within the context of this thesis and the TRANSNAP project overall, the sites that only contained fine grains (i.e. Chersa Beach and Latrun) were considered to be of great environmental and archaeological importance. Consequently, whilst single-grain dating was considered necessary for accurate age determination at these sites, it was only possible to apply OSL dating methods at the small aliquot or fine grain dating scale. Therefore, small aliquot and fine grain dating methods were used to obtain OSL ages for the samples, acknowledging that where complex dose distributions exist, the calculated age may be erroneous. Where partial bleaching is the cause of a complex dose distribution, the resulting ages will be erroneously high. The size and direction of the error caused by post-depositional mixing cannot be predicted. Consequently, caution is required when interpreting the dates produced for the coastal samples, particularly the palaeosol units, which should be viewed only as approximations.

Typical decay curves from single-grain, small aliquot and fine grain scales of measurement are shown in Figures 10.3, 10.4 and 10.5. Luminescence signals from all of the Libyan material are characterised by a rapid signal decay and fast ratio values of > 20, suggesting the dominance of the fast component in the initial part of the OSL signal (Durcan & Duller, 2012).

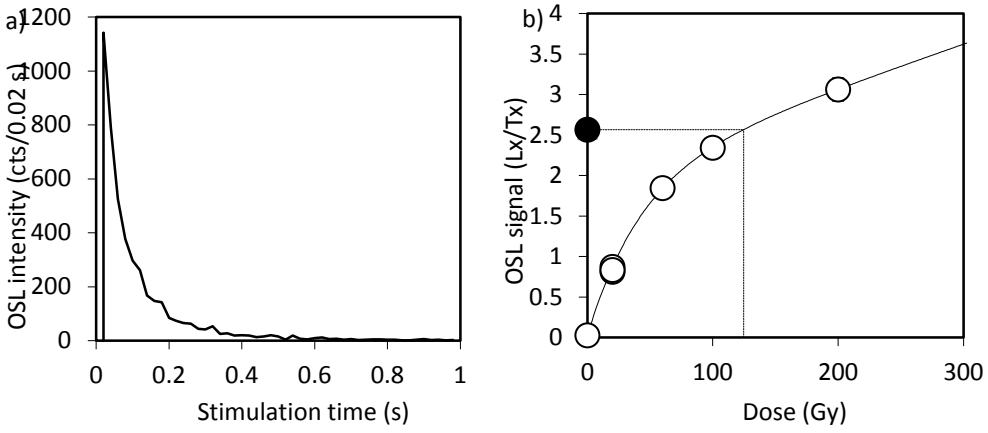

Figure 10.3. A typical (a) decay curve and (b) dose response curve for OSL 1, a single-grain sample that passed the rejection criteria and that is dominated by the fast OSL component.

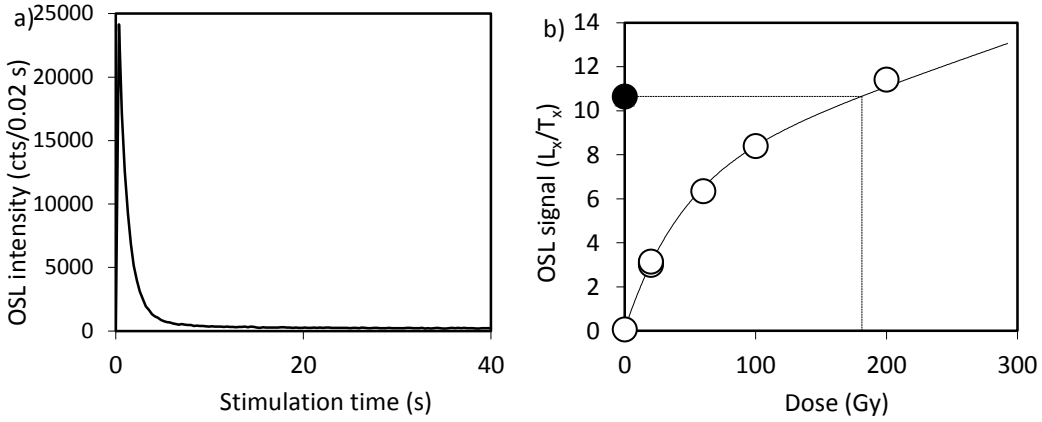

Figure 10.4. A typical (a) decay curve and (b) dose response curve for OSL 17, a small aliquot sample that passed the rejection criteria and that is dominated by the fast OSL component.

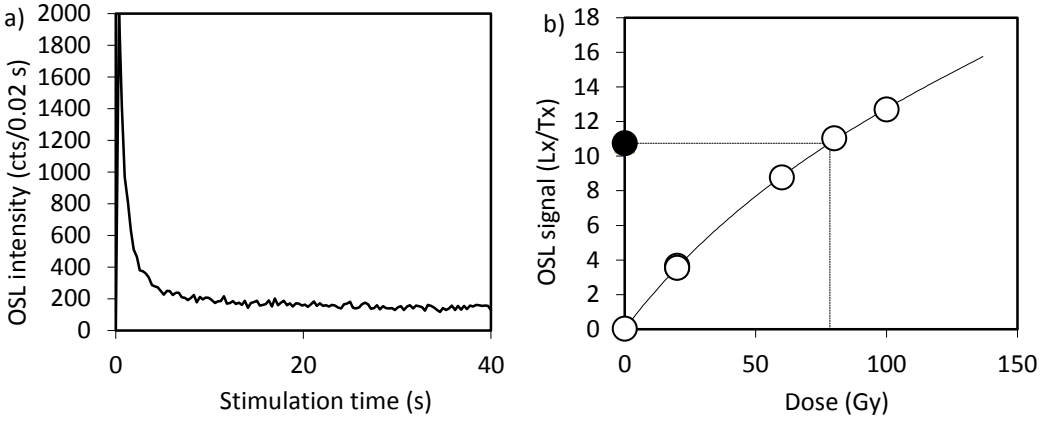

Figure 10.5. A typical (a) decay curve and (b) dose response curve for OSL 8, a fine grain sample that passed the rejection criteria and that is dominated by the fast OSL component.

Cumulative light sum plots produced for the single-grain samples suggest that 5-25% of the grains in the Libyan samples contribute 90% of the total light sum (Figure 10.6). In comparison with data reported by Duller (2000), which suggests that only c. 5% of grains yield a luminescence signal, the Libyan material appears to contain a relatively high proportion of luminescent grains.

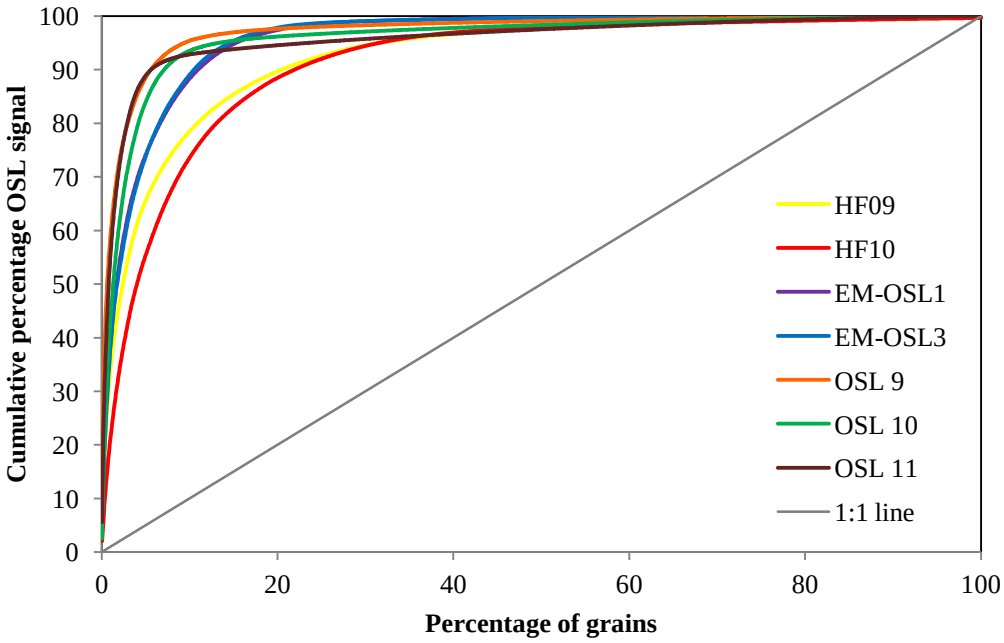

Figure 10.6. Cumulative light sum plots for the single-grain Libyan samples measured in this study. Grains are ranked by brightness, with the brightest grain being plotted first.

Single aliquot dose recovery preheat plateau experiments were performed using the method of Murray and Wintle (2003) for samples at each site. 24 aliquots were measured using the methodology outlined in Chapter 4. Overall, the results demonstrate that the Libyan samples are relatively insensitive to preheating conditions, and a PH1 temperature of 260 °C and PH2 temperature of 220 °C was adopted for the Libyan samples. Example dose recovery preheat plateau experiment results are presented in Figure 10.7.

Appendix 3 provides a summary of all D_e and D_r values used to calculate the age for the Libyan samples in this thesis.

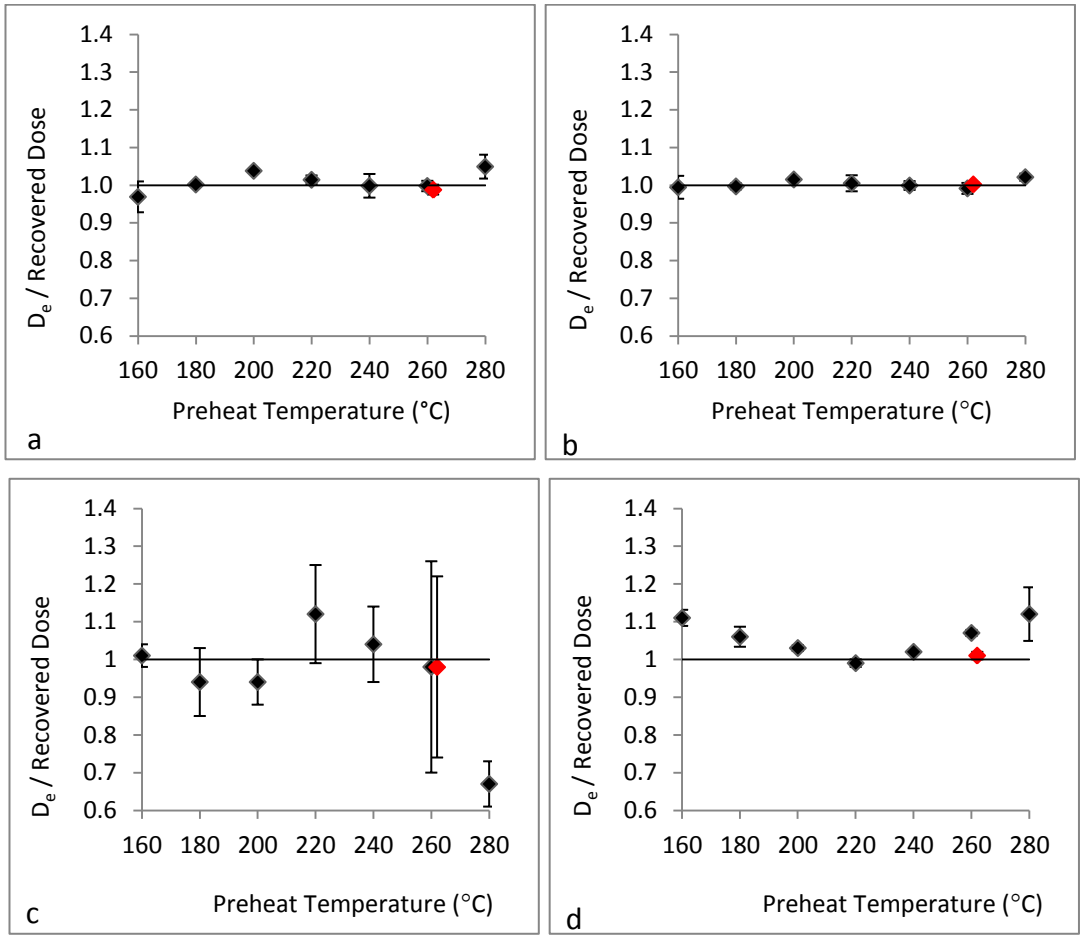

Figure 10.7. Dose recovery preheat plateau results for a) HF09, b) HF10, c) OSL 1, and d) OSL 3. PH1 temperatures are plotted on the x-axis. Black symbols represent aliquots measured using a 160 °C cut-heat for PH2, whereas red symbols represent aliquats which received a 220 °C, 10 second PH2. The red symbols are offset on the x-axis by 2 °C for clarity. Each data point represents the mean of three aliquots, with one standard deviation uncertainties. The chosen preheating regime was a 260 °C 10 second PH1, a 220 °C 10 second PH2. Aliquots measured using this preheating regime are represented by the red diamonds.

10.3. The Haua Fteah cave

The Haua Fteah cave is a limestone karstic cave located on the seaward side of the Gebel Akhdar upland massif (see Figure 10.1) (Barker et al., 2007). Two OSL samples from within the Haua Fteah cave were analysed in this study, though a larger number of samples were analysed by Dr Zenobia Jacobs. The samples measured in this study were taken at depths of 6.3 m (HF10) and 7.5 m (HF09). HF10 was taken from the basal section of the middle trench in context 524, which is associated with the start of Levallois-Mousterian Middle

Palaeolithic lithic industries (Barker et al., 2010) (see Figures 10.8 and 10.9). HF09 was taken from the top of the deep sounding, which is associated with Pre-Aurignacian lithic material throughout (Barker et al., 2010).

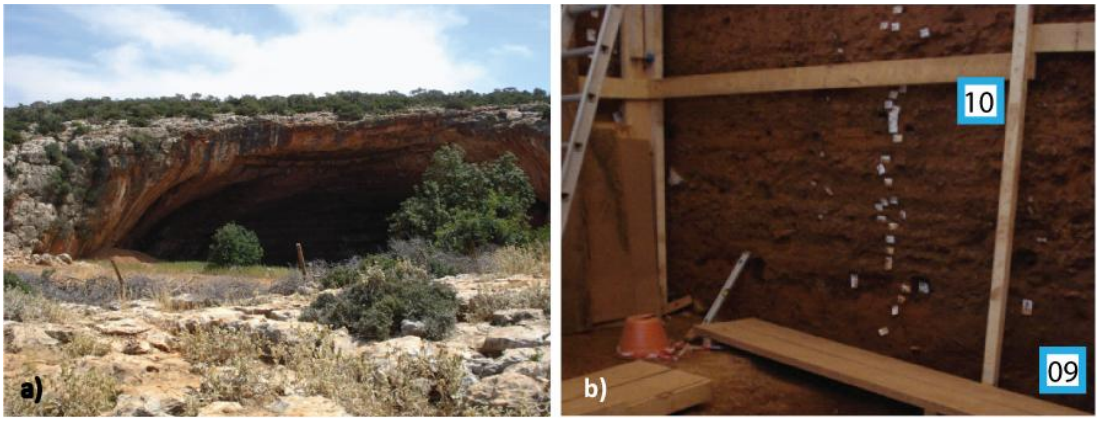

Figure 10.8. a) Haua Fteah cave. b) Location of sample HF10 from within the middle trench, and HF09 from within the deep sounding. Both samples are indicated by the presence of a blue box containing the sample number.

The Pre-Aurignacian lithics identified by McBurney (1967) are present from the base of the deep sounding to Layer XXXV, which is located at the base of the Middle Trench. This lithic industry contains a flake and blade flake industry with burins and points, and was named after the earliest blade industry of the European Upper Palaeolithic. Using the original age model for the site, McBurney assigned an age range of c. 80-65 ka BP to the Pre-Aurignacian lithic material. Succeeding the Pre-Aurignacian at the site, McBurney (1967) identified a Levallois-Mousterian industry broadly comparable with similar industries in the Levant and Europe. Two human mandibles, now believed to belong to robust modern humans, were discovered in the sediments associated with Levallois-Mousterian lithics in the middle trench (Barker et al., 2008). McBurney assigned an estimated age range of c. 65-40 ka BP to this section of the middle trench.

Although McBurney (1967) identified two separate lithic industries, re-analysis of the lithics by Reynolds (2012) suggests that rather than comprising two distinct industries, the Pre-Aurignacian and Levallois-Mousterian lithic assemblages are both likely to be of modern human origin, and that variations between the two assemblages are most likely due to sampling variants (i.e. differing sampling strategies).

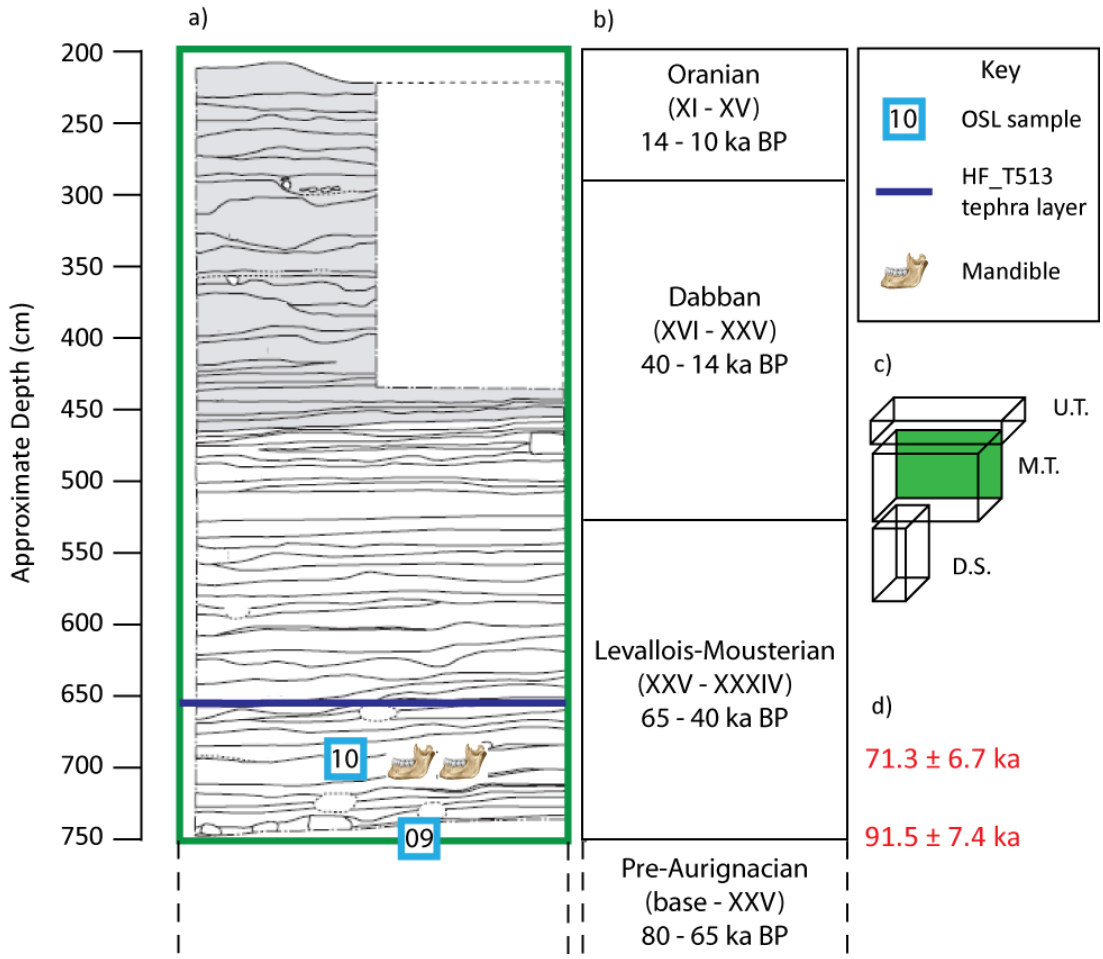

Figure 10.9. Section diagram for the Haua Fteah cave site. a) Section diagram showing the location of OSL samples HF10 (10) and HF09 (9), the location of the two human mandibles, and the location of the HF_T513 tephra layer (blue line) within the Haua Fteah Middle Trench contexts. The dashed black vertical lines extending below the section diagram indicate the start of the deep sounding, and the start of the corresponding Pre-Aurignacian lithic industry. The Upper Trench (not shown in this diagram) lies in the 0 - 200 cm above the Middle Trench. b) Table showing the corresponding McBurney (1967) lithic industries, layers, and suggested ages from the original site age model. c) Plan diagram showing the orientation of the McBurney trenches, including the Upper Trench (U.T.), Middle Trench (M.T.), and the Deep Sounding (D.S.). d) OSL ages produced as part of this thesis are marked in red to the right of the McBurney information, aligned with the according sample. Figure adapted from Barker et al. (2008, 2009) and Douka et al. (2014).

Soil micromorphological investigations from within the cave suggest that the basal section of the middle trench was dominated by significant hiatuses in deposition and a number of inwash events (Barker et al., 2010). Whilst continuous micromorphological investigations were not completed throughout the deep sounding, it is likely that similar depositional processes are responsible for the sedimentation in these layers. According to Douka et al.

(2014), the sediments between 7.5 m and 6.5 m in depth are dominated by red-orange silt layers, believed to have been reworked from the immediate area of the cave and potentially from further afield. Recycling of sediment blown into the cave via aeolian processes is also thought to have occurred. These sediments are interrupted with clay rich soil material transported into the cave from the surrounding hill slopes via inwash events. Consequently, partial bleaching and grain to grain variability are likely to affect the OSL samples from the Haua Fteah, due to the complex depositional and burial histories of the cave sediments.

The original age model for the cave produced by McBurney (1967) was developed by obtaining radiocarbon ages in the top part of the cave sequence. Ages for the lower levels were subsequently calculated by extrapolation, using an estimate of the sedimentation rate derived from the radiocarbon dated levels and a comparison with the emerging marine isotopic record (Douka et al., 2014). The Pre-Aurignacian material was originally thought to range from 80 – 65 ka BP, whilst the Middle Palaeolithic material was dated to between 65 – 40 ka BP (Barker, 2007; McBurney, 1967)(Figure 10.9). The OSL ages produced as part of this thesis will be combined and compared with a suite of other chronological techniques (including radiocarbon dating, U-series dating, and tephrochronology) in an attempt to produce an accurate, multi-technique age model for human occupation within the cave. HF10 represents a duplicate sample from a suite of 12 OSL samples that were taken throughout the Middle Trench by a team from Wollongong University, Australia. Independent dating by both teams sought to achieve an inter-laboratory comparison, which would test the accuracy of the technique within the cave.

As the potential for post depositional mixing within the Haua Fteah cave sediments (indicated by the micromorphological and sedimentological investigations) was high, single-grain dating was necessary to produce ages for these sediments. Due to the paucity of coarse grain quartz in these samples, following the experimental research outlined in Chapter 8, single grain discs were prepared by hand picking individual 60-90 µm quartz grains.

Overdispersion values of > 20% were obtained for both samples following the application of the Central Age Model. Similarly high overdispersion values have been interpreted as indicating the presence of more than one age component in a sample (Olley et al., 2004). Consequently, the Finite Mixture Model was applied to the datasets in an attempt to identify the individual components (Section 7.2.4). Radial plots (see Figure 10.10) show the

equivalent dose distributions for the two datasets, with the components identified by the FMM being expressed as grey and black lines. It is likely that post depositional mixing (resulting from inwash events and animal burrowing) within the cave has resulted in the complex D_e distributions shown by the radial plots.

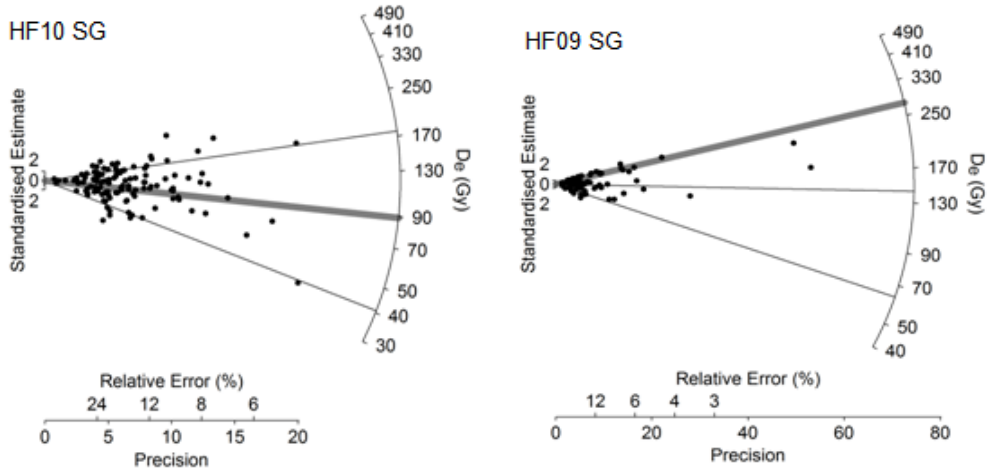

Figure 10.10. Radial plots showing the single-grain (SG) D_e distributions obtained from samples HF10 and HF09. The thick grey bars represent the dominant (>40%) components identified using the FMM. Black lines identify minor components, containing less than 40% of the grains measured.

HF10 and HF09 are comprised of 3 separate components at 16% and 20% overdispersion respectively. For sample HF10, the component containing the highest proportion of accepted grains (53%), yields an age of 35.9 ± 3.3 ka. Two smaller components yield ages of 16.5 ± 2.3 ka and 71.3 ± 6.7 ka and contain 12% and 35% of the remaining single-grain dataset respectively. The largest component (46%) obtained from HF09 suggests an age of 91.5 ± 7.4 ka. Smaller components comprising 16% and 38% of the D_e estimates yield ages of 21.1 ± 2.3 and 47.3 ± 4 ka respectively.

Whilst it has generally been assumed (e.g. Jacobs et al., 2008; Armitage et al., 2011) that the component which contains the highest proportion of grains is likely to be that relating to the true depositional age of a sedimentary deposit (i.e. an age of 35.9 ± 3.3 ka for HF10 and 91.5 ± 7.4 ka for HF09), independent tephrochronological results from the cave indicate that an age of 35.9 ± 3.3 ka for HF10 may be incorrect. The HF_T513 tephra layer (discovered in context 513, c. 35 cm above HF10 (see Figure 10.9)) has been chemically correlated with the TM-20-2a tephra layer in Lago Grande di Monticchio, and has been

assigned a varve age of 68,620 ± 2,600 calendar years. Additionally, the corresponding duplicate sample dated by the Wollongong team has been assigned an age of 60.9 ± 6.1 ka (Douka et al., 2014). For sample HF10, only the second largest component (35%, 71.3 ± 6.7 ka) yields an age in agreement with that for the tephra layer. Consequently, the second largest component for HF10 has been selected as the most likely age for the sample, due to its correlation with the independent tephrochronology and corresponding OSL age results. If this interpretation is correct, then it indicates that a very high degree of post-depositional intrusion of anomalously young material into sample HF10 has occurred. It is also notable that sample HF09, which overlies HF10, yields an age which is older than both HF10 and the HF-T513 tephra.

The ages obtained for HF10 (71.3 ± 6.7 ka) and HF09 (91.5 ± 7.4 ka) therefore suggest the presence of modern humans in the Haua Fteah cave around the time of the northern hemisphere interstadials MIS 5a and MIS 5c, far earlier than McBurney (1967) thought. Northern hemisphere interstadials have been shown to be periods of increased humidity in North Africa (e.g. Drake et al., 2011; Blome et al., 2012), and are therefore associated with enhancements in local resource availability. Since these resources would have supported modern humans living in the landscape around the cave, the ages presented are consistent with the archaeological evidence.

10.4 Coastal Sites

Barker et al. (2007) highlight the importance of studying the coastal region around the Haua Fteah cave for improving our understanding of environmental change and human activity in the area during the Quaternary. Sedimentary records in this area provide high resolution sequences documenting landscape change. These sequences contain raised beaches, fluvial gravel, scree / slope materials, palaeosols, tufas, and aeolian and lacustrine sediments. The discovery of lithics in several units in these sequences allows the relationship between humans in the landscape and the changing environment over time to be addressed (Barker et al., 2009). Furthermore, with tectonic uplift and sea level change complicating the overall landscape evolution record in the region (Barker et al., 2009), OSL dating may provide an important chronological contribution, aiding our understanding of the development of coastal sequences in the area.

During the 2010 field season four sites along two main coastal sections (Chersa Beach and Latrun) were investigated and selected for OSL dating (Figure 10.2). OSL dating was completed at the sites along the Latrun and Chersa Beach coastal sections, following the identification of in-situ lithic evidence, indicative of human activity in the area.

None of the OSL samples taken from the Chersa Beach and Latrun coastal sites contained measurable concentrations of quartz above 40 μm in diameter. Consequently, whilst single grain analysis would have been the preferred method for dating these sites, all OSL work at these sites was completed using aliquots of fine-grained quartz (4 – 11 μm). In the context of this thesis, these sites represent important evidence for human activity and environmental change along the Libyan coastline, a potential area of refuge during periods of increased aridity in North Africa. Consequently, whilst the utilisation of fine grain methods was likely to limit the accuracy of OSL dating at these sites, the anthropogenic and environmental importance of the sequences meant that it was important to attempt dating. Caution is therefore required when interpreting several of the dates produced for the Latrun and Chersa Beach samples.

The Central Age Model of Galbraith et al. (1999) was used to produce weighted mean equivalent doses and associated uncertainties for all of the fine grain samples.

10.4.1 Latrun

Latrun is a small town located on the coastline c. 8 km east of the Haua Fteah cave (22° N, 32° E) in an area that contains a number of headlands and bays, which exhibit signs of ephemeral human activity in the form of hearths and in-situ knapping floors (Figure 10.2). OSL work was undertaken in this area after Barker et al. (2009) identified a late Pleistocene sequence at Latrun, consisting of loess and mudflow deposits with three poorly developed palaeosols. The upper palaeosols were overlain by thin tufas, whilst the basal palaeosol unit contained evidence of Epipalaeolithic industries. Further signs of human activity including hearths were also discovered in the area, making this an important area for investigation.

To the east of the OSL study area at site 1800, Barker et al. (2009) identified a chert bedrock that was most likely formed by a wadi entering the area during warm and dry conditions. Overlying this bedrock unit, a sequence of aeolianites, mud flow gravels /

raised beach deposits, yellow and red silts, gravels, tufas and a capping calcareous unit are thought to represent the evolution and termination of a past lagoonal system in the area. Whilst no OSL dating samples were taken from these deposits during the 2010 field season, the sedimentary evidence suggests that this area would have most likely provided a rich source of resources for modern humans present in the landscape at some point in the past.

Site 1802/03 was located c. 200 m west of site 1800 in an adjacent bay. Here, a hearth bearing raised beach deposit (1803) was overlain by an 8 m palaeosol unit (site 1802) containing an in-situ knapping floor complete with hammer stone. The overall sequence at the site was underlain by a cemented beach gravel and capped by a small tufa deposit.

Lithic evidence from the Latrun area is currently thought to be associated with a modern human Epipalaeolithic industry (Barker et al., 2009), although detailed investigations into the lithics identified at site 1802/03 have not yet been completed. Consequently, OSL dating samples were taken from the sediment adjacent to the hearth and knapping floor in the raised beach and palaeosol deposits respectively (Figure 10.11). Samples taken from these locations sought to facilitate investigations into the timing of ephemeral human activity, the timing of environmental change, and the relationship between the two over time within the Latrun area.

OSL 7 was taken 11.3 m below the present land surface, from the hearth bearing raised beach deposit. The unit was a well sorted, cemented sandy carbonate containing small pebbles throughout. Based on the depositional environment inferred in the field, it was thought unlikely that this deposit would have experienced extensive partial bleaching or post depositional mixing, and therefore single grain dating was not considered necessary. Due to the cemented nature of the sediment it was not possible to obtain gamma spectrometry measurements from this unit.

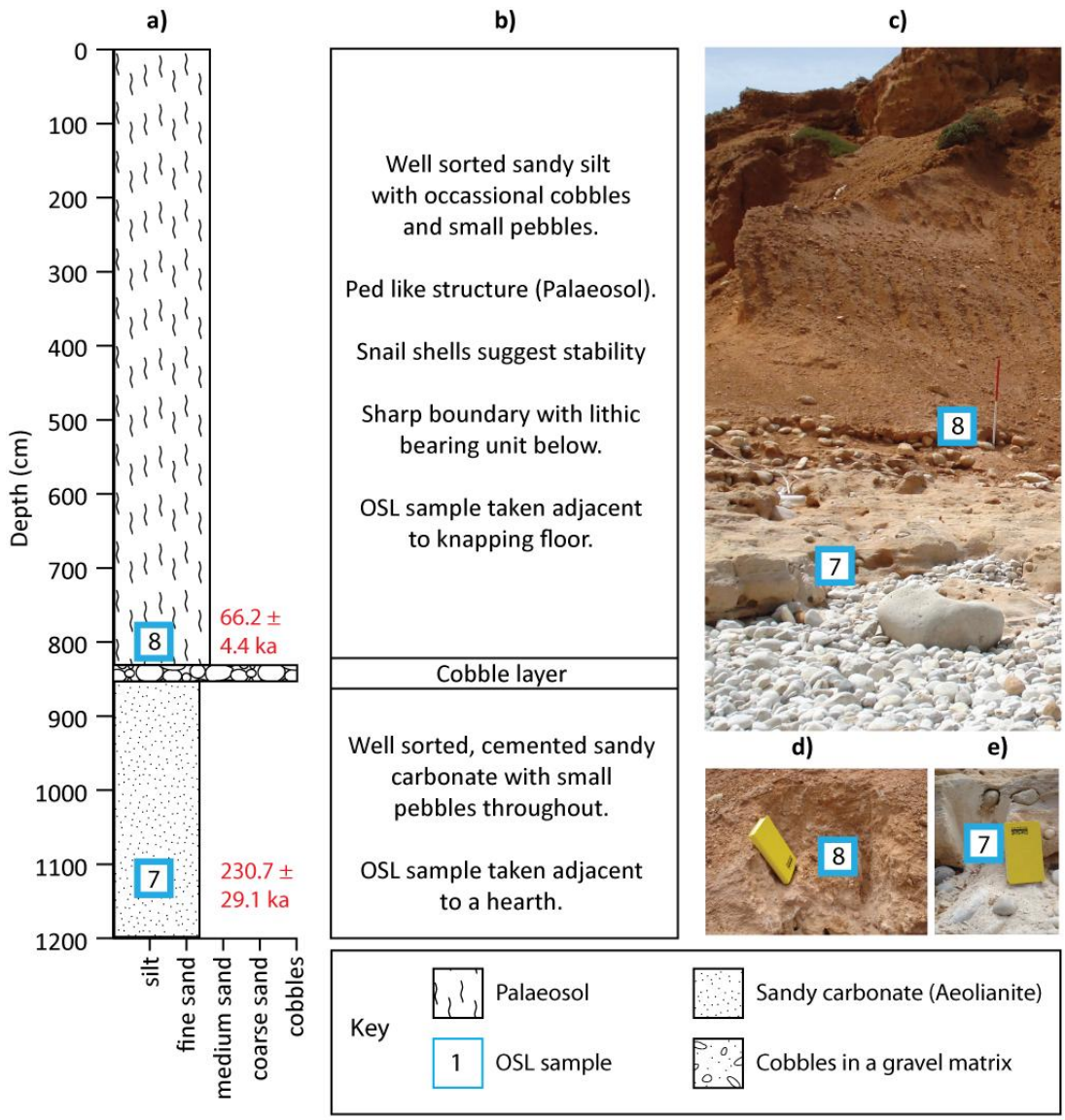

Figure 10.11. a) Field log of site Latrun, with b) sediment description and interpretation of key stratigraphic layers from which OSL samples were taken. Sharp contacts are indicated by solid lines. c) Photograph of the Latrun site with sample locations indicated by the blue boxes. Numbers in the boxes relate to the OSL sample number (i.e. 1 = OSL 1). d) Photograph of sediments surrounding OSL 8 sample location. e) Photograph of sediments surrounding OSL 7 sample location. OSL ages are shown in red to the right of the sediment log.

OSL 8 was taken from the palaeosol unit, 8 m below the present day land surface, adjacent to the knapping floor. Pebbles and cobbles were observed throughout the clay rich deposit, which appeared to have experienced "faulting/ slippage" in the past (Figure 10.11 c). "Slump" material, believed to represent that which may have "fallen" from the above section, was removed to expose a clean section face prior to sampling. Whilst the presence of intact snail shells suggested stability of the sediment unit (C. Hunt, *pers comm*. 2010), the potential for partial bleaching and post depositional mixing is high in soil samples. Consequently, this sample would ideally have been measured at the single-grain scale. However, insufficient coarse grained quartz was present in this sample to allow this approach, and hence it was dated using aliquots of fine grained (4-11 μm) material. Consequently, the age for this sample should be interpreted with caution.

Using the Central Age Model of Galbraith (1999), overdispersion values of < 20% were obtained for samples OSL 7 and OSL 8. For a single-grain dataset, this value would suggest that the samples contained only a single D_e component. However, for a fine-grained sample, it is likely that any grain to grain D_e variability in the dataset is masked by the averaging effect associated with measuring thousands of grains on a single disc. Consequently, the overdispersion value for these datasets cannot be used to infer the absence of a complex equivalent dose distribution.

The CAM D_e values for OSL 7 and OSL 8 yield ages of 230.7 ± 29.1 ka and 66.2 ± 4.4 ka respectively. These ages would place the development of the palaeosol at the beginning of MIS 4, and the raised beach deposition during MIS 7.

The presence of a fire hearth at Latrun c. 230 ka represents the earliest evidence of hominin occupation in Cyrenaica by a long way. Although Barker et al. (2009) suggest that evidence in the area indicates the presence of modern humans, the lack of confirmed lithic evidence makes it difficult to draw conclusions about which hominin species was present at the site. As discussed in the opening chapters of this thesis, anatomically modern humans are thought to have evolved in sub-Saharan Africa c. 200 ka, making the evidence for human occupation at Latrun c. 230 ka unlikely to be representative of an AMH population. Instead, it is possible that an archaic human population present along the Cyrenaican coastline at that time was responsible for the use of a fire hearth. A newly discovered hearth at Qesem Cave in Israel has recently been dated to c. 300 ka, and assigned to an archaic human population (Shahack-Gross et al., 2014). It is possible therefore, that a

similar hominin population was responsible for the hearth at Latrun, although this assumption requires further research.

As discussed earlier, the use of fine grain dating techniques on samples that are likely to contain complex dose distributions (i.e. partially bleached samples) may have resulted in the production of erroneously old ages. It is unlikely that the climate during MIS 4 provided the environmental conditions necessary for the development of an 8 m palaeosol unit. Furthermore, evidence for mass movement of the palaeosol unit increases the likelihood of partial bleaching and post depositional mixing at the site. Consequently, it is suggested that the age for OSL 8 is erroneously high, and that the development of the palaeosol unit is more likely to have occurred during the humid conditions of the MIS 3 interglacial. Without the completion of single-grain dating at the site it is impossible to verify this interpretation. It is therefore acknowledged that the attribution of an MIS 3 age to the palaeosol is, at best, an approximation of the true age.

Fine grain dating of a well sorted sediment that is likely to have been fully bleached prior to deposition can be considered far more appropriate. Whilst the age for sample OSL 8 must still be interpreted with caution, the deposition of a raised beach deposit during MIS 7, when sea level high stands have been reported by several authors (including Dutton et al., 2009), appears to be more realistic.

Overall, the ages produced for OSL 7 and OSL 8 at Latrun suggest that humans (both archaic and modern) were present along the Cyrenaican coastline during stages MIS 7 and MIS 4 respectively. Whilst the deposition of a raised beach deposit during humid climate periods associated with high sea level stands in MIS 7 seems appropriate, the development of an 8 m palaeosol unit during MIS 4 (a time usually associated with aridity in North Africa) does not. It is therefore suggested that the age produced for OSL 8 is erroneously old. Consequently, modern human presence along the coastline is tentatively attributed to the subsequent humid period associated with the MIS 3 interstadial instead, while an archaic human presence in the area is more confidently attributed to the high sea level stands in MIS 7. Latrun therefore potentially provides the earliest evidence for human occupation along the coastline in Cyrenaica.

10.4.2 Chersa Beach

OSL samples were taken from three sites along the Chersa Beach coastline at sites 1838, 1848/50 and 1851 (Figure 10.12). The stratigraphy of the coastal sections along the Chersa Beach coastline appeared to be broadly similar at each site. Underlain by a cemented raised beach, a sequence of archaeologically rich palaeosols and gravels were typically cut into by a second raised beach, that was in turn overlain by aeolianites and alluvial fan gravels (Barker et al., 2010). In all cases, the OSL samples were taken in association with either the lithic bearing palaeosols or the overlying aeolianite deposits. Consequently, a chronology for human activity and environmental change within the landscape could be developed.

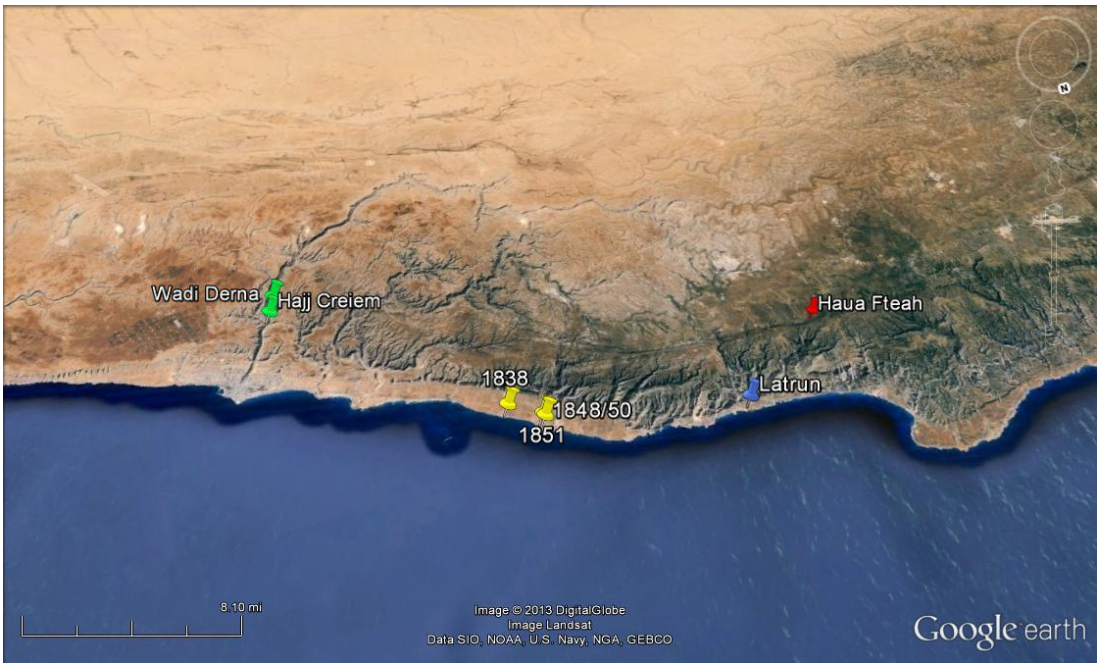

Figure 10.12. Google earth image showing the location of the Chersa Beach site locations (marked with yellow pins) in relation to the Haua Fteah, Latrun and Wadi Derna sites. The view is taken looking south onto the northern Libyan coastline.

10.4.2.1 Chersa Beach, 1838

Site 1838 contains a sedimentary sequence thought to reflect a change from a marine (cemented raised beach) to a terrestrial soil environment (palaeosol), which was interrupted briefly by a large flood event (gravel) before again returning to a period of soil development (palaeosol). A period of sea level rise (aeolianite) and cliff development then

followed the period of stability represented by the underlying thick palaeosol deposit (Figure 10.13). Eleven flakes, tentatively referred to as a knapping floor, were extracted from the lowest part of the palaeosol unit (below the gravel flood deposit). These lithics were tentatively assigned to the Middle Palaeolithic, and therefore modern human origins, although they have not yet been attributed to a specific lithic industry.

Sample OSL 21 was taken from the basal section of the lithic bearing palaeosol unit at a depth of 5.4 m below the present day land surface. This sample was taken from sediments associated with the knapping floor identified at the site. The palaeosol unit at this site is a poorly sorted red clayey silt, containing numerous clasts, from gravels to cobbles, throughout. The sample was taken c. 1 m above the raised beach deposit, between two gravel units. Under normal circumstances, fine grain dating would not have been utilised for the dating of this palaeosol unit due to the potential for partial bleaching. The paucity of quartz grains > 40 μm, however, meant that it was not possible to complete single-grain dating at this site.

Sample OSL 22 was extracted from the aeolianite deposit overlying the lithic bearing unit, at a depth of 1.7 m below the present day land surface. OSL dating in this location sought to provide a minimum age for the deposition of the underlying archaeology. The unit was comprised of a well sorted, cemented carbonate sand containing small clasts of gravel found sporadically throughout. The aeolianite unit which was located c. 10 m north of the main section containing the lithic bearing unit and appeared to bank up against the gravels, suggesting it was deposited after an erosion event. It was not possible to obtain gamma spectrometry measurements at this site due to the cemented nature of the aeolianite sediments. While small aliquot dating would have been preferable for this unit, utilisation of the fine grain dating method was considered more appropriate here than for the palaeosol deposit due to the well sorted nature of the aeolianite.

Equivalent doses produced using the CAM yield ages of 188.1± 18.4 ka and 78.3 ± 9.8 ka for the lithic bearing palaeosol (OSL 21) and overlying aeolianite deposit (OSL 22) respectively. According to these ages, human presence at the site is therefore suggested to have occurred at the end of MIS 7, into the beginning of MIS 6.

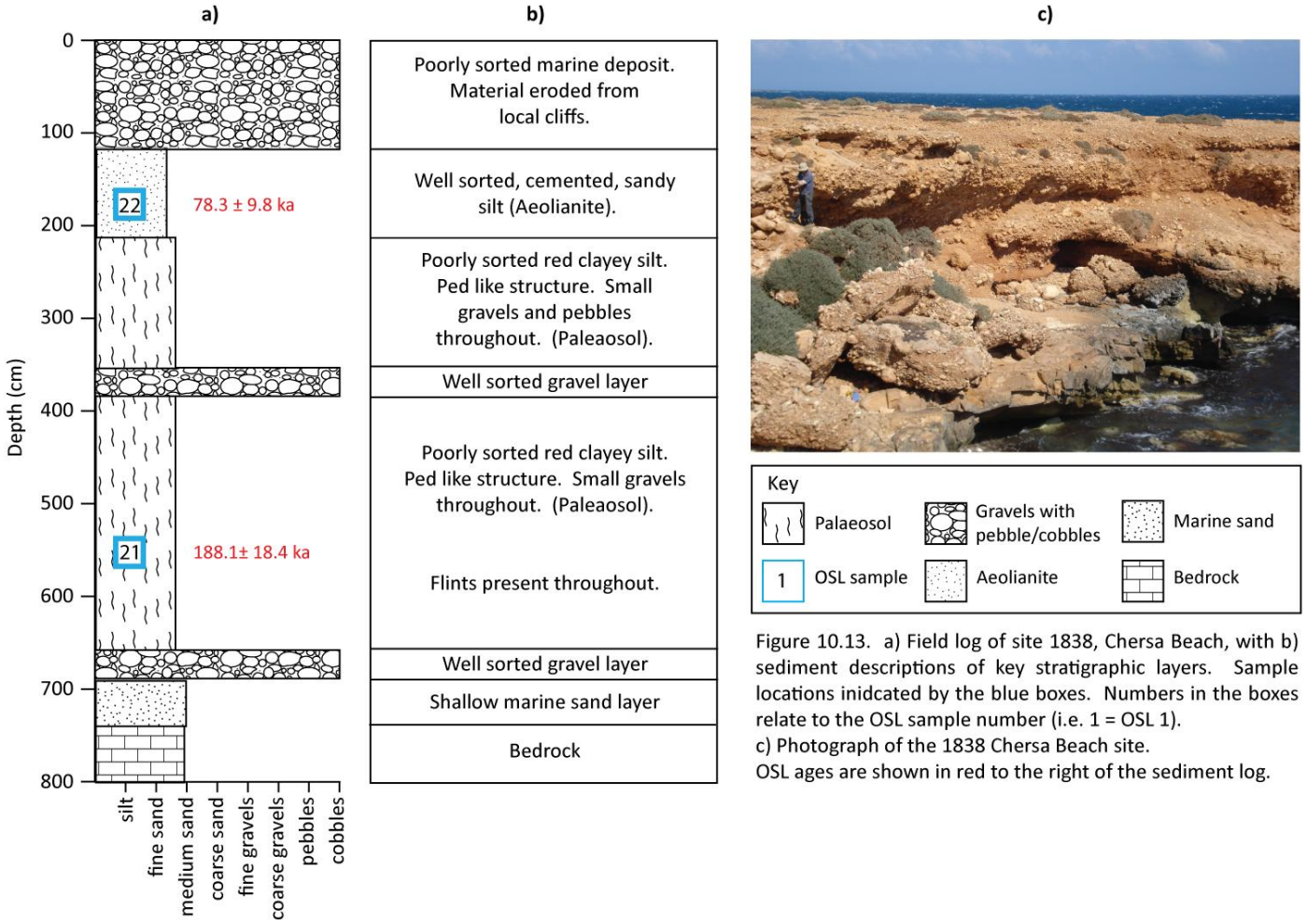

Figure 10.13. a) Field log of site 1838, Chersa Beach, with b) sediment descriptions of key stratigraphic layers. Sample locations inidcated by the blue boxes. Numbers in the boxes relate to the OSL sample number (i.e. 1 = OSL 1).
c) Photograph of the 1838 Chersa Beach site.
OSL ages are shown in red to the right of the sediment log.

Following a similar argument to that presented for OSL 8 at Latrun, it is likely that the fine grain age produced for the OSL 21 is erroneously old as a result of partial bleaching and/or post depositional mixing of the sampled palaeosol unit. The poorly sorted nature of the palaeosol unit, and presence of gravels which suggest episodic high-energy sediment transport, supports the interpretation that the measured equivalent dose may be subject to partial bleaching. If this is the case, then the resulting age determination is likely to be erroneously high. Consequently, while it is possible that human populations were able to remain in coastal areas for longer as the climate began to deteriorate (i.e. during early MIS 6), the development of a significant palaeosol unit during this period is unlikely. Assuming that the fine grain method has resulted in an overestimation of the age, it is possible that the development of the palaeosol unit at this site occurred earlier, during MIS 5. The humid climate reported for North Africa during MIS 5 (Drake et al., 2011, Blome et al., 2012) would have provided ideal conditions for the formation of a large palaeosol unit, which would not have been present during MIS 6. Furthermore, the presence of clay in a sediment is usually indicative of a stable wet environment during the time of formation. Again, single-grain dating would be required to test this interpretation, though it is not clear whether sediments suitable for this analysis exist at Chersa Beach.

Evidence from the overlying aeolianite unit provides support for the suggestion that the palaeosol unit developed during early to mid MIS 5. This aeolianite yielded an age of 78.3 ± 9.8 ka, indicating that it was deposited during a high sea-level stand during MIS 5a. Aeolianites can be deposited during glacial and interglacial conditions. In this instance, it is probable that the aeolianites represent fossil dune systems formed by pulses of sedimentation, provided by sea level high stands during interglacial periods (Brooke, 2001). Quartz grains deposited by aeolian (i.e. wind-blown) processes are likely to have been fully bleached prior to burial, reducing the likelihood of partial bleaching, making the age produced more reliable than for the complex palaeosol unit.

In summary, whilst caution must be exercised when interpreting the ages produced at Site 1383, it is suggested that humans were present along the Chersa Beach coastline during MIS 5. Due to the nature of the dating method used, it is not possible to attribute human activity to a specific sub-stage, however it is likely that humans were present prior to MIS 5a during the humid interglacial conditions.

10.4.2.2 Chersa Beach 1848/50

At site 1837, located c. 3 km along the coast to the west of 1838, flake technologies were also identified in a similar palaeosol unit (Barker et al., 2010). As at site 1838, the palaeosol was interrupted at one point by the occurrence of a flood event (gravel layer) and overlain by an aeolianite unit. While it was not possible to access site 1837 during the 2010 field season, samples were taken from site 1850 located on the adjoining headland and within the adjacent bay. Here a sedimentary sequence similar to that at site 1838 was observed, with a cemented raised beach underlying a lithic bearing palaeosol, interrupted briefly by a gravel unit before again returning to a period of soil development. The sequence was again capped by an aeolianite deposit.

OSL 23 was taken 2.5 m below the present day land surface from within the capping aeolianite. This unit was located above the lithic bearing palaeosol, which was observed as a continuous unit across the headland and bay at sites 1837 and 1850 respectively. Whilst the aeolianite unit was thinner at 1850 than 1838, it was still possible to obtain a suitably sized sample by using the full thickness of the unit. The aeolianite was a well sorted, cemented carbonate sand containing small clasts of gravel sporadically throughout. It was not possible to obtain gamma spectrometry from this unit due to the cemented nature of the sediment.

OSL 24 was taken from the lithic bearing palaeosol unit, 5.5 m below the present day land surface at site 1848 (a bay located to the west of the 1850 headland) (Figure 10.14). Extracted from the basal part of the palaeosol unit, OSL 24 is a poorly sorted, red clayey silt, associated with in-situ lithics, carbonate nodules, and numerous clasts varying in size from gravels to cobbles.

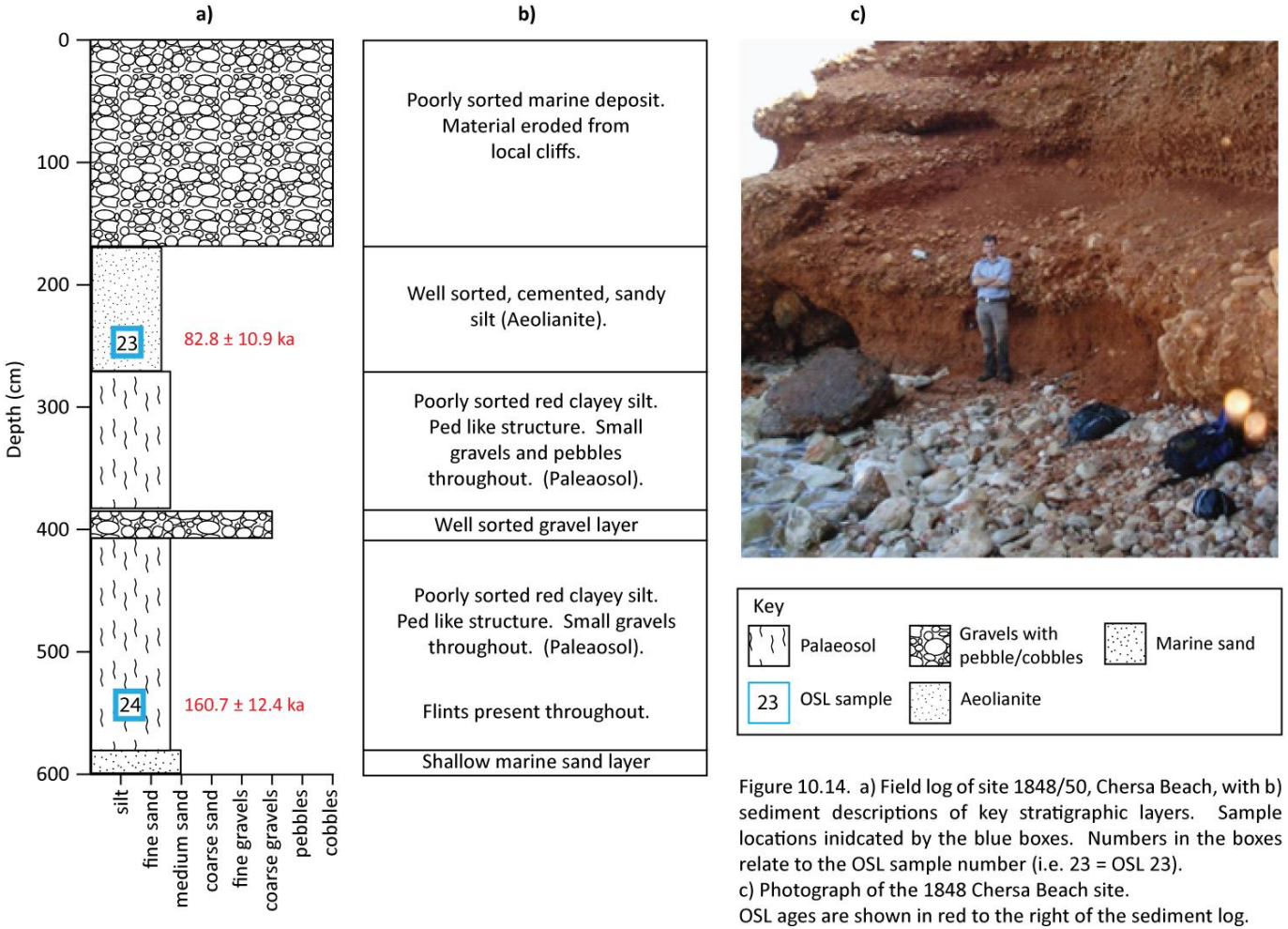

Figure 10.14. a) Field log of site 1848/50, Chersa Beach, with b) sediment descriptions of key stratigraphic layers. Sample locations inidcated by the blue boxes. Numbers in the boxes relate to the OSL sample number (i.e. 23 = OSL 23).
c) Photograph of the 1848 Chersa Beach site.
OSL ages are shown in red to the right of the sediment log.

The lithic bearing palaeosol (OSL 24) at this site yields an age of 160.7 ± 12.4 ka, while the overlying aeolianite (OSL 23) yields an age of 82.8 ± 10.9 ka. Similar to the other Chersa Beach and Latrun palaeosol units, the age produced for OSL 24 is likely to have overestimated the true age of the palaeosol at this site. Citing the limitations associated with fine grain dating of palaeosol units, it is suggested that the palaeosol unit at 1850 developed during MIS 5 rather than MIS 6 (as indicated by the calculated age). The ages produced for aeolianite samples OSL 22 and 23 are indistinguishable, supporting the hypothesis that the aeolianite samples yield reliable OSL ages, and suggesting that the two sediment bodies were deposited by the same high sea-level event during MIS 5a

As human presence along the coast (associated with the lithic bearing palaeosol) must have occurred prior to the deposition of the overlying aeolianite unit, evidence from the Chersa Beach sites suggest that modern humans were most likely present along the coastline during or prior to the MIS 5a interstadial period.

10.4.2.3 Chersa Beach 1851

Site 1851 was the final site investigated along the Chersa Beach coastline. Located at the western end of the Chersa Beach area, site 1851 exhibited a different sedimentary sequence from that observed at sites 1838 and 1848/50 (Figure 10.15). Here a cemented raised beach deposit was overlain by an aeolianite dune system, which was in turn overlain by a red brechiated sandy mud containing two gravel units. Finally, the red mud unit at this site was overlain by alluvial fan gravels containing small aeolianite sheets. OSL 25 was taken 5 m below the present day land surface from within the red sandy mud deposit, which contained a high concentration of fresh lithics. Although the lithics have not yet been assigned to a specific industry, archaeologists from the TRANSNAP team suggest that they were most likely produced by modern humans (S. Jones, *pers. comm.* 2010). The red mud at this site exhibited slightly different sedimentary characteristics from the palaeosol units observed at the other Chersa Beach sites. Specifically, the red mud unit here appears to be relatively well sorted, with weaker evidence of a “soil like” structure. OSL dating of this unit sought to provide a chronology for the deposition of the lithics, as well as determining whether or not this unit correlates with the palaeosol units from sites 1838 and 1850.

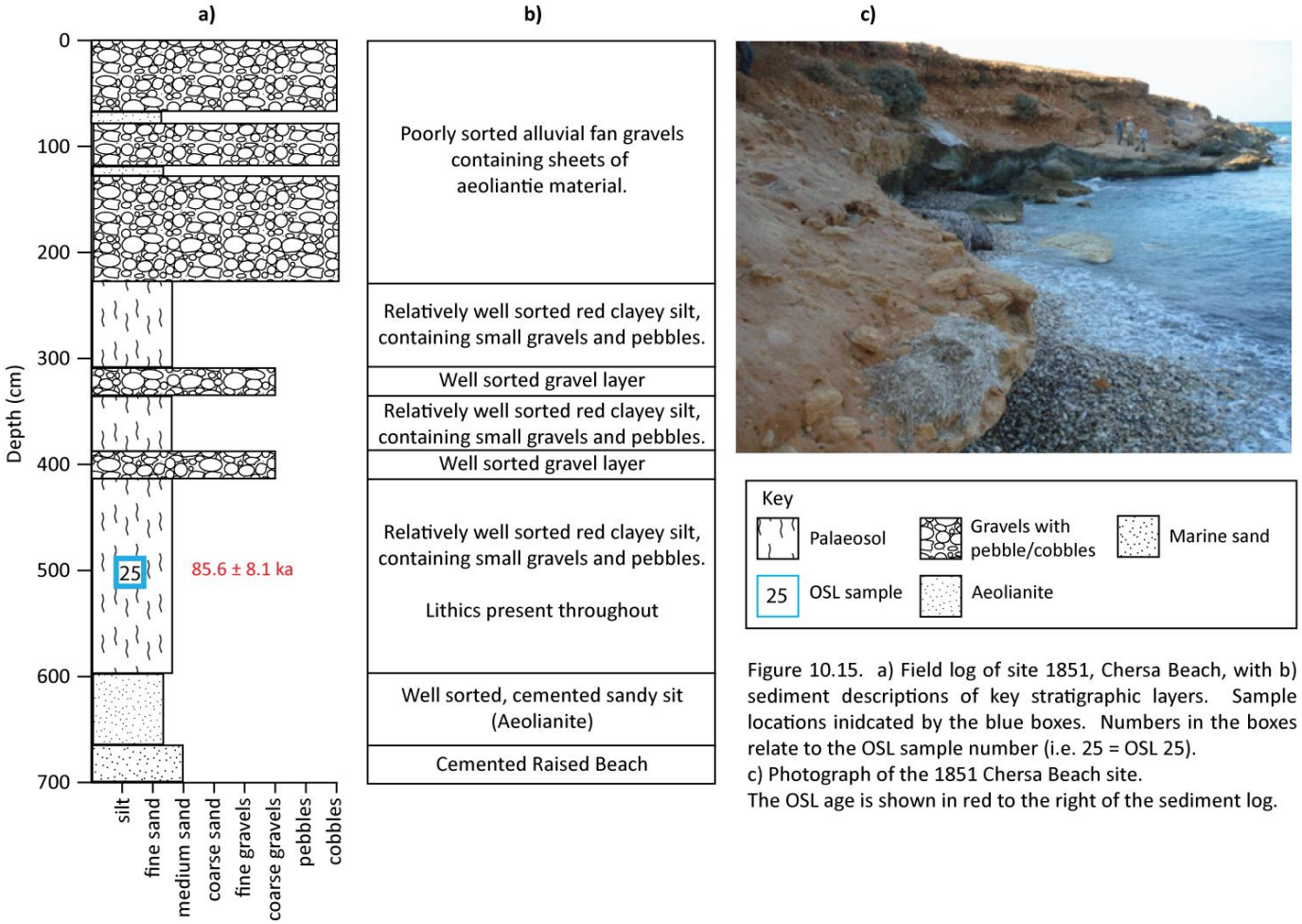

Figure 10.15. a) Field log of site 1851, Chersa Beach, with b) sediment descriptions of key stratigraphic layers. Sample locations inidcated by the blue boxes. Numbers in the boxes relate to the OSL sample number (i.e. 25 = OSL 25).
c) Photograph of the 1851 Chersa Beach site.
The OSL age is shown in red to the right of the sediment log.

An additional OSL sample was taken from the lower aeolianite unit, however no quartz could be extracted from this sample, and hence no OSL age was produced.

Sample OSL 25 yielded an age of 85.6 ± 8.1 ka, placing the timing of deposition of the lithic bearing red mud during the transition between MIS 5b and MIS 5a. Although the red mud unit appeared to be better sorted than the palaeosol units from the other Chersa Beach sites, caution is still necessary when interpreting the age produced. Without the use of single-grain dating, the extent of partial bleaching or post depositional mixing cannot be identified. However, deposition of the sandy mud deposit is likely to have occurred more rapidly than the development of large palaeosol sequences, and therefore an OSL age in MIS 5a is not unreasonable for this unit. Consequently, the units at site 1851 do not appear to directly correlate with the units identified at sites 1830 and 1850. Instead, OSL 25 suggests the presence of modern humans at this site during MIS 5a/b.

10.4.3 Coastal Summary

The OSL ages for samples from the section of coast from Latrun to Chersa Beach were produced using fine grain dating techniques. Whilst this technique may be appropriate in some environments, the presence of palaeosol units likely containing complex dose distributions at these sites requires the use of single-grain dating for accurate age determination. Single-grain dating methods facilitate the identification of the true overdispersion within the D_e distribution. In addition, the subsequent extraction of individual dose components and calculation of the most statistically likely age(s) would be possible. The paucity of coarse grain material at the sites prevented the optimal method being used, and it is therefore likely that several of the finite ages produced for the lithic bearing palaeosol units along the coast contain poorly bleached grains and may therefore produce erroneously old ages.

Despite these complications, the lithic bearing palaeosol units at sites 1838 and 1850 along the Chersa Beach coastline are tentatively assigned to early MIS 5, while the red mud unit at site 1851 is assigned to MIS 5a/b. The aeolianite samples, which overly the lithic bearing units at Chersa Beach, further support this notion, and were deposited late in MIS5, probably in MIS 5a. Whilst some caution is applied to these dates, the well sorted nature of the aeolianite units, and the processes by which constituent grains were

transported prior to deposition, mean it is less likely that these units have been affected by partial bleaching.

Latrun appears to represent a younger sedimentary sequence, which potentially places hominin occupation along the coastline earlier than previously thought. As at Chersa Beach, the OSL age produced for the palaeosol sample at Latrun is thought to overestimate the true age of the unit. Here, the palaeosol development is assigned to MIS 3 (rather than MIS 4, suggested by the measured age), however, the raised beach deposit (which is attributed a greater degree of confidence) is more confidently assigned to the high sea level stand of MIS 7. Dating at the site therefore provides evidence for the earliest human occupation to date in Cyrenaica.

Based on these data, it is concluded that human presence in the coastal landscape surrounding the Haua Fteah cave is most likely to have occurred during humid periods associated with insolation/monsoonal maxima which are synchronous with northern hemisphere interglacial periods. During these periods, more humid conditions were conducive to the presence of the food and fresh water resources essential for human survival. Furthermore, these conditions would have been more conducive for the production of large palaeosol units, containing clay rich deposits that are indicative of stable, wet conditions. It is possible, however, that the ages generated for the palaeosol units are accurate. In this scenario, modern humans would have been active along the coastline during the "arid" climatic periods associated with MIS 4 and MIS 6. Human presence at this time may have been facilitated by the weakening of the westerlies and subsequent increase in rainfall over the Cyrenaican landscape. Although detailed investigations into the origins of the lithics at these sites have not yet been completed, the lithic assemblages are tentatively assigned to modern human populations. It is likely therefore, that some of the humans present at Latrun and Chersa Beach were anatomically modern. A lack of lithics at the fire hearth site at Latrun prevents us from identifying the likely species present in the region at that time. The date of c. 230 ka, and similar findings at Qesem Cave in Israel, however, suggests an archaic population rather than AMH.

10.5 Wadi Derna and Hajj Creiem

Wadi Derna and Hajj Creiem are located c. 45 km east of the Haua Fteah cave (Figure 10.2). Wadi Derna is a dry river valley containing a series of lacustrine sequences c. 30-40 m thick

in places. These lacustrine deposits are thought to have been deposited behind a large tufa dam during the last interglacial-glacial cycle (Barker et al., 2009). Tufas are freshwater carbonate deposits that form at ambient temperatures in springs, waterfalls and lakes (Thomas & Goudie, 2000). Most tufa deposits are spring fed (Andrews, 2006) and actively form in warm and temperate climates, such as the Mediterranean (Pedley, 2009). There is a strong relationship between the production of soil CO_2 and tufa precipitation, with reductions in soil thickness and vegetation having been reported as major causes for tufa cessation (Goudie et al., 1993; Dominguez Villa et al., 2011). Consequently, tufa formation is commonly associated with interglacial periods throughout the Quaternary. Glover and Robertson (2003), however, suggest that periods of cool, but seasonally variable climate are also favourable for tufa formation along the coastal plain in Turkey, as this favours carbonate dissolution, aquifer recharge and profuse, uninterrupted spring discharge.

In the context of the TRANSNAP project, the lacustrine sequences reflect the presence of a perennial surface water body that would have been an important fresh water resource for modern humans in the area. The two sites investigated in Wadi Derna contained evidence for human activity (lithics and a knapping floor) in the area during the accumulation of these deposits. OSL dating samples were taken from one site in the main Wadi Derna channel and one site located in its tributary Hajj Creiem (Figure 10.16), with the aim of constraining the timing of fresh water availability and human activity along the wadi channel. The Hajj Creiem samples are associated with archaeology originally described by McBurney and Hey (1955), and hence represent a direct link between the availability of surface water and human occupation.

McBurney and Hey (1955) identified a number of flint artefacts and fossil bones projecting from the vertical face of the Hajj Creiem site, which graded into a tufa deposit a few metres downstream. They discovered a number of plant remains and fresh water shells within the sediment at the site, as well as the remains of some small and large mammals. Some examples of the mammalian species identified by McBurney and Hey (1955) include fragments of hippo or rhino, Barbary sheep, zebra, an extinct species of buffalo, and a small land tortoise.

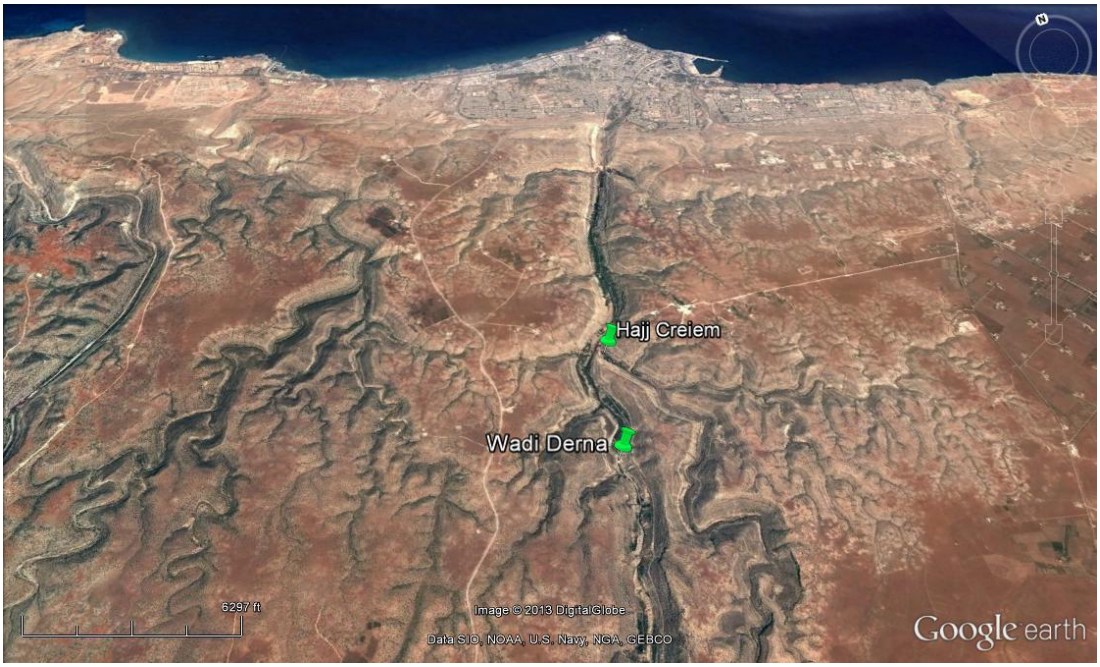

Figure 10.16. Google Earth image displaying the locations of Wadi Derna and the Hajj Creiem tributary sites.

Approximately 1500 lithics were collected from the Hajj Creiem site by McBurney and Hey (1955). Whilst the geological age of the site was not fixed, they suggested that deposition at the site most likely occurred during a relatively moist interval in the last interglacial, or in the early part of the last glaciation (Klein and Scott, 1986). Due to similarities identified between the lithics at the Hajj Creiem site and the Levallois Mousterian industry of Palestine, McBurney and Hey (1955) suggested that the deposit contained a predominantly Levallois-Mousterian human industry.

At several sites in Wadi Derna, major changes in the style of sedimentation, from tufaceous to lacustrine, were observed. These units were overlain by a series of large flood events, which probably reworked some of the underlying material, before themselves later becoming buried beneath carbonate layers. These water lain carbonate layers are interpreted as being indicative of high water table conditions (I. Candy, *pers. comm.* 2010). Consequently a major environmental question in this area concerns whether or not these changes are climatically significant or purely reflecting a series of major storm events. During this field season it was not possible to sample at a sufficiently high temporal resolution to produce a detailed environmental history of Wadi Derna. The sampling strategy used was intended to provide a broad chronology for freshwater deposition in

Wadi Derna, in preparation for a second field season which was eventually cancelled due to the 2011 civil war. Accordingly, OSL dating samples were obtained from units below the main tufa layer and above the tufa and lacustrine sediments, in an attempt to provide a coarse age range for the deposition of sediments in Wadi Derna.

10.5.1 Wadi Derna (Site 1816 and 1817)

The presence of a major tufa dam at Wadi Derna was most likely related to a temperate climate phase (Barker et al., 2009). OSL 17, taken at Site 1816, was taken 157 cm below the main tufa layer, directly above a carbonate layer and c. 40 m below the present day land surface at the base of the Wadi Derna valley (Figure 10.17). Sediments from the sampled unit consisted of a well sorted silty sand that was carbonate rich, and contained carbonate nodules throughout. The sediment at this site was too cemented to allow gamma spectrometry measurements.

Site 1817 is located at the top of the Wadi Derna channel sequence, above the tufa dam deposits and valley infill sediments, on the opposite side of the channel to site 1816 (Figure 10.17). Here a lithic bearing unit was identified directly below a sheet wash deposit. These features are interpreted to represent a time when humans were clearing the landscape of vegetation, leading to local landscape instability and increased sediment movement (C. Hunt, *pers. comm.* 2010). OSL 18 was taken directly below the sheet wash deposit within the lithic bearing unit. This lithic bearing unit is a well sorted silt deposit containing a small degree of red staining throughout. OSL dating of this unit sought to provide an age for modern human presence in the area, whilst also producing a minimum age for the valley fill tufa sediments located in the underlying units.

The coarsest quartz grains present in sufficient abundance to allow OSL dating at the Wadi Derna sites were those in the 90 – 125 μm size fraction. Because sedimentological investigations suggest that the well sorted lacustrine material sampled for OSL 17 and 18 were unlikely to have experienced post depositional mixing, and deposition occurred in a relatively low energy environment, which is unlikely to lead to partial bleaching, small aliquot dating was considered appropriate for age determination at these sites. The Central Age Model was employed to provide a weighted mean equivalent dose for each sample.

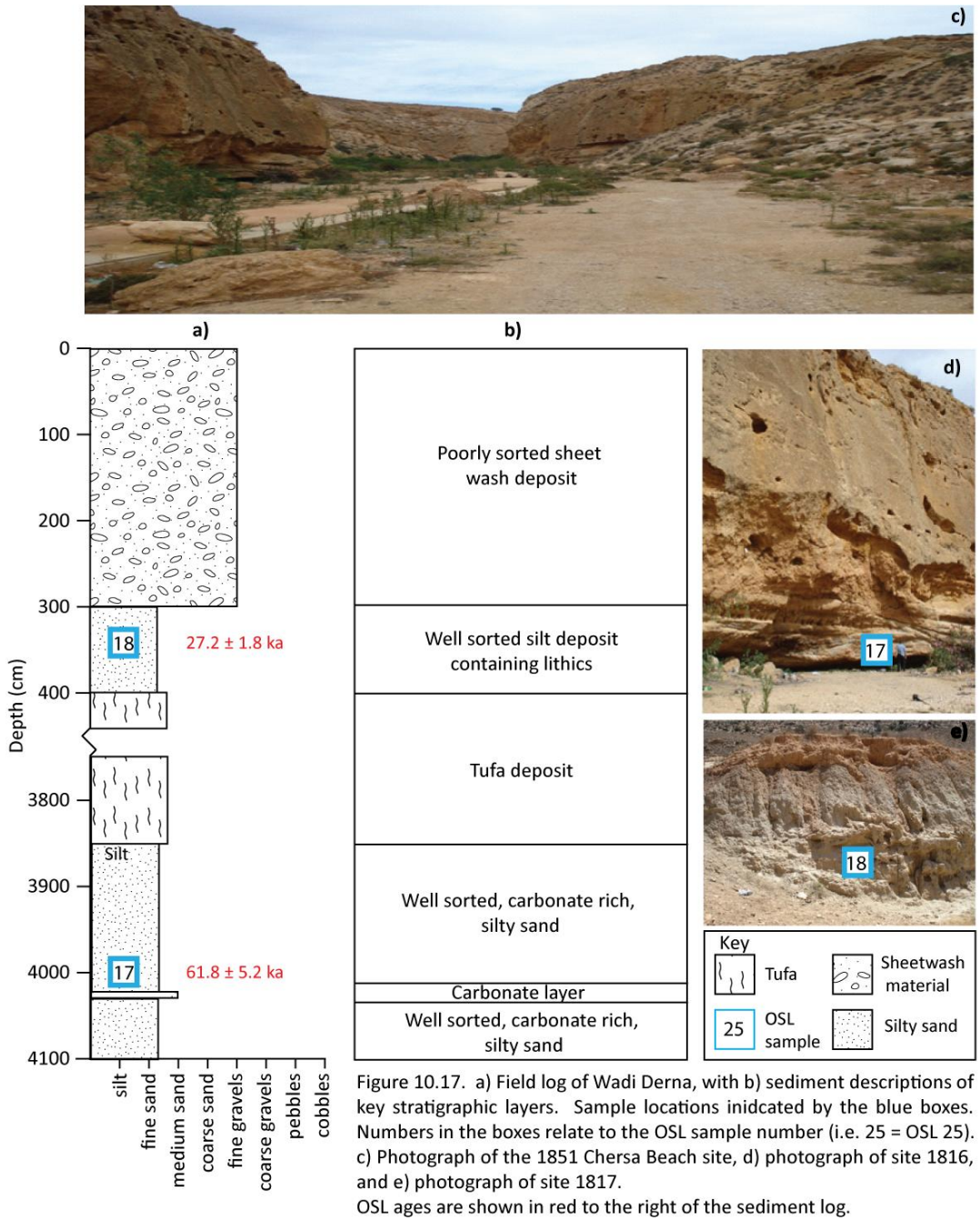

Figure 10.17. a) Field log of Wadi Derna, with b) sediment descriptions of key stratigraphic layers. Sample locations inidcated by the blue boxes. Numbers in the boxes relate to the OSL sample number (i.e. 25 = OSL 25). c) Photograph of the 1851 Chersa Beach site, d) photograph of site 1816, and e) photograph of site 1817.
OSL ages are shown in red to the right of the sediment log.

OSL ages from Wadi Derna channel suggests that tufa dam formation occurred during the MIS 3 interstadial, between 27.2 ± 1.8 ka (OSL 18) and 61.8 ± 5.2 ka (OSL 17). The presence of lacustrine material during MIS 4 (OSL 17), however, may also indicate that availability of fresh water resources in the environment surrounding the Haua Fteah during more arid climate phases. Valley inwash sediments capping the lacustrine and tufa dam material can be attributed a minimum age of 27.2 ± 1.8 ka (OSL 18). Furthermore, the lithic bearing

slope wash material can be assigned a maximum age of 27.2 ± 1.8 ka, which implies the presence of humans in the area in late MIS 2 / the early Holocene. Overall, evidence from the Wadi Derna site supports the notion that this coastal region of North Africa may have acted as a refuge for modern human populations during periods of more arid climate (MIS 4) in the Sahara, with the presence of fresh water resources in the landscape. Potentially, the MIS 4 age for OSL 18 may provide supporting evidence for humid conditions conducive to the formation of palaeosol units in MIS 4 (e.g. at Latrun).

10.5.2 Hajj Creiem

Hajj Creiem is located in a tributary of Wadi Derna, and lies downstream from the main valley lacustrine deposits at sites 1816 and 1817. The Hajj Creiem Mousterian site, initially excavated by McBurney and Hey (1955), contains flake archaeology (thought to be Levallois Mousterian) situated within water lain clayey silts. These silts are interpreted as indicating deposition under temperate environmental conditions (Barker et al., 2008). The archaeological units discovered at the site contained abundant small terrestrial gastropods, indicative of periods of low water stands and gentle current conditions.

An initial OSL dating sample (Hajj Creiem) was taken during the 2009 field season by Dr Kevin White from the sediment unit overlying the lithic assemblages identified at the site. These lithics matched the description of the Levallois Mousterian industry identified by McBurney and Hey (1955). Two additional OSL samples (OSL 19 and OSL 20) were taken during the 2010 field season, bracketing the "Hajj Creiem" OSL sample (and therefore also associated with the underlying archaeology) (Figure 10.18). Due to the archaeological and environmental importance of the site, three OSL samples were taken from the same unit to test the consistency of dates produced for the unit. Overall, the aim of OSL dating at Hajj Creiem is to provide a sound chronology for the archaeological and palynological site records that are currently under investigation, and to place the Hajj Creiem sediments into the overall context of the Wadi Derna environmental history. It was not possible to provide direct dating for the animal bones discovered by McBurney and Hey (1955), as it was unclear exactly where the specimens had been found within the section.

Samples OSL 19, Hajj Creiem and OSL 20 were taken at a depth of 105 cm, 130 cm and 140 cm below the present day land surface respectively. All of the samples were comprised of a well sorted sandy silt. These sediments are interpreted as having been deposited under

low energy conditions, and are therefore unlikely to have been affected by partial bleaching. There is no sedimentological evidence for post depositional mixing. OSL 20, the sample in closest proximity to the archaeology, was taken directly above a small carbonate layer which capped the lithic bearing unit (indicative of a previous high water table (I. Candy, *pers. comm.* 2010)).

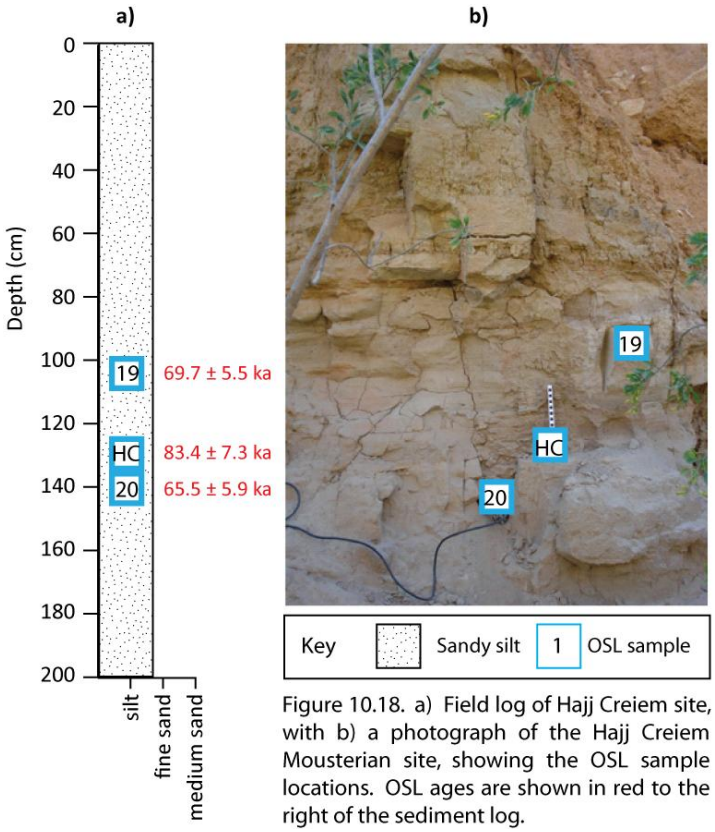

Figure 10.18. a) Field log of Hajj Creiem site, with b) a photograph of the Hajj Creiem Mousterian site, showing the OSL sample locations. OSL ages are shown in red to the right of the sediment log.

Whilst field sedimentology indicated that the samples would contain fully bleached quartz grains, unaffected by post depositional mixing, overdispersion values of > 20% were obtained from single aliquot datasets from all three samples. Where single-grain dating is employed, samples expressing overdispersion values of greater than 20% are thought to contain more than one distinct population of OSL signals.

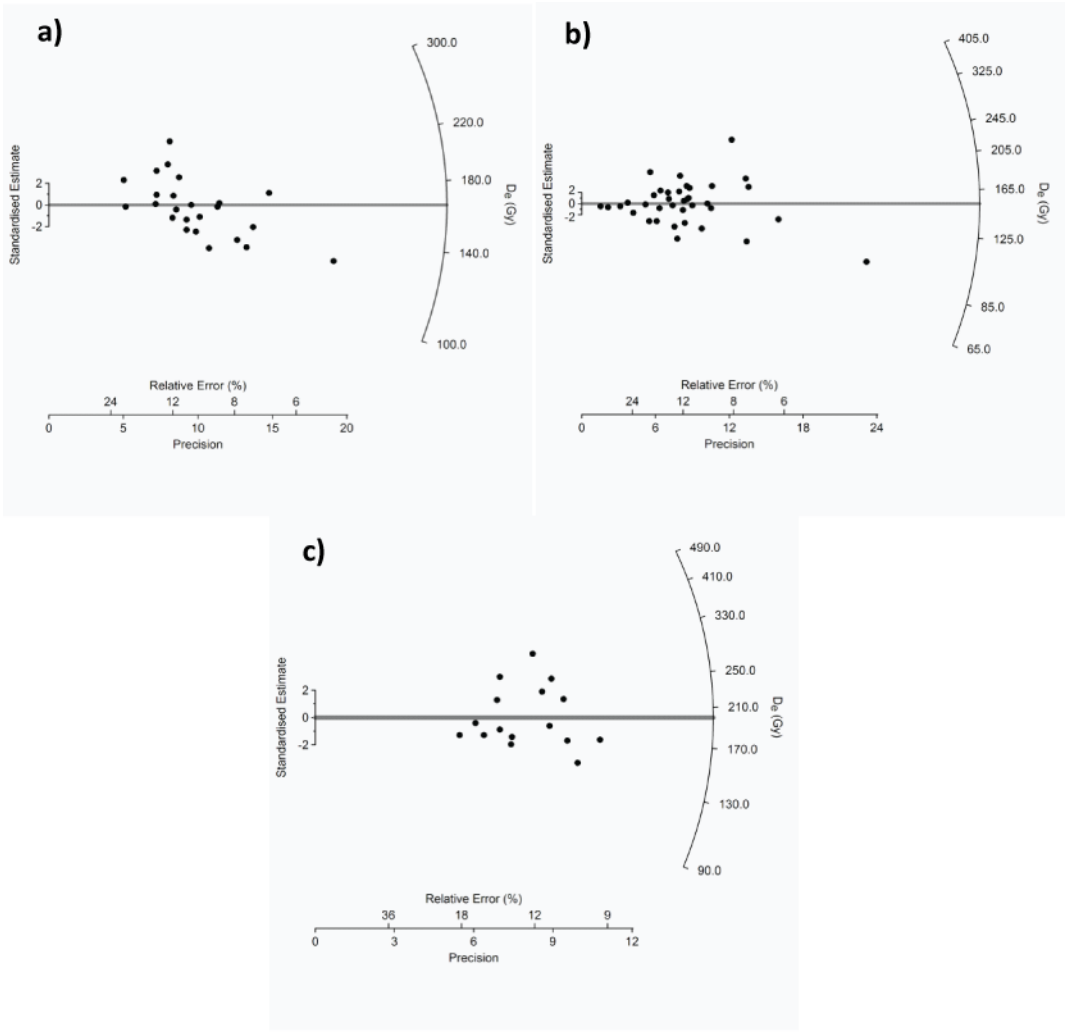

Figure 10.19. Radial plots showing the small aliquot D_e distributions obtained from samples a) OSL 19, b) Hajj Creiem, and c) OSL 20. The thick grey bars represent weighted mean D_e values identified using the CAM.

As the radial plots in Figure 10.19 show, the small aliquot equivalent dose values produced for each of the Hajj Creiem samples are relatively widely distributed around the CAM D_e, potentially reflecting the presence of more than one dose population within the samples. Whilst Arnold and Roberts (2009) and Russell and Armitage (2012) report that the use of the Finite Mixture Model is not appropriate for multiple grain aliquots, the three datasets from Hajj Creiem were, on this occasion, analysed using this model in an attempt to investigate further the dispersion of the datasets. The FMM identified two discrete components for OSL 19 and Hajj Creiem, and three discrete components for OSL 20 (Figure 8.20). In every case, the presence of a dominant component (containing > 60% of the total D_e values) was identified.

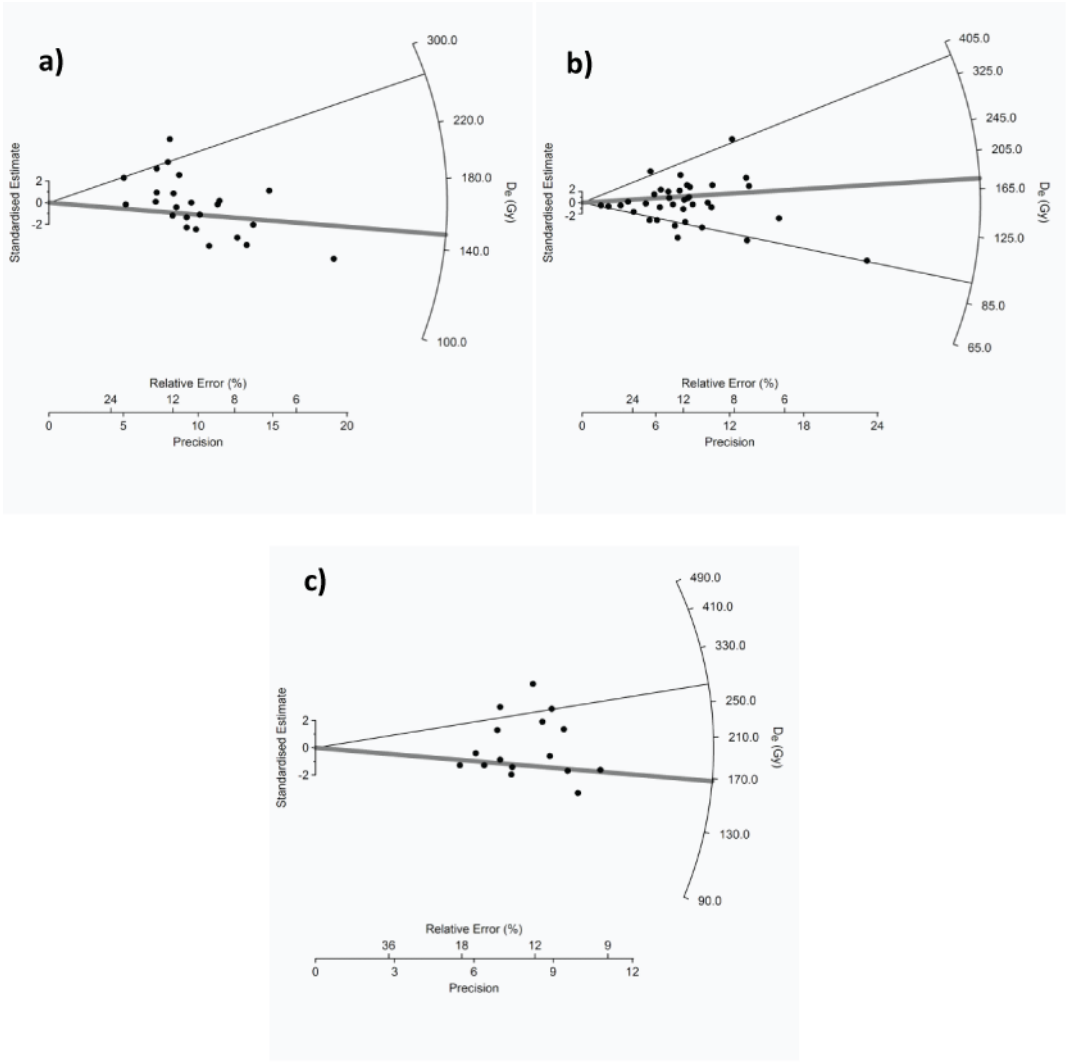

Figure 10.20. Radial plots showing the small aliquot D_e distributions obtained from samples a) OSL 19, b) Hajj Creiem, and c) OSL 20. The thick grey bars represent the dominant (>40%) components identified using the FMM. Black lines identify minor components, containing less than 40% of the grains measured.

Ages were produced for each sample using the CAM and FMM D_e results (Table 10.1). The D_e from the largest FMM component only is used here for age determination. A Student's t-test was used to compare the ages produced using the CAM and FMM. The test demonstrated that the D_e values produced by the largest FMM component and the CAM were statistically comparable for every sample using a 99% confidence interval, potentially suggesting that there may only be one component. Using the values from the FMM, the ages produced at Hajj Creiem are in good stratigraphical agreement, suggesting the presence of modern humans and standing fresh water resources prior to the termination of MIS 5a and onset of MIS 4. Similarly, the CAM ages suggest the presence of humans in a

lacustrine environment in the area at a time corresponding to the MIS 4 / 5a boundary, however, the ages produced are not in stratigraphical order. Furthermore, OSL 20, taken from a depth of 140 cm is assigned the youngest age, lying outside errors of the overlying Hajj Creiem sample which is attributed the oldest age.

Sample	CAM		FMM		
	Age (ka)	MIS	Age (ka)	%	MIS
OSL 19	69.7 ± 5.5	4	62.3 ± 4.2	80	4
Hajj Creiem	83.4 ± 7.3	5a	70.2 ± 5.8	65	4/5a
OSL 20	65.5 ± 5.9	4	78.4 ± 5.8	62	5a

Table 10.1. Finite ages produced using the weighted mean D_e from CAM analysis, and the statistically most likely component from FMM analysis.

The smaller components produced for OSL 19, 20 and Hajj Creiem would provide ages of 111.6 ± 12.9 ka (OSL 19), 41.1 ± 4.3 ka and 158.6 ± 24 ka (OSL 20), and 114 ± 11.1 ka (Hajj Creiem). Overall, the majority of the smaller components produce older ages than the CAM values. Consequently, it is possible that small amounts of lacustrine material may have been locally reworked, resulting in the partial bleaching of some quartz grains.

Whilst the FMM results produce the most stratigraphically coherent ages, the use of this age model on multi grain samples is generally deemed inappropriate. Accordingly, the CAM ages are utilised for the Hajj Creiem samples. Although there do appear to be some discrepancies between the CAM ages, there is generally a good agreement observed between the ages produced using the CAM and FMM. Consequently, confidence can be assigned to the ages produced, suggesting that the Hajj Creiem unit was deposited during the MIS 5a / MIS 4 transition. Modern humans therefore appear to have been present at the site during MIS 5a.

10.5.3 Wadi Derna summary

The presence of lacustrine material in Wadi Derna and Hajj Creiem from late MIS5 to late MIS3 suggests that fresh water was available in the landscape surrounding the Haua Fteah cave throughout this period. In particular, these data indicate that surface water was present during early MIS4, a period during which compilations of North African palaeoclimatic records (Drake et al., 2013, Blome et al., 2012) indicate increased aridity. This water would have provided an essential resource for modern human populations around the Haua Fteah at this time, suggesting that the Jebel Akhdar acted as an important environmental refuge. Furthermore, the dates produced for the Levallois Mousterian lithics at Hajj Creiem are in good agreement with the MIS 5a (71.3 ± 6.7 ka) age produced for the same industry dated as part of this thesis in the Haua Fteah cave.

10.6 Al Marj

Prior to the start of the 2010 field season, the Shuttle Radar Topography Mission (SRTM) digital elevation model (DEM) and remotely-sensed satellite imagery (Landsat TM) were used to locate potential lake basins in the Gebel Akhdar (Barker et al., 2010). A large internally-drained basin was identified in the Al Marj region, c. 125 km west of the Haua Fteah cave, and was targeted as a site for investigation due to its potential to act as a fresh water resource for modern humans in the region. The Al Marj basin is a fault bounded basin fed by a number of large ephemeral rivers that drain the highlands to the south, east and west, and some smaller rivers draining the low escarpment to the north (Barker et al., 2010). Today the centre of the depression contains seasonally flooded wetlands, in which ephemeral lakes form in response to exceptional rainfall events (Barker et al., 2010).

An artificial canal, dug during the 1970s to protect farmland from flooding by the river that drains the north-east corner of the basin, was located along the eastern edge of the basin. The canal runs roughly along a north-south transect for 8.5 km, reaching depths of up to 3 m and exposing a large number of sedimentary units. Many of these sedimentary units contain abundant archaeology including ancient hand axes, Levallois flakes, turtle shell cores and blades (Figure 10.21; Barker et al., 2010).

Figure 10.21. Google earth Image showing the location of the artificial channel in the Al Marj Basin. The EM 4 and Al Marj core sample locations are identified by the pink pins.

Sedimentological observations completed at several sites along a north-south transect within the canal suggested an increase in finer, better sorted material towards the south. This spatial pattern was interpreted as indicating that the processes responsible for the deposition of material at Al Marj shifted from predominantly slope wash in the north to a fluvially dominated environments downstream in the south.

Adjacent to the canal, towards the centre of the basin, a commercial drilling rig was used to extract a 30 m semi-continuous core at site EM 12 (Figure 10.22). Whilst the compactness of the sediments prevented the collection of a continuous record, four OSL dating samples were collected from the core at various depths, with the aim of providing a low resolution initial age model. A multi-proxy investigation of the core is now underway. To date, X-ray fluorescence (XRF), digital colour and magnetic susceptibility scans have been completed for the top 10 m of core. Micromorphological investigations are currently being carried out, and sub-sampling for tephra, phytoliths and pollen have been completed. To date, no mollusc, phytolith, diatom or pollen remains have been found in the core, however investigations are still ongoing.

Figure 10.22. Photograph of the coring site within the Al Marj basin, facing North.

10.6.1 Al Marj, EM 4

A large number of sedimentary units were exposed along the artificial channel at Al Marj, many of which contained rich deposits of mixed archaeological artefacts. At site EM 4, located at the northern end of the artificial channel, a large gravel unit interspersed with finer sediment lenses contains a large number of lithics. The gravel layer is overlain by a palaeosol deposit and underlain by a lacustrine unit. Five OSL samples were taken across the three main units in order to produce a chronology for deposition at the site, and also to give minimum ages for the archaeology contained within the gravel unit (Figure 10.23). Three samples were taken from the fine grained lenses within the lithic bearing gravel unit, to facilitate investigations into the timing of the main depositional events. Two further OSL samples were taken directly above and below the gravel unit in the palaeosol and lacustrine deposits respectively. These OSL dating samples sought to provide bracketing ages for the deposition of the reworked lithic assemblages contained in the gravel layer. Developing a chronology for the sequence also aimed to enhance our understanding of the environmental history in the lake basin.

OSL 1 was taken from the lacustrine unit underlying the lithic bearing gravels, 440 cm below the present day land surface (Figure 10.23). The lacustrine unit was a matrix supported, homogenous clayey silt containing a few small pebbles. A sharp boundary was observed with the overlying gravels, suggesting the erosion of the top part of the unit. Determining the age of this unit will facilitate the production of a maximum age for the deposition of the overlying reworked lithics, as well as timing of standing fresh water availability in the landscape.

A second sample (OSL 3) was taken from the palaeosol unit overlying the lithic bearing gravels (Figure 10.23). This unit is a well sorted clayey silt containing a few large clasts distributed throughout the deposit. The brown, soil like structure (i.e. containing peds) is characteristic of palaeosols found in this environment. OSL 3 was taken above the lithic bearing unit, directly below a small gravel lens to the left of the main section, 1.9 m below the present day land surface. OSL dating would therefore provide a minimum age for the reworked lithics within the underlying gravel unit. The sediment units containing OSL 1 and OSL 3 were too cemented to allow in-situ gamma spectrometry measurements.

Three samples, OSL 9, OSL 10 and OSL 11, were taken from the fine grained lenses that are interspersed within the main lithic bearing gravel unit (Figure 10.23). OSL 9 was taken 340 cm below the present day land surface and was comprised of a relatively well sorted, clast supported fine sand, containing some small pebbles. OSL 10 was taken 440 cm below the present day land surface. This lens consists of a relatively well sorted, clast supported, clayey silt, containing large gravels throughout. Finally, OSL 11 was taken 395 cm below the present day land surface. This lens unit consists of a clayey silt containing abundant gravel clasts.

Initial investigation of the lithics contained within the main gravel unit suggests that the artefacts belong predominantly, or exclusively, to the Middle Stone Age or Middle Palaeolithic period (Barker et al., 2010). The presence of bifacial hand axes suggests a potential Lower Palaeolithic origin, whilst the presence of Levallois cores and flakes indicate a modern human, Middle Palaeolithic source. Evidence for late Pleistocene and Arterian industries are absent from the gravel deposits. Due to the mixing of the artefact assemblages, however, it is likely that the source of the artefacts varied, or intermixing occurred over time during transportation and deposition of the gravel layers. However, many relatively fresh pieces were found within the gravel layer, which is interpreted as indicating short transport distances (S. Jones, *pers. comm.* 2010).

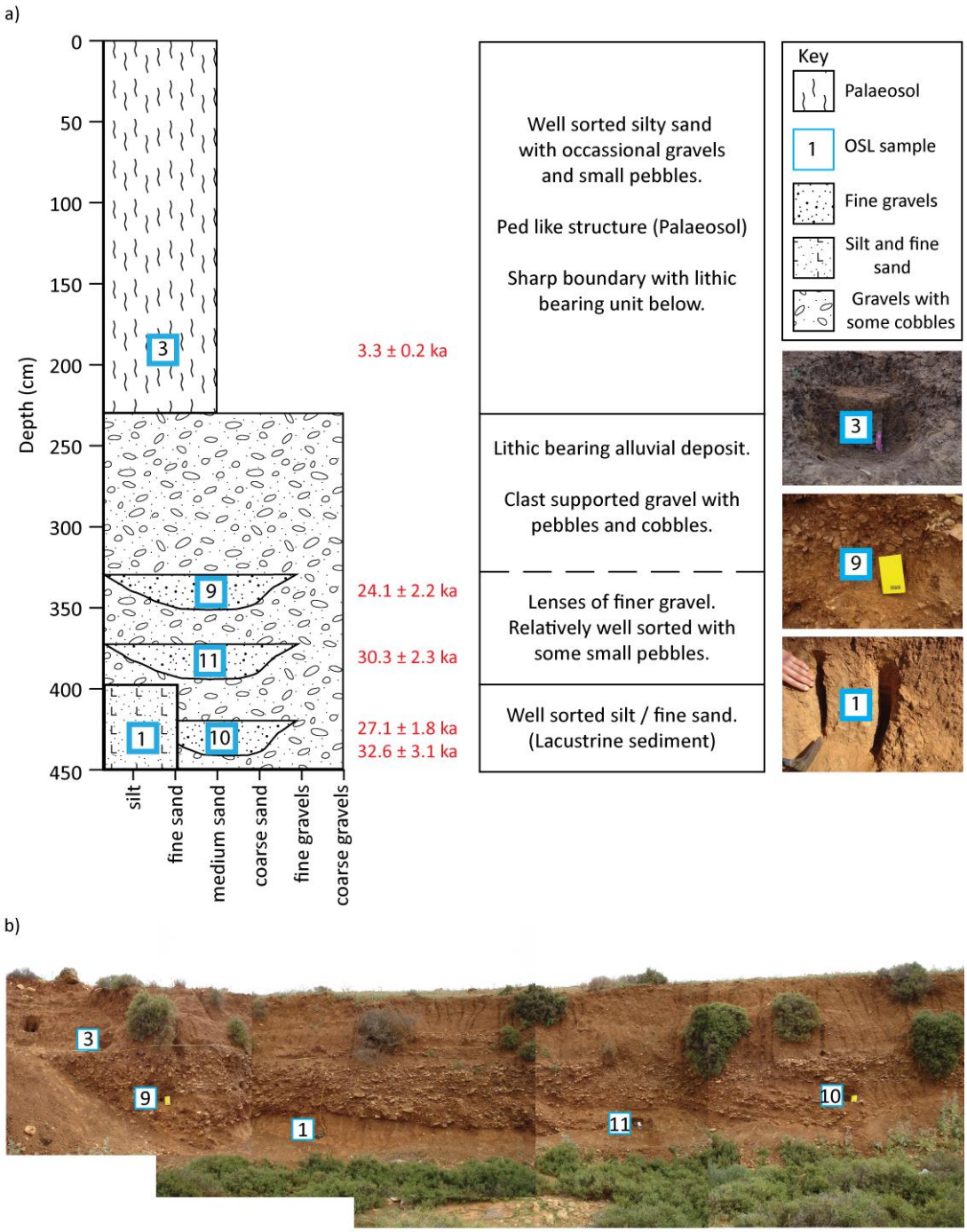

Figure 10.23. a). Field log of site EM 4, Al Marj, with sediment descriptions, interpretations and photographs of key stratigraphic layers from which OSL samples were taken. Sharp contacts are indicated by solid lines, graduated changes in sedimentology are indicated by a dashed line. b) Panoramic photograph of site EM 4 with sample locations indicated by blue boxes. Numbers in the boxes relate to the OSL sample number (i.e. 1 = OSL 1). OSL ages are shown in red to the right of the sediment log.

Due to the potential for post depositional mixing and partial bleaching at this site, single-grain dating was completed by hand picking the 90 – 125 µm quartz size fraction from each sample taken at Al Marj (Chapter 8). In every case, the samples yielded overdispersion values exceeding 20%, indicating the presence of more than one equivalent dose population. Consequently, the Finite Mixture Model was applied to all samples from EM 4 in an attempt to identify the most appropriate component for age determination.

The palaeosol at the top of the EM 4 sequence (OSL 3) yielded a Holocene age of 3.3 ± 0.2 ka, which was produced using the dominant FMM component (91% of accepted grains). Due to the humid conditions present in North Africa during the Holocene (Blome et al., 2012), this attribution was considered appropriate.

The basal lacustrine unit contained a more complex D_e distribution, with two major components identified by the FMM. An age of 32.6 ± 3.1 ka and 64.3 ± 5.7 ka was produced for components representing 45% and 55% of the sample respectively. The largest FMM component (containing 55% of the sample D_e values) would suggest the presence of standing water in the local environment during MIS 4, a period generally characterised by arid conditions in North Africa (Drake et al., 2011; Blome et al., 2012). Conversely, the slightly smaller FMM component (containing the other 45% of the D_e values from OSL 1) would place the deposition of the lacustrine sediments during the MIS 3 interstadial. Humid conditions present in North Africa during MIS 3 (Blome et al., 2012; Drake et al., 2013) would be more conducive to the development of a lacustrine environment in the Al Marj area. Furthermore, the high clay content of the unit is indicative of wet conditions, more likely to have been present during the humid MIS 3 climate (Blome et al., 2012; Drake et al., 2013). Consequently, whilst the younger MIS 3 age is obtained by the smaller of the two FMM components, it is suggested that this age provides the most likely age of the lacustrine unit at EM 4.

The three lenses interspersed within the main lithic bearing gravel exhibited similarly complex dose distributions, although OSL 10 and 11 did contain one dominant dose component. The ages produced by each of the FMM components for the three gravel lens samples are shown in Table 10.2.

Sample	Depth (cm)	Component 1		Component 2		Component 3		Component 4	
		Ka	%	Ka	%	Ka	%	Ka	%
OSL 9	340	4.2 ± 1.3	1	24.1 ± 2.2	28	44.1 ± 3.6	48	108.3 ±11.5	23
OSL 10	440	8.3 ± 0.6	25	27.1 ± 1.8	69	85.2 ± 12.4	6	-	-
OSL 11	395	17.7 ± 1.4	34	30.3 ± 2.3	66	-	-	-	-

Table 10.2. Ages produced using the Finite Mixture Model components from samples OSL 9, OSL 10 and OSL 11, taken from lenses interspersing the lithic bearing gravel unit at Site EM 4.

Assuming the largest components reflect the most likely age of the sediments, samples OSL 9, 10 and 11 yielded ages of 44.1 ± 3.6 ka, 27.1 ± 1.8 ka, and 30.3 ± 2.3 ka respectively. However, whilst the ages produced for OSL 10 and OSL 11 appear to be in good agreement with each other, OSL 9 which represents the stratigraphically shallowest unit, produces a significantly older age.

OSL 9, taken from a relatively poorly sorted clast supported gravel, was the least well sorted unit and exhibits the most complex dose distribution. As a clast supported unit, it is possible that this sediment was transported under relatively high energy conditions and therefore that some of the fine sand quartz material dated for this sample was not fully bleached during transport. It is possible therefore that the largest component produced for this sample does not represent the most accurate age for the deposition of the gravel unit. The age for the second largest component from OSL 9, however, is in good agreement with the ages produced for OSL 10 and OSL 11. On this basis, and the stratigraphic relationship between the samples, the age produced by the second largest equivalent dose population (24.1 ± 2.2 ka, 28% of accepted grains) is preferred for this sample.

The ages produced by the FMM at EM4 suggest that the deposition of the lithic bearing gravel occurred during late MIS 3 / early MIS 2, prior to the development of the overlying palaeosol unit during the Holocene. The underlying lacustrine material was most likely deposited during the MIS 3 interglacial, when humid conditions would most likely allow the presence of standing water bodies in the Gebel Akhdar.

As no bifacial hand axes were identified within the Haua Fteah cave sediments by McBurney (1967) or Barker (2013), it is likely that some of the lithics found at EM4 were produced by an archaic hominin population. Consequently, although further research is

required, it is possible that the reworked bifacial hand axes, indicative of a Lower Palaeolithic origin at EM4 (S. Jones, *pers. comm.* 2010), may have been produced by the same population responsible for the fire hearth identified at Latrun ~230 ka. While the necessary research required to investigate this suggestion fully is beyond the scope of this thesis, the TRANSNAP team will undoubtedly take this research forward in future publications.

10.6.2 Al Marj Core

During the extraction of the semi-continuous 30 m core, initial sedimentological investigations were completed to establish a low resolution environmental history of the lake basin. These initial investigations suggested a succession of distal alluvial fan and ephemeral lacustrine environments as the lake basin expanded and contracted in response to shifts in regional climate. Detailed sedimentological (micromorphology) and environmental proxy (phytoliths and pollen) investigations are currently being undertaken in the top 10 m of the core. It is anticipated that this multi-proxy investigation will facilitate the development of a high resolution record of lake level change in the area over time.

Initial OSL work was carried out on four samples from the core. These samples were intended to provide a coarse resolution chronology for the lake sediments, in an attempt to determine the timeframe covered by the record. Since the production of OSL dating has been completed, micromorphological investigations have started to render provisional results.

The Al Marj core samples only yielded fine grained quartz (4-11 µm) so there was no option but to perform fine grain measurements. However, this was considered to be the most appropriate method for these samples since they mainly contained clay, indicative of low energy depositional environments, and consequently ought to be well-bleached. The equivalent dose for these samples was calculated using the Central Age Model.

OSL 28, 31, 29 and 30 were taken at depths of 1.5 m, 2.98 m, 3.2 m and 10.2 m respectively (Figure 10.24).

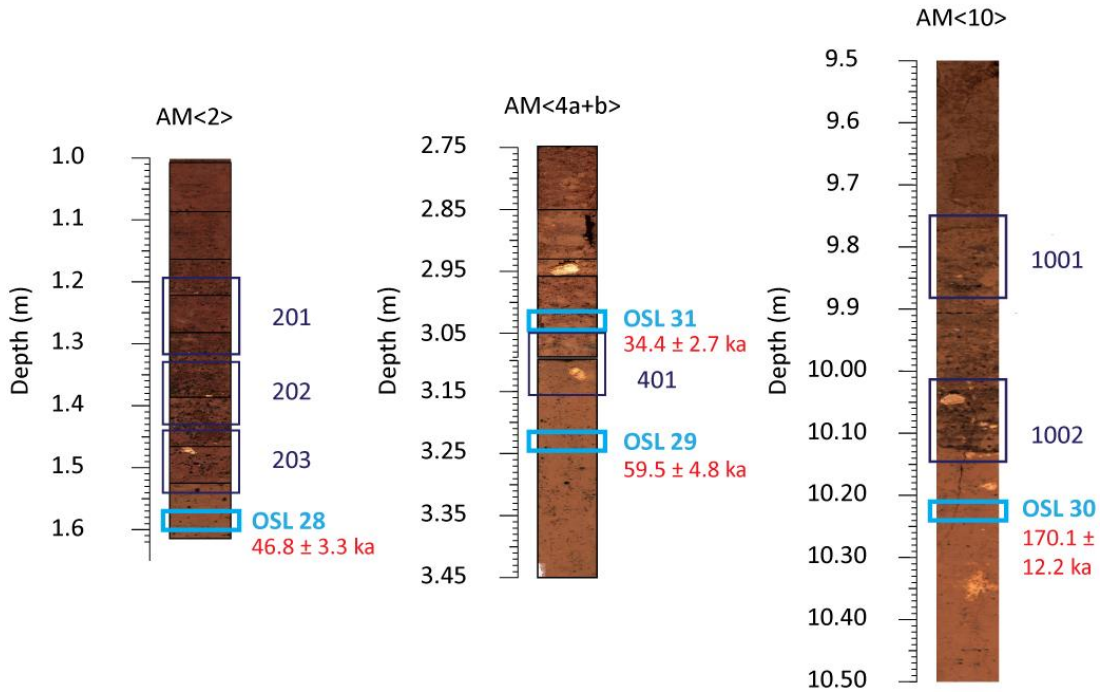

Figure 10.24. Photographs showing the Al Marj core sections dated as part of this thesis. OSL sample locations are indicated by blue boxes and soil micromorphology samples are indicated by dark blue boxes. Corresponding sample numbers are located adjacent to the sample boxes. OSL ages are shown in red below the corresponding sample number

OSL 28, taken from the upper part of the core, yielded an age of 46.8 ± 3.3 ka, suggesting the presence of standing fresh water in the Gebel Akhdar during MIS 3. Initial micromorphological investigations, however, suggest that OSL 28 represents a playa silty-clay, which underlies a thick, possibly multi-phased weathering horizon (R. Inglis, *pers. comm.* 2013). The accumulation of this type of sediment would require the presence of relatively humid conditions, which are not typical of glacial periods in North Africa (L. Farr, *pers. comm.* 2013; Blome et al., 2012).

OSL 29 was taken c. 5 cm above a potential weathering horizon (identified on the basis of an abrupt change in sediment colour, XRF and magnetic susceptibility data) at the top of a predominantly clay unit. OSL 31 was subsequently taken c. 15 cm below this horizon in an attempt to provide bracketing OSL ages for the event. Micromorphological work carried out across the horizon suggests that the weathered unit may be a fossil soil (R. Inglis, *pers. comm.* 2013). OSL 29 yielded an age of 59.5 ± 4.8 ka (late MIS 4), while OSL 31 is dated to 34.4 ± 2.7 ka (MIS 3).

The age reversal generated by OSL 31 (which provides a significantly younger age than OSL 28 and OSL 29) may be due to the delay between the initial sampling, and extraction of this later sample. As OSL 31 was sampled c. 1 year after the initial OSL sampling of the core, it is possible that the core (which was stored in cold storage room) may have dried out or been exposed to light conditions, potentially reducing the apparent luminescent age of the sample. Furthermore, as OSL 31 was taken from below a large carbonate nodule (Figure 10.24), it is also possible that the dose rate used for age calculation (ICP-MS/AES measurements on a sub-sample of OSL 31) is higher than that experienced by the sample during burial. Due to the agreement between the OSL 28 and 29 sample ages, the transition observed below OSL 29 is suggested to have occurred during the latter stages of MIS 4.

As climates began to ameliorate during the termination of MIS 4, increased humidity is likely to have enabled the development of soils. Additional OSL samples from below the weathered unit, and throughout the rest of the core, are required to fully test the accuracy of the current suggested age model.

The basal sample (OSL 30) was intended to provide a maximum age for the section of core currently being analysed for sedimentological and environmental proxies. This sample yielded an age of 170.1 ± 12.2 ka, suggesting that the presence of an ephemeral lake at Al Marj extended back until at least the MIS 6 glacial period.

10.6.3 Al Marj Summary

Preliminary OSL dating from the Al Marj core suggests the presence of an ephemeral lacustrine environment in the Al Marj region between MIS 6 and MIS 4. This suggests that fresh water resources were available in the region during two marine isotope stages associated with arid conditions across much of North Africa. The presence of lacustrine material in the basin during MIS 4 (which is also identified and dated by OSL 1 at the base of site EM 4) suggests that in the Jebel Akhadr, MIS 4 and MIS 6 were sufficiently humid to support ephemeral standing water bodies. Furthermore, the presence of fresh water resources in the environment during these times could have potentially supported modern human populations present in the area during periods of harsh climatic conditions.

Whilst the large gravel fan identified at EM4 did not reach the Al Marj core, the presence of some very fine gravel units within the core may be interpreted as evidence for very distal fan gravels. The increased sediment size associated with progradation of the gravel / fan over the lake deposits suggests an increase in energy in the environment surrounding the lake. Klinger et al. (2003) observed that periods of fan aggradation alternated with periods of lake high stands in the Dead Sea. They suggest that arid conditions in the region would have led to reduced vegetation cover, and increased regolith availability for transport, leading to progradation of the fan into the basin. Preliminary results from the Al Marj core micromorphological research (provided by Lucy Farr and Robyn Inglis) further supports this idea, suggesting that the gravel lenses and weathering horizons identified within the core represent lowlake stands during cold isotopic stages. The weathering horizons are most likely evidence for landscape degradation in the canal. Conversely, the core's clay units with gleying (soil formation) are likely evidence for warmer, wetter climatic phases. The lake has therefore most likely experienced an ephemeral history, with lake levels responding to regional climate changes.

OSL 1, taken from the lacustrine unit at EM 4, places the timing of a standing water body at Al Marj during the MIS 3 interstadial. The deposition of the overlying lithic bearing gravels, which are dated to late MIS 3 / early MIS 2, further suggests the presence of water in the region as late as MIS 2. A return to humid conditions in the basin is inferred by the overlying palaeosol unit at EM4, which was dated to the Holocene interglacial period. Evidence from EM4 thus suggests that humid conditions were present in the Al Marj basin during MIS 3 and the Holocene, with "wet" episodes prevalent during MIS 3/2 transition.

10.7 Environmental summary within a regional context

As discussed in Chapter 2, the causes of Pleistocene climatic change in North Africa, specifically the Saharo-Arabian desert belt, is a widely debated topic. Until recently the majority of palaeoclimatic data suggested that North Africa was humid during interglacial and interstadial periods, and arid during glacials. However, recent synopses of Mid to Late Pleistocene African climatic change produced by Blome et al. (2012) and Drake et al. (2013) provide evidence of climatic variability in North Africa during every MIS stage from MIS 6 to the Holocene. They suggest that these variations in African humidity are likely to have been driven by regional variations in the position of the ITCZ, associated monsoon system

in central and southern Africa, and the Westerlies along the north African coastline, rather than solely driven by high latitude processes. Due to the position of Cyrenaica along the North African coastline, it is unlikely that the ITCZ could have influenced an area this far north. It is therefore more likely that variations in mid-latitude Westerlies have driven precipitation changes in this Mediterranean region.

The North Atlantic Oscillation (NAO) is a climatic phenomenon in the North Atlantic which represents fluctuations in atmospheric pressure at sea level, as a result of variations in the strength of the Azores High and Icelandic Low (López-Moreno et al., 2011). Mid-latitude Westerlies form where cool dry air from the Icelandic Low collide with warm moist air from the Azores High, causing the moist air to rise, form clouds, and generate precipitation. When global temperatures fall, the Icelandic low is weaker and displaced south (Blome et al., 2012). In turn, this displacement causes the Westerlies to weaken and move south towards the equator, bringing moisture to the North African coastline.

Evidence obtained from the OSL dating of the sites from Cyrenaican landscape in this thesis supports the suggestion that mid-latitude Westerlies had a significant influence on precipitation along the North African coastline (Figure 10.25). In particular, it is clear that the Jebel Akhdar region supported standing water bodies during glacial / stadial periods when the Sahara itself was uninhabitably arid. As precipitation associated with monsoon systems is unlikely to have ever reached as far as the North African coastline, and small and large lake basins are thought to have receded or even dried up completely during glacial periods (Bar-Yosef and Meadow, 1995), the Westerlies represent the most likely source of precipitation during cooler, more arid periods.

Raised beach deposits at Latrun, dated to MIS 7, were most likely deposited during the high sea level stands associated with this interglacial period. A series of three sea level high stands were recorded by a number of submerged speleothems in Italy (Dutton et al., 2009). Dutton et al. (2009) used U-series techniques to date these three high sea level stands in the Mediterranean during MIS 7. One of these stands occurred between 248.9 ± 1.9 ka and 231 ±3 ka (MIS 7.5), a time synchronous with the insolation maximum. This high stand is in good agreement with the age produced for the raised beach deposition at Latrun.

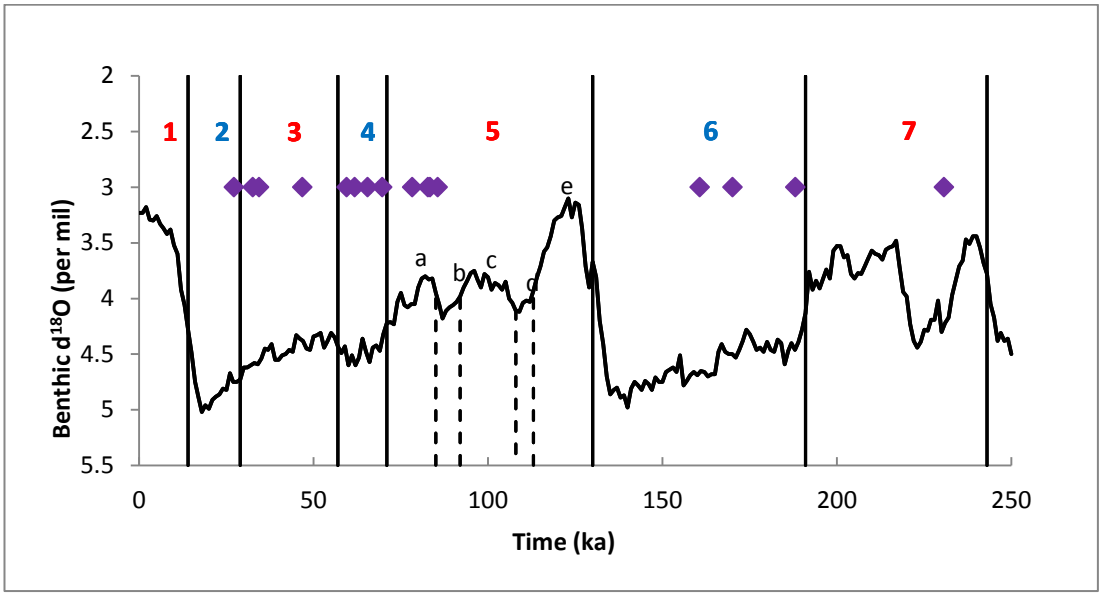

Figure 10.25. Summary plot showing the inferred timing of humid sediment accumulation in northern Libya and oxygen isotope data from the LR04 stack produced by Lisiecki and Raymo (2005) spanning the last 250 ka. OSL ages produced for lacustrine, palaeosol, raised beach and aeolianite deposits are indicated by the purple diamonds. MIS stage boundaries are marked by solid black lines. MIS 5 sub-stage boundaries, reported by Martrat et al., (2004), are represented by dashed lines and labelled appropriately. Interglacial/interstadial MIS stage numbers are labelled in red, while glacial MIS stage numbers are labelled in blue.

The OSL chronology produced for the Al Marj core suggests that the presence of an ephemeral lake in the Gebel Akhdar spanned the period from MIS 6 to MIS 4. Drake et al. (2013) suggest that while MIS 6 is traditionally thought of as a period of aridity, there is some evidence of humidity in the northern and central Saharan regions. Plotting ages for humid deposits as a probability density function, they report an increase in the probability peak in the Sahara at the end of MIS 6 c.138 ka. In addition, Blome et al., (2012) report the presence of spring-fed, groundwater and speleothem carbonate records from across North Africa (indicative of humid conditions) between 135-115 ka (end of MIS 6 – MIS 5e). While the lacustrine sediments from Al Marj appear to stretch further back into MIS 6, their presence provides further supporting evidence of ephemeral humid conditions during this period. This evidence suggests that while glacial periods in North Africa may have been more arid than interglacial periods, in the Gebel Akhdar at least, there is sufficient humidity to support standing water bodies. Speleothem evidence presented by Vaks et al. (2007, 2010) from six caves in the Negev Desert, Israel, also suggests that conditions along the

northern margins of the Saharo-Arabian desert belt were wetter during MIS 6 – MIS 5e. They suggest that a northward shift in the African monsoon due to increased orbital insolation would have increased precipitation over the desert region at this time.

Palaeosol units, which are generally considered to be formed during warm and humid interglacial periods (Boero et al., 1992), were dated to MIS6 at Chersa Beach. However, since these samples could only be dated using multi grain aliquots, it was not possible to test for partial bleaching. These ages are believed to be over-estimated due to partial bleaching, and an MIS 5 age for the Chersa Beach palaeosol deposits is preferred. A Red mud deposit from Chersa Beach was more confidently assigned to MIS 5a/b. The characteristic red colour of the palaeosol and mud units from Chersa Beach are characteristic of the Terra Rosa palaeosol units identified in the Mediterranean, thought to be the result of mineral weathering during warm periods of climate (Boero et al., 1992). Palaeoclimatic evidence from Soreq and Perquin Cave in Israel (Bar-Matthews et al., 2003) and 6 caves in the Negev Desert (Vaks et al., 2007, 2010) suggests that precipitation in the eastern Mediterranean increased during the full interglacial conditions of MIS 3 and MIS 5. Conversely, the speleothem evidence that they present suggests that precipitation levels fell in the region during stadial / glacial events of MIS 4 or MIS 6. Consequently, formation of these units is more likely to have occurred under full interglacial/interstadial conditions, than under the colder climates of MIS6. Further evidence for the development of palaeosol units during interglacial periods in North Africa is provided by the presence of a thick palaeosol unit at Al Marj, confidently dated to the Holocene. Accordingly, it is suggested that the presence of thick, red palaeosol units at Chersa Beach and Latrun are indicative of full interglacial conditions in North Africa.

The aeolianite deposits at Chersa Beach, which cap the palaeosol and red mud deposits, have been dated to late MIS5, probably MIS 5a. Humid conditions at these times would have been favourable for the production of carbonate, which would have cemented the raised dune systems that had been driven onshore by rising sea levels (Brooke, 2001). Potter et al. (2004) dated coral reef deposits using U/Th dating, reporting high global sea level stands during MIS 5c and MIS 5a (c. 101 ka and c. 81 ka). These dates are in good agreement with the Chersa Beach and Latrun sites, supporting the formation of the aeolianites during the sea level high-stand of MIS 5a.

Evidence from the Hajj Creiem tributary of Wadi Derna suggests the presence of lacustrine environments, and an associated humid climate, during late MIS 5a and early MIS 4.

Furthermore, evidence for humidity in early MIS 4 was identified by the presence of lacustrine material in the main Wadi Derna channel at this time. The presence of a major tufa dam in the main wadi channel throughout MIS 3, and into the beginning of MIS 2, also suggests the presence of relatively humid conditions at this time. Accordingly, evidence in this thesis from Wadi Derna and Hajj Creiem suggests that fresh water may have been available in the landscape surrounding the Haua Fteah from MIS 5 to the beginning of MIS 2. This means that in the Gebel Akhdar region, fresh water resources may have been present throughout MIS 4, which is uninhabitably arid further south in the Sahara.

The presence of lacustrine deposits at Al Marj during MIS 3 provides further evidence for humid conditions in the landscape surrounding the Haua Fteah during this interstadial. Although the OSL ages suggested that the palaeosol unit at Latrun was formed in MIS 4, this deposit is also attributed to the MIS 3 humid period. The deposition during the onset of MIS 2 of the large gravel unit at Al Marj suggests that the region may have been relatively humid until immediately prior to the Last Glacial Maximum.

Whilst Blome et al. (2012) suggests that North African climate records appear variable between early MIS 5a and MIS 3 (70-35 ka), North Africa is reported to have experienced predominantly arid climate conditions at this time, with the Sahara expanding between 65-50 ka (MIS 4). Palaeoclimatic evidence from the Levant further supports this notion, suggesting an increase in precipitation along the northern margins of the Saharo-Arabian desert belt during interglacial / interstadial periods, and more arid conditions during glacial / stadial periods (e.g. MIS 4) (Bar-Matthews et al., 2003; Vaks et al., 2007, 2010). Evidence from the Gebel Akhdar, however, demonstrates that local environmental change does not appear to have been solely driven by northern hemisphere glacial-interglacial cycles.

The presence of sedimentary units characteristic of humid conditions across glacial-interglacial boundaries suggests that the regional climate in North Africa was not entirely synchronous with Northern Hemisphere glaciations. Instead, it appears to have been affected by regional changes in climate, potentially driven by changes in the mid-latitude Westerlies in the region. Whilst the location of the ITCZ and precessional cycles are likely to have had dramatic influences on the southern margins of the Saharo-Arabian desert belt and the central African climate throughout the Quaternary period, it is unlikely that precipitation associated with the ITCZ reached the northern Cyrenaican region.

Blome et al. (2012) hypothesise that the westerlies are likely to have affected precipitation in North Africa, specifically during the period between 100-70 ka (MIS 5). Due to the elevated position of the Gebel Akhdar on the North African coastline, it is likely that this region was particularly sensitive to oscillations in the latitudinal position of the Westerlies. In particular, the data presented in this chapter support the hypothesis that peaks of Northern hemisphere high-latitude glaciation were associated with a southward shift of the westerlies, resulting in moisture delivery to the North African coastline.

10.8 Human presence within a regional context

The earliest fossil evidence for anatomically modern humans (AMH) leaving sub-Saharan Africa comes from the Levant, where the remains of more than 20 individual modern humans were found in the Mugharet es-Skhul and Jebel Qafzeh caves in Israel (Seddon, 2014). These remains were dated to between 119 – 85 ka (Carto et al., 2009), and are thought to represent the first wave of modern human migration out of Africa. Re-occupation of the Levant by AMH, followed by their expansion into Europe, is then thought to have occurred sometime between 60-80 ka (Eriksson et al., 2012; Seddon, 2014).

Recent evidence suggests that the coastal regions of North Africa provided important environmental refuges and corridors for the migration of modern humans during periods of climatic change (Stringer, 2000; Basell, 2008; Beyin, 2011). In this context, the availability of fresh water in the landscape is essential for the survival of human populations. Consequently, where lacustrine sediments have been identified in the landscape surrounding the Haua Fteah cave and Gebel Akhdar, it is reasonable to assume modern humans would have been able to thrive (Figure 10.26).

In recent years, the Arterian, a Middle Stone Age (MSA) lithic industry containing several markers indicative of symbolic behaviour and modernity (e.g. shell beads), has been regarded as a significant indicator for the appearance of modern humans in North Africa (Douka et al., 2013). Whilst no Arterian lithics were originally found in the Haua Fteah cave, or wider Cyrenaican landscape, re-analysis of the archive material from the cave by Reynolds (2012) suggests that there is a consistent presence of elements that could be considered Arterian in the cave. An increased interest in the industry has led to the re-dating of Arterian at several sites along the Moroccan and Libyan coastlines, revealing significantly older ages than previously thought. Spinapolice & Garcea (2013), suggest that

based on the re-examination of Arterian lithic industries in North Africa, modern humans may have been present along the Libyan and Moroccan coastlines as early as 160 ka. Barton et al. (2009) provide a more reserved estimate of 125 ka, based on the re-dating of the Arterian industry at Dar es-Soltan, a cave site located on the Moroccan coastline.

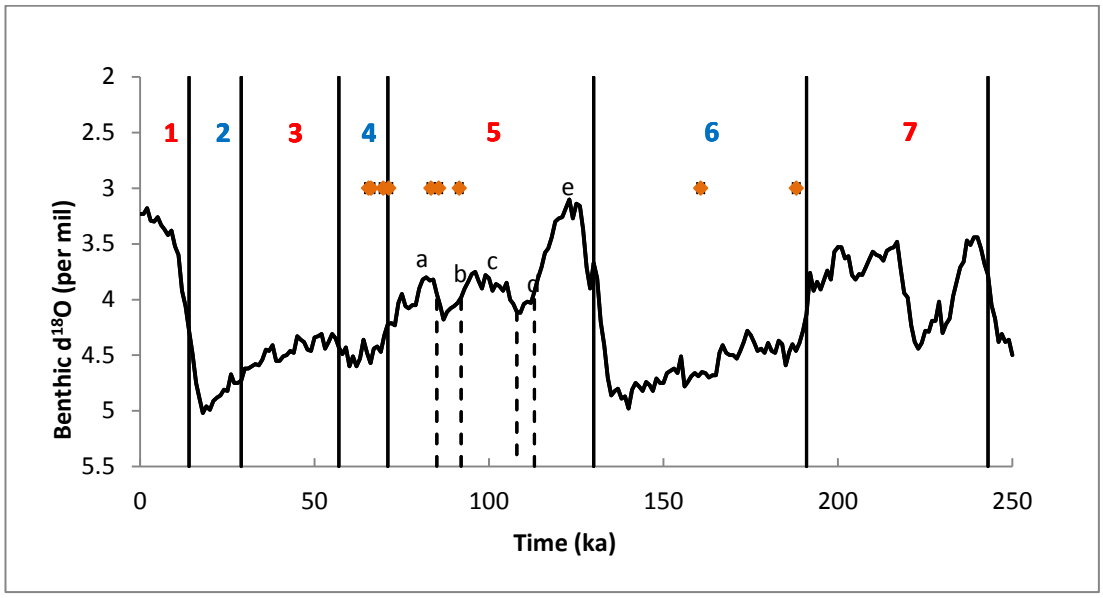

Figure 10.26. Summary plot showing the timing of human occupation in northern Libya and oxygen isotope data from the LR04 stack produced by Lisiecki and Raymo (2005) spanning the last 250 ka. OSL ages produced for lithic and fossil bearing deposits are indicated by the orange diamonds. MIS stage boundaries are marked by solid black lines. MIS 5 sub-stage boundaries, reported by Martrat et al., (2004), are represented by dashed lines and labelled appropriately. Interglacial/interstadial MIS stage numbers are labelled in red, while glacial MIS stage numbers are labelled in blue.

Fossil and archaeological evidence from within the Haua Fteah cave suggests that modern humans were present within the Cyrenaican landscape during MIS 5a and MIS 5c, far earlier than McBurney (1967) originally thought, but comfortably in line with the new dates produced for the Arterian in North Africa. OSL dating at the Hajj Creiem Mousterian site provides further supporting evidence for the presence of modern humans in the landscape at this time, with lithics at the site being dated to a minimum age of late MIS 5a / early MIS 4. Furthermore, the widespread distribution of MSA lithic assemblages across the Sahara

desert during MIS 5 (Frumkin et al., 2011; Seddon, 2014), suggests that AMH were successfully migrating out of sub-Saharan African earlier than previously thought.

At Chersa Beach, the lithic bearing palaeosol units are tentatively attributed to warmer, more humid, interglacial conditions during early MIS 5, and provide further evidence for human activity along the coastline at this time. The capping aeolianite at Chersa Beach provides a minimum age for human presence in the region of MIS 5a. Increased precipitation in central and North Africa during MIS 6 - MIS 5e (Bar-Matthews et al., 2003; Blome et al., 2012; Drake et al., 2013; Vaks et al., 2010) potentially facilitated the migration of modern humans across the Sahara-Arabian desert belt into North Africa, providing fresh water resources along the migration routes (Vaks et al., 2007.

Lithic assemblages identified in the palaeosol at Latrun place the presence of modern humans along the coastline during the subsequent MIS 3 interglacial. The deposition of reworked lithic assemblages in the gravels at Al Marj in MIS 2 further suggests that modern humans were present in the landscape prior to this time period.

Of significant interest is the presence of a fire hearth at the Latrun site which dates to c. 230 ka. As the Omo Kibish Formation and Herto-Bouri Ethiopian sites, which date to 195 ± 5 ka and 154 – 160 ka respectively, represent the locations for the earliest AMH fossils found in Africa (Frumkin et al., 2011), it is unlikely that the population responsible for the fire hearth at Latrun was modern human. While the evidence at the site is most likely representative of an archaic human population rather than AMH, this still provides evidence for the earliest hominin presence in the Cyrenaican landscape.

Evidence from Wadi Derna, Hajj Creiem and the Al Marj core suggest that standing fresh water resources were available in the Gebel Akhdar during MIS 6 and MIS 4, a time when most regions of North Africa were thought to be arid. The continued / ephemeral presence of these natural reservoirs, and the associated evidence for human presence in the landscape, supports the idea that the Gebel Akhdar acted as an area of refuge during periods of climatic deterioration.

10.9 Conclusions

Our current understanding of regional climatic change in North Africa, and the timing and distribution of modern humans in the area, is fragmentary. The OSL ages presented in this

chapter provide an addition to this fragmentary record. Evidence from this thesis therefore improves our understanding of the interaction between regional palaeoclimate and human occupation of North Africa.

Evidence of fresh water availability in the landscape surrounding the Haua Fteah cave during periods of Northern Hemisphere glaciation suggest that the regional climate in the Gebel Akhdar was not driven solely by Northern Hemisphere glaciations. Instead, the presence of humid conditions across MIS boundaries suggests that regional variations in climate are more likely to have been influenced by changes in the latitude of the Westerlies (driven by variations in the North Atlantic Oscillation).

OSL dating of lithic bearing units suggests that modern humans were present in the Gebel Akhdar during the MIS 5c, MIS 5a, MIS 3 and Holocene interglacial periods. Whilst no lithic evidence has been obtained during the glacial stages MIS 4 and MIS 6, the presence of ephemeral fresh water resources in the environment at these times probably allowed the survival of human populations in the area. López-Moreno et al. (2011) investigated the influence of the NAO (and Westerlies) on 15 mountainous areas in the Mediterranean regions. They suggest that the main contributor to water availability in the Mediterranean is runoff from mountainous regions, contributing 50-90% of the water supply in the area. The raised environmental setting of the Gebel Akhdar is therefore likely to have contributed to the more humid conditions as the Westerlies brought moisture to the area. Furthermore, the extension of the coastal landscape, associated with low sea level stands during these periods, and expansion of modern humans into new areas may have resulted in the loss of lithic evidence, as glacial sites have become submerged during subsequent sea level high stands (Basell, 2008).

Chapter 11 – Jebel Faya

11.1 Introduction

Jebel Faya is a 10 km long limestone mountain outlier that is part of an anticline structure located in the central region of the Sharjah Emirate (UAE). The archaeological rock shelter site FAY-NE1 is situated on the eastern side of Jebel Faya, approximately equidistant (60 km) from the Persian Gulf in the west, and the Gulf of Oman in the east (Figure 11.1). Excavations carried out at the site between 2003 and 2010 revealed a series of archaeological levels and artefacts that extended from the Iron and Bronze Ages, through the Neolithic, and into the Palaeolithic (Armitage et al., 2011; Bretzke et al., 2013).

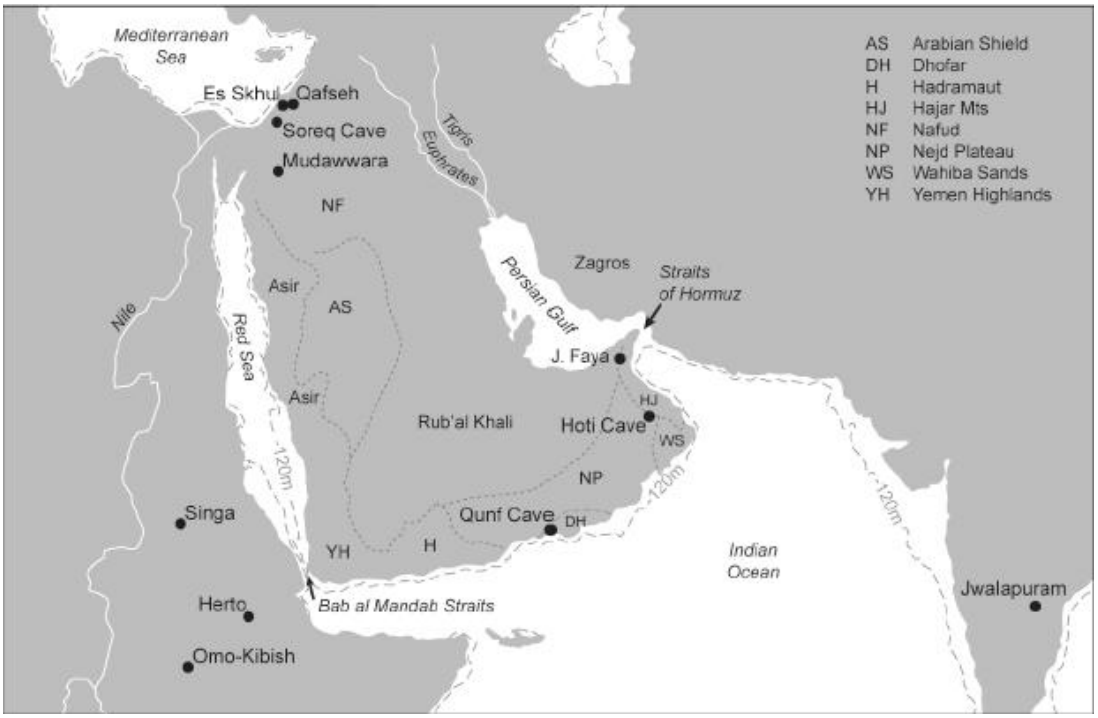

Figure 11.1. Map showing the location of FAY-NE1 (J. Faya), United Arab Emirates. Key AMH sites and geographical barriers to migration from Africa to Arabia/the Levant are shown. The dashed line represents the -120 m shoreline, which indicates the maximum exposure of land during glacio-eustatic marine low stands (source: Armitage et al., 2011).

Jebel Faya is located between the large dune fields of the Rub' al-Khali and the wide plain that reaches the western foot of the Hajar Mountains. This location is an ecotone, with access to a variety of habitats Bretzke et al. (2013). It is thought that Jebel Faya was used as a workshop, where modern humans utilised the site to re-provision with flint

instruments. The availability of raw material from the anticline structure, fresh water resources (Section 1.4.1), and the sheltered nature of the site would have made it an attractive settlement area for mobile hunter-gatherer groups dispersing into Arabia during the Pleistocene (Bretzke et al., 2013).

Armitage et al. (2011) produced the current chronology for FAY-NE1 using quartz single-grain optically stimulated luminescence dating. They published a suite of 7 OSL dates from key horizons within the rock shelter which suggest that the sedimentary and archaeological sequence spans at least the last 125 ka. Sample locations specifically focussed on three Palaeolithic layers, which have been designated Assemblage A, Assemblage B and Assemblage C (Figure 11.2) because they do not conform to any known Palaeolithic industries.

Assemblage C is the oldest lithic industry, and is located within the basal units at the site. Lithics from Assemblage B were superimposed onto Assemblage C, although the two were not always well separated. The uppermost Palaeolithic industry is represented by Assemblage A, which is separated from Assemblage B and C by an archaeologically sterile sand unit. Neolithic, Iron Age and Bronze Age layers, which overlie the Palaeolithic levels, are separated from the underlying Assemblage A by a sterile sand unit.

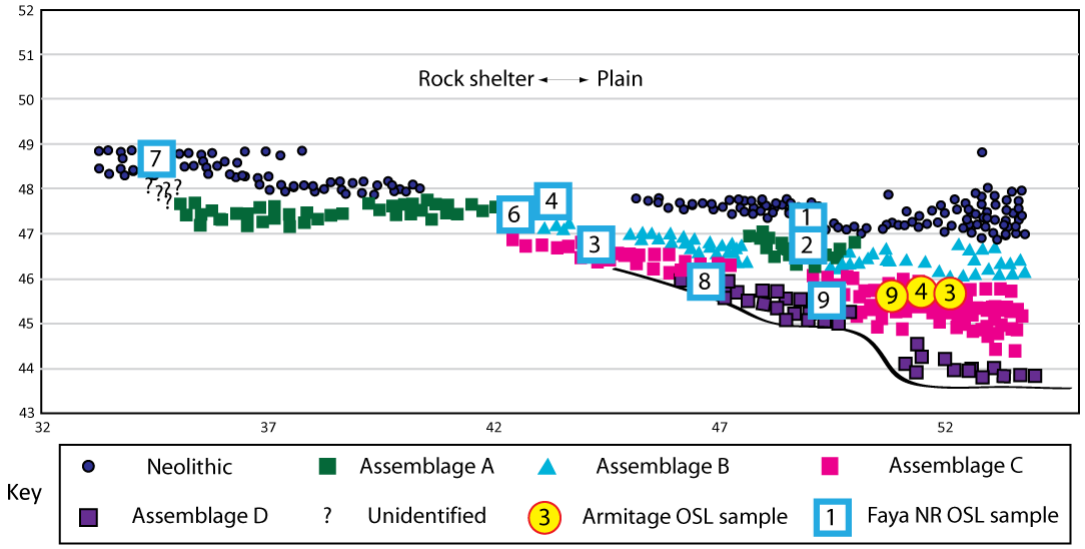

Figure 11.2. Schematic diagram showing the primary context of artefacts found during the excavation of the Jebel Faya site. The section runs from west to east, and shows the location of OSL samples taken as part of this thesis, OSL samples taken by Armitage et al. (2011), and the location of the main lithic industries. Adapted from information provided by Knut Bretzke in 2014.

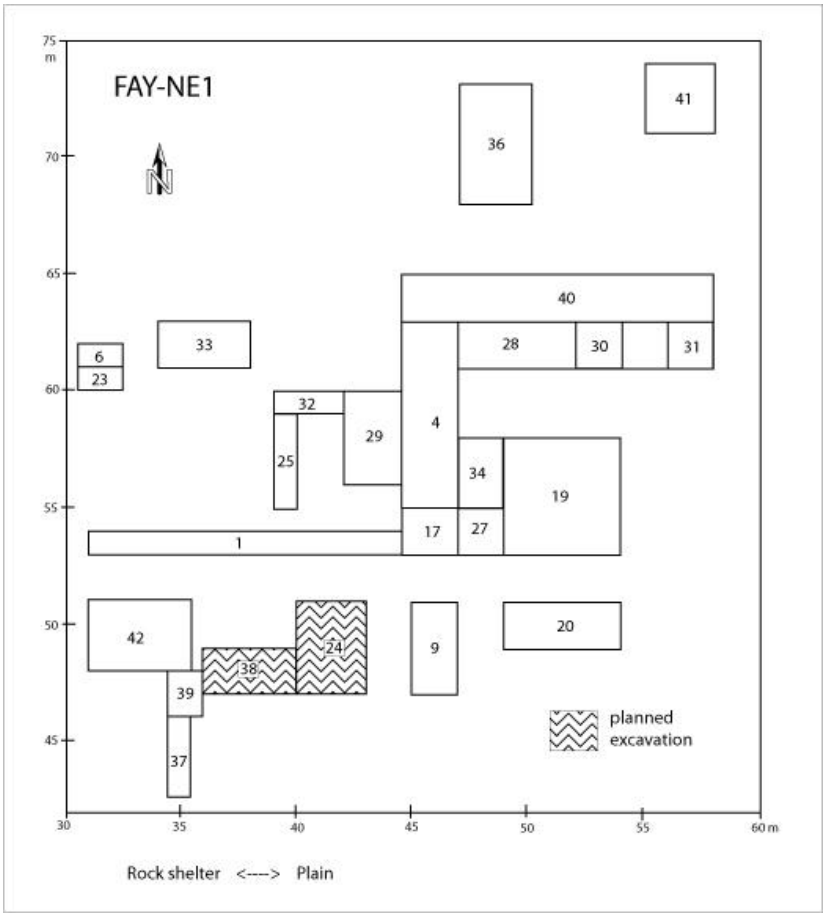

Figure 11.3. Schematic diagram showing the locations of the trenches excavated at FAY-NE1. Source: Armitage et al. (2011).

Whilst the Assemblage C lithics did not conform to the technological patterns identified within other Palaeolithic industries in Arabia, they did exhibit some similarities to East and northeast African assemblages, which are currently attributed to modern human populations (Armitage et al., 2011). Assemblages A and B, on the other hand, bear no affinity with Middle to Late Stone Age assemblages from East Africa, or the Upper Palaeolithic from the Levant and the Zagros. Consequently, Armitage et al. (2011) considered these assemblages to represent autochthonous development at Jebel Faya.

Three OSL samples taken from sandy pockets within the Assemblage C bearing sediments in Trench 19 (Figure 11.3) provided dates of 127 ± 16 ka, 123 ± 10 ka, and 95 ± 13 ka. Due to an inability to measure in-situ gamma dose rate for this sample, and the presence of large low radioactivity clasts within the FAY-NE1 sequence, the 95 ± 13 ka age is regarded as a minimum age by Armitage et al. (2011). This argument is provided in more detail by Bretzke et al. (2013). Using gamma spectrometry measurements from the other two

Assemblage C samples, Bretzke et al. (2013) suggest that the 95 ± 13 ka age has been underestimated by c. 15%, and that a corresponding age of 109 ± 15 ka may be more realistic, though it is difficult to attribute realistic uncertainties to this age. For the purpose of this chapter, only the two ages produced using direct gamma spectrometry measurements (127 ± 16 ka and 123 ± 10 ka) will be referred to from this point. Armitage et al. (2011) assert that Assemblage C represents evidence of modern human populations migrating from Africa during the transition from MIS 6 to MIS 5e. These populations then accessed the Jebel Faya site where they may subsequently have become disconnected from populations in southern Arabia during the arid conditions of MIS 5d and MIS 5b and probably after the start of MIS4. This disconnection led to the autochthonous development of Assemblage B. No radiometric age estimates are presently available for Assemblage B.

Armitage et al. (2011) processed OSL samples taken from Trench 4 and Trench 28 (Figure 11.3) within the Assemblage A sediments, and provided ages of 38.6 ± 3.1 ka and 40.2 ± 3.0 ka, placing the production of this industry in MIS 3. With no comparable lithic assemblages as yet identified in Africa or Arabia, Assemblage A was also considered to be a result of further autochthonous development, probably from Assemblage B.

The sterile sand unit that separates Assemblage A from the overlying Holocene lithics in Trench 4 and Trench 28 (Figure 11.3) was dated to between 38.6 ± 3.2 ka and 34.1 ± 2.8 ka, and 10 ka (using a combination of OSL dating in Assemblage A sediments, and radiocarbon dating in the overlying unit respectively), a period which coincides with hyper-aridity in Arabia during late MIS 3 and MIS 2. This sterile unit is therefore interpreted as marking the termination of human occupation at the site, until modern humans returned to the area during the Holocene.

Since the initial dating by Armitage et al. (2011) only focused on several key horizons within the FAY-NE1 site, producing OSL dates for the entire archaeological sequence will facilitate investigations into the settlement history of the site through the Palaeolithic and into the Holocene. Consequently, eight additional OSL samples, taken by the archaeological team during the 2010 field season, were dated as part of this thesis (Appendix 4). The location of the new samples sought to enhance the current resolution of the age model for FAY-NE1, facilitating further investigations into the timing of modern human occupation in Arabia and its relationship to periods of climatic fluctuation.

This chapter presents an enhanced chronology for environmental change and human activity at FAY-NE1, southeast Arabia. The new chronology is compared to published climatic and archaeological records to assess how the record at Jebel Faya fits in with the larger scale understanding of palaeoclimatic and anthropogenic variability in Arabia between MIS 6 and the Holocene. Consideration is given to how the advantageous geographical setting of Jebel Faya may have led to a stable populating of the region (Bretzke et al., 2013). Sediment descriptions, the climatic or anthropogenic significance of each sample location, and the sampling strategy employed in each unit, are also summarised in this chapter. The chapter concludes with a discussion concerning how the results from FAY-NE1 fit into the current debates concerning the potential routes and timings of our ancestors' migration out of sub-Saharan Africa.

11.2 Luminescence Properties

Most sediments at FAY-NE1 contain a high proportion of large clasts, which limited sampling to small sandy pockets within the lithic bearing sediments. While it is not possible to determine whether these sandy pockets were deposited during the slope wash events which emplaced the sediments at FAY-NE1, or subsequent aeolian infill into surface voids, Armitage et al. (2011) suggest that their deposition would have been effectively contemporaneous with the slope wash deposition.

All OSL samples from Jebel Faya were single-grain dated using quartz in the 180 – 212 µm size fraction. In every case, the Central Age Model yielded an overdispersion value of > 20%, suggesting the presence of a complex dose distribution (Section 7.2.1) (Galbraith et al., 2005; Olley et al., 2004). Accordingly, the Finite Mixture Model was used to extract the individual equivalent dose components and produce the most statistically likely age(s) for the samples.

All of the samples from FAY-NE1 which are presented in this thesis exhibited complex dose distributions, which contained 2 or more FMM components. The predominantly clast supported nature of the units at FAY-NE1 suggests that sediment deposition throughout the majority of the units at the site is likely to have occurred as a result of localised slope wash processes from the adjacent mountain slopes. Furthermore, evidence for post depositional reworking (i.e. Holocene gullies, burrows etc.) was also identified across the site. Sediments deposited via slope wash processes commonly contain partially bleached

grains, and reworked sediments are often subjected to the intrusion of younger material from the overlying units and/or older material from underlying units. These processes most likely explain the overdispersion observed in the datasets and therefore the complex nature of the dose distributions yielded by FAY-NE1 samples.

Typical decay curves from single quartz grains from FAY-NE1 are shown in Figures 11.4, 11.5, and 11.6. Luminescence signals from all of the FAY-NE1 material are characterised by a rapid signal decay and fast ratio values of > 20, suggesting the presence of a dominant fast component within the initial part of the OSL signal (Durcan and Duller, 2012). Following Armitage et al. (2011), and the arguments outlined in Chapter 7, dose response curves were fitted with a saturating exponential plus linear function.

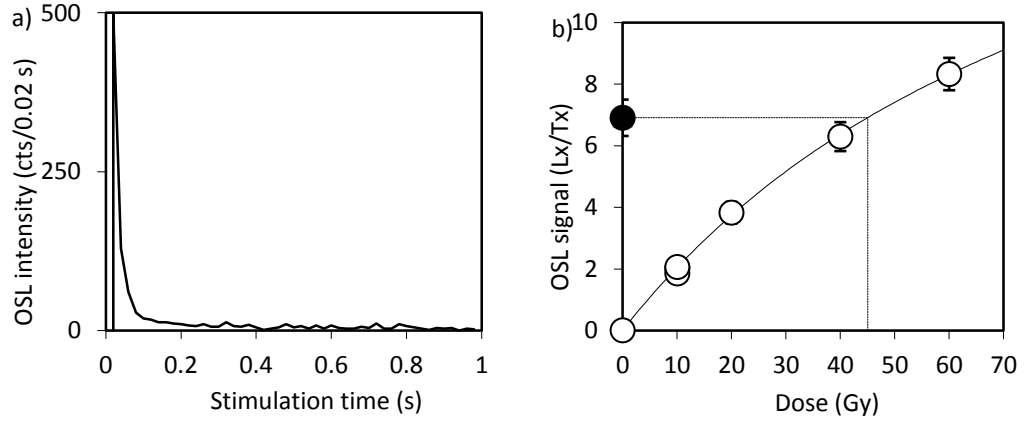

Figure 11.4. A typical (a) decay curve and (b) dose response curve for OSL Faya NR1, a single grain sample that passed the rejection criteria and that is dominated by the fast OSL component.

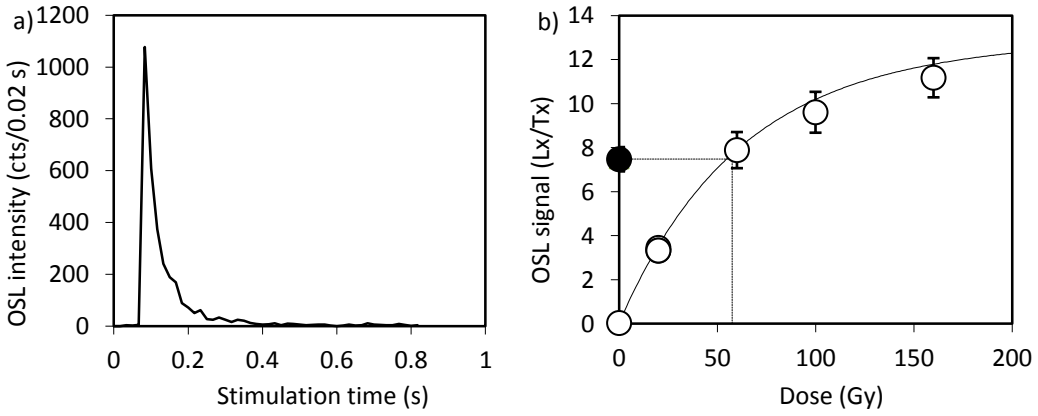

Figure 11.5. A typical (a) decay curve and (b) dose response curve for OSL Faya NR9, a "young" single grain sample that passed the rejection criteria and that is dominated by the fast OSL component.

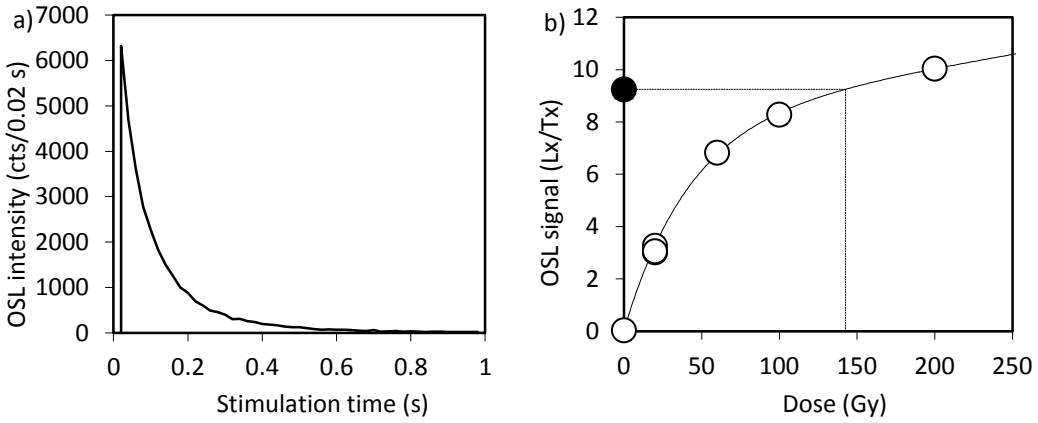

Figure 11.6. A typical (a) decay curve and (b) dose response curve for OSL Faya NR9, an "old" single grain sample that passed the rejection criteria and that is dominated by the fast OSL component.

Cumulative light sum plots produced for the single grain samples suggest that 28-58% of the grains in the FAY-NE1 samples contribute 90% of the total light sum (Figure 11.7), suggesting a high inherent sensitivity of the quartz measured at Jebel Faya. In comparison with data reported by Duller (2000), which suggests that only c. 5% of grains yield a luminescence signal, this Arabian material appears to contain a very high proportion of luminescent grains.

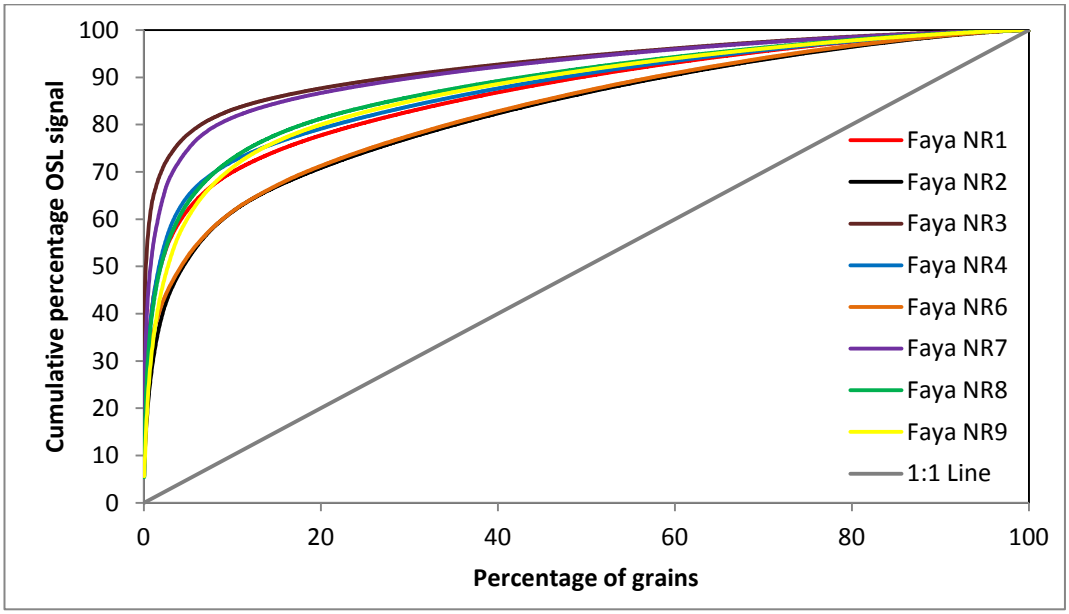

Figure 11.7. Cumulative light sum plots for all of the single grain FAY-NE1 samples measured in this study. Grains are ranked by brightness, with the brightest grain being plotted first.

Single aliquot dose recovery preheat plateau experiments were performed using the method of Murray and Wintle (2003) for two samples from FAY-NE1. 24 aliquots were measured using the methodology outlined in Section 5.2.2.4. The samples are relatively insensitive to preheating conditions, and a PH1 temperature of 260 °C and PH2 temperature of 220 °C was adopted for the FAY-NE1 samples. This preheating regime is identical to that employed by Armitage et al. (2011). Example dose recovery preheat plateau experiment results are presented in Figure 11.8.

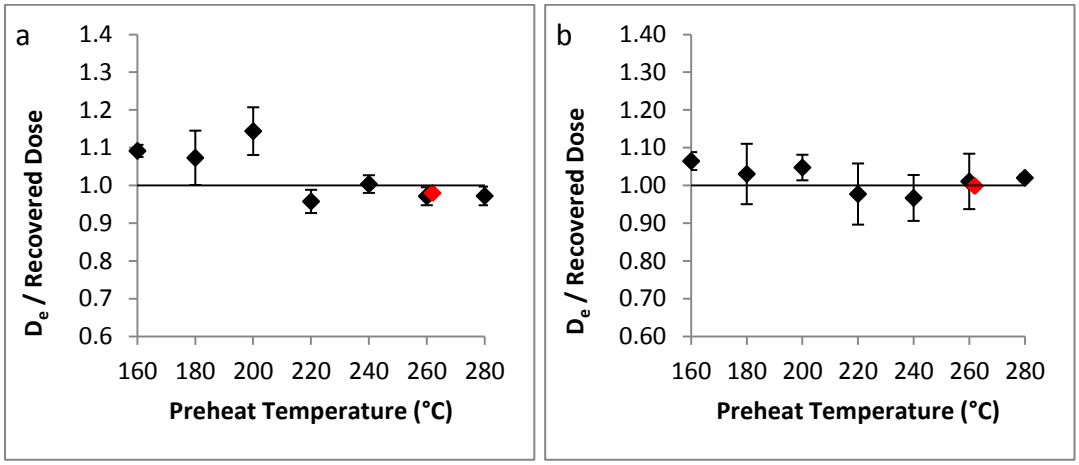

Figure 11.8. Dose recovery preheat plateau results for a) Faya NR1 and b) Faya NR2. PH1 temperatures are plotted on the x-axis. Black symbols represent aliquots measured using a 160 °C cut-heat for PH2, whereas red symbols represent aliquots which received a 220 °C, 10 second PH2. The red symbols are offset on the x-axis by 2 °C for clarity. Each data point represents the mean of three aliquots, with one standard deviation uncertainties. The chosen preheating regime was a 260 °C 10 second PH1, a 220 °C 10 second PH2. Aliquots measured using this preheating regime are represented by the red diamonds.

11.3 Dating the sterile sand layer at FAY-NE1

Following investigation of the sedimentology of the new trenches excavated during 2009/10, a sterile sand layer thought to correlate with that dated by Armitage et al. (2011) was identified in Trenches 27 and 36 (Figure 11.3). Unlike the sterile sand unit identified in Trench 4 and Trench 28, Assemblage A lithics were not found in the underlying clast rich units. Consequently, OSL dating samples were taken from the sand layer in Trench 36 and

Trench 27 to determine whether the layer did indeed represent the same depositional event as that reported by Armitage et al. (2011).

11.3.1 Sterile sand unit, Trench 36

OSL dating samples Faya NR1 and Faya NR2 were taken from a sterile sand unit located on the south facing section in Trench 36 (Figure 11.3). The sterile unit dated here underlies a matrix supported, clast rich unit containing Bronze and Iron Age lithics, including Fasad points, which were radiocarbon dated to the Holocene period (10,405 to 9711 cal. yr B.P. and 10,380 to 10,078 cal. yr B.P.) by Armitage et al. (2011). The Fasad points in this section were located directly on top of the sand unit, a sterile homogenous sand layer containing some small (0.5-1 cm) clasts. The unit situated below the sterile layer is a clast supported sediment containing a fine sand matrix, and is thought to correlate with the unit containing Assemblage A lithics in Trench 4 and Trench 28.

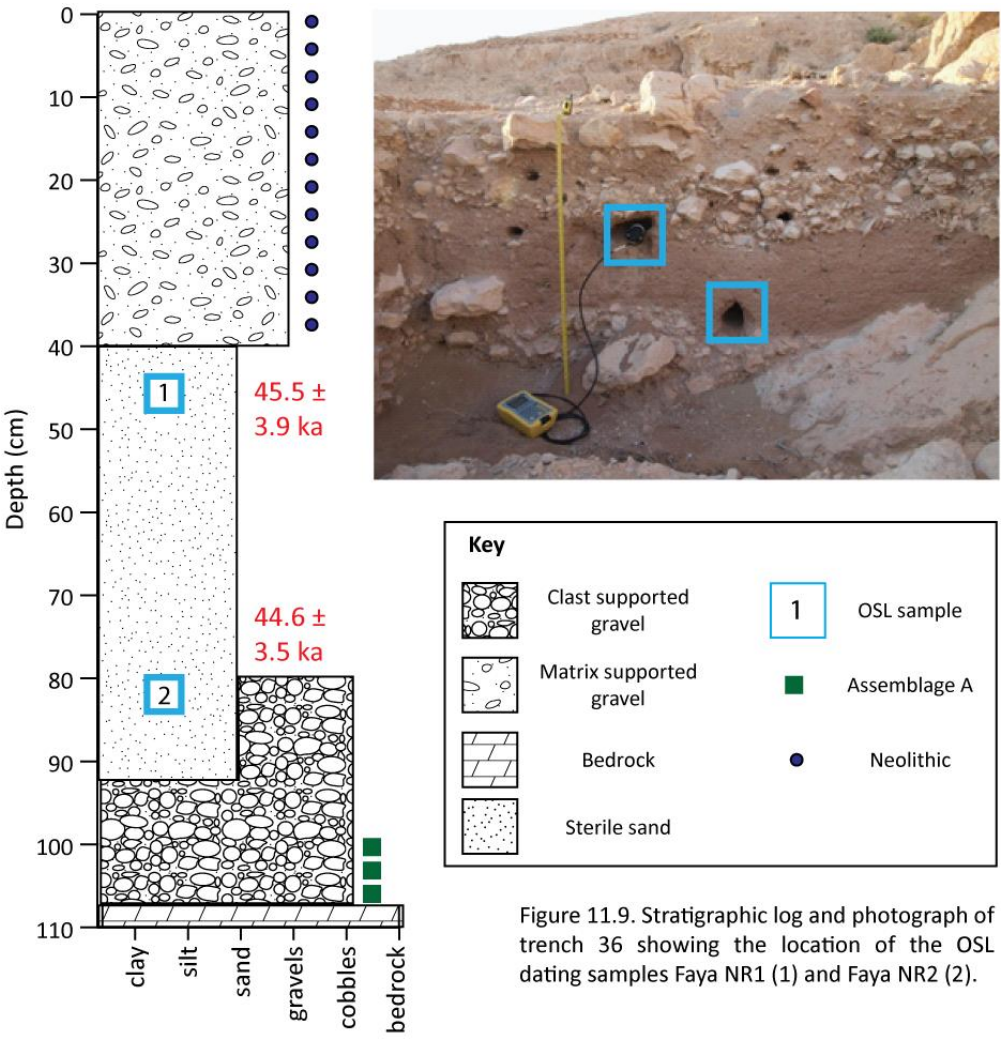

Figure 11.9. Stratigraphic log and photograph of trench 36 showing the location of the OSL dating samples Faya NR1 (1) and Faya NR2 (2).

OSL dating samples were taken from the top and bottom of the sterile sand layer in an attempt to provide minimum and maximum ages of deposition, and subsequently to determine whether or not this sterile unit correlates with the sterile sand dated by Armitage et al. (2011) (Figure 11.9). Furthermore, dating the unit will facilitate an investigation into the timing of human absence at the rock shelter. Faya NR1 was taken at the top of the sterile unit at a depth of 45 cm, c. 5 cm below the overlying Holocene layer, and Faya NR2 was taken from the base of the sterile unit at a depth of 85 cm, c. 5 cm above the underlying clast supported material (Figure 11.9).

Faya NR1 and Faya NR2 both exhibit complex dose distributions (Figure 11.10). Using the Finite Mixture Model three equivalent dose components were identified in Faya NR1, and two components were identified in Faya NR2. Both samples contained one dominant component containing > 50% of the accepted grains. Using these dominant components, ages of 45.5 ± 3.9 ka (66% of the accepted grains) and 44.6 ± 3.5 ka (92% of the accepted grains) were produced for Faya NR 1 and Faya NR2 respectively. Smaller components, containing 26% and 11% of accepted grains from sample Faya NR 1, yield ages of 6.4 ± 0.6 k and 21.2 ± 3.7 ka. The minor equivalent dose component (8% of accepted grains) from Faya NR2 yields an age of 8.9 ± 1.1 ka. These smaller, low dose components, are attributed to the post depositional intrusion of younger (predominantly Holocene) material from the overlying sediments into Faya NR1 and NR2 by bioturbation.

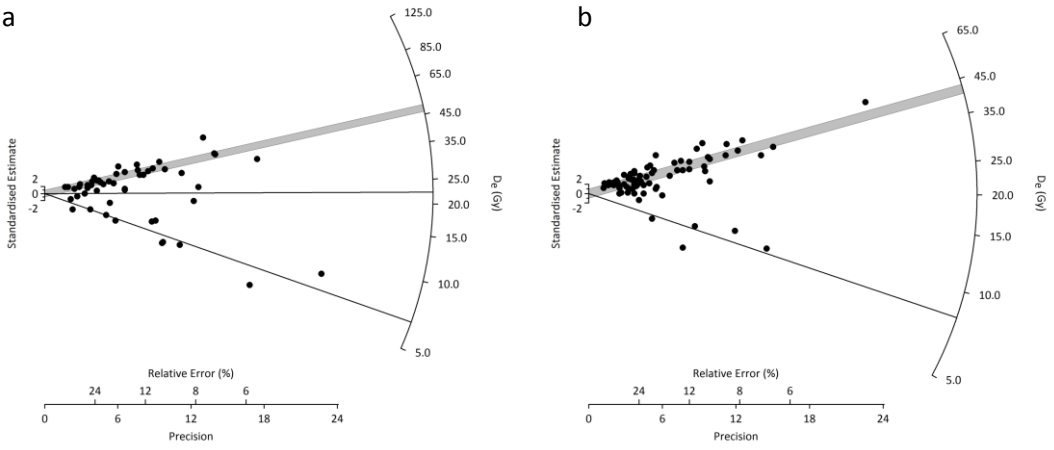

Figure 11.10. Radial plots showing the single-grain (SG) D_e distributions obtained from a) Faya NR1 and b) Faya NR2. The thick grey bars represent the dominant (>50%) components identified using the FMM. Black lines identify minor components, containing less than 50% of the grains measured.

As the ages produced using the dominant component for the two OSL samples fall within age uncertainties of each other, they suggest that the sterile sand unit was deposited during MIS 3. However, these ages are older than those produced for the sterile sand unit in trench 4 and trench 28 by Armitage et al. (2011), which were dated to 38.6 ± 3.2 ka and 34.1 ± 2.8 ka.

As the units are located in different trenches, it is possible that the sterile sand from which Faya NR1 and NR2 were taken is not the same depositional event investigated by Armitage et al., (2011). Initial correlation of the units was based solely on sedimentological investigation. Furthermore, Trench 36 is one of the most distal excavations at the FAY-NE1 site, and is thought to have been outside the limit of the shelter when it was occupied.

While the homogenous particle size of the sterile sand suggests that the material in this unit was transported and deposited via aeolian processes, possibly during a period of environmental deterioration / increased aridity, there is some evidence for local reworking. The identification of desiccation cracks, some small (0.5-1 cm) clasts, modern roots and burrows in the sterile sand provides evidence for post depositional mixing of the unit. Whilst care was taken to avoid sampling these latter features, it is possible that the introduction of younger aged populations into the unit may be the cause of an underestimation of the age. Visual inspection of Figure 11.10 shows that the equivalent doses in the largest component are tightly clustered, suggests that this population represents the “true” burial age.

11.3.2 Sterile sand unit, Trench 27

Faya NR 3 was taken from an archaeologically sterile sand layer located beneath a roof fall boulder 290 cm below the present day land surface on the north facing section of Trench 27 (Figure 11.11). The sterile layer was a homogenous sand unit containing no large clasts, and no evidence for bioturbation. Underlying the sand unit in Trench 27, a clast rich cemented sandy unit was identified. This unit was stratigraphically correlated to Trench 19, where the same unit was found to contain lithics that were attributed to the Assemblage C industry. The presence of imbrication in parts of the unit is indicative of deposition by water, probably as slope wash. Clasts contained within the unit are sub angular and range from 1-30 cm in diameter. Towards the base of the section, the clast rich unit becomes more cemented, before reaching bedrock.

OSL dating in this location sought to determine the timing of the rock fall event at the site, and establish whether the sterile unit in Trench 27 is the same as that identified in Trench 4 and 28. Furthermore, dating this sample provides a minimum age for the underlying lithic bearing unit, although lithics were not identified in the section directly below the sample location in this trench.

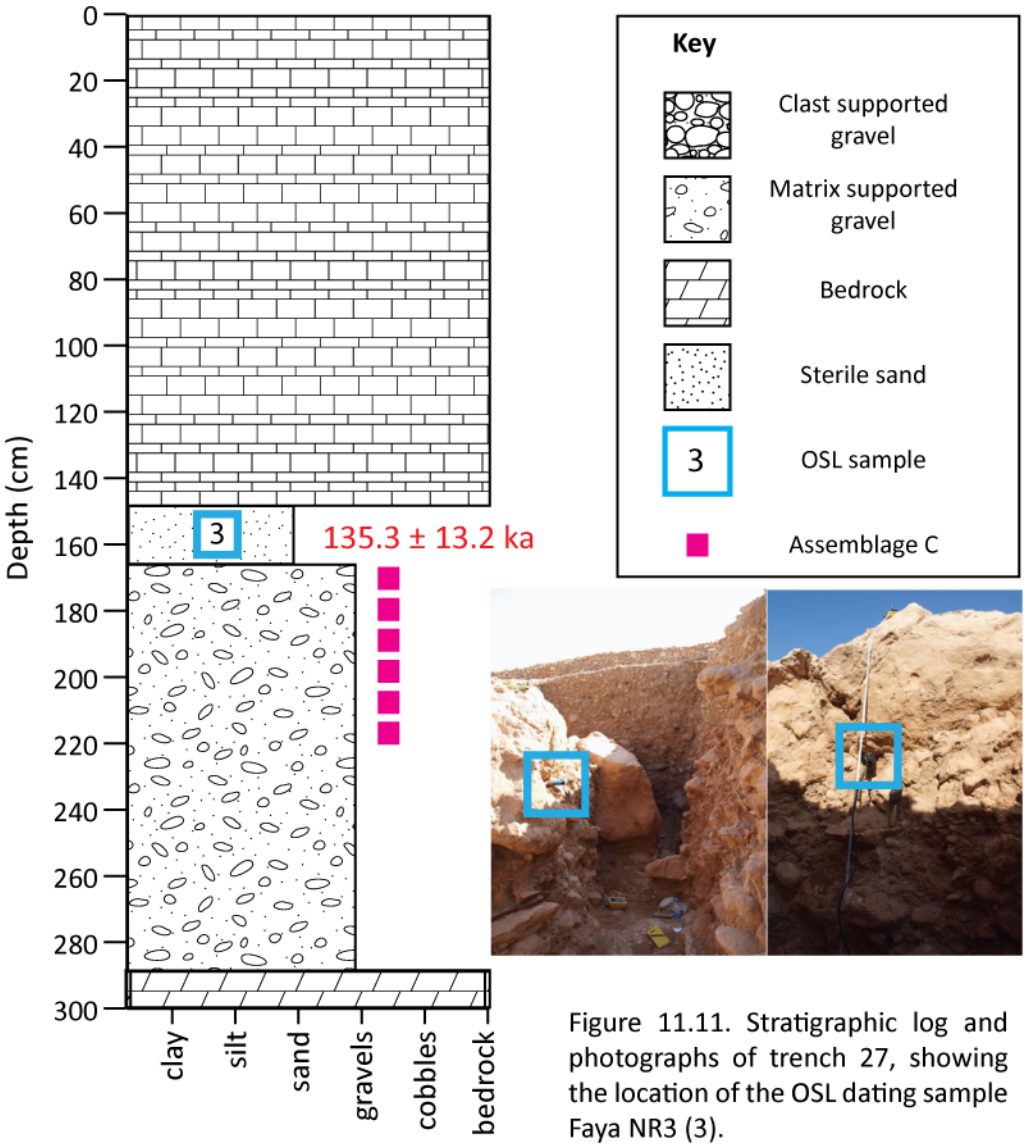

Figure 11.11. Stratigraphic log and photographs of trench 27, showing the location of the OSL dating sample Faya NR3 (3).

Unlike the samples taken in Trench 36, Faya NR3 did not contain a particularly complex dose distribution. A single dominant equivalent dose component, containing 96% of the accepted grains, was present in this sample, and was used to generate the OSL age (Figure 11.12). This component yielded an age of 135.3 ± 13.2 ka, placing its deposition during the

MIS 6 / MIS 5e boundary. The smaller component, comprising 4% of the equivalent dose values from the sample, produced a date of 19.1 ± 7.5 ka (MIS 2), which most likely represents the post depositional intrusion of younger grains into Faya NR3.

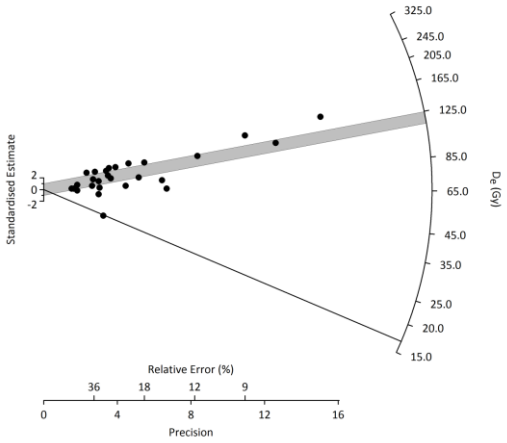

Figure 11.12. Radial plot showing the single-grain (SG) D_e distribution obtained from Faya NR3 . The thick grey bar represents the dominant (96%) component identified using the FMM. The black line identifies the minor component, containing 4% of the grains measured.

It is apparent that the sandy unit identified in this trench does not correlate chronologically with the sterile unit identified and dated by Armitage et al. (2011).

Trench 27 (where Faya NR3 was taken) is adjacent to Trench 19 (Figure 11.3), which is where the OSL samples associated with Assemblage C were collected by Armitage et al. (2011). Consequently, by tracing the stratigraphic units across the two trenches, the ages produced for Assemblage C (127 ± 16 ka and 123 ± 10 ka) should represent the sediment unit underlying the sterile sand dated by Faya NR3. Although slightly older, the age for Faya NR3 is indistinguishable from those for Assemblage C presented by Armitage et al. (2011). The rock fall event capping the lithic bearing unit was therefore deposited during or following the deposition of the Assemblage C levels. It is therefore possible to support the assertion made by Armitage et al. (2011) that modern humans were present at the FAY-NE1 site by MIS 5e, if not earlier.

11.4 Evidence for Holocene gullying

As shown in Figure 11.2, evidence for Holocene gullying was identified by Armitage et al. (2011) in Trenches 4, 19, 27 and 34. Although the gullying had not disturbed all of the sediments in these trenches, during the formation of these features, materials from the underlying units had been reworked in some areas. The Palaeolithic material was completely washed away on the west facing section of Trench 39, and replaced by a large Holocene channel deposit. These relatively modern deposits highlight the significance of slope wash processes in forming the sediments at FAY-NE1, and the potential for partial bleaching or post depositional mixing at the site.

Two of the samples dated as part of this thesis appear to have been affected by similar Holocene gullying processes, resulting in highly complex dose distributions and the subsequent underestimation of ages for the associated lithic technologies. These samples are discussed in the following sub-sections (Section 11.4.1 and 11.4.2).

11.4.1 The Neolithic, Trench 17

Faya NR 4 was taken from the west facing section of Trench 17, in a unit containing Neolithic material. In this section the bedrock was overlain by a clast supported, sandy unit containing cobbles and boulders. Above this unit, a lithic bearing matrix supported sandy unit containing small clasts (ranging from gravels to pebbles) was identified. The overall sequence was capped by a matrix supported, coarse sandy gravel layer containing clasts ranging in size from gravels to cobbles. Faya NR4 was taken from the lithic bearing sandy unit 40 cm below the present day land surface (Figure 11.13), with the aim of providing an age for the deposition of the Neolithic material identified within.

Evidence for Holocene gullying was identified on the west facing section of Trench 17, although at the time of sampling, there was no clear evidence for similar processes on the north facing section where the OSL dating samples were taken.

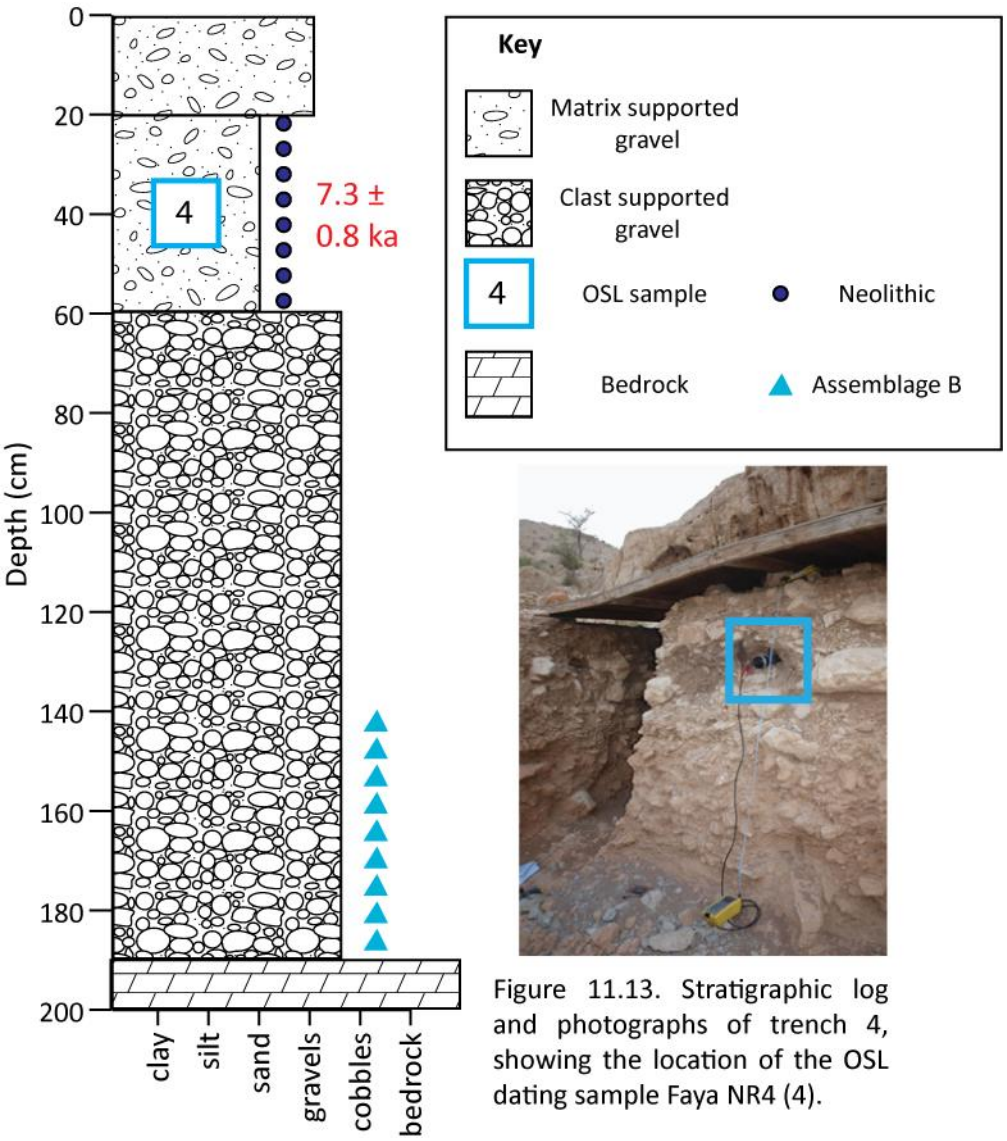

Figure 11.13. Stratigraphic log and photographs of trench 4, showing the location of the OSL dating sample Faya NR4 (4).

The Finite Mixture Model identified four components within the single-grain data for Faya NR4, indicating a complex dose distribution in which no component contained > 50% of the accepted grains. The radial plot (Figure 11.14) shows the dispersed nature of the single-grain sample, which is likely to have been affected by partial bleaching or post depositional mixing processes.

The largest component identified by the FMM containing 42% of the accepted grains was used to produce an age for Faya NR4, and the associated lithic artefacts. This equivalent dose component yielded an age of 7.3 ± 0.8 ka. The ages calculated using the equivalent dose components containing fewer grains were 2.4 ± 0.3 ka (25% of the accepted grains), 21 ± 3 ka (22%) and 52.2 ± 15.3 ka (11%).

The “older” components can be explained by the intrusion of older grains from the underlying units during post depositional mixing, or inadvertent sampling of the underlying material. Partial bleaching may also provide a valid explanation for the inclusion of “older” grains and subsequent overdispersion of the dataset.

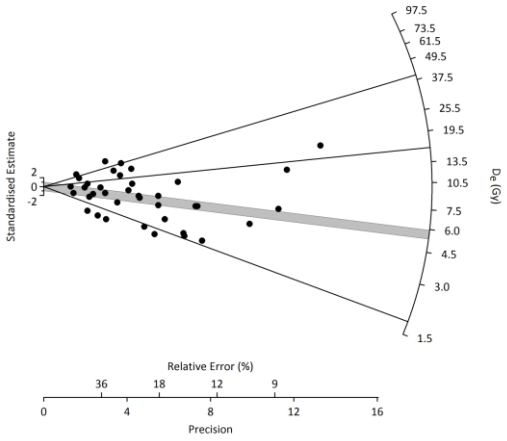

Figure 11.14. Radial plot showing the single-grain (SG) D_e distribution obtained from Faya NR4. The thick grey bar represents the largest (42%) component identified using the FMM. The black lines identify the minor components, containing < 30% of the grains measured.

The finite age of 7.3 ± 0.8 ka produced by the largest component within the sample, suggests that the Neolithic material was deposited during the early-mid Holocene, a time when humid conditions are likely to have supported the presence of modern humans in the Arabian landscape.

11.4.2 Assemblage A, Trench 1

Armitage et al. (2011) utilised OSL samples taken from Trench 4 and Trench 28 (Figure 11.3) to produces finite ages of 38.6 ± 3.1 ka and 40.2 ± 3.0 ka for sediments containing Assemblage A lithics. They also produced ages of 38.6 ± 3.2 ka and 34.1 ± 2.8 ka for the sterile sand unit that separates Assemblage A from the overlying Holocene lithics in Trench 4 and Trench 28 (Figure 11.3). Faya NR 6 was taken from the south facing sterile sediments located directly beneath the Assemblage A lithic bearing unit in Trench 1 (Figure 11.3), 95

cm below the present day land surface (Figure 11.15). Analysis of sample Faya NR6 sought to provide a maximum age for Assemblage A by dating the underlying sterile sediments.

A Holocene erosion channel was identified adjacent to the Assemblage A lithic material in this Trench. Care was taken to avoid sampling in the Holocene erosion channels, which were at risk of having been locally reworked during slope wash events in the recent past.

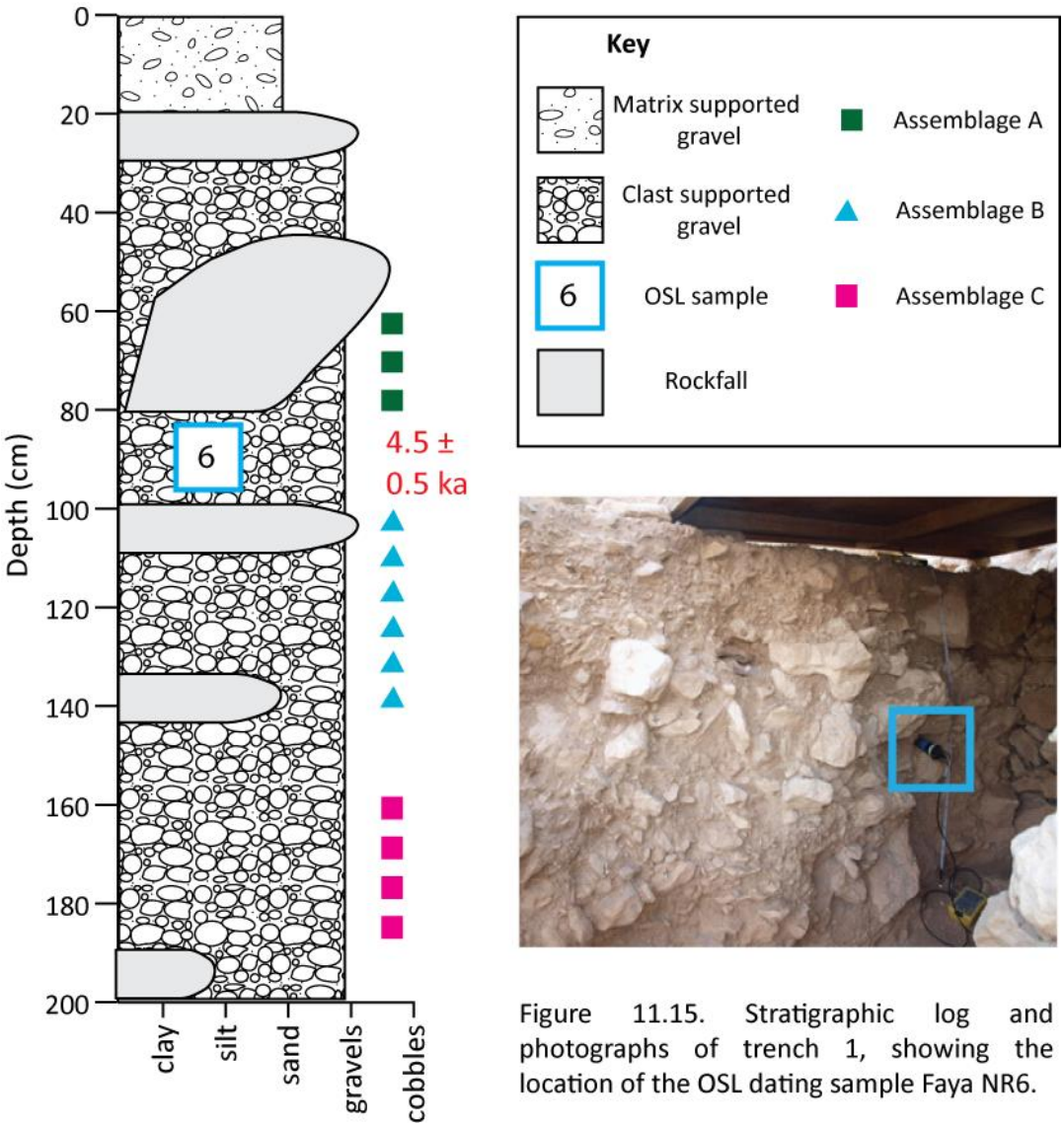

Figure 11.15. Stratigraphic log and photographs of trench 1, showing the location of the OSL dating sample Faya NR6.

Once again, a complex dose distribution was identified by the Finite Mixture Model, which suggests the presence of 4 components within the Faya NR6 sample. The dominant component, containing 50% of the accepted grains, yields an age of 4.5 ± 0.5 ka, placing the

deposition of the unit in the Holocene period. Smaller components identified by the FMM suggest finite ages of 10.1± 1.1 ka (27% of the accepted grains) and 31.8 ± 3.4 ka (23%).

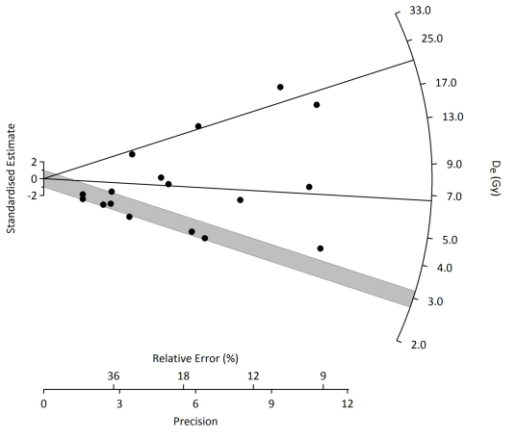

Figure 11.16. Radial plot showing the single-grain (SG) D_e distribution obtained from Faya NR6. The thick grey bar represents the dominant (50%) component identified using the FMM. The black lines identify the minor components, containing < 30% of the grains measured.

Due to the presence of predominantly Holocene aged material within this section, and the presence of a Holocene erosion channel in the adjacent section, it is suggested that the lithic bearing unit dated by Faya NR6 has been locally reworked. The smallest component, containing 23% of the accepted grains suggests an age of 31.8 ± 3.4 ka. This age is considered to be the one most likely to represent the "true" age of the Assemblage A lithics, since it is in the best agreement with the ages produced by Armitage et al. (2011) for Assemblage A. The 31.8 ± 3.4 ka age is inconsistent with the published ages for Assemblage A (38.6 ± 3.1 ka and 40.2 ± 3.0 ka). It is suggested therefore, that Assemblage A material was deposited during MIS 3, as suggested by Armitage et al. (2011). The poor agreement of the Faya NR6 age with those published by Armitage et al. (2011), and the younger components reported for Faya NR6 are attributed to the intrusion of Holocene material during post depositional mixing, following channel formation and gullying in this period.

11.5 Layer 3, a new lithic assemblage in Trench 38

Material within Layer 3 potentially represents a new lithic industry, recently identified in a unit located on the west facing section of Trench 38. The unit containing Layer 3 is located below a large boulder that itself underlies Neolithic material. Layer 3 is directly above a unit containing lithics assigned to the Assemblage A industry. The sediment within the layers in this trench do not vary significantly. Instead, the units were identified on the basis of small variations in colour, and the size and frequency of clasts.

Faya NR7 was taken 195 cm below the present day land surface, directly below a large boulder thought to represent roof fall. The sample was taken from a clast supported, sandy gravel unit containing Layer 3 lithics (Figure 11.17). The sediment units across the sections in Trench 38 were highly cemented. OSL dating at this location sought to produce an age for the Layer 3 lithics, which will assist in determining whether or not these lithics represent a new lithic industry, or are actually part of Assemblage A.

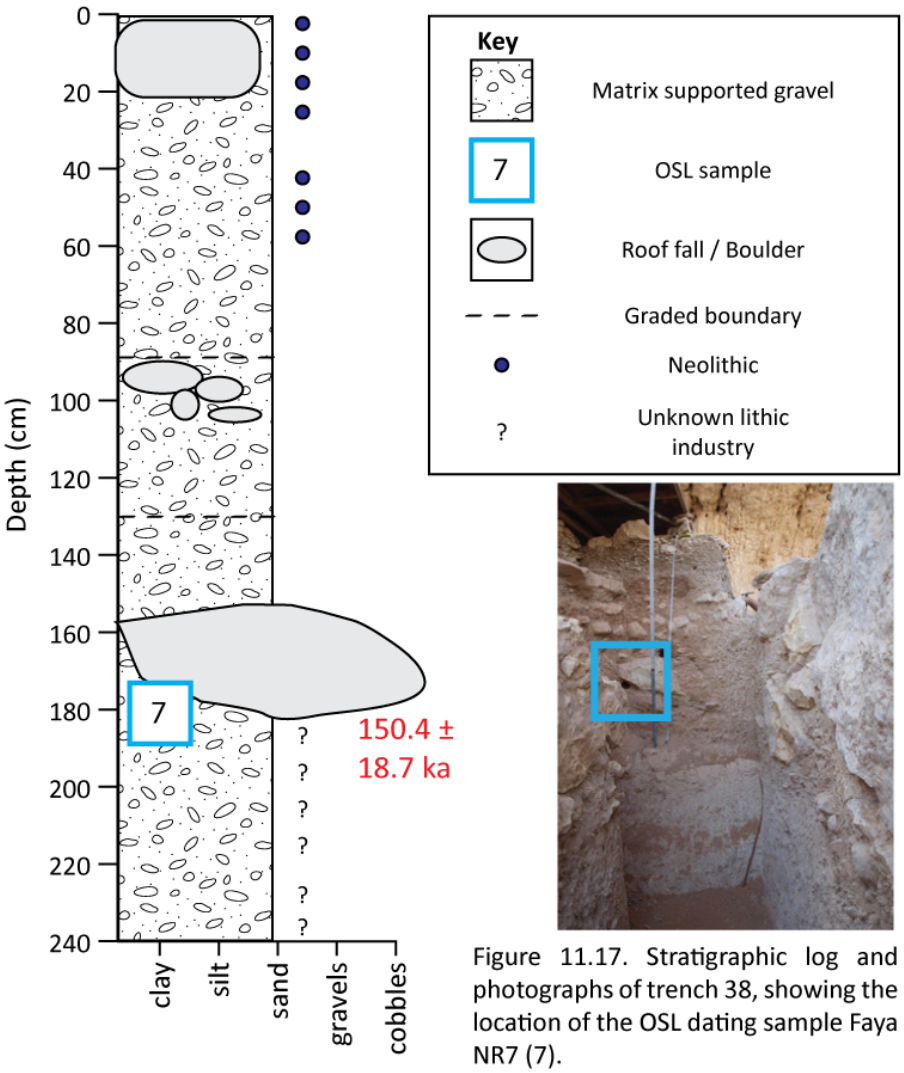

Figure 11.17. Stratigraphic log and photographs of trench 38, showing the location of the OSL dating sample Faya NR7 (7).

Three components were identified by the FMM (Figure 11.18). A dominant component containing 72% of the accepted grains produced an age of 150.4 ± 18.7 ka. However, due to the location of Assemblage A lithics below this sample, and the proximity to the overlying Holocene sediments, this age is markedly older than is reasonable on the basis of the associated archaeology. Smaller components containing 3% and 25% of the accepted grains produce ages of 10.2 ± 2.6 ka and 79.2 ± 21.3 ka respectively. Consequently, only 3% of the sample population produces an age that would be in good agreement with radiocarbon ages (10,405 to 9711 and 10,380 to 10,078 calendar years before present (Armitage et al., 2011)) produced for the Holocene lithics, and the archaeological understanding of the site.

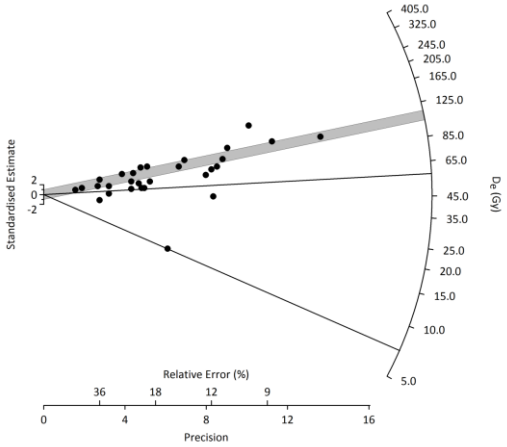

Figure 11.18. Radial plot showing the single-grain (SG) D_e distribution obtained from Faya NR7. The thick grey bar represents the dominant (>50%) component identified using the FMM. Black lines identify minor components, containing less than 50% of the grains measured.

It is not clear why OSL dating of this unit has been unsuccessful. It may be a result of contamination from the eboulis roof fall boulders, as in-situ decomposition of ancient rock released older material into the surrounding sediment. However, Armitage et al. (2011) dissolved a large clast of limestone bedrock, which yielded a proportion of quartz grains that was far too low to make this explanation likely. In this instance, the OSL dating has failed to produce an age which is consistent with the archaeology, and therefore further sample(s) from this assemblage are required.

11.6 Assemblage C

Assemblage C lithics in Trench 19 were dated to 127 ± 16 ka and 123 ± 10 ka by Armitage et al. (2011), and Faya NR3 yielded an indistinguishable age (135.5 ± 13.2 ka). All three of these samples yielded complex dose distributions which are likely to be a result of partial bleaching and/or post depositional mixing via slope wash processes. Armitage et al. (2011) suggest that younger populations present within their samples are a result of the intrusion of younger grains from overlying sediments. The dose distribution for sample TR19-04, which produced the older of the two dates (127 ± 16 ka), was highly scattered and contained a high equivalent dose component which contained 22% of the accepted grains. This high dose component was attributed to partial bleaching and the dominant component (77% of the accepted grains) was used for age determination instead.

In this thesis, samples were taken from units below Assemblage C levels in an attempt to provide a maximum age for human occupation at the site.

11.6.1 Faya NR8, beneath Assemblage C

Faya NR 8 was taken below the lithic bearing unit containing Assemblage C on the south facing section in Trench 27 (Figure 11.3). A clast supported, fine sand Holocene unit (containing Neolithic material capping the section at this site) directly overlies a clast supported, cobble layer containing abundant boulders. It is thought that this boulder rich layer lines the base of a Holocene gully channel that stretches across the trench. Underneath this Holocene channel, a clast supported, sandy unit extends down to the bedrock. Assemblage B and C lithics were found in discrete layers in this unit to a depth of c. 200 cm. Faya NR8 was taken at a depth of 235 cm below the present land surface, in a sterile section below Assemblage C, with the aim of providing a maximum age for the industry (Figure 11.19).

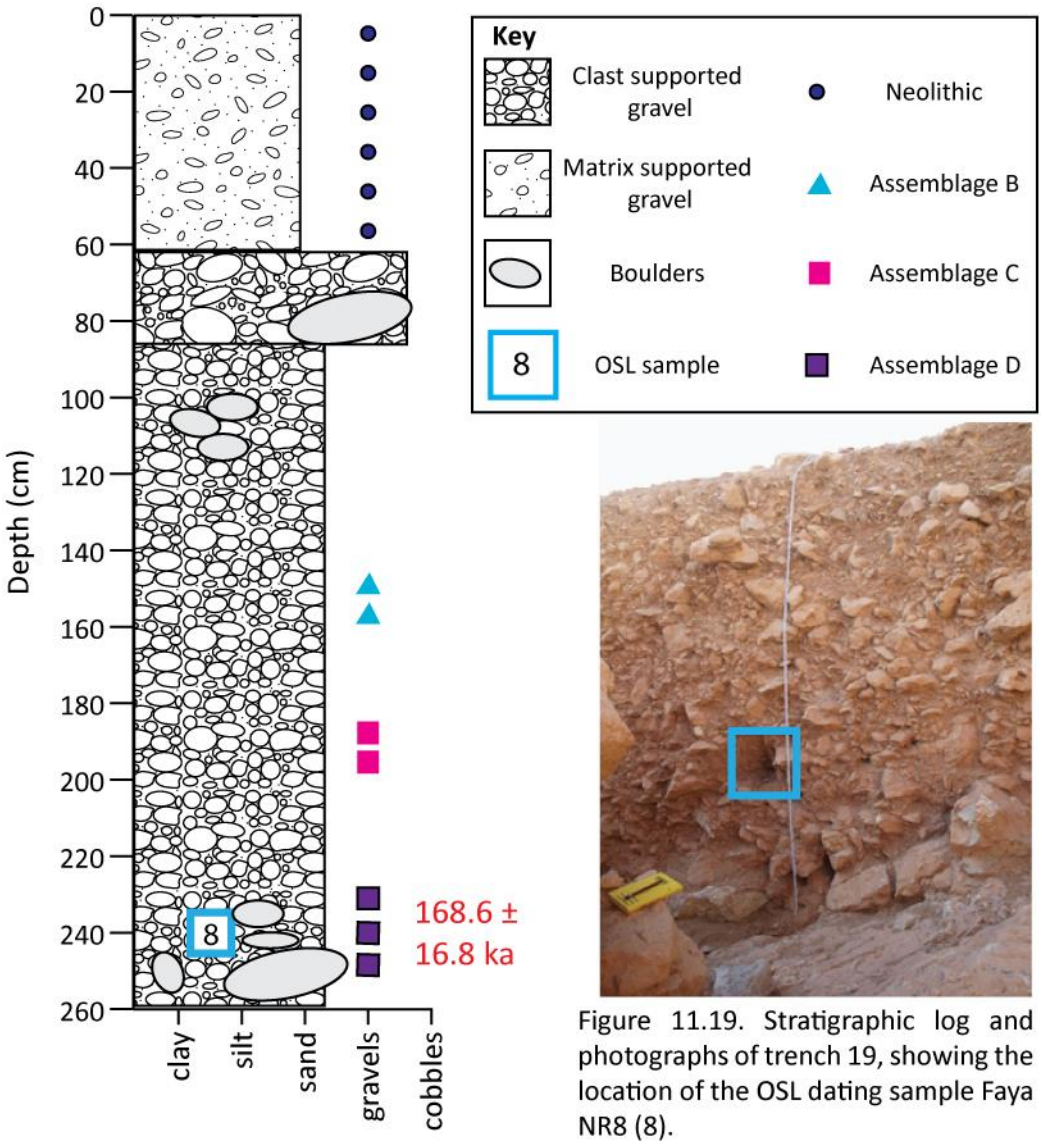

Figure 11.19. Stratigraphic log and photographs of trench 19, showing the location of the OSL dating sample Faya NR8 (8).

The Finite Mixture Model indicates that Faya NR8 has a complex dose distribution. In this instance two equally large components comprising 49% of the dose values are identified (Figure 11.20). The presence of a small (2%) younger component (9.9 ± 3.2 ka) is indicative of the intrusion of bleached grains during sampling, and is therefore not considered to represent the true age of the deposit.

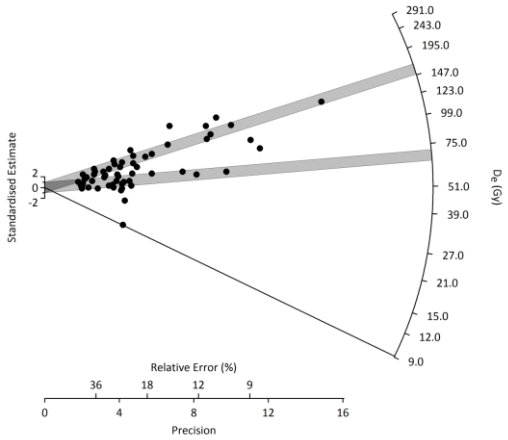

Figure 11.20. Radial plot showing the single-grain (SG) D_e distribution obtained from Faya NR8. The thick grey bars represents the dominant (49%) components identified using the FMM. The black line identifies the minor component containing 2% of the grains measured.

Two components containing 49% of the accepted grains yield ages of 73.4 ± 7.9 ka and 168.6 ± 16.8 ka. Due to the equal size of both components (i.e. each containing 49% of the accepted grains), it would be difficult to determine which component represents the most likely age of the sample without any previous chronological or archaeological understanding of the site. In this instance, however, using the evidence from the overlying Assemblage C that has already been dated by Armitage et al. (2011) and Faya NR3 to the MIS6/5 transition, it is unlikely that an age of 73.4 ± 7.9 ka represents the "true" age of the sample.

Based on the stratigraphical location of Faya NR8 beneath Assemblage C, it is most likely that the older component represents the true age of the underlying material. A similar component was removed by Armitage et al. (2011) amidst concerns that it contained erroneously high dose values due to partial bleaching. Out of interest, a mean age was calculated for Faya NR8 using the two dominant components containing 49% of the accepted grains each. Although there are no grounds for this calculation, the mean age of 121 ka is very similar to the existing ages produced for the Assemblage C samples by Armitage et al. (2011).

In an attempt to identify whether the constraints of the Finite Mixture Model were, in this instance, forcing apart a single component into two separate components, measurements were made using the model up to 30% overdispersion values. No change was observed,

and the three components were once again found to represent the statistically most likely components. Interestingly, when the weighted mean of the two largest components was calculated using the Central Age Model, the material underlying Assemblage C yielded an age of 105.4 ± 11.5 ka, a value which lies within errors of the two aged produced by Armitage et al. (2011). However, the overdispersion value reported for Faya NR8 was 43%, and therefore it is argued that the CAM age would not represent the most accurate age for the sample.

With the caveats outlined above, the age of 168.6 ± 16.8 ka is considered to be most likely to represent the true depositional age of sample Faya NR8. This places the deposition of the material underlying Assemblage C in MIS 6. The decision to prefer this age over other possibilities was made based on the stratigraphical position of the sample beneath the relatively well dated Assemblage C unit. The archaeological sterility of this layer probably indicates that hominins were not present at Jebel Faya at this time. This was probably due to locally arid conditions making the site uninhabitable to the hominins already in Arabia, and arid conditions in Africa and Arabia, which would have prevented the migration of modern humans out of sub-Saharan Africa.

11.6.2 Faya NR9, Assemblage D

Following the dating of Assemblage C in Trench 19 by Armitage et al. (2011), a small number of lithics were identified at the base of the trench, which exhibited technological variations when compared to lithics from Assemblage C. These lithics have tentatively been assigned to a new industry, named Assemblage D. In an attempt to determine whether or not these lithics form part of a new, older, industry, an OSL dating sample was taken in association with the "new" lithics.

Faya NR9 was taken at a depth of 295 cm below the present day land surface on the west facing section of Trench 19, in association with Assemblage D lithics (Figure 11.21). The OSL sample was taken from a lithic bearing, clast supported, sandy sediment, containing prevalent cobbles and boulders. It is interpreted as slope wash material. With increasing depth, clast size and abundance increased throughout the unit. Overlying the clast supported unit, a layer of boulders lined a Holocene channel containing a matrix supported gravel, which contained large clasts throughout. Overall, the unit was capped with a clast supported, Holocene slope wash deposit containing Neolithic material.

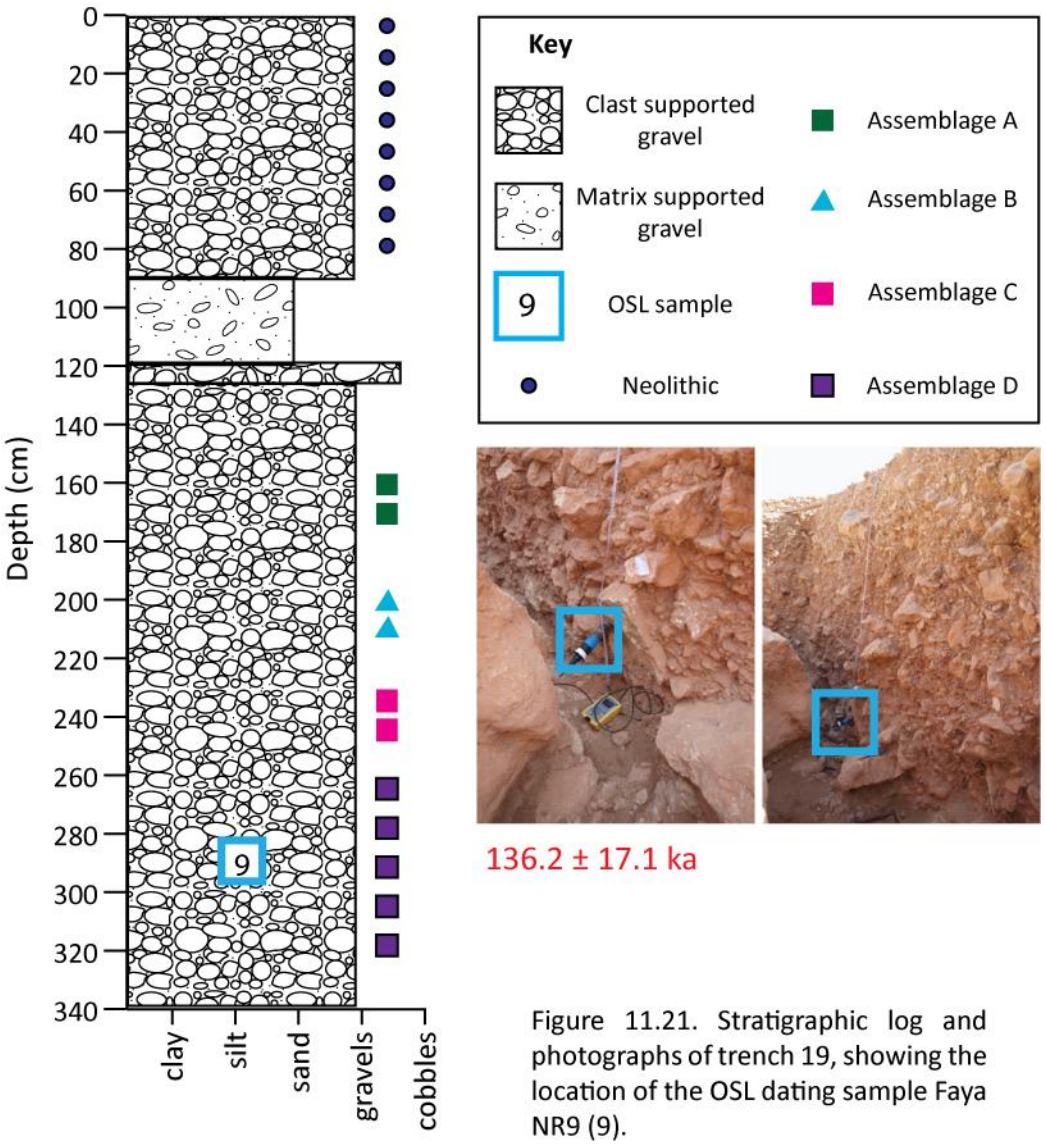

Figure 11.21. Stratigraphic log and photographs of trench 19, showing the location of the OSL dating sample Faya NR9 (9).

Four components were identified by the Finite Mixture Model. The two largest components, containing 48% and 31% of the accepted grains were used to calculate ages of 58.5 ± 6.1 ka and 136.2 ± 17.1 ka respectively (Figure 11.22). Two smaller components comprising 8% and 13% of the sample produced ages of 7.9 ± 1.5 ka and 24.1 ± 2.9 ka. Following Armitage et al., (2011), these smaller components are attributed to the intrusion of younger grains from overlying sediments, potentially as a result of bioturbation (e.g. animal burrowing).

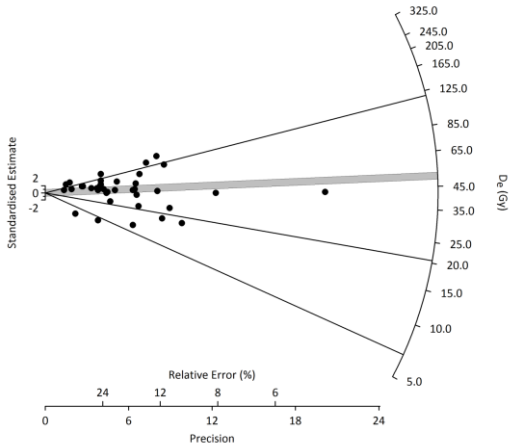

Figure 11.22. Radial plot showing the single-grain (SG) D_e distribution obtained from Faya NR9. The thick grey bar represents the largest component (48%) identified using the FMM. Black lines identify minor components, containing less than 40% of the grains measured.

The largest component produces an age that is not in stratigraphic agreement with the overlying sediments. An age of 58.5 ± 6.1 ka is significantly lower than the reported age of the overlying Assemblage C lithics at this site (here and Armitage et al., 2011). Consequently, the second largest component is taken to represent the "true" age of the Assemblage D lithics, which are assigned an age of 136.2 ± 17.1 ka. This age is in good agreement with the overlying Assemblage C lithics, and places the production of Assemblage D during the transition from MIS 6 into MIS 5e, probably late MIS 6.

Lithics from Assemblage D have not yet been fully investigated. It is therefore not clear what species of hominin produced these tools, or whether they are of African affinity like Assemblage C. At present there is no evidence to suggest that they were produced by modern humans. Once the assemblage has been fully investigated, it will be possible to answer a number of these questions, and consider how this potentially new lithic industry fits into the out of Africa migration theory.

11.7 Jebel Faya within an environmental context

As discussed in Chapter 2, the current understanding of regional climatic change in Arabia is fragmentary due to the limited amount of research that has been carried out in the area. Drake et al. (2013) published a synopsis of Mid to Late Pleistocene Arabian humidity

indicators from MIS 6 to MIS 2. Using probability density function (PDF) analysis, they synthesised evidence for humidity in the Arabian desert, obtained from regional lacustrine, tufa, calcrete, travertine and fluvial deposits (Section 2.4.2). They suggest that the regional climate was variable throughout all of the MIS stages.

Overall, the OSL chronology produced as part of this thesis suggests a termination of human occupation in Jebel Faya (as indicated by the presence of sterile sand units) occurred during MIS 3, MIS 5d, and MIS 6. Whilst the presence of the sterile sandy layers might also indicate the onset of aridity in the region, without corroboration from other climatic records they cannot be used to build an aridity record.

Bretzke et al. (2013) suggest that MIS 3 was a complex period in Arabia, with fluctuations between arid and humid conditions driven by Heinrich events and monsoon strength respectively. Armitage et al. (2011) dated the presence of a sterile sand layer at FAY-NE1 to 38.6 ± 3.2 ka and 34.1 ± 2.8 ka, during the transition between MIS 3 and MIS 2. Arabia was characterised by arid conditions at this time, with mega dunes forming across the Rub 'al Khali and Wahiba deserts, and the drying up of lakes in the region between 38-34 ka (Bretzke et al., 2013). Furthermore, marine core evidence suggests wide spread aridity in the region from 33 ka, corresponding with the occurrence of the H3 Heinrich event (Schulz et al., 1998). The two sterile sand units dated in this thesis from FAY-NE1 are also likely to have been deposited via aeolian processes during periods of aridity in Arabia. Faya NR1 and Faya NR2, however, suggested an earlier onset of aridity than that identified by Armitage et al., (2011). The dates produced for the samples in Trench 36 suggest arid conditions were present in the area c. 45 ka, during MIS 3. Carto et al., (2009) report the occurrence of Heinrich events 16, 22, 30, 38, 45, 65, 85 and 105 ka. Therefore, whilst the age of the unit in Trench 36 is similar to that dated by Armitage et al., (2011), it is suggested that the sterile sand here may represent an earlier period of aridity in the region, driven by the Heinrich event 45 ka.

The second sterile sand unit dated in this thesis also appears to have been deposited earlier than the one investigated by Armitage et al., (2011). If it is assumed that the sterile sands do reflect arid conditions at FAY-NE1, Faya NR 3 (taken from a sterile sand unit overlying Assemblage C lithics) suggests the presence of arid conditions in the region 135.5 ± 13.2 ka. An increase in dust levels identified in marine cores indicated increases in aridity during MIS 6, MIS 5d and MIS 5b in Arabia (Drake et al. 2013). Due to the stratigraphical location of the sterile sand unit dated by Faya NR3 above Assemblage C lithics (attributed to MIS

5e), it seems most likely that the overlying sand unit represents the arid conditions that were present during MIS 5d. The PDF produced by Drake et al., (2013) (Figure 2.7) provides further supporting evidence for aridity in Arabia during this time, with a humidity trough present at the onset of MIS 5d.

Although MIS 6 is traditionally considered to be a period dominated by aridity, some evidence for humidity has been reported in Arabia during this time. Drake et al. (2013) suggest that the decline in humidity appears reduced in the Arabian Peninsula during MIS 6, and present scattered evidence for humidity centred around 138, 154 and 180 ka. Whilst the large errors associated with MIS 6 ages are acknowledged to have reduced the precision with which the PDF can represent periods of humidity, pluvial periods at this time would have facilitated human migration into the area. Additional findings from speleothem records further suggest that there was an abrupt increase in rainfall over Arabia during the end of MIS 6 and into MIS 5e, c. 130 ka to c 120 ka (Bar-Matthews et al., 2003; Burns et al., 1998, 2001; Drake et al., 2013; Fleitmann et al., 2011; Vaks et al., 2007, 2010). This increase in humidity led to an extensive network of lakes across the northern Arabian peninsula during MIS 5e and MIS 5a, although periods of aridity returned during MIS 5b and MIS 5d. speleothem evidence presented by Vaks et al. (2007, 2010) from six caves in the Negev Desert, Israel, suggests that conditions along the northern margins of the Saharo-Arabian desert belt were also wetter during MIS 6 – MIS 5e. They suggest that a northward shift in the African monsoon due to increased orbital insolation would have increased precipitation over the desert region at this time.

Sedimentological and phytolith data produced by Bretzke et al. (2013) suggests that the lithic bearing units at FAY-NE1 were deposited during humid climatic periods. Increased proportions of organic matter and silt, combined with the poorly sorted nature of the clast rich units, are indicative of wetter climatic conditions. Increased surface runoff, resulting from increased precipitation, is likely to have been a primary driver in the slope wash processes responsible for the deposition of the units. Armitage et al. (2011) dated Assemblage A to 38.6 ± 3.1 ka and 40.2 ± 3.0 ka (MIS 3), and Assemblage C to 127 ± 16 ka and 123 ± 10 ka (MIS 5e), supporting the palaeoenvironmental data presented by Bretzke et al. (2013). Furthermore, the additional dating completed as part of this thesis is also in agreement with the relative timing of deposition for the lithic bearing units under humid conditions.

Faya NR9 was taken in association with Assemblage D lithics. The age produced by the OSL sample in this location yielded an age of 136.2 ± 17.1 ka, placing the deposition of the lithic bearing unit during the period of humidity associated with the MIS 6 / 5 transition period in Arabia. Faya NR8, taken below the lithic bearing units in Trench 19, produced an age of 168.6 ± 16.8 ka, providing a maximum age for the overlying lithic assemblages. This absence of lithics at the site during a period of hyper-aridity in MIS 6 again reinforces the link observed between humidity and human presence at the site.

During MIS 4 there was extensive dune deposition in Arabia, particularly in the Wahiba sands c. 71-57 ka (Bretzke et al., 2013). Whilst a lack of evidence for human occupation at the site during this time is to be expected, the absence of a sterile sand unit (such as that identified in MIS 2) is a little surprising considering the likely hyper-arid conditions. It is possible that any aeolian material has been reworked during MIS 3, when pluvial conditions facilitated the reworking of material via slope wash processes.

Although Faya NR4 and Faya NR6 were complicated by Holocene gullying processes, the ages generated by these samples also support the notion that the lithic bearing units were deposited during periods of increased humidity. Faya NR6 yielded an age of 31.8 ± 3.4 ka, placing its deposition in MIS 3, while the unit containing Neolithic material (Faya NR4) yielded an age of 7.3 ± 0.8 ka, positioning its deposition in the Holocene.

In summary, the OSL dating of samples completed as part of this thesis appear to be in good agreement with the dates produced by Armitage et al. (2011). The environmental evidence supports the theory proposed by Bretzke et al. (2013), that the lithic bearing units at site FAY-NE1 were deposited during humid climate periods, while sterile units were deposited during periods of aridity. Unlike the evidence obtained from Libya (Chapter 8), it is not possible to determine what forces were responsible for driving regional climate change in Arabia, due to the limited number of samples and sites dated. However, evidence for aridity during the MIS 3 interglacial, at a time correlating with the occurrence of a Heinrich event, potentially supports a northern hemisphere influence on the southern Arabian climate.

11.8 Jebel Faya within an archaeological context

A critical prerequisite for the presence and survival of modern humans within an environment is the availability of fresh water. As discussed in Section 11.1, Jebel Faya is located in an ecotone setting with easy access to a variety of habitats (Bretzke et al., 2013). The relatively wet conditions in the wide plain adjacent to Jebel Faya resulted in an area characterised by relatively well developed vegetation. Under favourable conditions, the confluence of precipitation draining from the Hajar mountains into the Inland Basin (via surface runoff and underground flow) results in the presence of standing surface water near FAY-NE1 (Bretzke et al., 2013). This availability of fresh water, presence of vegetation, and raw material availability for lithic production from the anticline would have made Jebel Faya an attractive settlement area for mobile hunter-gatherer groups dispersing into Arabia during the Pleistocene.

Armitage et al. (2011) suggest that the archaeological sequence at Jebel Faya spans at least 125 ka, a notion supported by the additional OSL dating completed as part of this thesis. They attribute Assemblage C to modern humans expanding out of Africa during the transition from MIS 6 to early MIS 5 because of the technological affinities of the industry with those from African lithic assemblages. Climatic evidence presented in Section 2.4, suggests the occurrence of interglacial, humid conditions in Arabia during this period. In addition, during the MIS 6/5 boundary, Bretzke et al. (2013) report the lowering of sea levels by approximately 120 m, consequently reducing the width of the Bab al-Mandab Straits to < 4 km. Due to a time lag of 5 ka between the peak of the Indian Monsoon index and the increase in sea levels to peak interglacial high stand conditions during MIS 5e, this means that there were full interglacial conditions at the same time as low sea levels in Arabia during the MIS 6/5 transition. Modern humans present along the East African coastline of the Red Sea during late MIS 6 would have therefore been presented with a window of opportunity for expansion into Arabia during the transition period into MIS 5e. Southern Arabia has strong floral (and some faunal) affinities with east Africa, potentially making the migration more favourable for the African populations (Bretzke et al., 2013; A. Parker, *pers.comm*. 2012). At this time, the Njed plateau would have also opened, enabling human migration to, and occupation of, the Jebel Faya rock shelter (Bretzke et al., 2013).

Evidence from the OSL chronology presented here supports the findings of Armitage et al. (2011), placing the timing of human occupation at the site during the Holocene, MIS 3, and MIS 6 / MIS 5e humid interglacial phases (Figure 11.23). Furthermore, the sample dated in

association with the Assemblage D (Faya NR9) lithics, suggests that modern humans may have been present at the site as early as 136 ka, although it is acknowledged that the associated dating errors could comfortably place their presence in MIS 5.

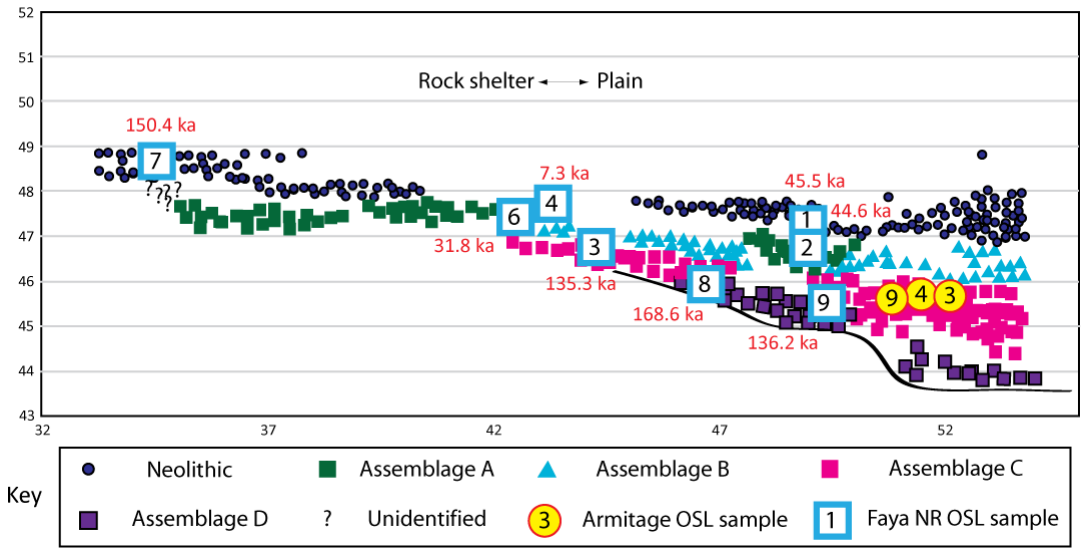

Figure 11.23. The schematic diagram from Figure 11.2, adapted to show the primary context of artefacts found during the excavation of the Jebel Faya site and associated OSL ages. The section runs from west to east, and shows the location of OSL samples taken as part of this thesis and their associated ages (marked in red), OSL samples taken by Armitage et al. (2011), and the location of the main lithic industries. Adapted from information provided by Knut Bretzke in 2014.

Many authors believe that modern humans successfully dispersed out of Africa c. 75 – 80 ka (Rosenberg et al. 2011) following evidence provided by genetic analysis (Forster, 2004; Macaulay et al. 2005). However, recent re-examination and re-dating of Arterian lithic industries in North Africa suggests that modern humans may have been present along the Libyan and Moroccan coastlines c. 125 ka (Barton et al., 2009), and potentially as early as 160 ka (Spinapolice & Garcea., 2013). The presence of lithic industries (attributed to modern humans) recovered in the basal units at FAY-NE1 during MIS 6/5e supports the notion that modern humans were able to disperse out of sub-Saharan Africa much earlier than previously thought. As such, the chronology of the FAY-NE1 site is of critical importance for our understanding of the climatic controls upon human migration, and the routes taken.

What is also apparent from the Jebel Faya site is that there is a strong relationship between regional climate and human occupation dynamics during the Pleistocene, with human presence at the site restricted to favourable humid conditions. However, the lack of human fossil remains at the site does limit the findings of the research. The results from this study, and that completed by Armitage et al. (2011), hinge on the attribution of the Palaeolithic industries to the correct hominin species.

Whilst the timing of modern human presence at Jebel Faya coincides with the Levantine Middle Palaeolithic, the lithics in Assemblage C are not typologically similar to those identified in the Levant and therefore a technological correlation cannot be drawn between the two. Furthermore, the presence of the Assemblage D lithics, which are not currently assigned to a specific hominin population, raises further questions about the timing and species present in Arabia 136.2 ± 17.1 ka. If Assemblage D was produced by modern humans, this would suggest the presence of AMH in Arabia even earlier than previously thought. If, however, Assemblage D is assigned to an archaic hominin population, this could raise questions about the certainty with which modern humans are assigned to Assemblage C. Until modern human fossil remains are found in association with similar industries (or at Jebel Faya) a modern human presence cannot be unequivocally proven, although the lithic evidence from Assemblage C here is convincing.

The emergence of modern humans out of sub-Saharan Africa remains widely debated. Fossil evidence from the Mugharet es-Skhul and Jebel Qafzeh caves in Israel suggests that modern humans first migrated out of Africa between 119 – 85 ka (Carto et al., 2009; Seddon, 2014). Recent re-dating of the Arterian lithic industry in Dar es-Soltan in Morocco further supports this notion, placing modern humans in North Africa c. 125 ka (Barton et al., 2009). Furthermore, evidence from this thesis suggests that modern humans were present in the Cyrenaican landscape at least c. 91 ka. While modern humans are traditionally believed to have taken the “northern route” out of Africa through the Levant, into the Middle East, and on into Eurasia, it is possible that modern humans took a “southern route” through Arabia. Lithic evidence suggesting the presence of modern humans at Jebel Faya c. 125 ka (Armitage et al., 2011), and potentially as early as c. 136 ka (as presented in this thesis) provides strong evidence for an early expansion of modern human populations out of Africa during late MIS 6, along this “southern route”.

Chapter 12 – Conclusions

This thesis presents a chronology for human occupation and abrupt climatic and environmental change in Libya (North Africa) and southern Arabia during the Mid to Late Pleistocene. Our current understanding of regional climatic change in North Africa and Arabia is fragmentary, and the timing and distribution of modern humans in these areas remains widely debated. Using applications of optically stimulated luminescence dating, this thesis has provided an improved regional understanding of palaeoclimate and human occupation histories in Libya and southeast Arabia, enhancing our knowledge about how and when modern humans dispersed out of sub-Saharan Africa.

Experimental work, outlined in two of the chapters in this thesis, also discussed the appropriateness of standard methods and rejection criterion used for age determination for the Arabian and Libyan datasets. This thesis has sought to address these research topics, and uses the most appropriate OSL dating methods as the basis for developing a chronology for human occupation and environmental change in the two regions.

12.1 Luminescence conclusions

The first component of this thesis centred on the development of the most appropriate method for age determination of fine grain sedimentary quartz using OSL dating. A paucity of coarse grain quartz material in some of the complex Libyan samples meant it was not possible to produce true single-grain data (i.e. one grain per recess) using standard methods (Section 2.5.1). Experimental work was therefore undertaken to test the appropriateness of using very small aliquots containing c. 14 to 20 grains as an alternative to true single-grain dating. Chapter 8 suggests that the inclusion of "rogue grains" in multi grain measurements adversely affects the measurement of D_e, resulting in the measurement of higher equivalent dose values than obtained using true single-grain measurements. For these reasons, where possible, true single-grain measurements are preferred for samples which exhibit complex dose distributions.

It has been suggested that when a dose response curve is produced for the fast component (fitted using a single saturating exponential function), it is possible to determine accurate D_e values up to a dose value of around $2D_0$ (Wintle and Murray, 2006 and Bailey, 2000). Pawley et al. (2010) however, argued that that the application of the $2D_0$ rejection criterion

limited dose measurements. Chapter 9 presents the results from experimental work carried out as part of this thesis, investigating the applicability and affect of the $2D_0$ rejection criterion on the Libyan and Arabian datasets. The evidence suggests that in most cases, the application of the $2D_0$ rejection criterion limits the upper age of each sample by truncating the D_e distribution at higher doses. This was particularly evident when radial plots were used to compare the dataset dose values that were accepted prior to, and post, the application of the $2D_0$ rejection criterion.

Similar results were observed when a single saturating exponential fit was used to fit the datasets, rather than an exponential plus linear function (which best appeared to fit the data). In this instance, the removal of the upper, linear part of the function, limited the maximum level of the growth curve, causing some previously accepted grains/aliquots to fail the "no L_n/T_n intersection" rejection criterion. Whilst the luminescence community remains divided on the use of the linear part of the growth curve, with some authors suggesting that its use may result in underestimations / overestimations of the age, evidence presented here suggests that it is appropriate for the samples in this thesis.

In conclusion, this thesis suggests that the application of the $2D_0$ rejection criterion, and the removal of the additional linear function from the growth curve, has a significant effect on the majority of samples analysed (particularly single grain measurements with higher equivalent doses). Accordingly, all of the Libyan and Arabian datasets in this thesis were fitted with an exponential plus linear function, and the $2D_0$ rejection criterion was not applied.

12.2 Palaeoenvironmental and Archaeological conclusions

In Chapter 1 (Section 1.2.2), a series of research questions were outlined, which I have attempted to answer in this thesis.

12.2.1 When were modern humans present in the landscape surrounding the Haua Fteah cave, Libya, and the Jebel Faya rock shelter, Arabia?

An absence of modern human fossils in all bar one of the sites investigated in this thesis meant that the presence of Middle Palaeolithic lithics with affinities to industries found at sites which do contain AMH remains were taken to represent the presence of modern

human populations. Whilst the limitations associated with this assumption are widely acknowledged, in the case of this thesis, as well as many other studies, the presence of lithics represents the only evidence available for investigation.

The OSL based chronology in this thesis suggests that modern humans were present in the Libyan landscape during the MIS 5c, MIS 5a, MIS 3 and Holocene periods. Although none of the lithic evidence identified at the Libyan sites was dated to the glacial stages MIS 4 and MIS 6, the presence of ephemeral fresh water resources in the environment may have facilitated the survival of human populations in the area during these times.

Chronological evidence for occupation at the Jebel Faya rock shelter also suggests that modern humans were present in the Arabian landscape during late MIS 6, MIS 5, MIS 3 and the Holocene. Armitage et al. (2011) suggest that the autochthonous development of the lithic industries at the site is indicative of continual human occupation in the region through Assemblage C to A, although they would not always have been at the site itself. Technological affinities observed between the "oldest" lithic assemblages discovered (Assemblage C) at Jebel Faya, and modern human East African assemblages, is used to support the attribution to modern human populations. Further investigations into the characteristics of the new Assemblage D lithics are required before this industry can confidently be assigned to a modern or archaic hominin origin.

In conclusion, modern humans appear to have dispersed into the Libyan and Arabian landscapes during MIS 5 (and potentially late MIS 6), where their presence at the site was observed in each of the following humid periods.

12.2.2 How has regional climate change affected the timing of human activity in these regions?

The lithic bearing units at site FAY-NE1, and the sites in the landscape surrounding the Haua Fteah cave (except Al Marj which did not represent the primary depositional environment of the lithics), were all deposited under humid climate periods. Furthermore, the sterile units were deposited during periods of aridity. Humid climatic periods are represented by the presence of lacustrine, palaeosol, slope wash and raised beach deposits, which all required interglacial conditions for formation.

12.2.3 How closely do North African and Arabian Quaternary environmental changes reflect northern hemisphere glacial and interglacial cycles?

Overall, the OSL chronology produced for Jebel Faya, suggests termination of human occupation at the site (as indicated by the presence of sterile sand units) during MIS 3, MIS 5d, and MIS 6. Unlike the evidence obtained from Libya (Chapter 10), it is not possible to determine what forces were responsible for driving regional climate change in Arabia, due to the limited number of samples available. However, evidence for aridity and human absence at the site during MIS 5d and MIS 6 coincides with evidence of the northern hemisphere stadial and glacial periods. Speleothem (Bar-Matthews et al., 2003) and lake level evidence (Bar-Yosef and Meadow, 1995) indicate precipitation levels in the Levant and North African regions were reduced at this time. Furthermore, the evidence for aridity at Jebel Faya during the MIS 3 interglacial, a time generally associated with increased precipitation in the Levant and North Africa (Bar-Matthews et al., 2003; Vaks et al., 2007,2010), correlates with the occurrence of a Heinrich event, thus supporting a northern hemisphere influence on the southern Arabian climate.

Conversely, evidence of fresh water availability in the landscape surrounding the Haua Fteah cave during periods of Northern Hemisphere glaciation, suggests that the regional climate in northern Libya was not driven solely by Northern Hemisphere glacial / interglacial cycles. Instead, following Blome et al. (2012) and Drake et al. (2013), the presence of water lain, lacustrine sediment units (characteristic of humid conditions) during MIS 6, MIS 4 and MIS 2, suggests that regional variations in Libyan climate were more likely to have been influenced by changes in the mid-latitude westerlies. Essentially, as global temperatures fall, the mid-latitude Westerlies are weakened, causing them to move south towards the equator, bringing moisture to the North African coastline (Blome et al., 2012; López-Moreno et al., 2011). As precipitation associated with the ITCZ and monsoon systems is unlikely to have ever reached as far as the North African coastline, and precipitation was thought to reduce during glacial periods (Bar-Matthews et al., 2003; Bar-Yosef and Meadow, 1995; Vaks et al., 2010), the Westerlies represent the most likely source of precipitation in the region during cooler, more arid periods.

It is concluded that northern hemisphere glacial/interglacial cycles do not represent the sole driving force behind regional climate changes in North Africa (and possibly Arabia). Instead, it is a complex combination of northern hemisphere forcing, and the position of

the westerlies, that appears to drive climatic change in along the North African coastline during the Pleistocene.

12.2.4 Do the data presented in this thesis support a "pre" or "post Toba" dispersal model out of sub-Saharan Africa?

Genetic evidence has recently been used by Mellars et al. (2013) to support the traditional view that modern humans did not disperse out of Africa until after the Toba super eruption 74 ka (i.e. "post Toba"). The chronological evidence provided in this thesis, however, suggests that modern humans were present in the landscape surrounding both the Haua Fteah cave and the Jebel Faya rock shelter during MIS 5. Fossil remains found in the Mugharet es-Skhul and Jebel Qafzeh caves in Israel (Seddon, 2014) place modern humans in the Levant c. 119 – 85 ka (Carto et al., 2009), fully supporting the "pre-Toba" dispersal model. Furthermore, re-dating of the Arterian lithic industry by Barton et al. (2009) again suggests the arrival of modern humans in North Africa c. 125 ka, "pre" the Toba eruption.

Whilst the majority of evidence for modern humans in this thesis is based on the presence of lithics with affinities to industries found at sites which do contain AMH remains, the presence of modern human mandibles in the Haua Fteah cave during MIS 5a, unequivocally supports the "pre Toba" dispersal theory. Furthermore, the enhanced chronology produced for Jebel Faya in this thesis is in excellent agreement with Armitage et al. (2011), suggesting that modern humans were able to disperse out of Africa much earlier than previously thought, during the MIS 6 / MIS 5 transitional boundary. At either site, the presence of modern humans significantly before the Toba eruption indicates that they were geographically well-placed to begin a wider dispersal.

12.2.5 Did modern humans migrate out of sub-Saharan Africa along a northern or southern route?

Of all the research questions posed, this represents the most difficult to address, as evidence presented here suggests that modern humans were present in Libya and Arabia during similar time periods.

Human presence in both regions has been tied to the MIS 5 interglacial, suggesting that modern humans were successfully able to utilise both northern and southern routes during humid climatic conditions. The Haua Fteah cave provides the only human fossil evidence from all of the sites dated in this thesis. Consequently, the "northern route" represents the only route containing absolute evidence for modern human presence at this time (MIS 5a). This evidence is further supported by the fossil remains from the Mugharet es-Skhul and Jebel Qafzeh caves in Israel, which date to 119 – 85 ka (Carto et al., 2009), and the Arterian lithic evidence from Morocco dated to c. 125 ka (Barton et al., 2009). Chronological evidence produced for Jebel Faya lithics, however, places the timing of modern human presence in Arabia during the earlier stage of MIS 5e. Furthermore, the presence of a new lithic industry (Assemblage D), which may be associated with modern humans, at the base of the Jebel Faya excavation, may provide evidence for an even earlier arrival during late MIS 6. Assuming the Assemblage C (and potentially D) lithics do in fact represent modern humans at each location, it is concluded that the "southern route" into Arabia represents the earliest dispersal route taken by our modern human ancestors out of Africa.

12.3 Further research

Although the overarching aim of this thesis, to develop a robust chronology for human occupation and environmental change in Libya and Arabia using OSL dating, has been achieved, further research into the following topics is recommended:

1) Additional research into the effect of the $2D_0$ rejection criterion on a larger range of samples from different geographical locations, depositional environments, and ages, would provide a more general assessment of the method.
2) Further research needs to be completed into our understanding of the linear part of the growth curve. Currently this part of the curve is commonly removed as it is not well understood, despite representing the best fit for the dataset in many instances.
3) Work published by Russell and Armitage (2012) should be extended to assess the applicability of small multi grain aliquot to samples reflecting a wider range of deposit ages and sedimentary environments.

4) Where OSL dating was unsuccessful, or complex dose distributions complicated the dating process, new samples should be taken and dated to enhance the confidence in the age models produced at these sites.
5) New excavations at FAY-NE1 and other sites in the Jebel Faya area are currently being undertaken. OSL dating of the lithic bearing units identified during these excavations will further increase our understanding of the settlement history at Jebel Faya. Furthermore, increasing archaeological investigations at the site and in the region will aid our understanding of the importance of the region for early modern human dispersals out of sub-Saharan Africa.

References

- Abbate, E., Sagri, M., 2011. Early to Middle Pleistocene Homo dispersals from Africa to Eurasia: geological, climatic and environmental constraints. Quaternary International 267, 3-19.
- Adamiec, G., 2005. OSL decay curves – relationship between single- and multiple-grain aliquots. Radiation Measurements 39, 63-75.
- Adamiec, G., Aitken, M., 1998. Dose-rate conversion factors: Update. Ancient TL 16, 37-50.
- Aitken, M.J., 1985. Thermoluminescence dating. Academic Press, London.
- Aitken, M.J., 1998. An Introduction to Optical Dating. The Dating of Quaternary Sediments by the Use of Photon-stimulated Luminescence. Oxford University Press, Oxford.
- Andrews, J.E., 2000. Palaeoclimatic records from stable isotopes in riverine tufas: Synthesis and review. ISOtopes in PALaeoenvironmental reconstruction (ISOPAL) 75, 85-104.
- Armitage, S.J., Duller, G.A.T., Wintle, A.G., 2000. Quartz from southern Africa: sensitivity changes as a result of thermal pre-treatment. Radiation Measurements 32, 571-577.
- Armitage, S.J., Bailey, R.M., 2005. The measured dependence of laboratory beta dose rates on sample grain size. Radiation Measurements 39, 123-127.
- Armitage, S.J., Drake, N.A., Stokes, S., El-Hawat, A., Salem, M.J., White, K., Turner, P., McLaren, S.J., 2007. Multiple phases of North African humidity recorded in lacustrine sediments from the Fazzan Basin, Libyan Sahara. Quaternary Geochronology 2, 181-186.
- Armitage, S.J., Jasim, S.A., Marks, A.E., Parker, A.G., Usik, V.I., Uerpmann, H.P., 2011. Southern Route “Out of Africa”: Evidence for an Early Expansion of Modern Humans into Arabia. Science 331, 453-456.
- Armitage, S.J., King, G.E., 2013. Optically stimulated luminescence dating of hearths from the Fazzan Basin, Libya: A tool for determining the timing and pattern of Holocene occupation of the Sahara. Quaternary Geochronology 15, 88-97.
- Arnold, L.J., Roberts, R.G., 2009. Stochastic modelling of multi-grain equivalent dose (D_e) distributions: Implications for OSL dating of sediment mixtures. Quaternary Geochronology 4, 204-230.

- Arnold, L.J., Demuro, M., Navazo Ruiz, M., 2012. Empirical insights into multi-grain averaging effects from 'pseudo' single-grain OSL measurements. Radiation Measurements 47, 652-658.
- Athanassas, C., 2011. Constraints on the precision of SAR in equivalent dose estimations close to saturation in quartz. Geochronometria 38, 413-423.
- Bailey, R.M., 2000. Circumventing possible inaccuracies of the single aliquot regeneration method for the optical dating of quartz. Radiation Measurements 32, 833-840.
- Bailey, R.M., 2001. Towards a general kinetic model for optically and thermally stimulated luminescence of quartz. Radiation Measurements 33, 17-45.
- Bailey, R.M., 2004. Paper I – simulation of dose absorption in quartz over geological timescales and its implications for the precision and accuracy of optical dating. Radiation Measurements 38, 299-310.
- Bailey, R.M., Smith, B.W., Rhodes, E.J., 1997. Partial bleaching and the decay form characteristics of quartz OSL. Radiation Measurements 27, 123-136.
- Bailey, R.M., Armitage, S.J., Stokes, S., 2005. An investigation of pulse-irradiation regeneration of quartz OSL and its implications for the precision and accuracy of optical dating (Paper II). Radiation Measurements 39, 347-359.
- Bailey, G., Carrion, J.S., Fa, D.A., Finlayson, C., Finlayson, G., Rodriguez-Vidal, J., 2008. The coastal shelf of the Mediterranean and beyond: Corridor and refugium for human populations in the Pleistocene. Quaternary Science Reviews 27, 2095-2099.
- Bailey, R.M, 2010. Direct measurement of the fast component of quartz optically stimulated luminescence and implications for accuracy of optical dating. Quaternary Geochronology 5, 559-568.
- Ballarini, M., Wallinga, J., Wintle, A.G., Bos, A.J.J., 2007. A modified SAR protocol for optical dating of individual grains from young quartz samples. Radiation Measurements 42, 360-369.
- Bar-Matthews, M., Ayalon, A., Kaufman, A., 1997. Late Quaternary palaeoclimate in the eastern Mediterranean region from stable isotope analysis of speleothems at Soreq Cave, Israel. Quaternary Research 47, 155-168.

- Bar-Matthews, M., Ayalon, A., Gilmour, M., Matthews, A., Hawkesworth, C.J., 2003. Sea-land oxygen isotopic relationships from planktonic foraminifera and speleothems in the Eastern Mediterranean region and their implication for paleorainfall during interglacial intervals. Geochimica et Cosmochimica Acta 67, 3181-3199.
- Bar-Yosef, O., Meadow, R.H., 1995. The origins of agriculture in the Near East. In: Price, T.D., Gebauer, A.B. (Eds.), Last hunters - first farmers: new perspectives on the prehistoric transition to agriculture. Sante Fe: School of American Research Press, 39-94
- Bar-Yosef, O., Cohen, A.B., 2001. From Africa to Eurasia – early dispersals. Quaternary International 75, 19-28.
- Barker, G. A., Hunt, C., Reynolds, T., Brooks, I., el-Rishi, H., 2007. The Haua Fteah, Cyrenaica (Northeast Libya): renewed investigations of the cave and its landscape, 2007. Libyan Studies 38, 93–114.
- Barker, G., Basell, L., Brooks, I., Burn, L., Cartwright, C., Cole, F., Davison, J., Farr, L., Grun, R., Hamilton, R., Hunt, C., Inglis, R., Jacobs, Z., Leitch, V., Morales, J., Morley, I., Morley, M., Pawley, S., Pryor, A., Reynolds, T., el-Rishi, H., Roberts, R., Simpson, D., Stimpson, C., Touati, M., van der Veen, M., 2008. The Cyrenaican Prehistory Project 2008: the second season of investigations of the Haua Fteah cave and its landscape, and further results from the initial (2007) fieldwork. Libyan Studies 39, 1-47.
- Barker, G., Antoniadou, A., Candy, I., Drake, N., Farr, L., Hunt, C., Ibrahim, A., Inglis, R., Jones, S., Morales, J., Morley, I., Mutri, G., Rabett, R., Reynolds, T., Simpson, D., Twati, M., White, K., 2009. The Cyrenaican Prehistory Project 2009: the third season of investigations of the Haua Fteah cave and its landscape, and further results from the 2007-2008 fieldwork. Libyan Studies 40, 1-42.
- Barker, G., Antoniadou, A., Armitage, S., Brooks, I., Candy, I., Connell, K., Douka, K., Drake, N., Farr, L., Hill, E., Hunt, C., Inglis, R., Jones, S., Lane, C., Lucarini, G., Meneeley, J., Morales, J., Mutri, G., Prendergast, A., Rabett, R., Reade, H., Reynolds, T., Russell, N., Simpson, D., Smith, B., Stimpson, C., Twati, M., White, K., 2010. The Cyrenaican Prehistory Project 2010: the fourth season of investigations of the Haua Fteah cave and its landscape, and further results from the 2007–2009 fieldwork. Libyan Studies 41, 63–88.

- Bartov, Y., Goldstein, S.L., Stein, M., Enzel, Y., 2002. Catastrophic arid episodes in the Eastern Mediterranean linked with the North Atlantic Heinrich events. Geology 31, 439-442.
- Basell, L.S., 2008. Middle Stone Age (MSA) site distributions in eastern Africa and their relationship to Quaternary environmental change, refugia and the evolution of *Homo sapiens*. Quaternary Science Reviews 27, 2484-2498.
- Berger, W.H., Labeyrie, L.D., 1987. Abrupt climatic change – Evidence and Implications. D Reidel Publishing Company, Holland.
- Berger, A., Loutre, M.F., 2007. Astronomical theory of palaeoclimates. Comptes Rendus Geoscience 336, 701-709.
- Beyin, A., 2006. The Bab al Mandab vs the Nile-Levant: an appraisal of the two dispersal routes for early modern humans out of Africa. African Archaeological Review 23, 5-30.
- Beyin, A., 2011. Upper Pleistocene Human Dispersals out of Africa: A Review of the Current State of the Debate. International Journal of Evolutionary Biology 2011, 1-17.
- Blome, M.W., Cohen, A.S., Tryon, C.A., Brooks, A.S., Russell, J., 2012. The environmental context for the origins of modern human diversity: A synthesis of regional variability in African climate 150,000-30,000 years ago. Journal of Human Evolution 62, 563-592.
- Boero, V., Premoli, A., Melis, P., Barberis, E., Arduino, E., 1992. Influence of climate on the iron oxide mineralogy of Terra Rossa. Clays and clay Minerals 40, 8-13.
- Bond, G., Heinrich, H., Broecker, W., Labeyrie, L., McManus, J., Andrews, J., Huon, S., Jantschik, R., Clasen, S., Simet, C., Tedesco, K., Klas, M., Bonani, G. and Ivy, S., 1992. Evidence for massive discharges of icebergs into the North Atlantic ocean during the last glacial period. Nature 360, 245-249.
- Bond, G., Broecker, W., Johnsen, S., McManus, J., Labeyrie, L., Jouzel, J., Bonani, G., 1993. Correlations between climate records from North Atlantic sediments and Greenland ice. Nature 365, 143-147.
- Bötter-Jensen, L., Andersen, C.E., Duller, G.A.T., Murray, A.S., 2003. Developments in radiation, stimulation and observation facilities in luminescence measurements. Radiation Measurements 37, 535-541.

- Bretzke, K., Armitage, S.J., Parker, A.G., Walkington, H., Uerpmann, H.P., 2013. The environmental context of Paleolithic settlement at Jebel Faya, Emirate Sharjah, UAE. Quaternary International 300, 83-93.
- Broecker, W.S., Hemming, S., 2001. Climate swings come into focus. Paleoclimate 294, 2308-2309.
- Brooke, B., 2001. The distribution of carbonate eolianite. Earth Science Reviews 55, 135-164.
- Bulur, E., 1996. An alternative technique for optically stimulated luminescence (OSL) experiment. Radiation Measurements 26, 701-709.
- Burns, S.J., Matter, A., Frank, N., Mangini, A., 1998. Speleothem-based palaeoclimate record from northern Oman. Geology, 26, 499-502.
- Burns, S.J., Fleitmann, D., Matter, A., Neff, U., Mangini, A. 2001. Speleothem evidence from Oman for continental pluvial events during interglacial periods. Geology, 29, 623-626.
- Buylaert, J.P., Jain, M., Murray, A.S., Thomsen, K.J., Thiel, C., Sohbati, R., 2012. A robust feldspar luminescence dating method for Middle and Late Pleistocene sediments. Boreas 41, 435-451.
- Cabrera, V.M., Abu-Amero, K.K., Larruga, J.M., Gonzalez, A.M., 2009. The Arabian peninsula: Gate for human migrations out of Africa or cul-de-sac? A mitochondrial DNA phylogeographic perspective. In: Petraglia MD, Rose JI. (Eds.), The evolution of human populations in Arabia. Dordrecht: Springer, 79–87.
- Cacho, I., Grimalt, J.O., Pelejero, C., Canals, M., Sierro, F.J., Flores, J.A. and Shackleton, N.J., 1999, Dansgaard-Oeschger and Heinrich event imprints in Alboran Sea palaeotemperatures. Palaeoceanography 14, pp.698-705.
- Carto, L.S., Weaver, A.J., Hetherington, R., Lam, Y., Wiebe, E.C., 2009. Out of Africa and into an ice age: on the role of global climate change in the late Pleistocene migration of early modern humans out of Africa. Journal of Human Evolution 56, 139-151.
- Choi, J.H., Duller, G.A.T. Wintle, A.G., Cheong, C.S., 2006. Luminescence characteristics of quartz from the Southern Kenyan Rift Valley: Dose estimation using LM-OSL SAR. Radiation Measurements 41, 847- 854.
- Choi, J.H., Duller, G.A.T., Wintle, A.G., 2006b. Analysis of quartz LM-OSL curves. Ancient TL 24, 9-20.

- Close, A.E., Minichillo, T., 2007. Global Expansion 300,000-8000 years ago, Africa. In: Elias, S.A. Encyclopedia of Quaternary Science, 99-107.
- Cooke, R.U., Warren, A., Goudie, A., 1993. Desert Geomorphology. University College London Press, London.
- Dansgaard, W., Johnsen, S.J., Clausen, H.B., Dahl-Jensen, D., Gundestrup, N.S., Hammer, C.U., Hvidberg, C.S., Steffensen, J.P., Svelnbjörnsdottir, A.E., Jouzel, J. and Bond, G., 1993. Evidence for general instability of past climate from a 250-kyr ice-core record. Nature 364, pp.218-220
- Delanges, A., Crassard, R., Bertran, P., Sitzia, L., 2013. Cultural and human dynamics in southern Arabia at the end of the Middle Palaeolithic. Quaternary International 300, 234-243.
- DeMenocal, P., Ortiz, J., Guilderson, T., Adkins, J., Sarnthein, M., Baker, L., Yarusinsky, M., 2000. Abrupt onset and termination of the African Humid Period: rapid climate responses to gradual insolation forcing. Quaternary Science Reviews 19, 347-361.
- Domínguez-Villar, D., Vázquez-Navarro, J.A., Cheng, H. and Edwards, R.L., 2011, Freshwater tufa record from Spain supports evidence for the past interglacial being wetter than the Holocene in the Mediterranean region, Global and Planetary Change 77, 129–141
- Douka, K., Jacobs, Z., Lane, C., Grun, R., Farr, L., Hunt, C., Inglis, R.H., Reynolds, T., Albert, P., Aubert, M., Cullen, V., Hill, E., Kinsley, L., Roberts, R.G., Tomlinson, E.L., Wulf, S., Barker, G., *in prep*. The chronostratigraphy of the Haua Fteah cave (Cyrenaica, northeast Libya). Journal of Human Evolution.
- Drake, N., Bristow, C., 2006. Shorelines in the Sahara: geomorphological evidence for an enhanced monsoon from palaeolake Megachad. The Holocene 16, 901-911.
- Drake, N.A., El-Hawat, A.S., Turner, P., Armitage, S.J., Salem, M.J., White, K.H., McLaren, S., 2008. Palaeohydrology of the Fazzan Basin and surrounding regions: the last 7 million years. Palaeogeography, Palaeoclimatology, Palaeoecology 263, 131-145.
- Drake, N.A., Blench, R.M., Armitage, S.J., Bristow, C.S., White, K.H., 2011. Ancient watercourses and biogeography of the Sahara explain the peopling of the desert. Proceedings of the National Academy of Sciences 108, 458-462

- Drake, N.A., Breeze, P., Parker, A., 2012. Palaeoclimate in the Saharan and Arabian Deserts during the Middle Palaeolithic and the potential for hominin dispersals. Quaternary International 300, 48-61.
- Duller, G.A.T., 2000. Optical dating of single sand-sized grains of quartz: sources of variability. Radiation Measurements 32, 453-457.
- Duller, G.A.T., 2003. Distinguishing quartz and feldspar in single grain luminescence measurements. Radiation Measurements 37, 161-165.
- Duller, G.A.T., 2004. Luminescence dating of Quaternary sediments: recent advances. Journal of Quaternary Science 19, 183-192.
- Duller, G.A.T., 2007. Assessing the error on equivalent dose estimate derived from single aliquot regenerative dose measurements. Ancient TL 22, 15-24.
- Duller, G.A.T., 2008(a). Luminescence dating guidelines on using luminescence dating in archaeology. English Heritage.
- Duller, G.A.T., 2008 (b). Single-grain optical dating of Quaternary sediments: why aliquot size matters in luminescence dating. Boreas 37, 589-612.
- Duller, G.A.T., 2012. Improving the accuracy and precision of equivalent doses determined using the optically stimulated luminescence signal from single grains of quartz. Radiation Measurements. 47, 770-777.
- Duller, G.A.T., Botter-Jensen, L., Murray, A.S., Truscott, A.J., 1999. Single grain laser luminescence (SGLL) measurements using a novel automated reader. Nuclear Instruments and Methods in Physics research B 155, 506-514.
- Duller, G.A.T., Bøtter-Jensen, L., Murray, A.S., 2000. Optical dating of single sand-sized grains of quartz: sources of variability. Radiation Measurements 32, 453-457.
- Durcan, J.A., 2013. Luminescence dating of sediments in Punjab, Pakistan: implications for the collapse of the Harappan Civilisation. Unpublished PhD thesis. Aberystwyth University.
- Durcan, J.A., Duller, G.A.T., 2011. The fast ratio: A rapid measure for testing the dominance of the fast component in the initial OSL signal from quartz. Radiation Measurements 46, 1065-1072.
- Dutton, A., Bard, E., Antonioli, F., Esat, T.M., Lambeck, K., McCulloch, M.T., 2009 Phasing and amplitude of sea-level and climate change during the penultimate interglacial. Nature Geoscience 2, 355-359.

- Emiliani, C., McBurney, C.B.M., 1967. Palaeotemperature analysis by the oxygen isotope method at the Haua Fteah. In: McBurney, C.B.M. (Eds.), The Haua Fteah (Cyrenaica) and the Stone Age of the South-East Mediterranean. Cambridge University Press, 54–59.
- Eriksson, A., Betti, L., Friend, A.D., Lycett, S.J., Singarayer, J.S., von Cramon-Taubadel, N., Valdes, P.J., Balloux, F., Manica, A., 2012. Later Pleistocene climate change and the global expansion of anatomically modern humans. PNAS 109, 16089-16094.
- Field, J.S., Lahr, M.M., 2005. Assessment of the Southern Dispersal: GIS-based analyses of potential routes at oxygen isotopic stage 4. Journal of World Prehistory 19, 1-45.
- Finlayson, C., Pacheco, G.P., Rodriguez-Vidal, J., Fa, D.A., Lopez, J.M.G., Perez, A.D., Finlayson, G., Allue, E., Preysler, J.B., Caceres, I., Carrion, J.S., Jalvo, Y.F., Gleed-Owen, C.P., Espejo, F.J.J., Lopez, P., Saez, J.A.L., Cantal, J.A.R., Marco, A.S., Guzman, F.G., Brown, K., Fuentes, N., Valarino, C.A., Vilalpando, A., Stringer, C.B., Ruiz, F.M., Sakamoto, T., 2006. Late survival of Neanderthals at the southernmost extreme of Europe. Nature 443, 850-853.
- Fleagle, J.G., Assefa, Z., Brown, F.H., Shea, J.J., 2008. Paleoanthropology of the Kibish Formation, southern Ethopia: Introduction. Journal of Human Evolution 55, 360-365.
- Fleitmann, D., Matter, A., 2009. The speleothem record of climate variability in Southern Arabia. Comptes Rendus Geoscience 341, 633-342.
- Fleitmann, D., Burns, S.J., Pekala, M., Mangini, A., Al-Subbary, A., Al-Aowah, M., Kramers, J., Matter, A. 2011. Holocene and Pleistocene pluvial periods in Yemen, southern Arabia. Quaternary Science Reviews, 30, 783-787.
- Foley, M.M., Lahr, R.A., 1998. Towards a theory of modern human origins: geography, demography, and diversity in recent human evolution. Yearbook of Physical Anthropology 41, 137-176.
- Forster, P., 2004. Ice Ages and the Mitochondrial DNA Chronology of Human Dispersals: A Review. Philosophical Transactions: Biological Sciences 359, 255–64.
- Galbraith, R.F., Roberts, R.G., Laslett, G.M., Yoshida, H., Olley, J.M., 1999. Optical dating of single and multiple grains of quartz from Jinmium rock shelter, Northern Australia: Part I, BuylExperimental design and statistical models. Archeometry 41, 339-364.

- Galbraith, R.F., Roberts, R.G., Yoshida, H., 2005. Error variation in OSL palaeodose estimates from single aliquots of quartz: a factorial experiment. Radiation Measurements 39, 289-307.
- Galbraith, R.F., Roberts, R.G., 2012. Statistical aspects of equivalent dose and error calculation and display in OSL dating: An overview and some recommendations. Quaternary Geochronology 11, 1-27.
- Garcea, E.A.A., 2008. Africa, North| Sahara, Eastern. Encyclopedia of Arcaheology. Academic Press, 56-61.
- Glover, C., Robertson, A.F., 2003/ Origin of tufa (cool-water carbonate) and related terraces in the Antalya area, SW Turkey. Geological Journal 38, 329-358.
- Goudie, A.S., Viles, H.A. and Pentecost, A., 1993, The late-Holocene tufa decline in Europe, The Holocene 3, 181-186
- Groucutt, H.S., Blinkhorn, J., 2013. The Middle Palaeolithic in the desert and its implications for understanding hominin adaptation and dispersal. Quaternary International 300, 1-12.
- Groucutt, H.S., Petraglia, M.D., 2012. The prehistory of the Arabian peninsula: Deserts, dispersals, and demography. Evolutional Anthropology 21, 113-125.
- Guérin, G., Murray, A.S., Mayank, J., Thomsen, K.J., Mercier, N., 2013. How confident are we in the chronology of the transition between Howieson's Poort and Still Bay? Journal of Human Evolution 64, 314-317.
- Hays, J.D., Imbrie, J., Shackleton, N.J., 1976. Variations in the earth's orbit: Pacemaker of the ice ages. Science 194, 1121-1132.
- Higham, T., Compton, T., Stringer, C., Jacobi, R., Shapiro, B.,Trinkaus, E., Chandler, B., Groning, F., Collins, C., Hillson, S., O'Higgins, P., FitzGerald, C., Fagan, M., 2011. The earliest evidence for anatomically modern humans in northwestern Europe. Nature 479, 521-524.
- Hooghiemstra, H., Stalling, H., Agwu, C.O.C., Dunport. L., 1992. Vegetational and climatic changes at the northern fringe of the Sahara 250,000-5000 years BP: evidence from 4 marine pollen records located between Portugal and the canary Islands. Review of Palaeobotony and Palynology 74, 1-52.
- Hong, D.G. 1998. Luminescence stimulated from quartz by green light: developments relevant to dating. Unpublished PhD Thesis. University of Edinburgh.

- Huntley, D.J., Lian, O.B., 2006. Some observations on tunnelling of trapped electrons in feldspars and their implications for optical dating. Quaternary Science Reviews 25, 2503-2512.
- Hütt, G., Jaek, I., Tchonka, J., 1988. Optical dating: K feldspars optical response stimulation spectra. Quaternary Science Reviews 7, 318-385.
- Inglis, R.H., 2013. Human occupation and changing environments during the middle to later stone ages: soil micromorphology at the Haua Fteah, Libya. Unpublished PhD thesis. Magdalene College, University of Cambridge.
- Issar, A.S., 2010. Climate change as a draw bridge between Africa and the Middle East. Global and Planetary Change 72, 451-454.
- Jacobs, Z., Duller., G.A.T., Wintle, A.G., 2003. Optical dating of dune sand from Blombos Cave, South Africa: II-single grain data. Journal or Human Evolution 44, 613-625.
- Jacobs, Z., Wintle, A.G., Duller, G.A.T., 2006. Evaluation of SAR procedures for D_e determination using single aliquots of quartz from two archaeological sites in South Africa. Radiation Measurements 41, 520-533.
- Jacobs, Z., Roberts, R.G., Galbraith, R.F., Deacon, H.J., Grun, R., Mackay, A., Mitchell, P., Vogelsand, R, Wadley, L., 2008(a). Ages for the Middle Stone Age of Southern Africa: Implications for Human Behaviour and Dispersal. Science 322, 733-735.
- Jain, M., Murray, A.S., Botter-Jensen, L., 2003. Characterisation of blue light stimulated luminescence components in different quartz samples: implications for dose measurements. Radiation Measurements 37, 441-449.
- Kim, J.C., Duller, G.A.T., Roberts, H.M., Wintle, A.G., Lee, Y.I., Yi, S.B., 2010. Re-evaluation of the chronology of the Palaeolithic site at Jeongokri, Korea, using OSL and TT-OSL signals from quartz. Quaternary Geochronology 5, 365-370.
- Labeyrie, L., Skinner, L., Cortijo, E., 2007. Sub-Milankovitch (D-O/Heinrich) Events, In: Elias, S.A., (Eds.), Encyclopedia of Quaternary Science. Elsevier, 1964-1974.
- Li, B., Li, S.H., 2006. Comparison of De estimates using the fast component and the medium component of quartz OSL. Radiation Measurements 41, 125-136.
- Li, B., Li, S.H., Wintle, A.G., 2006b. Observations of thermal transfer and the slow component of OSL signals from quartz. Radiation Measurements 41, 639-648.

- Lian, O.B. 2007. Optically-Stimulated Luminescence. In: Elias, S.A. The Encyclopedia of Quaternary Science, (Eds.), Elsevier, 1491-1505.
- Lisiecki, L.E., Raymo, M.E., 2005. A Pliocene-Pleistocene stack of 57 globally distributed benthic $\delta^{18}O$ records. Paleoceanography 20, 1-17.
- Lowe, J.J., Walker, M.J.C., 1997. Reconstructing Quaternary Environments. Pearson Prentice Hall, Harlow.
- Lowick, S.E., Preusser, F., Wintle, A.G., 2010. Investigating quartz optically stimulated luminescence dose-response curves at high doses. Radiation Measurements 45, 975-984.
- Macaulay, V., C. Hill, A. Achilli, C. Rengo, D. Clarke, W. Meehan, J. Blackburn, O. Semino, R. Scozzari, F. Cruciani, A. Taha, N. K. Shaari, J. M. Raja, P. Ismail, Z. Zainuddin, W. Goodwin, D. Bulbeck, H.-J. Bandelt, S. Oppenheimer, A. Torroni, and M. Richards., 2005. Single, Rapid Coastal Settlement of Asia Revealed by Analysis of Complete Mitochondrial Genomes. Science 308, 1034–36.
- Marean, C.W., Bar-Matthews, M., Bernatchez, J., Fisher, E., Goldberg, P., Herries, A.I.R., Jacobs, Z., Jerardino, A., Karkanas, P., Minichillo, T., Nilssen, P.J., Thompson, E., Watts, I., Williams, H.M., 2007. Early use of marine resources and pigment in South Africa during the Middle Pleistocene. Nature 449, 905-909.
- Marks, A., 1992a. Upper Pleistocene archaeology and the origins of modern man: a view from the Levant and adjacent areas. In: Akazawa, T., Aoki, K., Kimura, T. (Eds.), The evolution and Dispersal of Modern Human in Asia, Tokyo, Japan. Hokusen-Sha, 229-251.
- Marks, A. 1992b. Typological variability in the Levantine Middle Palaeolithic. In: Dibble, H.L., Mellars, P.A. (Eds.), The Middle Paleolithic: Adaptations, Behaviour and Variability. University of Pennsylvania Museum Press, 127-141.
- Maslin, M., Seidov, D., Lowe, J., 2001. Synthesis of the Nature of Rapid Climate Transitions During the Quaternary. Geophysical monograph series 126, 9-52.
- Mayya, Y. S., Morthekai, P., Murari, M.K., Singhvi, A.K., 2006. Towards quantifying beta microdosimetric effects in single-grain quartz dose distribution. Radiation Measurement 41, 1032-1039.
- McBurney, C.B.M., 1967. The Haua Fteah (Cyrenaica). And the Stone Age of the South-East Mediterranean. Cambridge University Press, UK.

- McBurney, C.B.M., Hey, R.W., 1955. Prehistory and Pleistocene geology in Cyrenaican Libya. Occasional Publications of the Cambridge University Museum of Archaeology and Ethniology 4.
- McDougall, I., Brown, F. H., Fleagle, J.G., 2005. Ethiopia is top choice for cradle of *Homo sapiens*. Nature 433, 733–736.
- Mejdahl, V., 1979. Thermoluminescence dating: Beta-dose attenuation in quartz grains. Archaeometry 21, 61-72.
- Mejdahl, V., 1987. Internal radioactivity in quartz and feldspar grains. Ancient TL 5, 10-17.
- Mellars, P., 2006. Why did modern human populations disperse from Africa ca. 60,000 years ago? A new model. PNAS 103, 9381-9386.
- Mellars, P., Gori, K.C., Carr, M., Soares, P.A., Richards, M.B., 2013. Genetic and archaeological perspectives on the initial modern human colonization of southern Asia. PNAS, Early edition.
- Murray, A.S., Roberts, R.G., 1998. Measurement of the equivalent dose in quartz using a regenerative-dose single-aliquot protocol. Radiation Measurements 29, 503-515.
- Murray, A.S., Wintle, A.G., 1998. Factors controlling the shape of the OSL decay curve in quartz. Radiation Measurements 29., 65-79.
- Murray, A.S., Wintle, A.G., 2000. Luminescence dating of quartz using an improved single-aliquot regenerative- dose protocol. Radiation Measurements 32, 57-73.
- Murray, A.S., Olley, J.M., 2002. Precision and accuracy in the optically stimulated luminescence dating of sedimentary quartz: A status review. Geochronometria 21, 1-16.
- Murray, A.S., Wintle, A.G., Wallinga, J., 2002. Dose estimation using quartz OSL in the non-linear region of the growth curve. Radiation Protection Dosimetry 101, 371-374.
- Murray, A.S., Funder, S., 2003. Optically stimulated luminescence dating of a Danish Eemian coastal marine deposit: A test of accuracy, Quaternary Science Reviews 22, 1177-1183.
- Murray, A.S., Wintle, A.G., 2003. The single aliquot regenerative dose protocol: potential for improvements in reliability. Radiation Measurements 37, 377-381.

- Murray, A., Buylaert, J.P., Henriksen, M., Svendsen, J.I., Mangerud, J., 2008. Testing the reliability of quartz OSL ages beyond the Eemian. Radiation Measurement 43, 776-780.
- Nathan, R.P., Thomas, P.J., Jain, M., Murray, A.S., Rhodes, E.J., 2003. Environmental dose rate heterogeneity of beta radiation and its implications for luminescence dating: Monte Carlo modelling and experimental validation. Radiation Measurements 37, 305-313.
- National Climatic Data Centre, 2008. *Heinrich and Dansgaard-Oeschger events*. Available at: http://www.ncdc.noaa.gov/paleo/abrupt/data3.html (Accessed June, 2013).
- Olley, J.M., Murray, A., Roberts, R.G., 1996. The effects of disequilibria in the uranium and thorium chains on burial dose rates in fluvial sediments. Quaternary Science Reviews 15, 751-760.
- Olley, J., Caitcheon, G., Murray, A., 1998. The distribution of apparent dose as determined by Optically Stimulated Luminescence in small aliquots of fluvial quartz: Implications for dating young sediments. Quaternary Science Reviews 17, 1033-1040.
- Olley, J.M., Pietsch, T., Roberts, R.G., 2004. Optical dating of Holocene sediments from a variety of geomorphic settings using single grains of quartz. Geomorphology 60, 337-358.
- Oppenheimer, S., 2009. The great arc of dispersal of modern humans: Africa to Australia. Quaternary International 202, 2-13.
- Osborne, A.H., Vance, D., Rohling, E.J., Barton, N., Rogerson, M., Fello, N., 2008. A humid corridor across the Sahara for the migration of early modern humans out of Africa 120,000 years ago. Proceedings of the National Academy of Sciences of the United States of America 105, 16444-16447.
- Parker, A.G., 2009. Pleistocene Climate Change in Arabia: Developing a Framework for Hominin Dispersal over the Last 350 ka. In: Petraglia, M.D., Rose, J.I., (Eds.), The Evolution of Human Populations in Arabia. Palaeoenvironments, Prehistory and Genetics. Springer, Netherlands, 39-49.
- Partridge, T.C., Demenocal, P.B., Lorentz, S.A., Paiker, M.J., Vogel, J.C., 1997. Orbital forcing of climate over South Africa: A 200,000-year rainfall record from the Pretoria saltpan. Quaternary Science Reviews 16, 1125-1133.

- Pawley, S.M., Bailey, R.M., Rose, J., Moorlock, B.S.P., Hamblin, R.J.O., Booth, S.J., Lee, J.R., 2008. Age limits on Middle Pleistocene glacial sediments from OSL dating, north Norfolk, UK. Quaternary Science Reviews 27, 1363-1377.
- Pawley, S.M., Toms, P., Armitage, S.J., Rose, J., 2010. Quartz luminescence dating of Anglian Stage (MIS 12) fluvial sediments: Comparison of SAR age estimates to the terrace chronology of the Middle Thames valley, UK. Quaternary Geochronology 5, 569-582.
- Pedley, M., 2009. Tufas and travertines of the Mediterranean region: a testing ground for freshwater carbonate concepts and developments. Sedimentology 56, 221-246.
- Petit-Marie, N., Carbonel, P., Reyss, J.L., Sanlaville, P., Abed, A., Bourrouilh, R., Fontugne, M., Yasin, S., 2010. A vast Eemian palaeolake in Southern Jordan (29°N). Global and Planetary Change 72, 368-373.
- Petraglia, M.D., Alsharekh, A.M., Crassard, R., Drake, N.A., Groucutt, H., Parker, A.G., Roberts, R.G., 2011. Middle Palaeolithic occupation on a Marine Isotope Stage 5 lakeshore in the Nefud Desert, Saudi Arabia. Quaternary Science Reviews 30, 1555-1559.
- Petraglia, M.D., Alsharekh, A., Breeze, P., Clarkson, C., Crassard, R., Drake, N.A., Groucutt, H.S., Jennings, R., Parker, A.G., Parton, A., Roberts, R.G., Shipton, C., Matheson, C., al-Omari, A., Veall, M.A., 2012. Hominin Dispersal into the Nefud Desert and Middle Palaeolithic Settlement along the Jubbah Palaeolake, Northern Arabia. PLOS ONE 7, 1-21.
- Potter, E.K., Esat, T.M., Schellmann, G., Radtke, U., Lambeck, K., McCulloch, M.T., 2004. Suborbital-period sea-level oscillations during marine isotope substages 5a and 5c. Earth and Planetary Science Letters 225, 191-204.
- Prescott, J.R., Hutton, J.T., 1988. Cosmic ray and gamma ray dosimetry for TL and ESR. International Journal of Radiation Applications and Instrumentation. Part D. Nuclear Tracks and Radiation Measurements, 14, 223-227.
- Prescott, J.R., Hutton, J.T., 1994. Cosmic ray contributions to dose rates for luminescence and ESR dating: Large depths and long-term time variation. Radiation Measurements 23, 497-500.
- Preusser, F., Chithambo, M.L., Götte, T., Martini, M., Ramseyer, K., Sendezera, E.J., Susino, G.J., Wintle, A.G., 2009. Quartz as a natural luminescence dosimeter. Earth Science Reviews 97, 184-214.

- Reed, F.A., Tishkoff, S.A., 2006. African human diversity, origins and migrations. Current Opinion in Genetics & Development 16, 597-605.
- Rees-Jones, J., 1995. Optical dating of young sediments using fine-grain quartz. Ancient TL 13, 9-14.
- Reimer, P.J., Baillie, M.G.L., Bard, E., Bayliss, A., Beck, J.W., Blackwell, P.G., Ramsey, C.B., Buck, C.E., Burr, G.S., Edwards, R.L., Friedrich, M., Grootes, P.M., Guilderson, T.P., Hajdas, I., Heaton, T.J., Hogg, A.G., Hughen, K.A., Kaiser, K.F., Kromer, B., McCormac, F.G., Manning, S.W., Reimer, R.W., Richards, D.A., Southon, J.R., Talamo, S., Turney, C.S.M., van der Plicht, J., Weyhenmeyer, C.E., 2009. IntCal09 and Marine09 radiocarbon age calibration curves, 0-50,000 years cal BP. Radiocarbon 51, 1111-1150.
- Rhodes, E.J. 2011., Optically Stimulated Luminescence Dating of Sediments over the Past 200,000 Years. Annual Review of Earth and Planetary Sciences 39, 461-488.
- Rhodes, E.J., Schwenninger, J.L., 2007. Dose rates and radioisotope concentrations in the concrete calibration blocks at Oxford. Ancient TL 25, 5-8.
- Roberts, H.M., 2008. The development and application of luminescence dating to loess deposits: a perspective on the past, present and future. Boreas 37, 483-507.
- Roberts, R., Walsh, G., Murray, A., Olley, J., Jones, R., Morwood, M., Tuniz, C., Lawson, E., Macphail, M., Bowdery, D., Nauman, I., 1997. Luminescence dating of rock art and past environments using mud-wasp nests in northern Australia. Nature 387, 696-9.
- Roberts, R., Bird, M., Olley, J., Galbraith, R., Lawson, E., Laslett, G., Yoshida, H., Jones, R., Fullagar, R., Jacobsen, G., Hua, Q., 1998. Optical and radiocarbon dating at Jinmium rock shelter in northern Australia. Nature 393, 358-362.
- Roberts, R.G., Galbraith, R.F., Yoshida, H., Laslett, G.M., Olley, J.M., 2000. Distinguishing dose populations in sediment mixtures: a test of single-grain optical dating procedures using mixtures of laboratory-dosed quartz. Radiation Measurements 32, 459-465.
- Roberts, H.M., Duller, G.A.T., 2004. Standardised growth curves for optical dating of sediment using multiple-grain aliquots. Radiation Measurements 38, 241-252.
- Rodnight, H., Duller, G.A.T., Wintle, A.G., Tooth, S., 2006. Assessing the reproducibility and accuracy of optical dating of fluvial deposits. Quaternary Geochronology 1, 109-120.

- Rodnight, H., 2008. How many equivalent dose values are needed to obtain a reproducible distribution? Ancient TL 26, 3-10.
- Rose, J.I., Petraglia, M.D., 2009. The Evolution of Human Populations in Arabia: Palaeoenvironments, Prehistory and Genetics, Netherlands. Springer Press.
- Rosenberg, T.M., Preusser, F., Fleitmann, D., Schwalb, A., Penkman, K., SChmid, T.W., al-Shanti, M.A., Kadi, K., Matter, A., 2011. Humid periods in southern Arabia: Windows of opportunity for modern human dispersal. Geology 39, 1115-1118.
- Russell, N.J., Armitage, S.J. 2012. A comparison of single-grain and small aliquot dating of fine sand from Cyrenaica, northern Libya. Quaternary Geochronology. 10. 62-67.
- Schefuß, E., Schouten, S., Jansen, J.H.F., Sinninghe Damste´ , J.S., 2003. African vegetation controlled by tropical sea surface temperatures in the mid-Pleistocene period. Nature 422, 418–421.
- Shea, J.J., 2008. Transitions or turnovers? Climatically-forced extinctions of *Homo sapiens* and Neanderthals in the east Mediterranean Levant. Quaternary Science Reviews 27, 2253-2270.
- Singarayer, J.S., Bailey, R.M., 2003. Further investigations of the quartz optically stimulated luminescence components using linear modulation. Radiation Measurements 37, 451-458
- Singarayer, J.S., Bailey, R.M., 2004. Component-resolved bleaching spectra of quartz optically stimulated luminescence: preliminary results and implications for dating. Radiation Measurements 38, 111-118.
- Singarayer, J.S., Bailey, R.M., Ward, S., Stokes, S., 2005. Assessing the completeness of optical resetting of quartz OSL in the natural environment. Radiation measurements 40, 13-25.
- Smith, B.W., Aitken, M.J., Rhodes, E.J., Robinson, P.D., Geldard, D.M., 1986. Optical dating, methodological aspects. Radiation Protection Dosimetry 17, 229-233.
- Smith, B.W., Rhodes, E.J., 1994. Charge movements in quartz and their relevance to optical dating. Radiation Measurements 23, 329-333.
- Smith, M.A., Prescott, J.R., Head, M.J., 1997. Comparison of 14C and luminescence chronologies at puritjarra rock shelter, central Australia. Quaternary Science Reviews 16, 299-320.
- Spooner, N.A., 1994. On the optical dating signal from quartz. Radiation Measurements 23, 593-600.

- Spooner, N.A., Prescott, J.R., Hutton, J.T., 1988. The effect of illumination wavelength on the bleaching of the Thermoluminescence (TL) of quartz. Quaternary Science Reviews 7, 325-329.
- Spooner, N.A., Questiaux, D.G., 2000. Kinetics of red, blue and UV Thermoluminescence and optically-stimulated luminescence from quartz. Radiation Measurements 32, 659-666.
- Straus, L.G., Bar-Yosef, O., 2001. Out of Africa in the Pleistocene: and introduction. Quaternary International 75, 1-3.
- Stringer, C., 2000. Paleoanthropology: Coasting out of Africa. Nature 405, 24-27.
- Stokes, S., Colls, A.E.L., Fattahi, M., Rich, J., 2000. Investigations of the performance of quartz single aliquot D_e determination procedures. Radiation Measurements 32, 585-594.
- Sutton, S.R., Zimmerman, D.W., 1976. Thermoluminescence dating using zircon grains from archaeological ceramics. Aracheometry 18, 125-134.
- Thomas, D.S.G., Goudie, A.S., 2009. The dictionary of physical geography. Blackwell Publishing, London.
- Thomas, P.J., Jain, M., Juyal, N., Singhvi, A.K., 2005. Comparison of single-grain and small-aliquot OSL dose estimates in <3000 years old river sediments from South India. Radiation Measurements 39, 457-469.
- Thomsen, K.J., Bøtter-Jensen, L., Denby, P.M., Moska, P., Murray, A.S., 2005. Developments in luminescence measurement techniques. Radiation Measurements 41, 768-773.
- Trauth, M.H., Deino, A.L., Bergner, A.G.N., Strecker, M.R., 2003. East African climate change and orbital forcing during the last 175 kyr BP. Earth and Planetary Science Letters 206, 297-313.
- Trauth, M.H., Larrasonaña, J.C., Mudelsee, M., 2009. Trends, rhythms and events in Plio-Pleistocene African climate. Quaternary Science Reviews 28, 399-411.
- Trinkaus, E., 2005. Early modern humans. Annual Review of Anthropology 34, 207-230.
- Tsukamoto, S., Duller, G.A.T., Murray, A.S., Choi, J.H., 2009. Introduction to the special issue on application of luminescence dating in geomorphology. Geomorphology 109, 1.
- Tyron, C.A., 2006. “Early” Middle Stone Age lithic technology of the Kapthurin Formation (Kenya). Current Anthropology 47, 367-375.

- Uerpmann, H.P., 2008. The environment of Jebel al-Buhais: human geography of a Neolithic landscape. In: Uerpmann, H.P., Uerpmann, M., Jasim, S.A. (Eds.), The Natural Environment of Jebel al-Buhais: Past and Present. Kerns Verlag, Tübingen, 9-16.
- Vandenberghe, D., Corte, F, D., Buylaert, J.P., Kucera, J., Van den haute, P., 2008. On the internal radioactivity in quartz. Radiation Measurements 43, 771-775.
- Walter, R.C., Buffler, R.T., Bruggemann, J.H., Guillaume, M.M.M., Berhe, S.M., Negassi, B., Libsekal, Y., Cheng, H., Edwards, R.l., Cosel, R., Néraudeau, D., Gagnon, M., 2000. Early human occupation of the Red Sea coast of Eritrea during the last interglacial. Nature 405, 65-69.
- White, T.D., Asfaw, B., DeGusta,D., Gilbert, H.,Richards, G. D., Suwa, G. & Clark Howell, F., 2003. Pleistocene *Homo* sapiens from Middle Awash, Ethiopia. Nature 423, 742–747.
- Willoughby, P.R., 2007. The Evolution of Modern Humans in Africa: A Comprehensive Guide. Altamira, New York.
- Wintle, A.G., 1973. Anomalous Fading of Thermo-Luminescence in Mineral Samples. Nature 245, 143-144.
- Wintle, A.G., 2008. Luminescence dating: where it has been and where it is going. Boreas 37, 471-482.
- Wintle, A.G., Murray, A.S., 2000. Quartz OSL: Effects of thermal treatment and their relevance to laboratory dating procedures. Radiation Measurements 32, 387-400.
- Wintle, A.G., Murray, A.S., 2006. A review of quartz optically stimulated luminescence characteristics and their relevance in single-aliquot regeneration dating protocols. Radiation Measurements 41, 369-391.
- Wolpoff, M.H., Hawks, J., Caspari, R., 2000. Multiregional, not multiple origins. American Journal of Physical Anthropology 112, 129-136.
- Yoshida, H., Roberts, R.G., Olley, J.M., Laslett, G.M., Galbraith, R.F., 2000. Extending the age range of optical dating using single 'supergrains' of quartz. Radiation Measurements 32, 439-446.

Appendix 1 – Abbreviations

D_e	Equivalent dose
D_r	Dose rate
PH1	Preheat 1
PH2	Preheat 2
L_n	Natural OSL intensity
T_n	Natural test dose OSL intensity
L_x	Regenerated OSL intensity
T_x	Regenerated test dose OSL intensity
α	alpha
β	beta
γ	gamma

Appendix 2 – Calculation of the environmental dose rate: a worked example

Environmental dose rate calculations in this thesis have been completed using the Aberystwyth Luminescence Database (LDB2005) software written by Professor Geoff Duller. To ensure that the database is calculating the environmental dose rate correctly, a worked example for OSL3 is presented here. All values reported in this Appendix have been rounded to two decimal places following calculation.

K, U and Th concentrations

ICP MS and ICP AES were used to calculate the alpha and beta contributions of U and Th, and K concentrations respectively. In-situ gamma spectrometry measurements were used to determine the gamma contributions of K, U and Th where possible.

The U, Th and K concentrations determined for OSL 3 using ICP MS and ICP AES are:

U 2.50 ± 0.25 ppm

Th 14.18 ± 1.41 ppm

K 1.40 ± 0.14 %

The U, Th and K concentrations determined for OSL 3 using in-situ gamma spectrometry are:

U 2.21 ± 0.16 ppm

Th 11.24 ± 0.65 ppm

K 1.09 ± 0.04 %

Environmental dose rates

Using the conversion factors from Adamiec and Aitken (1998), the "dry" alpha, beta and gamma dose rates can be calculated from the U, Th and K concentrations:

U D_α 2.50 * 2.78 = 6.96 Gy/ka

U D_β 2.50 * 0.15 = 0.37 Gy/ka

U D_γ 2.21 *0.11 = 0.25 Gy/ka

Th D_α 14.18 * 0.07 = 1.04 Gy/ka

Th D_β 14.18 * 0.03 = 0.39 Gy/ka

Th D_γ 11.24 *0.05 = 0.54 Gy/ka

K D_β 1.40 * 0.78 = 1.09 Gy/ka

K D_γ 1.09 *0.24 = 0.27 Gy/ka

Grain size attenuation for alpha and beta (not for gamma)

The "dry" alpha and beta dose rates must be corrected for attenuation due to grain size (90-125 µm) using the conversion factors of Bell (1980) and Mejdahl (1979):

U D_α 6.96 * 0.23 = 1.58 Gy/ka

U D_β 0.37 * 0.90 = 0.33 Gy/ka

Th D_α 1.04 *0.26 = 0.27Gy/ka

Th D_β 0.39 * 0.86 = 0.33 Gy/ka

K D_β 1.09 * 0.96 = 1.05 Gy/ka

Alpha efficiency correction

An alpha efficiency correction is then completed for the "dry" alpha dose rates using correction factor of 0.04 ± 0.02 from Rees-Jones (1995):

U D_α 1.58 * 0.04 = 0.06 Gy/ka

Th D_α 0.27 * 0.04 = 0.01 Gy/ka

Water Attenuation

The "dry" alpha beta and gamma dose rates must then be corrected for the water content of 6 ± 1%:

U D_α 0.06 / (1+(1.50*0.06)) = 0.06 Gy/ka

U D_β 0.33 / (1+(1.25*0.06)) = 0.31 Gy/ka

U D_γ 0.25 / (1+(1.14*0.06)) = 0.24 Gy/ka

Th D_α 0.01 / (1+(1.50*0.06)) = 0.01 Gy/ka

Th D_β 0.33 / (1+(1.25*0.06)) = 0.31 Gy/ka

Th D_γ 0.54 / (1+(1.14*0.06)) = 0.50 Gy/ka

K D_β 1.05 / (1+(1.25*0.06)) = 0.98 Gy/ka

K D_γ 0.27 / (1+(1.14*0.06)) = 0.25 Gy/ka

The cosmic dose rate

The cosmic dose rate was calculated using the equations in Prescott and Hutton (1988) and the COSMIC programme written by Dr Robert Clark.

D_c 0.16 ± 0.02 Gy/ka

At FAY-NE1 and the Haua Fteah cave site, the cos2theta protocol was completed to calculate the proportion of cosmic dose shielded from the samples by the cave / rock shelter roof.

Following Smith et al. (1997) in calculating the dose rate, the angular distribution of the cosmic rays was taken to follow the cos2Ø-zenith angle dependence of Allkofer (1975). Using trigonometry, the angular distribution of cosmic rays passing through a determined thickness of rock (i.e shielded) and/or sediment was calculated. These distributions included dose rates for sediments that were "unshielded" (i.e. the cosmic rays did not pass through the rock shelter) and "shielded" (i.e. the cosmic rays had to pass through the roof or wall of the rock shelter). Cosmic dose rates for each of these angular distributions were calculated using the equations in Prescott and Hutton (1988) and the COSMIC programme written by Dr Robert Clark.

A cosmic correction factor was then calculated:

(Total unshielded D_c – Total shielded D_c) / Total unshielded D_c = Correction factor

This correction factor is then used to correct the cosmic dose rate for the sample.

Calculation of the Total Environmental dose rate

The alpha, beta and gamma dose rates are calculated by summing the corrected U, Th and K contributions:

D_α 0.06 + 0.01 = 0.07 Gy/ka

D_β 0.31 + 0.31 + 0.98 = 1.59 Gy/ka

D_γ 0.24 + 0.50 + 0.25 = 0.99 Gy/ka

The total environmental dose rate is the sum of the alpha, beta, gamma and cosmic dose rates:

D_r 0.07 + 1.59 + 0.99 + 0.16 = 2.81 Gy/ka

The environmental dose rate of OSL 3 is 2.81 Gy/ka.

Errors associated with these numerical values were propagated in quadrature throughout the calculation.

Appendix 3 – Libya summary table

Sample ID	D_e (Gy)	D_r (Gy/ka)	Age (ka)
HF09 DS	274.57 ± 13.51	3.00 ± 0.17	91.50 ± 7.40
HF10	177.00 ± 12.10	2.48 ± 0.14	71.30 ± 6.70
OSL 1	106.13 ± 8.13	3.25 ± 0.16	32.60 ± 3.10
OSL 3	9.40 ± 0.20	2.82 ± 0.13	3.30 ± 0.20
OSL 7	136.85 ± 4.77	0.59 ± 0.07	230.70 ± 29.10
OSL 8	78.30 ± 0.83	1.18 ± 0.07	66.20 ± 4.40
OSL 9	62.60 ± 4.50	2.59 ± 0.13	24.10 ± 2.20
OSL 10	70.50 ± 2.10	2.61 ± 0.13	27.10 ± 1.80
OSL 11	88.00 ± 4.10	2.91 ± 0.15	30.30 ± 2.30
OSL 17	227.26 ± 9.76	3.34 ± 0.19	68.10 ± 5.20
OSL 18	75.06 ± 1.73	2.76 ± 0.14	27.20 ± 1.80
OSL 19	165.14 ± 9.09	2.37 ± 0.11	69.70 ± 5.50
OSL 20	152.53 ± 10.56	2.33 ± 0.11	65.50 ± 5.90
Hajj Creiem	199.91 ± 13.47	2.40 ± 0.12	83.40 ± 7.30
OSL 21	250.78 ± 9.91	1.33 ± 0.11	188.10 ± 18.40
OSL 22	83.24 ± 1.58	1.06 ± 0.13	73.80 ± 9.80
OSL 23	83.84 ± 2.44	1.01 ± 0.13	82.80 ± 10.90
OSL 24	283.79 ± 7.13	1.77 ± 0.12	160.70 ± 12.40
OSL 25	66.64 ± 2.07	0.78 ±0.07	85.60 ± 8.10
OSL 28	167.86 ± 3.36	3.59 ± 0.22	46.80 ± 3.30
OSL 29	207.00 ± 9.23	3.48 ± 0.21	59.50 ± 4.80
OSL 30	529.35 ± 13.86	3.11 ± 0.19	170.10 ± 12.20
OSL 31	111.24 ± 4.70	3.24 ± 0.19	34.40 ± 2.70

Table A3. Summary table reporting the equivalent dose values, dose rates, and ages for the Libyan samples.

Appendix 4 – Arabian summary table

Sample ID	D_e (Gy)	D_r (Gy/ka)	Age (ka)
Faya-NR-1	47.70 ± 2.60	1.05 ± 0.06	45.50 ± 3.90
Faya-NR-2	41.70 ± 1.50	0.93 ± 0.06	44.60 ± 3.50
Faya-NR-3	119.10 ± 7.40	0.88 ± 0.06	135.30 ± 13.20
Faya-NR-4	5.60 ± 0.50	0.76 ± 0.04	7.30 ± 0.80
Faya-NR-6	2.98 ± 0.30	0.66 ± 0.04	4.50 ± 0.50
Faya-NR-7	7.30 ± 1.80	0.72 ± 0.05	10.20 ± 2.60
Faya-NR-8	155.70 ± 10.80	0.92 ± 0.06	168.60 ± 16.80
Faya-NR-9	117.20 ± 11.90	0.86 ± 0.06	136.20 ± 17.10

Table A4. Summary table reporting the equivalent dose values, dose rates, and ages for the Arabian samples.

Appendix 5 – Arabian sample radial plots

Faya NR 1

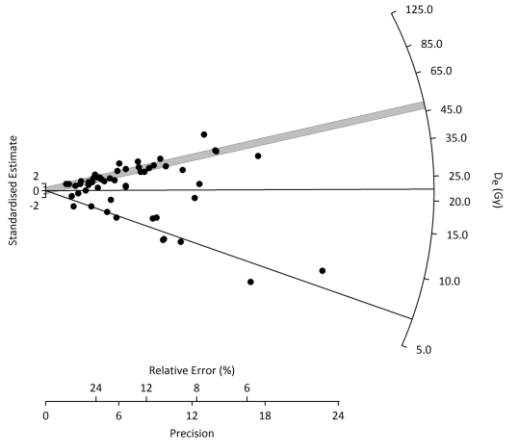

Faya NR 2

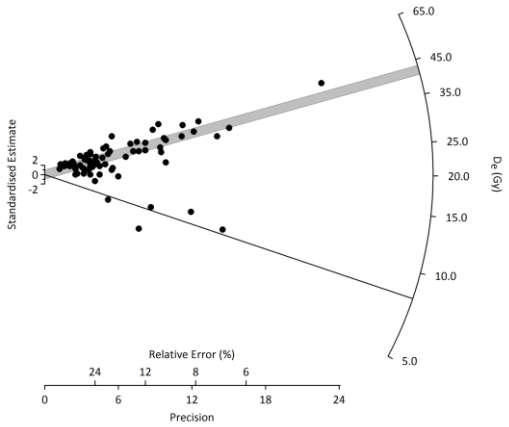

Faya NR 3

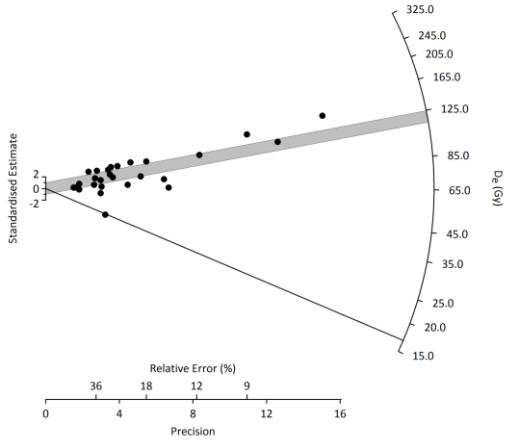

Faya NR 4

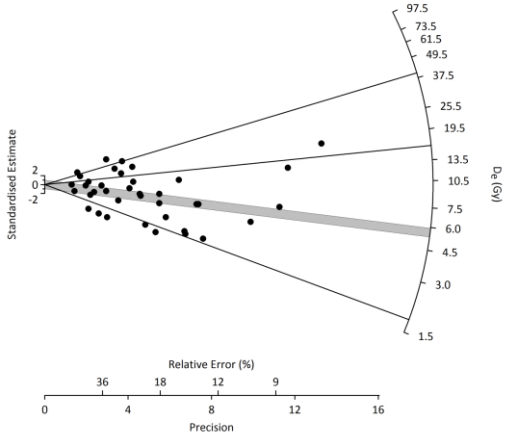

Figure A5.1. Radial plots showing the single-grain (SG) D_e distributions obtained from Faya NR1 (top left), Faya NR2 (top right), Faya NR 3 (bottom left), and Faya NR 4 (bottom right). The thick grey bars represent the dominant component identified using the FMM. Black lines identify minor components.

Faya NR 6

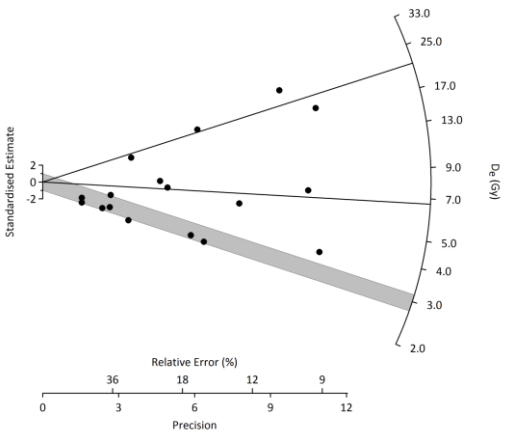

Faya NR 7

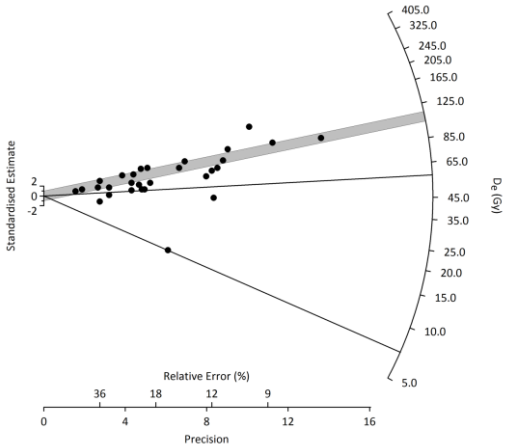

Faya NR 8

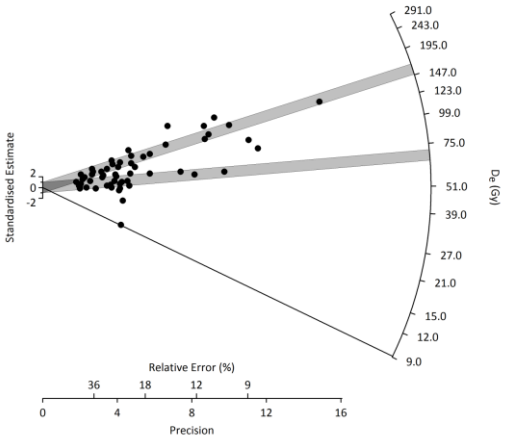

Faya NR 9

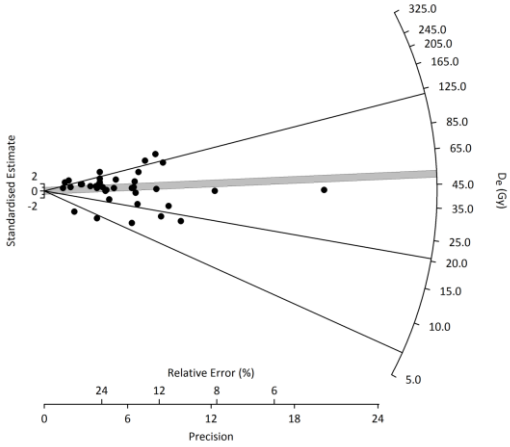

Figure A5.2. Radial plots showing the single-grain (SG) D_e distributions obtained from Faya NR6 (top left), Faya NR7 (top right), Faya NR 8 (bottom left), and Faya NR 9 (bottom right). The thick grey bars represent the dominant components identified using the FMM. Black lines identify minor components.